INFORMATION TO USERS

This manuscript has been reproduced from the microfilm master. UMI films the text directly from the original or copy submitted. Thus, some thesis and dissertation copies are in typewriter face, while others may be from any type of computer printer.

The quality of this reproduction is dependent upon the quality of the copy submitted. Broken or indistinct print, colored or poor quality illustrations and photographs, print bleedthrough, substandard margins, and improper alignment can adversely affect reproduction.

In the unlikely event that the author did not send UMI a complete manuscript and there are missing pages, these will be noted. Also, if unauthorized copyright material had to be removed, a note will indicate the deletion.

Oversize materials (e.g., maps, drawings, charts) are reproduced by sectioning the original, beginning at the upper left-hand corner and continuing from left to right in equal sections with small overlaps.

ProQuest Information and Learning
300 North Zeeb Road, Ann Arbor, MI 48106-1346 USA
800-521-0600

UMI®

Random Dynamics of a Structurally Nonlinear Airfoil in Turbulent Flow

by
Dominique C.M. Poirel

Department of Mechanical Engineering
McGill University
Montreal, Canada
February 2001

A thesis submitted to the Faculty of Graduate Studies and Research
in partial fulfilment of the requirements of the degree of

Doctor of Philosophy

©D. Poirel 2001

National Library of Canada
Bibliothèque nationale du Canada

Acquisitions and Bibliographic Services
Acquisitions et services bibliographiques

395 Wellington Street
Ottawa ON K1A 0N4
Canada

395, rue Wellington
Ottawa ON K1A 0N4
Canada

Your file Votre référence

Our file Notre référence

The author has granted a non-exclusive licence allowing the National Library of Canada to reproduce, loan, distribute or sell copies of this thesis in microform, paper or electronic formats.

L'auteur a accordé une licence non exclusive permettant à la Bibliothèque nationale du Canada de reproduire, prêter, distribuer ou vendre des copies de cette thèse sous la forme de microfiche/film, de reproduction sur papier ou sur format électronique.

The author retains ownership of the copyright in this thesis. Neither the thesis nor substantial extracts from it may be printed or otherwise reproduced without the author's permission.

L'auteur conserve la propriété du droit d'auteur qui protège cette thèse. Ni la thèse ni des extraits substantiels de celle-ci ne doivent être imprimés ou autrement reproduits sans son autorisation.

0-612-70129-8

Canada

ABSTRACT

The main objective of this thesis is to investigate the effects of turbulent flow on the random dynamics of structurally nonlinear airfoil. A secondary objective is to articulate a more comprehensive picture of the contribution of the longitudinal component of turbulence, as experienced by the airfoil, be it linear or nonlinear. In this regard, a systematic and detailed numerical analysis of the airfoil experiencing random flutter/Hopf bifurcation is presented. Some aspects of the divergence/pitchfork problem are also discussed.

The airfoil is modelled as a flexibly mounted rigid flat plate with degrees-of-freedom in pitch and heave. The principal nonlinearity considered is a hardening cubic torsional spring. The aerodynamics is incompressible and linear. Unsteady aerodynamic effects due to arbitrary motion and turbulence are modelled. Both longitudinal and vertical components of the Gaussian turbulence are considered. Longitudinal turbulence acts as a parametric excitation, whereas the latter represents an external forcing.

A Monte Carlo simulation is performed to solve numerically the system of random differential equations. The time history solutions are then studied in terms of their mean-square, probability density function and power spectral density. The largest Lyapunov exponent is also calculated.

The bifurcation, stability and response characteristics of the airfoil are examined. For the linear airfoil, it is found that the coalescence flutter speed is always advanced by the longitudinal component of turbulence, and generally dominated by the very low frequency range of the excitation. Divergence can be either advanced or postponed, but the magnitude of the shift is not significant compared with flutter. Furthermore, it is shown that in general longitudinal turbulence decreases the overall stability of the airfoil, be it linear or nonlinear.

For the nonlinear airfoil, it is the vertical component of turbulence that determines the essential features of the *stochastic bifurcation* and the qualitative characteristics of the response. The interplay between turbulence and nonlinear stiffness has a significant impact on the probability structure of the aeroelastic response. Uni-, bi- and double bi-modal distributions are observed,

and found to occur at different airspeeds depending on which state variable is considered. Furthermore, the spectral content displays *noise-controlled*, and *noise-induced*, time scales.

ABRÉGÉ

Le but principal de notre recherche est l'étude des effets d'un écoulement turbulent sur la dynamique aléatoire d'un profil d'aile ayant une nonlinéarité structuralle. Un but secondaire est d'articuler un portrait d'ensemble de la contribution de la composante longitudinale de la turbulence, comme en témoigne le comportement du profil, soit linéaire ou nonlinéaire. Une analyse systématique et détaillée du profil en condition de flottement/bifurcation de Hopf aléatoire est présentée. Quelques aspects du problème de divergence/pitchfork sont aussi abordés.

Le profil d'aile est modélisé comme une plaque plane et rigide, avec deux degrés-de- liberté en tangage et en déplacement vertical. La nonlinéarité étudiée consiste principalement en un ressort en torsion qui se durcit selon une loi cubique. Les forces aérodynamiques sont incompressibles et linéaires. Les effets non-stationnaires dûs au mouvement du profil et à la turbulence sont modélisés. Les composantes longitudinale et verticale de la turbulence Gaussienne sont considérées. La turbulence longitudinale agit comme une excitation paramétrique, tandis que la verticale représente une force externe.

Une simulation de type Monte Carlo est effectuée afin de solutionner numériquement le système d'équations différentielles aléatoires. Les solutions temporelles sont ensuites étudiées en terme de leur carré-moyen, fonction de densité de probabilité et densité spectrale. Le plus grand exposant de Lyapunov est aussi calculé.

Les caractéristiques de bifurcation, stabilité et réponse du profil d'aile sont examinées. En ce qui à trait au profil linéaire, il est observé que la vitesse de flottement de coalescence est toujours avancée par la turbulence longitudinale, et est généralement dominée par la gamme de trés basses fréquences de l'excitation. La vitesse de divergence peut être avancée ou retardée, mais la grandeur du déplacement n'est pas importante en comparaison avec celle du flottement. De plus, il est démontré qu'en général la composante longitudinale de la turbulence réduit la stabilité d'ensemble du profil, qu'il soit linéaire ou nonlinéaire.

Pour le profil nonlinéaire, c'est la composante verticale de la turbulence qui détermine les particularités éssentielles de la *bifurcation stochastique* et les caractéristiques qualitatives de la réponse. L'intéraction réciproque entre la turbulence et la rigidité nonlinéaire a un impact important sur la structure de probabilité de la réponse aéroélastique. Des distributions uni-, bi- et doublement bi-modales sont observées, et se manifestent à différentes vitesses d'écoulement dépendamant de quelle variable d'état est considérée. De plus, le contenu spectral présente des échelles de temps dites *contrôlées-par-le-bruit* et *provoquées-par-le-bruit.*

ACKNOWLEDGEMENTS

A number of people have contributed directly and indirectly to this thesis. First, I would like to acknowledge the openness, frankness and responsiveness of my supervisor, Professor S.J. Price. I am also specially indebted to Dr. B.H.K. Lee who acted as a mentor, without perhaps knowing it. He also gave me the opportunity to spend two years, during the course of this research, at the CNRC/Institute for Aerospace Research as a guest worker.

In addition, I have some thoughts for Mr. M. Zgela. He has been one of the first sources of inspiration; I recall our discussions on the CF18 limit cycle oscillations. Mr. Nghi Nguyen was also extremely helpful in setting up the computer hardware and software infrastructure.

Without naming them, other people have been instrumental as well. Their contributions have been either specific or indirect but nevertheless important. Finally, credit must be given to the Department of National Defence, specifically the Directorate of Technical Airworthiness and the Royal Military College of Canada/Department of Mechanical Engineering, and the National Research Council of Canada, as organizations, for enabling the pursuit of this endeavour.

STATEMENT OF CONTRIBUTION

An in-depth and systematic analysis of the random dynamics of an airfoil, linear and nonlinear, in turbulent flow has been performed. To the author's knowledge, this is the first time that this problem has been reported. Specifically, the following aspects have been solved.

- It is determined that the supercritical Hopf and pitchfork bifurcations are fundamentally modified by pure longitudinal turbulence. In both cases, *Dynamical* (D-) and *Phenomenological* (P-) bifurcation types are observed. When vertical turbulence is considered, with or without the longitudinal component, the D-bifurcation disappears and a single P-bifurcation remains. Furthermore, the post-Hopf bifurcation motion type is not unique and depends on turbulence variance. This is also the first time that an aeroelastic problem has been studied within the framework of stochastic bifurcation theory.

- It is determined that the flutter point is advanced by the longitudinal component of turbulence, due mainly to parametric, combination difference type, resonances with the very low frequency range in the excitation. Furthermore, the nature of the shift of the random flutter point is similar to deterministic classical flutter, in that it is mainly stiffness controlled and associated with an advancement of the frequency coalescence. On the other hand, the divergence airspeed can be either postponed or advanced by longitudinal turbulence, but the magnitude of the shift is not significant in comparison with the advancement in flutter speed.

- In general, it is shown that the nonlinear aeroelastic response, both qualitatively and quantitatively, is highly dependent on the vertical turbulence characteristics and magnitude of the nonlinearity. For the linear airfoil and/or small nonlinear effects, longitudinal turbulence may become significant mainly because of its destabilizing effect.

- The nonlinear aeroelastic response exhibits complex behaviour due purely to the nonlinear-random interaction. This original dynamics is evidenced in both the uni-dimensional and bi-dimensional probabilistic structure of the response and in its spectral content where *noise-controlled* and *noise-induced* time scales are identified.

From the more general and fundamental perspective of random dynamical systems, this thesis also adds to the very short list of published simulated data on nonlinear dynamical systems excited by multiplicative and additive coloured noise. More specifically, we believe it is the first time that the robustness of the random bifurcation exhibited with multiplicative noise is critiqued explicitly in light of the ubiquitous additive noise component.

TABLE OF CONTENT

NOMENCLATURE

a_i	output of congruential generator (uniform random number)
a_h	distance between mid-chord and elastic axis normalized by semi-chord
A_1, A_2, b_1, b_2	Wagner's function coefficients
A_3, A_4, b_3, b_4	Küssner's function coefficients
b	semi-chord
c	chord
C	multiplier for congruential generator
$C(k)$	Theodorsen function
D_h	structural damping coefficient in heave
D_θ	structural damping coefficient in pitch
$E[x^2]$	mean-square of x (x is a dummy variable)
$F(k)$	real part of Theodorsen function
$G(k)$	imaginary part of Theodorsen function
G^*_{wn}	Gaussian white noise
h	heave
i	imaginary unit number, $\sqrt{-1}$
I_{EA}	airfoil mass moment of inertia about elastic axis
k	reduced frequency, $\omega b/U^*_m$
k_1, k_2	system eigenfrequencies
k_3	non-dimensional nonlinear cubic stiffness coefficient, K_3/K_θ
k_f	(deterministic) flutter reduced frequency
k_p	PSD peak reduced frequency

K_h	linear heave stiffness coefficient
K_θ	linear pitch stiffness coefficient
K_3	nonlinear cubic stiffness coefficient
L^*	scale of turbulence
L	non-dimensional scale of turbulence, L^*/b
L_C	circulatory lift
L_{NC}	non-circulatory lift
L_ψ	lift due to vertical turbulence
L_φ	lift due to arbitrary motion and longitudinal turbulence
m	airfoil mass per unit length
M	modulus
M_{EA}	aerodynamic moment about elastic axis (EA)
$M_{EA\varphi}$	aerodynamic moment about EA due to arbitrary motion and longitudinal turbulence
$M_{EA\psi}$	aerodynamic moment about EA due to vertical turbulence
M_{EAC}	circulatory aerodynamic moment about EA
M_{EANC}	non-circulatory aerodynamic moment EA
N	number of steady state iterations
N_{FFT}	number of data points to perform a Fast Fourier Transform
p	probability density (function)
p_s	steady state, or stationary, probability density
P	probability
r	central frequency of narrow band excitation
$r_\theta{}^2$	radius of gyration squared, I_{EA}/mb^2

t, s	time
$T_{u,Uf}$	turbulence intensity in reference to flutter speed, σ_T/U_f
U_f	non-dimensional (deterministic) flutter speed
U_L	non-dimensional limit speed
U_D	non-dimensional design speed
U_d	non-dimensional (deterministic) divergence speed
u_1, u_2	uniform distributed numbers
U^*	airspeed
U	non-dimensional airspeed, $U^*/b\omega_\theta$
U^*_m	mean airspeed
U_m	non-dimensional mean airspeed, $U^*_m/b\omega_\theta$
U_{m1}	U_m at dynamical bifurcation point
U_{m2}, U_{m3}	U_m at phenomenological bifurcation point
u^*_T, v^*_T, w^*_T	longitudinal, lateral and vertical turbulent velocities, respectively
u_T, w_T	non-dimensional longitudinal and vertical turbulent velocities, respectively, $u^*_T/b\omega_\theta$, $w^*_T/b\omega_\theta$
unf	$U(\tau)/U_m$
unsf	$(U(\tau)/U_m)^2$
$\vec{v}_m$	vector field of mean free-stream velocities
$\vec{v}_T$	vector field of turbulent velocities
w^*	downwash
$w^*_{3/4}$	downwash at three-quarter chord
x_θ	static unbalance; distance between EA and centre of mass normalized by semi-chord
(x, y, z)	airfoil-fixed system of coordinates

(x_m, y_m, z_m)	mean free-stream-fixed system of coordinates
$z_{1,2}$	non-dimensional aerodynamic states, $z^*_{1,2}\, b^2 / U^*_m$
$z^*_1, \dot{z}^*_1$	aerodynamic states due to Wagner's function
$z^*_2, \dot{z}^*_2$	aerodynamic states due to Kussner's function
α	angle of attack
$\Delta\tau$	numerical integration time step
ΔT	FFT sampling time interval
Φ_{LT}	power spectral density of longitudinal turbulent velocity
Φ_{VT}	power spectral density of vertical turbulent velocity
ϕ_{LT}	non-dimensional power spectral density of longitudinal turbulent velocity
ϕ_{VT}	non-dimensional power spectral density of vertical turbulent velocity
ϕ_{wn}	non-dimensional power spectral density of Gaussian white noise
ϕ_θ	non-dimensional power spectral density of pitch angle
ϕ_ξ	non-dimensional power spectral density of heave
φ	Wagner's function
λ_{max}	non-dimensional largest Lyapunov exponent
μ	airfoil/air mass ratio, $m/\rho\pi b^2$
θ	pitch
ρ	air density
σ^{*2}_T	variance of turbulence
σ_T^2	non-dimensional variance of turbulence, $\sigma^{*2}_T/(b\,\omega_\theta)^2$
τ	non-dimensional time, $t\, U^*_m/b$
$\bar{\omega}$	frequency ratio, ω_h/ω_θ

ω	radial frequency
ω_h	uncoupled structural natural frequency in heave, $(K_h/m)^{1/2}$
ω_n	natural frequency
ω_θ	uncoupled structural natural frequency in pitch, $(K_\theta/I_{EA})^{1/2}$
ξ	non-dimensional heave, h/b
ψ	Kussner's function
ζ_h	damping ratio in heave, $D_h/2(mK_h)^{1/2}$
ζ_θ	damping ratio in pitch, $D_\theta/2(mK_\theta)^{1/2}$
$[A]$	linear aeroelastic system state matrix
$[A_3]$	nonlinear stiffness term matrix
$\{B\}$	external forcing vector
$[D]$	damping matrix
$[K]$	linear stiffness matrix
$[K_3]$	nonlinear stiffness matrix
$[M]$	mass matrix
$\dot{} = d\ /dt$	time derivative
$\ddot{} = d^2\ /dt^2$	second time derivative
$' = d\ /d\tau$	non-dimensional time derivative
$'' = d^2\ /d\tau^2$	non-dimensional second time derivative
LT	subscript for longitudinal turbulence
VT	subscript for vertical turbulence
CT	subscript for combined (longitudinal and vertical) turbulence

CHAPTER 1

INTRODUCTION

1.1 Aeroelasticity Fundamentals

The discipline of aeroelasticity and, more generally, fluidelasticity deals essentially with the interaction of structural and aerodynamic (or fluid) forces. One main area of interest is the structural deformations induced by aerodynamic forces, due to turbulence for example. This is generally known as a *response* problem. In many instances, the structural deformations also affect significantly the aerodynamic forces, thus leading to a feedback mechanism between the two sets of forces. The response of the aeroelastic system, for example an airfoil, to any external forcing will depend on this feedback mechanism. It may also lead to a *stability* problem since the feedback mechanism can be negative or positive depending on the value of the system parameters, in particular the airspeed. For low airspeeds, the feedback is generally negative. In this case, the system will return to its initial state after being disturbed; it is said to be stable. Past a critical airspeed, the feedback becomes positive. Any disturbance will in theory grow to infinity if the system is linear. In practice, nonlinearities are present thus restraining the growing motion. Consequently, the system settles on a new state or attractor. The change in dynamics experienced by the nonlinear system as the airspeed is increased through the instability point is termed a *bifurcation*.

A simple but extremely useful model for understanding the fundamentals of aeroelastic dynamics is the flexibly mounted, two-dimensional rigid airfoil known as the *typical section*. It is illustrated in Figure 1.1 with degrees of freedom in torsion (pitch) and translation (heave). Also shown is the airspeed, U^*.

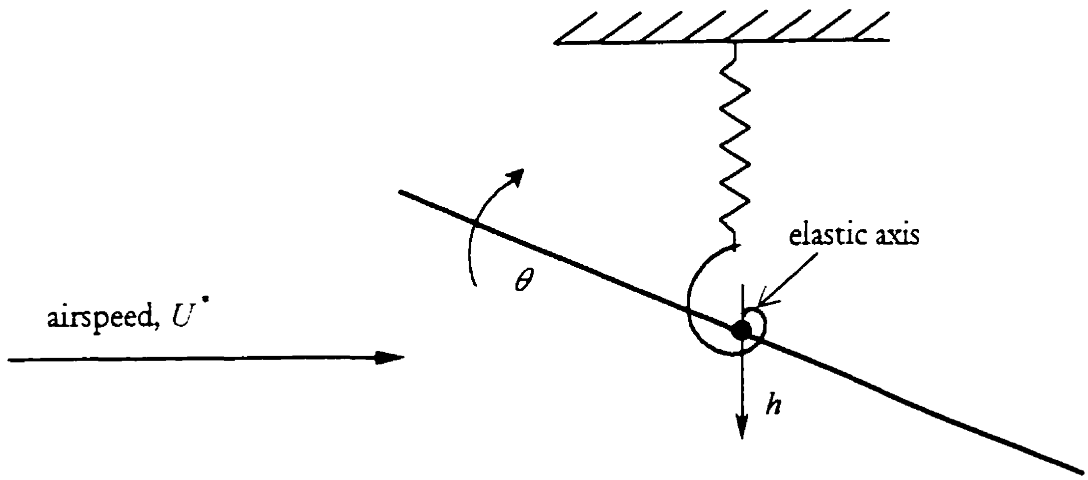

Figure 1.1 - The typical section.

This model has been, and still is used extensively for research, see Lee et al. [1999] for example, as well as for pedagogical purposes in standard aeroelasticity text books, for example Fung [1955]. The dynamics of the linear model is well known and documented. One of the classical problems concerns the stability of the system. The airfoil generally encounters two types of instability, *divergence* and *binary flutter*. Divergence is a static instability and is solely dependent on the system's torsional (structural and aerodynamic) stiffness properties. Bringing the axis of rotation (elastic axis) of the airfoil forward has a stabilising effect.

Flutter is a more complex problem. It is a dynamic instability meaning that the unstable motion grows in an oscillatory fashion. There exists different types of flutter mechanisms but the most common one for this aeroelastic model is binary flutter. It requires the coupling between the two degrees of freedom. Furthermore, for this coupling to be able to extract energy from the airflow, the two vibratory motions must have closely spaced frequencies (i.e. frequency coalescence) such that a desired phase difference is maintained. The dependence of coalescence flutter on the system frequencies makes this type of instability very sensitive to the system stiffness properties. In contrast, structural damping does not have a significant impact [Fung, 1955]. Binary flutter is also called classical, coupled, coalescence or two-degree-of-freedom (2DOF) flutter.

On the other hand, the nonlinear (structural or aerodynamic) airfoil is still a rich source of unexplored dynamic behaviour. For instance, research on the airfoil with structural non-linearities is currently being undertaken at various institutions [i.e. Alighanbari and Price, 1996; Liu and Zhao, 1992; Lee and Desrochers, 1987] where a number of interesting phenomena have been predicted. For example, regions of limit cycle oscillations below the main flutter boundary have been predicted, and for certain airfoil parameters the existence of chaotic oscillations was suggested and then demonstrated via calculation of the Lyapunov exponents [Alighanbari and Price, 1996].

However, it must be admitted that the system being considered in previous investigations is an idealization of the real problem. One particular idealization is that the airfoil is generally assumed to be free of any sources of perturbation, such as mechanical vibrations or turbulent flow, which in reality are always present. This raises, from both a practical and theoretical point of view, the question of the presence of random noise.

Turbulence is felt by the airfoil via two basic forms, as an external forcing and as a parametric excitation. Due to its three-dimensional nature, the turbulent excitation is not only felt as an external forcing by way of its vertical and lateral components, which is the usual approach in classical linear aeroelastic analysis, but as a parametric excitation as well due to its longitudinal component. As we will see in more detail in the next chapter, the in-plane, or longitudinal, turbulence excitation acts directly on the aerodynamic damping and stiffness terms via the airspeed, as for example $U^*(t) = U^*_m + u^*_T(t)$, where U^*_m is the mean airspeed equivalent to the deterministic airspeed. This component of turbulence is a source of difficulty for the mathematical treatment of the problem, because it makes the equation of motion time-varying, and is also the origin of a potentially rich pool of dynamic behaviour.

For the typical section, being a two-dimensional problem, lateral turbulence is not considered; see Figure 1.2 for a two-dimensional representation of turbulence. u^*_T represents longitudinal turbulence and w^*_T is the vertical component.

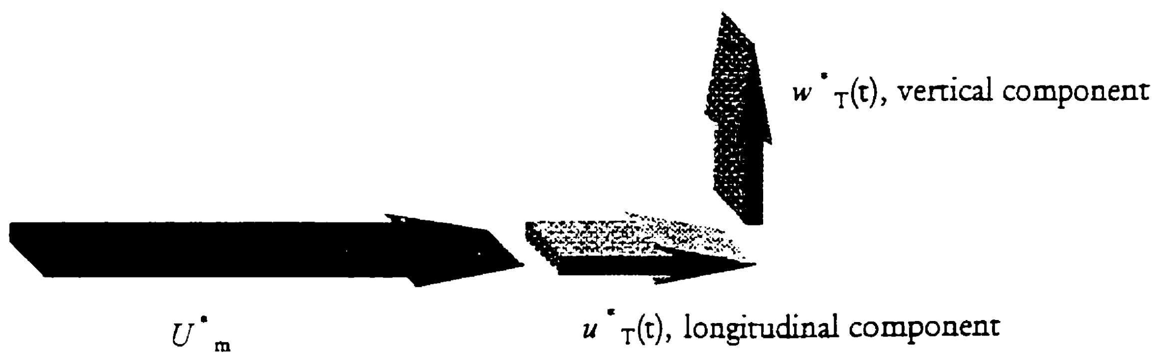

Figure 1.2 - Turbulence components in 2D flow.

The interaction between turbulence and aeroelastic forces (structural and aerodynamic) is represented functionally in Figure 1.3. The airfoil-structure block relates aerodynamic loads (and any external forcing) as inputs with structural deflections as output. Notice that the aerodynamics is broken down into two blocks. One block relates the vertical component of turbulence as input, w^*_T, to aerodynamic load as output. For the other block the input is the structural deflection and the output is the load. This second block is a function of the longitudinal component of turbulence, u^*_T.

A detailed description of the airfoil structure and of the two different types of aerodynamic load is given in Chapter 2. For example, the aerodynamic block relating vertical turbulence to aerodynamic load is represented by equations (2.14) for the airfoil in incompressible inviscid attached flow. The other block relating structural deflection and aerodynamic load is expressed as equations (2.16). From this diagram, it is shown that u^*_T affects directly the stability of the system since it is embedded in the feedback loop, whereas w^*_T has a direct impact on the response.

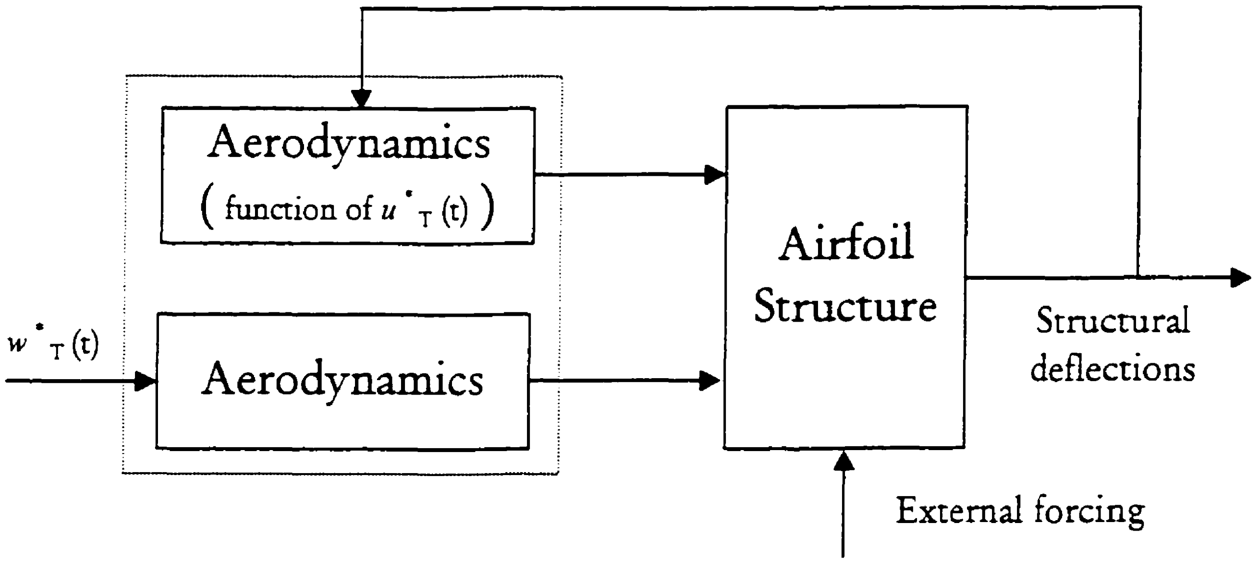

Figure 1.3 - Aeroelasticity-turbulence functional diagram representation.

Note that we consider the turbulent excitation velocities to be independent of the structural deformations. Hence, in many cases the physical origin of the turbulence is not the aeroelastic body itself, such that its characteristics may be determined *a priori*. This type of random excitation is referred to as external noise in the physics literature (not to be confused with external forcing in engineering terminology).

In other circumstances which will not be treated in this thesis, the turbulence is created by the aeroelastic body itself, hence self-induced turbulence. This is similar to internal noise described in the physics literature. For instance, this is the case in separated flow over an airfoil where the turbulence characteristics determine, and are determined by, the buffeting motion of the airfoil.

1.2 Conceptual Framework

In the past two decades, physicists have studied the problem of stochastic fluctuations in light of the recent interest and understanding of chaotic behaviour and related nonlinear dynamics. They have revised the classical, intuitive reasoning that considers randomness in a system as a secondary effect. In fact, it can no longer be argued that stochastic fluctuations should automatically be averaged, or filtered out of signals arising from nonlinear deterministic systems. Furthermore, it is now realised that a nonlinear system excited by random noise can produce original bifurcation phenomena and organized behaviour, some of which have no analog in their deterministic counterparts. These phenomena have been designated as *noise-induced transitions*[1] [Horsthemke and Lefever, 1984]. They are a product of the interplay between stochastic fluctuations and nonlinear dynamics. Examples of the effect of random nonlinear dynamics include either postponement or advancement of the bifurcation points, an increase or decrease in the amplitude of attractors, and more dramatically, completely new types of attractors and bifurcations, the so-called *pure noise-induced transitions* [Fronzoni et al., 1987].

The term *stochastic bifurcation* is also now commonly used although its interpretation and strict definition remain an open question [Arnold, 1995; 1998]. Two schools of thought, with their own perspective and background, have opposite points of view. On one hand, we have the mathematicians and dynamical system theorists, found mainly at the Institute for Dynamical Systems, Bremen University, Germany. On the other hand, there are the physicists, engineers and other scientists whose approach relies more on observation and physical interpretation [Ariaratnam, 1994]. The debate is exemplified by the two basic types of stochastic bifurcation being proposed: *dynamical* and *phenomenological* bifurcations. The dynamical (D-) bifurcation, advocated by the first group, is related to the Lyapunov exponents. The phenomenological (P-) bifurcation is determined by the shape of the response probability density function (PDF). For a deterministic system these two interpretations coincide (for example the bifurcation of a fixed point into a limit cycle oscillation), but not necessarily for a randomly excited problem.

In the modelling and interpretation of fluctuating systems, Millonas [1996] has identified four basic levels of sophistication. The first level, labelled the *deterministic paradigm,* neglects totally the effect and presence of noise; hence, it considers solely the deterministic dynamics. The next

---

[1]In this work, a distinction will be made between *transition* and *bifurcation*. Although the referenced authors use the term *transition*, we believe they actually mean *bifurcation* in the sense of a qualitative change of the system dynamics as a control parameter is changed. Their use of *transition* perhaps stems from their specific areas of research in physics and chemistry. For our case, the word *transition* will be used to describe a superficial and to a certain extent artificial, as opposed to fundamental, change in the system dynamics. The distinction will be made clearer in the analysis of marginal PDFs.

level, which he calls the *equilibrium paradigm*, considers noise but purely as a source of disorder about the deterministic stable attractor. Next in line is the *passive noise paradigm*. A clear example is found on a multi-stable system. In this case, the system may exhibit an irregular, noisy, motion with jumps between the different deterministic multiple stable attractors, hence *basin hopping*. *Active noise paradigm* is the highest level. This is the level of sophistication which is generally associated with the previously mentioned pure noise-induced transition phenomena. Alternatively, the attractors are not pure deterministic objects but are defined by the noise as well.

The equilibrium and passive noise paradigms are related to *additive noise*, or *random external forcing* in engineering terminology. The active noise paradigm is mainly associated with *multiplicative noise*, or *random parametric excitation*. These two types of noise can be classified as *dynamical noise* because they affect and determine the dynamics of the system. On the other hand, *observational*, or *measurement noise*, does not affect the system dynamics, but is simply superimposed (added literally) on the response. It characterises the noise in the measurement system.

As pointed out by Schreiber [1999], "The description of a particular time series by an empirical model will of course be guided by the paradigm adopted for the study". An inappropriate choice of noise model to analyse a noisy time series may hence lead to erroneous conclusions with regards to the type of dynamics which this time series represent. For example, Casdagli [1991] discusses the case of a randomly behaving time series. He mentions that in trying to distinguish between randomness and chaotic motion, some researchers concluded the data to be chaotic on the basis that it could not be adequately described by a limit cycle with additive noise. As remarked by Casdagli, a more plausible alternative to chaos could have been found by using the multiplicative noise instead of the additive noise model.

Schreiber also defines a set of paradigms in the nonlinear-stochastic space. Schematized in Figure 1.4, two of its antipodes represent the usual paradigms: nonlinear deterministic and linear stochastic. Embedded in a solid mathematical framework and nourished by a strong cultural bias, they essentially determine how we choose to analyse and interpret a particular problem. For example, with respect to the linear stochastic perspective, which is equivalent to Millonas's equilibrium paradigm, randomness is addressed within the framework of linearity. Put another way, it is common to model the dynamics by a mean value, defined by the deterministic component of the linearized model, on which are superimposed random fluctuations. Randomness is implicitly considered as secondary effect. Again, Schreiber articulates that these underlying paradigms must be generalized in order to expand our knowledge and grasp of observed dynamic behaviour. Applied to the problem of aeroelasticity, it is in this context that the present thesis is conducted.

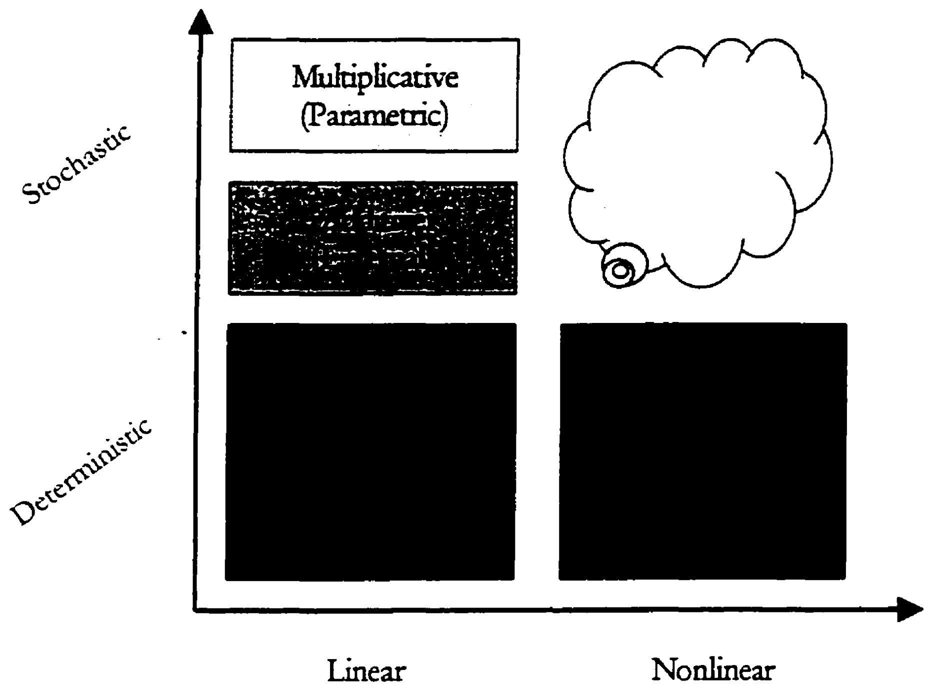

Figure 1.4 - The nonlinear-stochastic paradigm space.

Stepping back in time, let us mention that the shift from a linear to a nonlinear deterministic conception of aeroelastic dynamics seems to have been formally effected in the mid 1970's by Dowell's book [1974] on panel flutter, Brietbach's pioneering paper [1978] on the effects of structural nonlinearities on aircraft vibration and flutter, and more subtly by Holmes [1977] in his proposed alternative definitions for flutter and divergence within the framework of nonlinear theory which takes into account the post-instability behaviour[2].

Along this train of thought, we point out that in many instances a linear description of

[2] To remove any ambiguity, this comment should not be interpreted in the sense that nonlinear aeroelastic behaviour had been discarded before that time. Indeed, nonlinear effects have been treated earlier, namely with regard to panel flutter [Fung, 1955] or wing and control surface flutter [Woolston et al., 1957]. However, we believe that the mid 1970's mark a higher level of maturity in this regard.

divergence cannot capture the proper behaviour of the system in the vicinity of the bifurcation point, even at pre-divergence airspeeds, nor its instability point. Divergence, or pitchfork bifurcation in nonlinear dynamics terminology, is a structurally unstable bifurcation. As illustrated in Figure 1.5, in the presence of a bias (due for example to gravity or camber) the pre-divergence nonlinear fixed point solution does not bifurcate, and an additional saddle-node bifurcation appears at a higher airspeed, whereas for the linear model the instability point for the perturbed and non-perturbed problems are the same.

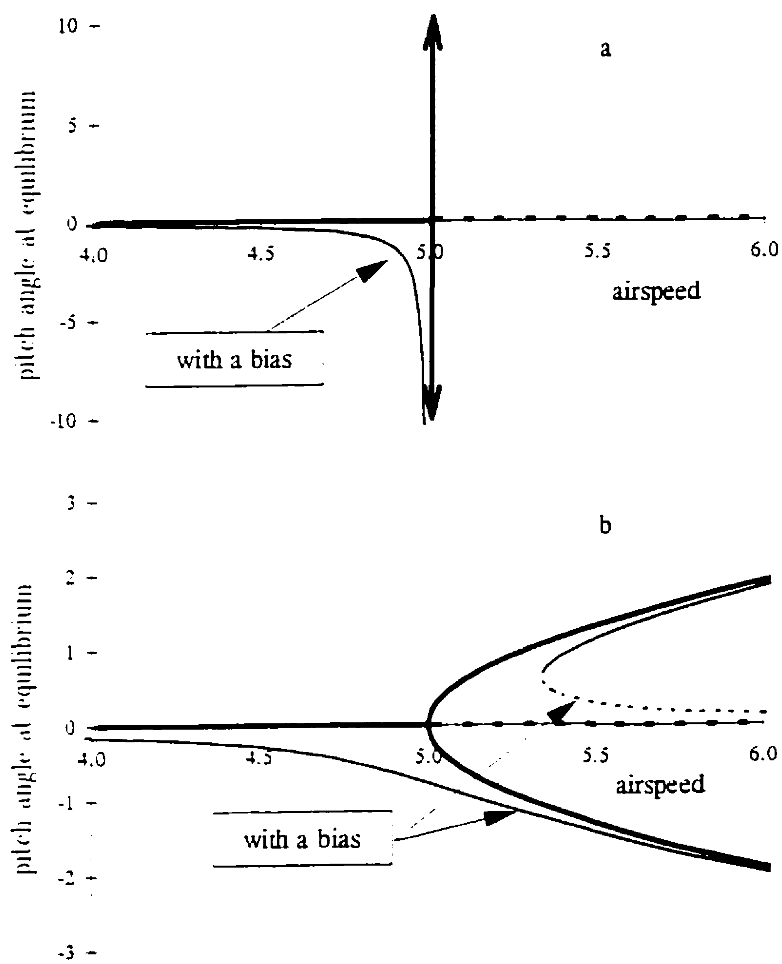

Figure 1.5 - The divergence bifurcation scenario; a) linear case; b) nonlinear case.
(Dark lines: without a bias; Thin lines: with a bias)

1.3 Theoretical Background

1.3.1 Probabilistic, and statistical, analysis and noisy bifurcations

In establishing the theoretical background for this investigation, let us examine the following first-order differential equation:

$$\dot{x} = f(x) = f_\lambda(x) + \lambda_t\, g(x) = h(x) + \lambda q(x) + \lambda_t\, g(x) \tag{1.1}$$

where $h(x)$, $q(x)$ and $g(x)$ are general nonlinear functions of x. λ is constant and λ_t is a parameter which is allowed to fluctuate randomly as:

$$\lambda_t = \sigma\, \xi_t \tag{1.2}$$

ξ_t is a stationary random process of zero mean value and unit intensity; the intensity of λ_t is σ^2. Hence, equation (1.1) can be expressed as:

$$\dot{x} = h(x) + \lambda\, q(x) + \sigma g(x)\, \xi_t \tag{1.3}$$

Assuming the random process is white and Gaussian, we can use Stratonovich[3] calculus formulation for the stochastic differential equation

$$dx = [\, h(x) + \lambda\, q(x)\,]dt + \sigma g(x) \circ dW_t = f_\lambda(x)\, dt + \sigma g(x) \circ dW_t \tag{1.4}$$

The first term on the right is called the drift (vector) and the second term is the diffusion (matrix).

[3]Without getting lost in the mathematical subtleties of stochastic differential equation theory, it is appropriate to mention that Stratonovich calculus is normally used for "real" white noise, i.e. the white-noise limit of a colored-noise process, whereas Ito's formulation is useful for treating the more theoretical "true" white noise idealization. Both formulations are coherent. It is a question of how to interpret the results. Finally, we add that the switch between the two formulations can be easily implemented by a simple transformation in the drift vector [Horsthemke and Lefever, 1984].

W_t is the Wiener process[4]. For this case, based on the Fokker-Planck equation[5], the probability density function (PDF) at steady state, $p_s(x) = \lim p(x, t\to\infty)$, can generally be obtained by solving the following equation [Horsthemke and Lefever, 1984]:

$$f_\lambda p_s - (gg'p_s + g^2 p_s')\,\sigma^2/2 = 0 \tag{1.5}$$

The extrema, or peaks of the steady state PDF, which we argue are in some sense the stochastic analogue of the deterministic equilibrium points are then given by the condition:

$$p_s' \equiv dp_s/dx = 0 \tag{1.6}$$

Hence,

$$f_\lambda p_s - gg'p_s\,\sigma^2/2 = 0$$

$$f_\lambda(x) - g(x)\,g'(x)\,\sigma^2/2 = 0 \tag{1.7}$$

We can immediately recognize the deterministic idealization, i.e. with $g(x) = 0$, giving the well known definition for a fixed point: $f_\lambda(x) = 0$. In the more general stochastic scenario, there are essentially two cases, multiplicative and additive noise. As introduced earlier, additive noise, known as random external forcing in the engineering literature, is independent of the state of the system. In the second case, multiplicative noise or parametric noise acts directly on the parameters, thus its intensity effectively varies with the system states. According to equation (1.3), the type of noise is defined by the diffusion term g as:

$$g = g(x), \qquad \text{multiplicative noise;}$$

$$g = 1 \neq g(x), \quad \text{additive noise.}$$

[4]The Wiener process has zero mean and is Gaussian distributed, with continuous but highly irregular sample path. It is related to the white noise process by the following: $W_t = \int_0^t \xi_s ds$. See Arnold [1974] or Horsthemke and Lefever [1984] for details.

[5]The Fokker-Planck equation governs the evolution of the transition probability density function, $p(x,t)$. See Arnold [1974] or Horsthemke and Lefever [1984] for details.

For the case of additive noise, i.e. $g' = 0$, we are again left with $f_\lambda(x) = 0$. This automatically leads to the conclusion that the deterministic equilibrium points are equivalent to the extrema of $p_s(x)$ for a first-order system excited by additive noise, thus supporting our previous analogy.

With parametric excitation, the zeros of equation (1.7) are no longer independent of the noise intensity. In addition, depending on the relative order of the polynomials of $g(x)$ and $f_\lambda(x)$, not only the position of the zeros but their number can change. This dramatic new "order through fluctuations", or pure noise-induced transition, requires the excitation to be directly acting on a nonlinear term. In the context of this research, the random excitation which originates from turbulence expresses itself in part as a time-varying airspeed, thus random aerodynamic forces. Since we will only consider linear aerodynamics, the number of zeros will not change. Nevertheless, the multiplicative excitation will play a fundamental role in the dynamics of the aeroelastic system.

1.3.1.1 Deterministic Landau equation

To illustrate the problem described above in a simple form, consider the Landau equation [Mackey et al., 1990], where λ acts as the control parameter on the linear term:

$$\dot{x} = f(x) = \lambda x - x^3 \tag{1.8}$$

Note that in deterministic nonlinear dynamic theory, it represents both the pitchfork bifurcation and the r-component (when expressed in polar coordinates) of the normal form for a Hopf bifurcation. The deterministic equilibrium points are:

$$x = 0,\ x = \pm \sqrt{\lambda} \tag{1.9}$$

We can also define the potential, $V(x)$:

$$V(x) = - \int f(x)\, dx = - \lambda x^2/2 + x^4/4 \tag{1.10}$$

The stable equilibrium points given by equation (1.9) correspond to the valleys of the potential well, as shown in Figure 1.6. At steady state, for $\lambda < 0$ the system will stay permanently at $x = 0$ since this is the only stable position, while for $\lambda > 0$ it will remain in either of the two wells as dictated by their respective basin of attraction and the initial conditions.

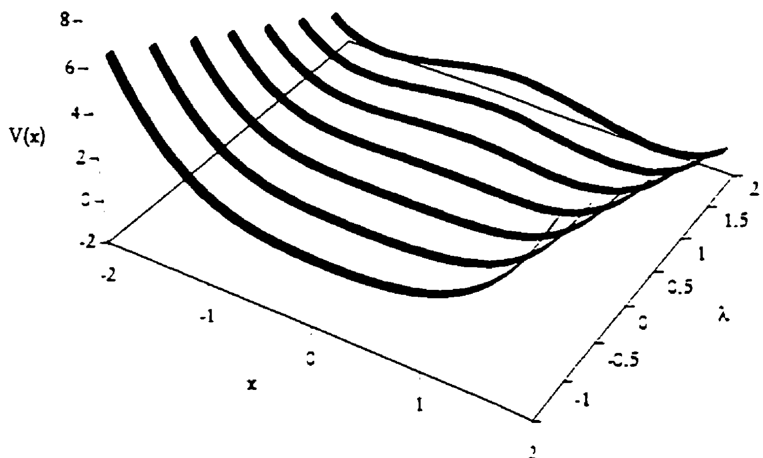

Figure 1.6 - Potential for the Landau equation.

1.3.1.2 Landau equation with additive noise

For the stochastic case, again we decompose the problem into additive and multiplicative excitation. For the additive problem, $g = 1$, we have the following equation:

$$\dot{x} = \lambda x - x^3 + \lambda_t \;=\; \lambda x - x^3 + \sigma\,\xi_t = f_\lambda(x) + \sigma\,\xi_t \qquad (1.11)$$

The steady state probability density is obtained by solving equation (1.5) and gives the general solution [Horsthemke and Levefer, 1984]:

$$p_s(x) = N \exp\,[\,2/\sigma^2\,(\int f_\lambda(x)\,dx)\,] = N \exp\,[\,2/\sigma^2\,(-V(x))\,] \qquad (1.12)$$

and in particular for the potential given in equation (1.10):

$$p_s(x) = N \exp\,[\,\lambda x^2/\sigma^2 - x^4/2\sigma^2\,] \qquad (1.13)$$

where N is a normalization constant such that $\int p_s(x)\, dx = 1$. Imagining the system state to be represented by a ball in a potential well, under the random external perturbations it will jiggle about the single equilibrium point for $\lambda < 0$. For $\lambda > 0$, it will also initially jiggle about one of the two equilibrium points, but will in time jump over the energy barrier into the second well, and so on. In general, the amount of time spent in each well can be characterized by $p_s(x)$. We immediately see the correspondence between potential and steady state PDF. Hence, the valleys of the potential correspond to the peaks of the PDF, and inversely, as shown in Figure 1.7. Qualitatively speaking, the steady state PDF is the inverse image of the potential.

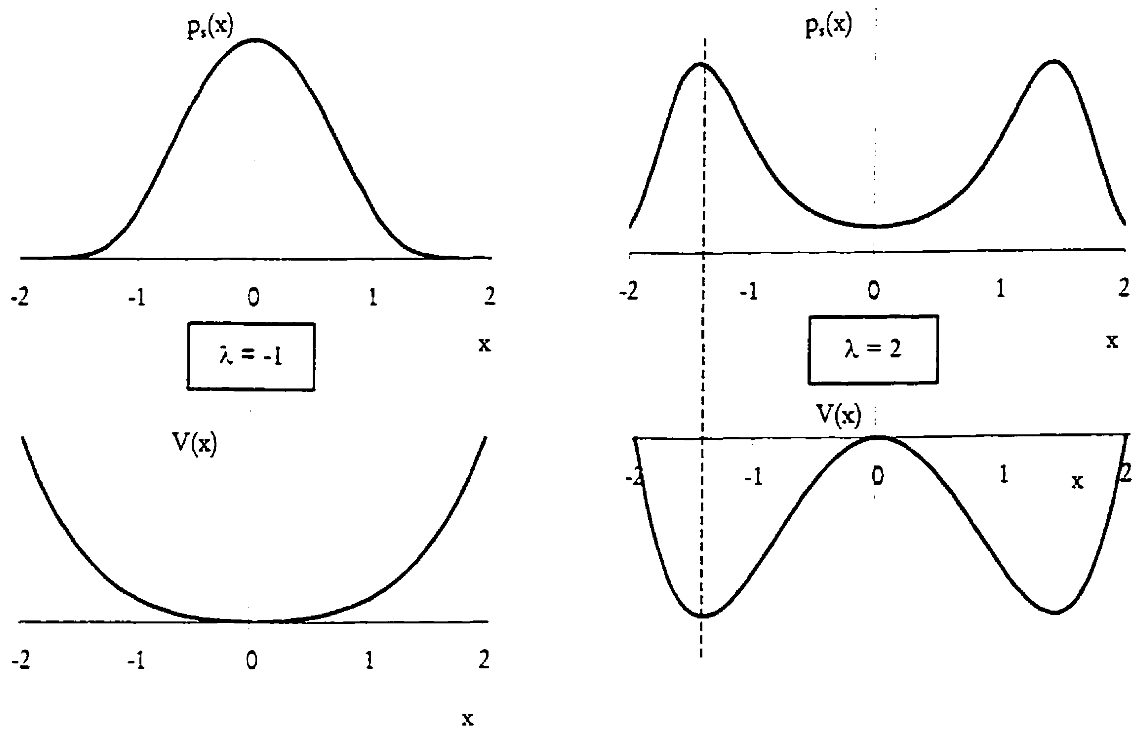

Figure 1.7 - Comparison of potential and PDF for the Landau equation with additive noise.

1.3.1.3 Landau equation with multiplicative noise

We now consider the Landau equation under multiplicative excitation, i.e. with $g = x$

$$\dot{x} = \lambda x - x^3 + \lambda_t x \;=\; \lambda x - x^3 + \sigma x \xi_t = f_\lambda(x) + \sigma x \xi_t \tag{1.14}$$

The extrema of the steady state PDF can be obtained easily from equation (1.7). For this particular problem, we have:

$$f_\lambda(x) = \lambda x - x^3$$
$$g(x) = x$$
$$g'(x) = 1$$

which when introduced into equation (1.7) give:

$$f_\lambda(x) - g(x)\, g'(x)\, \sigma^2/2 = \lambda x - x^3 - x\, \sigma^2/2 = x\,(\lambda - \sigma^2/2 - x^2) = 0 \qquad (1.15)$$

The zeros, i.e. extrema, are

$$x = 0,\ x = \pm \sqrt{(\lambda - \sigma^2/2)} \qquad (1.16)$$

Note that the second set of zeros appears for $\lambda > \sigma^2/2$, indicative of a shift in the bifurcation according to the extrema of the PDF. The steady state probability density function is also obtained by solving equation (1.5) and gives the general solution [Horsthemke and Levefer, 1984]:

$$p_s(x) = N \exp\left[\, 2/\sigma^2 \left(\int f_\lambda(x)/g^2(x)\, dx - \sigma^2/2\ \ln g(x)\right) \right] \qquad (1.17)$$

and in particular:

$$p_s(x) = N \exp\left[\, 2/\sigma^2 \left(\lambda \ln |x| - x^2/2 - \sigma^2/2 \ln |x|\right) \right] \qquad (1.18)$$

Under this form, $p_s(x)$ is only defined for values of $\lambda > 0$. For $\lambda \leq 0$, $p_s(x)$ cannot be normalized[6], and is represented by the delta Dirac generalized function, $p_s(x) = \delta(x)$. Figure 1.8 shows the steady state probability density function for three ranges of the control parameter. In this example, the noise intensity is set at $\sigma^2 = 1$ such that the bifurcation in PDF occurs for a value of the control parameter $\lambda = 0.5$, as per equation (1.16).

[6] In other words, $p_s(x)$ is integrable over $(-\infty,\infty)$ only for $\lambda > 0$. Expressing equation (1.18) as $p_s(x) = N\, x^{2\lambda/\sigma 2 - 1} \exp[\, -x^2/\sigma^2\,]$, we can notice that for $\lambda = 0$, the power term $2\,\lambda/\sigma^2 - 1 = -1$. This makes the improper integral, $\int p_s(x)\, dx$, diverge at $x = 0$.

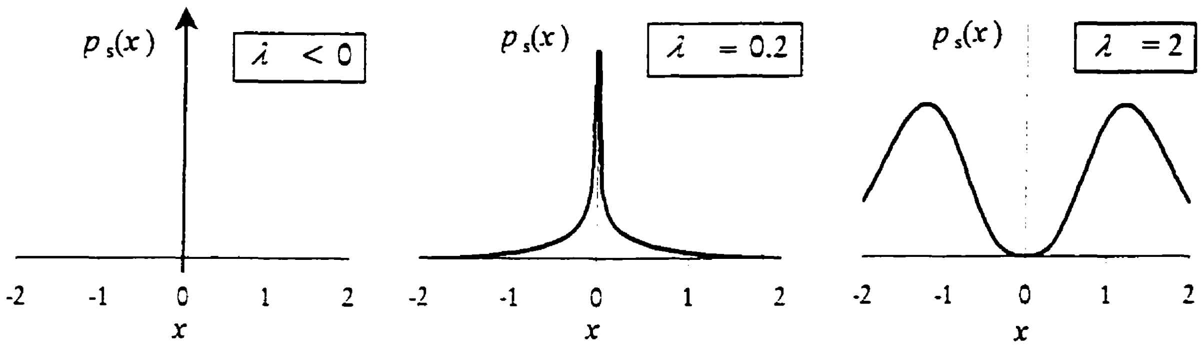

Figure 1.8 - PDFs for the Landau equation with multiplicative noise.

Three distinct regions of dynamic behaviour are observed. For $\lambda < 0$, there is no dynamics. The system does not move; it is fixed at zero. For $\sigma^2/2 > \lambda > 0$ (for example $\lambda = 0.2$ in Figure 1.8), the dynamics is also concentrated about the zero axis, but there is some diffusion about this point. For $\lambda > \sigma^2/2$ ($\lambda = 2.0$ in Figure 1.8), there are two peaks, also with movement about these two extrema.

For this first-order system, the first transition point, at $\lambda = 0$, corresponds to the deterministic instability. However, for the stochastic (multiplicative) case, it cannot be picked up by monitoring the extrema of the PDF, even though a qualitative change in its shape has occurred. In the very recent and quickly evolving theory of stochastic nonlinear dynamical systems, this transition has been termed *Dynamical* or *D-bifurcation* [Arnold, 1995; Arnold and Kedai, 1994]. As we will see later it is associated with a critical slowing down phenomenon, and is purely determined by the linear terms, hence the linear bifurcation point. The D-bifurcation is determined by a change in sign of the largest Lyapunov exponent of the linearized system.

The second transition occurs at $\lambda = \sigma^2/2$, where the qualitative change from single to double peak density is observed. As argued earlier, the peaks are in some sense the stochastic analogues of the deterministic fixed points and correspond to the most probable values the system state will have. This noise-induced transition is labelled as a *Phenomenological* or *P-bifurcation*, and is also sometimes called the nonlinear bifurcation point in contrast with the first. It is postponed compared with the deterministic bifurcation. In this case, no change in sign or discontinuity in the behaviour of the largest Lyapunov exponent is exhibited (Arnold [1998]).

To recap, for this single variable (first-order) system, we have found that additive Gaussian white noise does not modify the bifurcation portrait: there is a single bifurcation point and it occurs for the same value of control parameter as the deterministic case. On the other hand, multiplicative noise creates a second bifurcation which is postponed compared with the deterministic one; the first stochastic bifurcation and the deterministic bifurcation occur at the same point. Without proof, let us mention intuitively that a system excited by both additive and multiplicative noise will not show any indication of a dynamical bifurcation. Hence, as pointed out by Ariaratnam [1994], a real system will not display an abrupt bifurcation, but rather a gradual and continuous increase in response amplitude. In this sense, the concept of P-bifurcation may be more appropriate for some applications. However, using the phenomenological concept in isolation of the dynamical concept, and vice versa, may be to the detriment of a more profound understanding of the dynamics and its fundamental tenets.

1.3.1.4 Multi-variable systems

Multiplicative noise

We will now examine briefly the case of multi-variable stochastic systems, more specifically the (stochastic) Hopf bifurcation problem, whose complexity is magnified in terms of its analytical treatment. Without going into the same level of detail as for the previous case, let us mention that similarly to the Landau dynamics, the Hopf bifurcation exhibited from a multi-variable system excited by multiplicative noise will also be characterized by three distinct regions of dynamic behaviour, hence two bifurcation points. The first region has no dynamics and can be represented as a Dirac delta function at the equilibrium point, the second region is also concentrated about the equilibrium point with some diffusion (we may then speak of a ***stochastic equilibrium point***), and the third region is characterized by a crater-like shaped PDF (***stochastic limit cycle oscillation***).

The similarities stop there. In effect, it has been shown that the first bifurcation point no longer coincides automatically with the deterministic instability point [Ariaratnam, 1994;

Knobloch and Weisenfeld, 1983]. For example, Ariaratnam and Tam [1979] obtained destabilization of a stable deterministic 1DOF system, while Prussing [1981] showed that physical white noise could stabilize an unstable 1DOF system. Similarly, the second (nonlinear) bifurcation point has also been observed to require either higher or lower values of the control parameter. Although Fronzoni et al. [1987] noted that only postponements have been observed in laboratory experiments [Kabashima and Kawakubo, 1979] and numerical simulations, some authors [Lefever and Turner, 1986] have predicted advancements, which is contrary to existing experience for single variable systems.

In this respect, Nicolis and Nicolis [1986] have clearly illustrated the dependence of the shift not only on the coupling between the noise and the slow variable experiencing the critical slowdown, but also on the coupling with the fast variables. Critiquing the universality of the normal forms in the presence of noise, they use the example of the Hopf bifurcation by comparing the solutions obtained from two different approaches. First, they discuss the approach of starting with the deterministic normal form of the r-component, $\dot{r} = ar + br^3$, and then adding phenomenologically a random component to $a \to a + \sigma\xi_r$. The resulting equation is similar to the Landau equation (1.14) excited by multiplicative noise. We have seen that no shift in D-bifurcation is possible, and only a postponement in the P-bifurcation is realizable. On the other hand, they derive a normal form by considering the coupling between the noise and the slow and fast variables, thus, as they put it, maintaining the sensitivity of the stochastic Hopf bifurcation to the specific structure of the system. Finally, they obtain an expression of the noisy normal form of the radial variable in terms of a stationary PDF which exhibits a dependance on the rotation variable, i.e. the LCO frequency. It is this dependance, originating from the coupling with the noise, that enables a shift in the D-bifurcation and an advancement in the P-bifurcation. For example, Lefever and Turner [1986] have shown that for their specific two-dimensional system exhibiting a Hopf bifurcation, postponement of the P-bifurcation occurs when the period of the LCO is smaller than the noise correlation time, whereas advancement happens when the noise is the fastest process. Note that advancement of the P-bifurcation necessarily implies advancement of the D-bifurcation. Knobloch and Weisenfeld [1983] also touch upon the sensitivity of the normal form on the structure of the noisy system and obtain a shift in D-bifurcation even for the pitchfork problem. They go further and show that if the initial system is limited to a single variable by eliminating the inertia term, the shift is no longer possible.

Additive noise

Except for the single variable system excited by additive Gaussian white noise, for which we have argued that the bifurcation is not influenced by the noise, at least when simple local bifurcation types, such as pitchfork, are considered, published literature on either multi-dimensional and/or coloured noise excited systems is contradictory. For example, Knoblock and Weisenfeld [1983] address the case of a single DOF (i.e. two-dimensional) system excited by additive Gaussian white noise, which has no effect on the bifurcation point. On the other hand, cases where additive white and coloured noises influence the bifurcation scenario of two-dimensional nonlinear systems are discussed by Schimansky-Geier et al. [1985]. Similarly, the same is argued by Lugiato et al. [1989] for a single variable system excited by additive coloured noise, and by Longtin [1991] and Longtin et al. [1990] for a single variable delay-differential equation[7] excited by additive white and coloured noise. These issues will be further discussed in Chapter 4 in light of our results.

Arguing that additive noise can influence the bifurcation scenario may in some sense be counter-intuitive considering that our intuition is in many respects nourished by the classical linear problem, one of Schreiber's two antipodes paradigms. It is well known that an external forcing function does not modify the stability behaviour of a linear time-invariant system. Take for example the Lyapunov exponents (to be discussed later) which are determined by the behaviour of the variational (perturbation) variables. For the linear problem the variational system does not depend on the reference trajectory, hence it is independent of the external forcing. However, the influence of the external forcing, via the behaviour of the reference trajectory, can be felt by the variational states if a nonlinearity is considered. On a more physical note, the influence of an external forcing on the stability behaviour can be observed with the divergence problem as discussed earlier, and shown in Figure 1.5. However, this deterministic example is complicated by the unstable nature of the pitchfork bifurcation. Take the case of flutter leading to a Hopf bifurcation, which is structurally stable [Argyris et al., 1994], the linear system will lose stability at an airspeed whose value does not depend on any external forcing, be it constant, harmonic or random. The nonlinear system will also bifurcate at this same airspeed if no forcing is present. On the other hand, the Hopf bifurcation will be shifted to another value of airspeed if, for example,

[7] A delay-differential equation can be considered to be infinite dimensional [Longtin, 1990, 1991].

a constant forcing is imposed [Sipcic and Morino, 1991].

This discussion serves to highlight, and gain some insight into, some of the particularities and fundamental differences for bifurcation phenomena that a noisy system can exhibit in comparison with its usual deterministic counterpart. Accordingly, we have restricted the topic to the simplest cases. However, for the system under investigation in this thesis, its specific structure does not lend itself to a "simple" analysis as described above. For example, we will see that it is excited by both additive and multiplicative coloured noise. Other complications, for multiplicative noise, are the nature of the excitation, which takes different forms and the number of parameters which are excited. We will have parameters excited with linear noise, say $u^{*}_{T}(t)$, and others with quadratic noise, $u^{*}_{T}{}^{2}(t)$. Obviously, the quadratic excitation will not be Gaussian distributed, and its mean will not be zero. Finally, the system is high-dimensional.

1.3.2 Resonance considerations and spectral analysis

Turning our attention to the more traditional and classical frequency analysis, let us briefly introduce the problem of resonance in the context of external, and parametric, excitations. Resonance in an externally forced system usually occurs when the forcing frequency, Ω, is close to one of its natural frequencies. For a linearized n-degree-of-freedom system, with natural frequencies ω_{ni}, $i = 1$ to n, the condition for resonance is expressed as $\Omega \approx \omega_{ni}$, and is the ***primary*** or ***main resonance***. If nonlinear effects become important, the system may exhibit ***secondary (harmonic) resonances***, and ***combination (external) resonances*** for the multi-degree-of-freedom case, which depend on the order and type of the nonlinearity. For example, consider a cubic nonlinearity, secondary resonance may occur at $\Omega \approx \frac{1}{3}\,\omega_{ni}$, or $3\,\omega_{ni}$ and combination resonance with the external excitation might exist at $\Omega \approx \omega_{ni} \pm \omega_{nj} \pm \omega_{nk}$, $\Omega \approx \omega_{ni} \pm 2\,\omega_{nj}$, $\Omega \approx 2\,\omega_{ni} \pm \omega_{nj}$, $\Omega \approx (\omega_{ni} \pm \omega_{nj})/2$ [Nayfeh and Mook, 1979]. Another type of combination resonance is possible between a natural frequency and combinatory harmonic external excitations in the case of multifrequency excitation. Again for the cubic system, the condition is, $\omega_n \approx \Omega_1 \pm \Omega_2 \pm \Omega_3$, $\omega_n \approx \Omega_1 \pm 2\,\Omega_2$, $\omega_n \approx 2\,\Omega_1 \pm \Omega_2$, $\omega_n \approx (\Omega_1 \pm \Omega_2)/2$.

Contrary to the previous problem, a system which is parametrically excited will resonate at a forcing frequency close to twice one of its natural frequencies. The condition, $\Omega \approx 2\,\omega_{ni}$, is called *principal parametric resonance*. Other resonance frequencies are given by the more general condition, $\Omega = 2\,\omega_n/m$, where m is an integer, ie m = 1, 2, 3, ...[McLachlan, 1964]. Taking for example the archetypal Mathieu's equation in its damped form:

$$\ddot{x} + 2\zeta\omega_n \dot{x} + (\omega_n^2 - 2q\cos\Omega t)\,x = 0 \qquad (1.19)$$

the stability chart is schematized in Figure 1.9. Centered about $(2\,\omega_n/\Omega)^2 = 1$ is the *principal parametric zone*. We see that, contrary to the well known external resonance case where the presence of damping renders the system always stable, for parametric forcing damping modifies the stability chart by enlarging the stability region; Otherwise in the unstable region, the system will grow to infinity even in the presence of positive damping (or in practice until some nonlinear effect takes over). The system is also subject to combination resonance between combinatory harmonic parametric excitations and twice one of its natural frequencies [Cartmell, 1990].

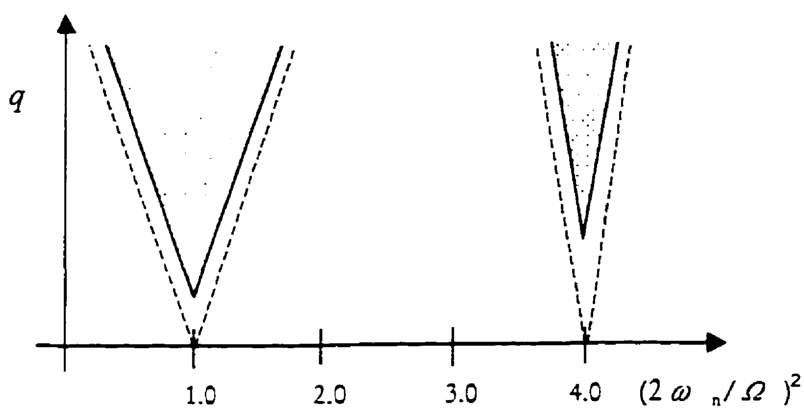

Figure 1.9 - Damped Mathieu's equation schematized stability chart [McLachlan, 1964]. (shaded regions are unstable; dashed lines mark the undamped stability boundary)

Another particularity of parametric excitation is that under certain conditions, it may stabilize an otherwise unstable system, as exemplified again with Mathieu's equation under a more general form, and where the constant stiffness term, k, is negative:

$$\ddot{x} + c\,\dot{x} + (k - 2q\cos\Omega t)\,x = 0 \qquad (1.20)$$

The schematized stability chart for negative values of k is shown in Figure 1.10. For a non-excited system, ie $q = 0$, the fixed point is unstable. However, as the magnitude of the periodic forcing is increased, a relatively small region of stability is possible. It is indicated by the unshaded region left of the y axis.

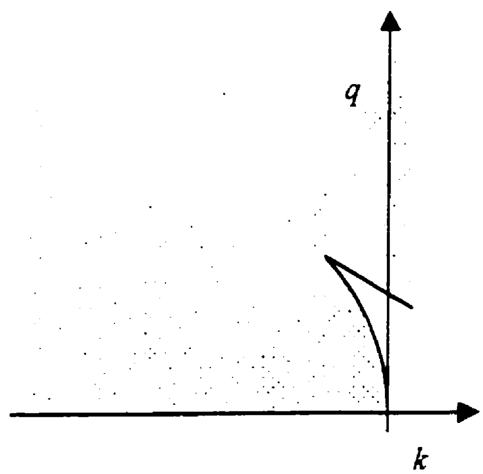

Figure 1.10 - Damped Mathieu's equation schematized stability chart, for $k < 0$. [Nayfeh and Mook, 1979]. (shaded regions are unstable)

Multi-degree-of-freedom parametrically excited systems can also exhibit resonance when the excitation frequency is close to a combination of the system natural frequencies. The condition, $\Omega \approx (\omega_{nj} \pm \omega_{nl})/m$, where m is an integer is called *combination (parametric) resonance.* As pointed out by Cartmell [1990], combination resonances are not limited to pairs only, however higher combinatory orders are more elusive and require stronger excitation levels to materialize. Note, as well, that contrary to the single-degree-of-freedom system where viscous damping is always stabilizing, Nayfeh and Mook [1979] discuss its possible destabilizing effect on combination resonances with parametric excitation.

Other types of resonance, such as internal and autoparametric, are also possible for nonlinear multi-degree-of freedom systems [Nayfeh and Mook, 1979]. However, for the type of nonlinearity considered in this research, we will not be concerned with them.

In many respects, resonance behaviour under random excitation is a natural extension of the previous discussion. In this case, the input and output spectra are in general broad, depending on the noise model. In other words, the system responds to a continuous range of frequency inputs. Resonance effects are characterized by a sensitivity of the response at frequencies which correspond to the primary resonance ($\Omega \approx \omega_n$) for the external excitation, to the principal resonance ($\Omega \approx 2\,\omega_n$) for the parametric problem, and to any secondary and combination resonances for the nonlinear and multi-degree-of-freedom cases, respectively. The intensity of the noise excitation is a critical factor at these resonant frequencies. For example, for a two-degree-of-freedom, linear system excited parametrically by coloured narrow band noise[8], Lin [1996] reports reduced stability regions when the excitation peak corresponds to twice the frequency of the mode experiencing critical slow down ($2\,\omega_1$), or to the difference between the slow and fast mode frequencies (ω_1 - ω_2). The principal parametric resonance condition exhibits the greater effect, followed by the difference combination.

Considering the linear problem, but parametrically excited with broad band noise either in stiffness, or damping or both, a number of authors have reported analytical results demonstrating the role of the noise power spectral density at twice the system natural frequency for its stability condition. For example, Ariaratnam and Tam [1979] studied the single-degree-of-freedom system with randomly excited stiffness and damping, in addition to an external random excitation:

$$\ddot{x} + \omega_n\,(2\zeta + \sigma_1\,\xi_{t1})\,\dot{x} + \omega_n^2\,(1 + \sigma_2\xi_{t2})\,x = \sigma_3\,\xi_{t3} \tag{1.21}$$

They obtained destabilisation of the system, and derived the condition where the deterministic damping must be greater than a certain critical value, $\zeta > \zeta_{cr}$, for stability. They showed that ζ_{cr} depends on the value of the excitation (ξ_{t1} and ξ_{t2}) spectral and cross-spectral densities at $2\omega_n$, and at zero frequency for ξ_{t1}, the damping excitation. They also showed that for this linear system, the additive term, ξ_{t3}, had no effect.

Inversely, stabilization of an unstable, negative stiffness type, deterministic system by parametric white noise was also obtained for a linear single-degree-of-freedom system [Prussing, 1981]. Later, Prussing and Lin [1982] attributed the stabilizing effect to "a change in system

[8]Unless specified otherwise, the noise is considered Gaussian with zero mean.

damping in a particular manner". Although no physical explanation was given, Mitchell and Kozin [1974] also reported stabilization of a negative stiffness type instability. Both sets of authors modelled damping and stiffness random excitation, but Prussing used the same noise excitation, with different intensities, for his study.

Note that Katafygiotis et al. [1997] and Khasminskii [1980] have shown that a one-dimensional unstable deterministic system cannot be stabilized by parametric noise. More generally, the stability of a one-dimensional (first-order) deterministic system is not affected by parametric noise [Arnold, 1974]. This result is coherent with the probabilistic analysis of the Landau equation discussed earlier; see Figure 1.8.

For the nonlinear problem, in addition to the resonance phenomena described earlier, other types of behaviour are expected to occur. As pointed out by Cai and Lin [1997] for the case of a nonlinearity in stiffness, localized broadening of the spectrum may be observed due to a varying natural frequency of the system. Consider the case of a cubic stiffness:

$$\ddot{x} + 2\zeta\omega_n \dot{x} + \omega_n^2 x^3 = \sigma\xi_t \tag{1.22}$$

one may imagine an effective linear stiffness to be $\omega_n^2 x^2$, hence varying with the square of the response amplitude.

Recently[9], the notion of *stochastic resonance* has been introduced to describe situations when a weak periodic force in a nonlinear system can be amplified by external noise. The initial definition requires that all three features, namely nonlinearity, periodic external forcing and random excitation, be present simultaneously [Dykman et al. 1994]. However, since its first interpretation, a number of related phenomena have been observed and the concept of stochastic resonance has been generalized. For instance, Ditzinger et al. [1994] define *stochastic resonance without periodic force*. In this case, the periodicity in the signal originates not from an external forcing, but from either a monostable limit cycle oscillation or from the jumping action between two stable attractors. Ditzinger et al. [1994] studied the response spectrum of a deterministic

[9]According to Dykman et al. [1994], the concept of stochastic resonance dates back to 1982 and is due to Nicolis [1982] and Benzi et al. [1982].

nonlinear (cubic) system subject to additive white noise, without any external periodic forcing, and exhibiting a bi-stability (i.e. two stable fixed points). They found that for low noise intensity the spectrum has one dominant peak at zero frequency, typical of a strong attraction of the system toward one of its fixed points. For increasing noise intensity, the peak broadens and moves toward non-zero frequencies, indicative of a coherent oscillation, termed *pseudo-regular oscillation* by Sigeti and Horsthemke [1989], due to hopping between the two basins of attraction. For larger intensity noise, the peak moves back toward $\omega = 0$ and loses its distinctive shape; the spectrum is nearly flat. As they put it, "the coherent oscillation stimulated by the noise is destroyed by the noise itself almost completely".

As suggested by many authors, this noise-induced frequency peak can be related to a period of oscillation which can be defined either as the *mean sojourn time* from an attractor, or *mean exiting time*, a concept used by McClintock and Moss [1989], or *mean first passage time* [Hänggi et al., 1985]. Others, such as Sigeti and Horsthemke [1989], prefer to use the *most probable time.*

1.3.3 Stochastic stability

Contrary to the deterministic problem, where the observation of a signal often leaves (relatively) very little room for interpretation, the determination of *stochastic stability* is in general not a trivial affair due in part to the different approaches or concepts one may use. We are however very cautious in this statement, since deterministic stability is not always a simple problem[10]. The choice of a stability concept depends on its relevance to the problem at hand. This means specifically the type of motion one is concerned with, the ease of implementation of the method, and finally its pertinence for any useful, engineering application. In other words, determining the stability of a system, or a trajectory, serves no purpose if it is not done within a context. For example, this has led to contradictory comments in the literature. Bucher [1991] states his preference for *sample stability*, or *almost sure stability* (probabilistic concept), over *mean-*

[10]The first example that comes to mind is for a chaotic trajectory which is defined as locally unstable (ie $\lambda_{max} > 0$; see next section) but can be interpreted to be globally stable (i.e. chaotic attractor). Another example, perhaps more subtle, concerns the limit cycle whose stability depends on the method chosen. Using the kinematic concept of Lyapunov, hence (kinematic) Lyapunov exponents, the limit cycle is not stable due to a vanishing λ_{max}. On the other hand, this closed trajectory is stable according to the orbital concept of Poincaré because it is not concerned with the phase difference between two reference points along the trajectory. This concept leads to the term *orbital Lyapunov exponent* [D'Souza and Garg, 1984; Wedig, 1991].

square stability (statistical concept) in engineering applications, due to the fact that the former concept is "related to directly observable events while mean-square stability requires averaging over an ensemble which, in reality, cannot be observed". On the other hand, Lin and Prussing [1982] appear to favour the mean-square stability, arguing that the known techniques to determine sample stability are "very difficult to apply for complicated systems...", while the "techniques for *moment stability* are more versatile ... and appear just as adequate for engineering design as almost sure stability". This dichotomy is symptomatic of the complexity of the treatment of stochastic stability.

Due to the innate random nature of a stochastic system, the most viable approaches are obviously statistical and probabilistic. Hence, in an effort to create a manageable approach to the problem, the different concepts of stochastic stability have been defined along these lines. The two main, fundamental, concepts are sample stability and moment stability[11]. Sample stability (also termed almost sure stability, or almost certain stability, or *stability with probability one*) describes the stability in terms of probability and ensures the stability of all sample functions except for some whose probability of occurrence is negligible. As we will further discuss in the next section, almost sure stability is controlled by the value of the largest Lyapunov exponent. For a more detailed discussion on sample stability, see the following references: Lin and Prussing [1982], Ibrahim [1985], Pugachev and Sinitsyn [1985], Arnold [1974], Sri Namachchivaya and Doyle [1994], Mitchell and Kozin [1974]. We wish to emphasize the meaningful physical insight given by Lin and Prussing in their description of the concept, as well as the very complete discussion by Ibrahim.

The other main notion used to describe stochastic stability is in terms of a statistical functional of samples. Here, we introduce the older concept of moment stability. According to Ariaratnam and Tam [1979], the system is considered asymptotically stable in the n^{th}-moment if the following condition is met:

$$\lim_{t \to \infty} E\left[\left\|x(t)\right\|^n\right] \to \text{finite value} \tag{1.23}$$

[11]There exist other basic types such as stability in distribution, stability in probability [Sri Namachchivaya and Doyle, 1994; Lin and Prussing, 1982; Ibrahim, 1985] and entropy stability [Ibrahim, 1985]. According to the authors, they are either too weak or unpractical.

where $\| x(t) \|$ is the Euclidian norm of the d-dimensional trajectory, and E [ ] is the expectation or the ensemble average. Although n can take different values, we will concentrate on the traditional second moment ($n = 2$) which provides a better physical insight. For this reason, as well as ease of implementation, mean-square stability appears to be the preferred choice for a number of engineering analyses [Lin and Prussing, 1982; Sri Namachchivaya and Doyle, 1994; Ibrahim, 1985].

According to Sri Namachchivaya and Doyle [1994], sample and moment stability of a linear system do not imply each other. For example, Mitchell and Kozin [1974] present results for a parametrically excited linear system which exhibits sample stability but is unstable in the sense of the second moment. It has been pointed out by some authors that this phenomenon is one of *large deviations* [Arnold et al.; 1997]. In contrast, numerical results for our nonlinear system (parametrically excited) have shown that the sample and mean-square stability points coincide.

1.3.4 Lyapunov exponents

The *Lyapunov exponents* express the stability characteristics of a reference trajectory, and more specifically its sensitivity to small perturbations in the initial conditions. Implicit in this description is the linear nature of the concept. Although they may characterize any trajectory whose origin is a linear or a nonlinear system, they depend only on the linear part of the flow. Hence, the Lyapunov exponents are a generalization of the real part of the eigenvalues, defined for a fixed point, to any arbitrary solution. We may then speak of exponential divergence (negative stability) or convergence (positive stability).

Given a d-dimensional continuous ergodic system, Osedelec [Argyris, 1994; Xie, 1990] has demonstrated the existence of d non-random exponents, some of which could coincide. Similarly to the eigenvalue problem, it is the value of the largest exponent, given as λ_{max}, which determines the stability of the trajectory, such that a negative λ_{max} implies a convergence of initially close trajectories, while a positive λ_{max} defines diverging trajectories. Local (trajectory) instability is not necessarily associated with a more global (attractor) instability. For example, a stable chaotic attractor has at least one positive Lyapunov exponent, thus expressing a local instability. However, given a dissipative system, the summation of all n exponents is negative, ensuring that the trajectories will be limited to a confined, but fractal, region in state space. Another characteristic of the Lyapunov exponents is the invariance of their respective magnitude for (almost) any reference trajectory within a given attractor.

No assumption has been made in the preceding on the determinism, or inversely randomness, of the dynamical system. In fact, the concept of Lyapunov exponents has been defined within the framework of random dynamical systems, where the deterministic problem is considered as a particular case of the more general random problem [Arnold and Crauel, 1991, Arnold and Chueshov, 1998]. Examining the d-dimensional linear dynamical system, $\dot{x} = A(t)\, x$, where A is a randomly time-varying d × d matrix, it has been shown analytically that a qualitative[12] change in stability, hence bifurcation, of the random fixed point occurs when the largest Lyapunov exponent changes sign. More specifically, a vanishing λ_{max} is indicative of a D-bifurcation [Arnold, 1995]. This change of sign of λ_{max} is also associated with the probabilistic concept of sample stability [Baxendale, 1991; Arnold et al. 1986].

Another interpretation of the largest Lyapunov exponent refers to its magnitude, which defines the time scale with which two initially close trajectories converge or diverge with respect to each other. Relatively speaking, a large, but negative, largest Lyapunov exponent is associated with the fast convergence of a strongly stable attractor. On the other hand, a small negative largest Lyapunov exponent indicates a stable system, but highly susceptible to excitations, hence the potential problem of large deviations introduced earlier. As the magnitude of λ_{max} decreases towards zero with a change of control parameter, a critical slow down is experienced up to the bifurcation point where λ_{max} vanishes.

In practice there exist different means for obtaining the largest Lyapunov exponent. One approach is the so-called tangent space method [Schreiber, 1999], in reference probably to the linearization process of the system to a reference trajectory. The largest Lyapunov exponent obtained by this method matches its theoretical definition since it calls for the calculation of the Jacobian, and subsequently the solution of the variational equations (see Schenk-Hoppé [1996] for a rigorous theoretical definition of the largest Lyapunov exponent). Although this approach

[12]Here a distinction is made between a qualitative and quantitative description of stability. Qualitative refers to the sign of λ, while quantitative expresses the magnitude of λ, hence the degree of stability.

has been applied to calculate the Lyapunov exponents from time series [for example Eckmann et al., 1986], it is particularly well suited for the case where the equations of motion are available.

There are essentially two avenues to determine the largest Lyapunov exponent via the tangent space method. One is to directly linearize the system by calculating the Jacobian about the reference, random trajectory, hence the requirement to simultaneously numerically integrate the linearized and nonlinear sets of equations. The largest Lyapunov exponent is then obtained from

$$\lambda_{max} = \lim_{t \to \infty} \frac{1}{t} ln \left(\frac{\|\tilde{x}(t)\|}{\|\tilde{x}_o\|} \right) \tag{1.24}$$

where $\tilde{x}(t)$ is the solution of

$$\dot{\tilde{x}} = \frac{\partial f(x,t)}{\partial x} |_{x_r(t)} \tilde{x} \tag{1.25}$$

and $x_r(t)$ is a solution of $\dot{x} = f(x,t)$ which, in general, contains both parametric and external random excitations. Take for example the case of a cubic nonlinearity with $f(x,t) = A(t)x + A_3x^3 + B(t)$, then

$$\dot{\tilde{x}} = \frac{\partial f(x,t)}{\partial x} |_{x_r(t)} \tilde{x} = \left[A(t) + 3A_3x^2\right]|_{x_r(t)} \tilde{x} \tag{1.26}$$

The parametric excitation is directly felt by the linear term $A(t)$, and indirectly by the nonlinear term via the reference trajectory, whereas the influence of the external excitation $B(t)$ is purely determined by the latter.

The second avenue to determine the largest Lyapunov exponent according to the tangent space method consists of twice solving the same system of nonlinear equations, with different but close initial conditions, but with the same noise realisation. In this case, the largest Lyapunov exponent is given by:

$$\lambda_{\max} = \lim_{t\to\infty} \tfrac{1}{t} \ln\left(\frac{\| \ \|_t}{\| \ \|_o}\right) \tag{1.27}$$

where $\| \ \|_t$ is the Euclidian norm between the two solutions at time t

$$\| \ \|_t = \left(\sum_{i=1}^{d}(y_i - x_i)^2\right)_t^{1/2} \tag{1.28}$$

Another series of methods, known as real space or direct methods, search for pairs of initially close trajectories and monitor divergence or convergence. This is the idea behind the algorithm developed by Wolf et al. [1985], and more recently by Kantz [1994], for time series analysis. For the case where the dynamical system is known, the spirit of the real space methods is followed by solving the equations twice, with different initial conditions and with different noise realizations.

1.3.5 Final remarks

We conclude this section on two notes. First, it transpires from the vast majority of the published literature on random nonlinear dynamical systems, more specifically on the subject of bifurcation, that the preferred exercise in trying to elucidate the D- versus P-bifurcation problem is to develop a formalism based on either the presence of multiplicative noise (most cases) or of additive noise (sometimes), but rarely with both noise components acting simultaneously. In fact, we are aware of only a few publications where the combined, additive and multiplicative, noise problem is systematically and explicitly addressed [Sri Namachchivaya, 1988; Sri Namachchivaya and Liang, 1996]. In this context, it is refreshing and stimulating that Arnold [1995] poses the very relevant question: "the real challenge for stochastic bifurcation theory is to explain and analyse what *stochastic Hopf bifurcation* could mean". We believe however that this question is rooted in a more fundamental one, which should take into account the universal property of nature where both multiplicative and additive noise co-exist. Essentially, treating the multiplicative noise problem in exclusion of its additive counterpart, and as a goal in itself, may be in some regards a limited exercise, especially for the nonlinear case. In this sense, Ariaratnam [1994] has alluded to the question by stating "In any physical system, in addition to parametric stochastic fluctuations, there is also present stochastic disturbances of an additive nature. In such systems, an abrupt bifurcation does not occur, but rather a gradual transition to higher and higher response amplitudes as the bifurcation point is crossed. Hence, from a physical viewpoint, the concept of bifurcation of probability density measure may be more realistic."

Second, it seems appropriate in closing to mention the very nice and relevant paper written by Yoon and Ibrahim [1995] on nonlinear coupled oscillators excited by parametric random noise. Relevant to this thesis not so much in depth as some other previously referenced papers, but in terms of breadth. It has the dual merit of investigating the problem with a combined analytical, numerical and experimental approach, and bringing together a number of concepts, some of which were discussed earlier.

1.4 Aeroelasticity in Turbulent Flow - History and Current Status

1.4.1 Preamble

Of the two fundamental problems treated in this thesis, random excitations and nonlinearities, the latter has certainly been addressed with much more drive and vigour in recent years from an aeroelastic point of view. Two recent review papers in the Journal of Aircraft confirm this unbalance. Friedmann [1999] on the "Renaissance of Aeroelasticity and Its Future" identifies nonlinearities as being one of the major areas of interest, but makes relatively little reference to turbulent, or random, excitations. Perhaps, he justifies indirectly this position in the context of rotary-wing aeroelasticity by stating that "Time-varying wake geometry, which is an important source of unsteady loads, vibration, and noise, is excruciatingly complex.". The other paper, by Livne [1999] on "Integrated Aeroservoelasticity Optimization: Status and Direction", offers a classification system of "space-time" behaviour which distinguish for example between linear and nonlinear problems, or between steady and unsteady (dynamic) problems. The random versus deterministic distinction is not offered. However, the gust-excitation situation is discussed but only in terms of (quantitative) response, thus indirectly neglecting the more fundamental aspects of the random-nonlinear interaction such as stochastic bifurcation, or basin hopping.

These operationally oriented positions are certainly motivated, and explained to a degree, by the combined influence of requirements, tools and paradigm bias. In this sense, it can be argued that the current state of technology of flight vehicles does not require a more detailed and up-front tackling of turbulent (random) excitation, which in any case is not possible due to the state of analysis tools available. In counterpoise to this view is the rapidly increasing rate of computer technology, the quickly evolving theory of random nonlinear dynamical systems, experienced and accelerated by other scientific disciplines[13], and the seemingly ever intensifying operational environment of flight vehicles.

For example on this last point, the early days of aeroelasticity were largely dominated by fixed-wing aircraft technology, with an emphasis on linear behaviour, where turbulence was mainly of geo-thermal (atmospheric) origin [see Fung, 1955; or Bisplinghoff and Ashley, 1962]. With the advancement of aircraft capabilities, both in speed and manoeuvres, came a higher intensity turbulence created by flow separation. The shock stall and abrupt pull-up stall on the main wing impacted the tail, hence tail buffeting. The 1960's and 70's marked a shift in interest from fixed- to rotary-wing technology. Along with that shift came the appreciation of the intrinsically nonlinear (structurally and aerodynamically) nature of rotary-wing aeroelasticity, along with the highly turbulent flow caused by the rotating blades cutting through their own shed wake and vortices [Friedmann, 1999; Done, 1996]. Then came the even higher turbulent flow intensity attributed to leading edge vortex breakdown, associated with current generation fighter aircraft at high angle of attack leading to fin buffeting [AGARD-LS-121, 1982; AGARD-CP-483, 1990]. For example, Lee et al. [1993; 1990] measured the turbulent flowfield with a vortex rake in the vicinity of the F-18 vertical fin. At subsonic speeds and angles of attack in the neighbourhood of 35°, RMS values of pressure fluctuations, normalised with the freestream dynamic pressure, in

[13]We are making reference to the disciplines of mathematics and physics which usually precede any engineering applications, and also to advancements in biology or chemistry notably by Horsthemke and Lefever [1984]. However, we wish to point out that closely related to the phenomenon of random dynamics is the probabilistic approach to the analysis and design of systems. In this light, the 40th American Institute of Aeronautics and Astronautics (AIAA) Structures, Structural Dynamics, and Materials Conference [1999] may have been an important turning point for the (North American) aerospace community as it was held in conjunction with the first Forum on Non-Deterministic Approaches. Furthermore, it is also worth pointing out the creation in 1986 of the Journal of Probabilistic Engineering Mechanics.

the order of 0.4 to 0.5 were obtained.

Today's fighter aircraft also experience nonlinear aeroelastic dynamics within their published operational envelope, and sometimes at airspeeds lower than the published flutter speed [Poirel and Landry, 1993; Lee and Tron, 1989]. In particular, limit cycle oscillations are being experienced [Trame et al., 1985; Meijer and Cunningham, 1991]. If there is a trend that emerges from this short historical perspective, it is the increasing practical importance of nonlinearities coupled with an intensifying turbulent operational environment.

1.4.2 Classical approach

The bulk of the published literature on aeroelasticity in turbulent flow concentrates on the response of the system. Moreover, the system is either linearized or sometimes quasi-linearized. Quasi-linearization in a random context is known as the equivalent gain method. It is analogous to the describing function method for deterministic harmonic signals, hence it is not limited to small amplitudes but requires, or assumes, that the response is Gaussian distributed [Lusebrink and Sonder, 1991]. In addition, the turbulent excitation is considered in its vertical, and lateral for a 3D analysis, components only. The longitudinal component is almost always not considered explicitly. The consequences of these simplifications are that the impact of turbulent flow on the stability and dynamics of the aeroelastic system is not known, and more generally the stochastic-nonlinear interaction is not well understood.

Let us add that in the design and certification of aerospace systems, the turbulence excitation is often treated as a deterministic input, known generally as the discrete gust model as opposed to the continuous turbulence model. The deterministic approach has been formulated in a practical form by Pratt in 1953 under the name of the 1-cos pulse model [Pratt and Walker; 1954]. The advantage of this model, which is still being used extensively to treat the response to atmospheric turbulence, lies in its empirical simplicity cultivated by an immense source of flight data [see for example AGARD-R-734, 1986]. It is only in the 1980's that the continuous turbulence model, with some of its limitations as described above, has been used for design in parallel with the discrete gust method [Saucray et al., 1991; Anon. (DOT), 1996].

Of the large number of published works following the classical approach, we wish to discuss two major contributions. Houbolt et al. [1964] in "Dynamic Response of Airplanes to Atmospheric Turbulence Including Flight Data on Input and Response" is particularly significant, in that it provides an exhaustive description of atmospheric turbulence as resolved from flight test data, and a discussion on the determination of the dynamic response of aircraft with a spectral approach. In conjunction with the research headed by Hoblit in the early 1960's, this report is the origin of the more rational continuous turbulence model used in aircraft design. The specific case of the longitudinal component is described initially in the context of the description of atmospheric turbulence. However, and symptomatic of most, if not all, publications, the contribution of longitudinal turbulence is totally discarded in the analysis of the aircraft dynamic response, with no explanation being given. The aircraft is also linearized.

The second work is Hoblit's book [1988] titled "Gust Loads on Aircraft: Concepts and Applications". It is the authoritative reference, and provides a comprehensive treatment of the subject, again from a design point of view. Remaining coherent with the classical approach that considers turbulence excitation only as an external forcing, he stresses the importance of properly modelling the frequency mid-range of the turbulence spectrum, in the same breath neglecting the contribution of the low frequencies. His argumentation is on firm theoretical grounds from the classical approach perspective, as the low frequencies typically excite only the aircraft rigid modes which have a small secondary and indirect influence on the elastic modes. On the other hand, as shown by Lin [1996] for example, in the context that the parametric excitation is considered, the turbulence low frequency range becomes important due to combination parametric resonance and the condition at zero frequency. This book is the only source found which proposes, although indirectly, a rationale for neglecting the longitudinal component (called head-on turbulence in his book). The argument is based on a very simple comparison between the lift increments due to head-on and vertical gusts. Among the simplifications used, the gust is discrete and of small intensity, the reaction of the aircraft is not considered and the aerodynamics is assumed as steady. Nevertheless, Hoblit mentions that longitudinal gusts can be important, but makes no mention of it in the rest of the book. The treatment of nonlinearities is also extremely narrow and superficial, i.e. two pages.

1.4.3 Non-classical initiatives

On the fringe of the classical analysis of aeroelastic response to turbulence are a relatively small number of individual and punctual initiatives. They appear to take their motivation from the specificity of the subject treated or from a more fundamental research interest. In this regard, these initiatives broaden the span of interest, usually limited to wings, control surfaces and fuselage in atmospheric turbulence described above, to other types of structural components, other sources of turbulent excitation and more generally random excitation, and/or to other types of fluid excitation.

In aeroelasticity, there seems to be one main subject which is directly concerned with the nonlinear-random interaction, that is panel flutter. Although an aeroelastic problem, it differs mainly from the airfoil case in that chordwise (streamwise) deformations are important, and supersonic flow is required [Fung, 1955; Dowell et al., 1978]. Nevertheless, it is similar to classical binary flutter of airfoils in that its instability mechanism is also a coalescence of two aeroelastic natural frequencies [Dowell et al., 1978]. A recent survey paper on nonlinear panel flutter is given by Mei et al. [1999]. Due to the very large number of papers published on the subject, the specific case of random excitations is exposed in a few lines, and brings in evidence the work of Ibrahim et al. [1990] with regards to in-plane random forces.

The initial works on stochastic panel flutter aimed at investigating the effect of low intensity excitation of the turbulent boundary layer, originating and acting on the same panel, ie self-induced turbulence. One of the first to observe experimentally and report such an effect was Dowell [Dowell, 1970; Dowell and Voss, 1965]. Wind tunnel experiments showed that the turbulent excitation had relatively more effect on the plate response at pre- rather than at post-flutter airspeeds. In the wake of the experimental observations came efforts to model analytically the phenomenon [for example Dowell, 1970; Eastep and McIntosh, 1971]. Eastep and McIntosh approached the problem by first assuming a phenomenological random pressure field based on known experimental data. The panel motion was then modelled as a previously determined deterministic response on which a small random response is added.

A significant shift in the appreciation of panel flutter followed shortly after with the use of a Monte Carlo technique, thus taking advantage of increasing computing power capabilities. Vaicaitis et al. [1974] integrated the stochastic nonlinear equations of motion in the time domain. The random excitations due to the turbulent boundary layer were, similarly to Eastep and McIntosh's model, considered independent of the panel response and determined from previous experimental data. The experimentally generated turbulence pressures, characterized by their power spectral densities (PSD) and assumed Gaussian distribution, were treated as an external forcing and simulated in the time domain. No parametric random excitations were modelled. In terms of the panel deflection, some relevant results are the following. The response PDF is uni-modal, and tending to a Gaussian structure at pre-flutter speeds, while it is bi-modal after the flutter point. From a physical point of view, the authors have attributed this behaviour to the fact that the rate of response is large when the panel goes through the neutral position, and is then slowed down as nonlinear effects become more important for large deflections. Another interesting observation is that the peak of the nonlinear response PSD, characterizing the LCO, occurs at a frequency slightly lower than the second mode (aeroelastic) natural frequency of the panel. It is not clear however if this change in frequency is due strictly to nonlinear effects or to the nonlinear-random interaction.

Using a very similar approach, the analogous problem of nonlinear panel flutter subjected to acoustic excitations is attacked by Abdel-Motagaly et al. [1999]. Although a number of their results match Vaicaitis et al.'s, a notable exception is the non-zero root-mean-square (RMS) panel response at zero dynamic pressure, whereas for the latter the RMS response tends to zero with dynamic pressure. This difference is not explained, but can be attributed to the source of the random excitation which for Abdel-Motagaly is independent of airspeed. On the other hand, a random excitation having an aerodynamic origin changes with airspeed.

A seemingly increased familiarity with semi-analytical probabilistic methods[14] in random dynamical systems based on the Fokker-Planck equation, enabled Ibrahim et al. [1990; 1991] to tackle stochastic panel flutter in this manner, in addition to including the effect of parametric random pressure loading on the aerodynamic stiffness. No random excitation of the aerodynamic damping terms was considered. They expressed the problem in terms of response statistics, thus

[14]For an in-depth description of the method, see the excellent book by Ibrahim [1985].

generating a set of first-order nonlinear differential equations describing the time evolution of the moments. These equations were then numerically integrated. Using the second-order moment, they were able to determine that, due to its in-plane component, the random turbulent boundary layer reduces the stability (i.e. mean-square stability) region of the system.

Another notable problem is the stability and response of rotor blades. In this case, the equations of motion are usually linearized about a periodic motion obtained from the deterministic nonlinear equations of motion. The turbulent excitation is then included in the linearized equation. The periodicity of the deterministic motion is a direct consequence of the rotating blades in forward flight. This problem is obviously physically different than the one under consideration in this thesis. Mathematically, one difference is expressed by a random parametric cyclostationary process excitation[15]. However, in conditions of hover, the parametric excitation becomes stationary, representative of atmospheric turbulence excitation, due to the loss of the inherent deterministic periodicity. This case has been studied by Lin et al. [1979] and Prussing and Lin [1982; 1983]. Some of the simplifications used are quasi-steady aerodynamics, linear (i.e. no quadratic noise $u^{*2}_T(t)$) and physical white noise excitation, and three degrees-of-freedom. Both damping and stiffness terms were randomly excited. Based of stochastic differential equation theory, they obtained closed-form solutions for the mean-square stability of the system. They showed that turbulence had a destabilizing effect on the uncoupled flapping motion. Introducing a coupling with other degrees of freedom, they further showed that turbulence could be stabilizing for the flap-lag problem. They initially speculated that the origin of the stabilizing effect of the parametric turbulence was the same as the one reported for the single-degree-of-freedom, negative stiffness type instability [Prussing, 1981], which is "a change in the system damping in a particular manner" [Prussing and Lin, 1982]. Later, they interpreted the origin of the stabilisation as an increase in damping of the lead-lag motion due to turbulence [Prussing and Lin, 1983]. On the other hand, the flap-pitch stability was always reduced by turbulence.

More recently, Tang and Dowell [1995] have studied analytically, and complemented this with experimentation, the response of a linear airfoil in a sinusoidal pulsating flow with longitudinal atmospheric turbulence. Although their problem is significantly different from the present one, in the sense that they attempt to simulate the periodic free-stream of a rotor blade

---

[15]Gaonkar [1981] provides a discussion on the response of rotors to nonstationary gust excitation.

in forward motion, it is relevant to highlight one of their aerodynamic modelling assumptions. As discussed later in the next chapter, an ambiguity exists with regard to what has been called an unsteady free-stream velocity versus fore-aft motion. In the later case, the unsteadiness in the airspeed is created by the fore-aft (chordwise) motion of the airfoil, whereas in the former case the origin of the fluctuations in airspeed is not the airfoil motion, but some other outside factor, for example, atmospheric turbulence. One consequence of this difference (others will be discussed in Chapter 2) has to do with additional added mass terms proportional to $\dot{U}$ (for instance $\pi\rho b^2\dot{U}\alpha$ in the lift force) that appears in the aerodynamic model, as for example in Greenberg's model used by Tang and Dowell. The appearance of this term is certainly valid for the fore-aft motion. On the other hand, our intuition suggests that for the unsteady-free stream case, the only added mass terms should be due to arbitrary motion of the airfoil in pitch and heave, since there is no accelerated motion chordwise. It is interesting to note that it appears that Tang and Dowell have not modelled this additional apparent mass term, not for the reason discussed above, but purely for matters of "simplicity". Otherwise, no rationale for neglecting this term was given.

Other, non-aeronautical aeroelastic problems include wind-excited bridges. For example, Bucher and Lin [1988; 1988; 1989] studied the stability of linear bridges randomly excited by wind. Both stiffness and damping terms were randomly excited. Based on a one-mode analysis, they obtained destabilisation in the mean-square sense due to longitudinal turbulence, whereas the system became more stable with the addition of other modes of vibration which had no effect on the deterministic stability. They argued that although longitudinal turbulence may destabilize individual modes acting separately, introducing a coupling with other modes helps in transferring the energy from the least stable to the more stable modes, thus stabilizing the overall system[16]. For a discrete model, the same conclusion was obtained for a 1DOF pitch model, as compared with a 2DOF pitch and heave model for which it was shown that turbulence could have a slight stabilizing effect [Lin and Li, 1993; Li and Lin, 1995; Lin, 1996]. The same authors also highlighted the significance of the excitation spectral level at frequencies corresponding to twice the flutter frequency (principal parametric resonance) and in conditions of combination

[16]Note that the flutter mechanism in this case is one-mode damping-controlled, as opposed to the classical two-mode coalescence airfoil flutter. This should be kept in mind before any hasty conclusions are drawn for classical flutter since coupling is an essential element for this instability to occur, but it could be of some significance for divergence even though divergence is a negative stiffness type instability.

parametric resonance for the 2DOF case[17]. Le Maître et al. [1999] have given a more exotic flavour to the aeroelastic problem by investigating, in the time domain using a Runge-Kutta scheme, the nonlinear interaction of atmospheric turbulence and a sail.

From a more general perspective, Heo and Ibrahim [Heo, 1985; Ibrahim and Heo, 1987] have examined the stochastic response of a nonlinear (quadratic) structure, consisting of two coupled beams with tip masses, under parametric and external white noise excitation. Although they claim their model is representative of an aeroelastic system, there is no attempt to take into account the specific nature of the aerodynamic forces. Among others, one consequence is that the relative magnitude of vertical to longitudinal excitations does not appear to have been considered per se; the same can be said about the relative proportion of random excitation intensity on the damping and stiffness terms. Without losing sight of this essential fact, some of their results are nevertheless relevant to this thesis. Using the same excitation magnitude for both stiffness and damping, they show that the random excitation of the stiffness terms generally has more impact on the system mean-square response than the random excitation of the damping terms. In addition, they conclude that the mean-square response is mainly governed by the external excitation in comparison with the influence of the parametric excitation.

Finally, the more general fluid-structure interaction scenario lends itself to the study of flexible tubes in cross-flow, a topic which has seen and is still receiving a lot of attention. This is an extremely vast topic and no attempt will be made to provide even a modest overview of the problem. We just want to highlight the recent paper by Romberg and Popp [1998] which brings an experimental perspective to the stochastic aeroelastic question. Using a grid of variable geometry they were able to create upstream turbulence with intensity ranging from 10% to 23%. Then, they investigated the stability behaviour of a single flexibly mounted tube in an otherwise fixed array, and determined that the turbulence, even at the lower intensity level (10%), had a significant stabilization effect on the tube. This is relevant in that this controlled experimental investigation provides credence to the physical manifestation of the more fundamental influence that turbulence can have on an aeroelastic system.

[17] The combination parametric resonance condition, $\omega_1 - \omega_2$, could be a contributing factor in the shift of the classical two-mode flutter instability point. As the flutter point is approached, the coalescence of the two modal frequencies makes this resonance condition tend to zero, which is in its own right another determinant for instability [Lin, 1996; Ariaratnam and Tam, 1979].

1.5 Research Motivations, Objectives and Scope

Motivations

As introduced earlier, the interest of the engineering community in the interaction of random excitations with deterministic chaos and related nonlinear dynamics is relatively recent. We have also seen that aeroelastic systems offer a potentially important domain of stochastic nonlinear dynamic phenomena. In this context, we are motivated by both the ubiquitous nature of turbulence, coupled with the ever increasing practical importance of nonlinearities, as well as the theoretical challenge and intellectual significance that the combined problem of random excitations and nonlinearities offer.

Objectives

Except for some recent contributions [Poirel and Price, 1996; 1997; 1999; submitted for publication], published work on the effect of turbulence on the idealized 2D airfoil (the typical section) has concentrated mainly on the linear externally excited (i.e. no longitudinal turbulence) problem. Conversely, the vast majority of studies on the nonlinear airfoil have been treated from a deterministic point of view. Accordingly, this thesis has two objectives:

1. *The principal aim of this thesis is to explore, describe and analyse some of the effects of turbulence on the dynamic characteristics of a flexible airfoil with a structural nonlinearity.*

2. *A secondary objective is to articulate a more detailed and comprehensive picture of the contribution of the longitudinal component of turbulence, as experienced by an airfoil, be it linear or nonlinear.*

Scope

Chapter 1 has established the conceptual framework, and theoretical background, upon which this thesis is constructed. The novelty and relevance of the undertaking have also been put forward through a discussion of random nonlinear dynamical systems theory, and with an historical perspective of turbulent aeroelasticity, linearized and nonlinear. In Chapter 2, the 2D airfoil-turbulence model used for this investigation is described. Particular emphasis is put on the aerodynamic model, since the turbulence excitation acts on the airfoil via the aerodynamic force and moment, considered to be linear and incompressible for this work. The model simulation and analysis methodology are then described in Chapter 3. Some particularities of time discretization and numerical integration of random differential equations are discussed. A discussion on the generation of (pseudo) random numbers is also provided.

The main results of this thesis are given in the next five chapters. The first four deal with the airfoil experiencing binary flutter. These four chapters form the heart of this thesis. Chapter 4 introduces the problem by first establishing the deterministic baseline, non-excited dynamics, and then providing a bifurcation analysis of the random flutter/supercritical Hopf bifurcation. Chapter 5 is concerned with the mechanism of the random instability and Chapter 6 discusses the nonlinear response. In Chapter 7, the second objective of this thesis is specifically addressed where the relative influence of the longitudinal component of turbulence, in the overall more realistic combined excitation problem, is examined.

Some aspects of the turbulence excited diverging airfoil are then discussed in Chapter 8. We conclude with Chapter 9.

Chapter 2

PROBLEM DESCRIPTION AND MODELLING

2.1 The Typical Section (Airfoil)

As shown in Figure 2.1, the airfoil is modelled as a rigid flat plate with two degrees of freedom in heave and pitch, h and θ respectively. Structural flexibility is provided by torsional and translational springs at the elastic axis, EA. By definition, the airfoil is a two dimensional model, hence three dimensional effects are not considered.

The semi-chord is given by b. The static unbalance, x_θ, is the distance from the elastic axis to the airfoil center of mass as a fraction of semi-chord. It is defined positive for the center of mass aft of the EA. a_h is the distance, also as a fraction of semi-chord, from the mid-chord point to the EA. It is defined positive for the EA aft of the mid-chord point. Also shown are the mean airspeed, U^*_m, and the longitudinal and vertical components of turbulent velocities, respectively $u^*_T(t)$ and $w^*_T(t)$.

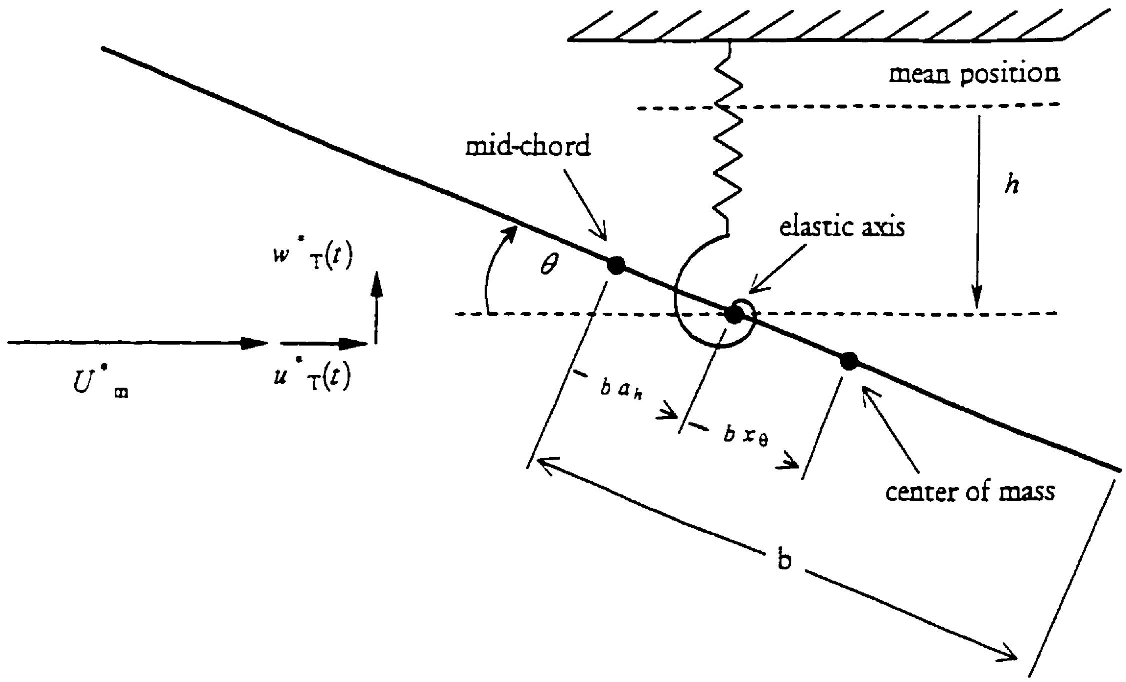

Figure 2.1 - Airfoil model schematic.

2.2 Elastic (Structural) Equations of Motion

The structural equations are obtained from Fung [1955], and modified to include viscous "structural" damping and a structural type nonlinearity in the form of a cubic hardening torsional spring. Note that this is the only source of nonlinearity, except for a few cases discussed in Chapter 8 where a cubic nonlinearity on the translational spring is also considered . Other nonlinearities, such as those of geometric origin have been neglected. Thus, oscillations are limited to small amplitudes, typically $\theta < 10°$, such that $\sin\theta \approx \theta$ and $\cos\theta \approx 1$. The pitch is defined as positive nose up, and the heave as positive downward.

$$I_{EA}\,\ddot{\theta} + m\,x_\theta b\,\ddot{h} + D_\theta\,\dot{\theta} + K\,\theta + K_3\,\theta^3 = M_{EA}(t) \tag{2.1 a}$$

$$m\,\ddot{h} + m\,x_\theta b\,\ddot{\theta} + D_h\,\dot{h} + K_h\,h = -\,L(t) \tag{2.1 b}$$

In addition to the parameters and variables shown in Figure 2.1, I_{EA} represents the mass moment of inertia about the elastic axis, and m is the airfoil mass. D_θ and D_h are the torsional and translational damping coefficients respectively. Similarly, K_θ and K_h are the linear spring coefficients, and K_3 is the cubic nonlinear torsional spring coefficient. The uncoupled natural frequencies in heave and pitch, respectively, are $\omega_h = (K_h/m)^{1/2}$ and $\omega_\theta = (K_\theta/I_{EA})^{1/2}$.

Coupling between the two degrees of freedom arises from the inertia terms in the case where the elastic axis and centre of mass do not coincide ($x_\theta \neq 0$), and otherwise from the aerodynamics. On the right hand side of the pitch and heave equations are the aerodynamic moment and lift force, respectively.

2.3 Aerodynamics

As opposed to previous works on linear or nonlinear airfoil systems, which for the most part modelled the aerodynamics as steady or quasi-steady in the presence of longitudinal turbulence, notably [Prussing and Lin, 1983; Heo, 1985[1]], unsteady aerodynamics is considered in this thesis.

2.3.1 Unsteady aerodynamics due to arbitrary motion of the airfoil

The aerodynamics is considered to be linear as the motion is restricted to small amplitude oscillations, and compressibility effects are neglected. The 2D unsteady aerodynamics accounting for memory effects is modelled, assuming incompressible inviscid attached flow, via Duhamel's integral and the two-state representation of Wagner's function, $\varphi(t)$, given by Jones [Fung, 1955]. This is usually referred to as arbitrary-motion theory. Classically it considers motion in the structural degrees of freedom only, where the downwash is taken at the three-quarter chord position, $w^*_{3/4}(t)$. Realizing that because of the pitch motion, the downwash is not uniform along the chord, $w^*_{3/4}(t)$ represents the effective downwash on the airfoil. Due to its significance in unsteady aerodynamics, the three-quarter chord point is called the rear aerodynamic center [Fung,

---

[1] As we mentioned earlier in Chapter 1, Heo claimed to investigate the flutter behaviour of an aeroelastic body representing an airfoil, in nonlinear stochastic conditions. However, there is no attempt to model the specifics of aerodynamics.

1955]. This effective downwash is given by:

$$w^*_{3/4} = \dot{h} + U^* \alpha + b\,(0.5 - a_h)\,\dot{\alpha} \tag{2.2}$$

Note that for the static problem, the downwash is simply $w^* = U^* \sin\alpha \approx U^*\alpha$. For the similar situation, aerodynamically speaking, of a steady downward translation, an effective angle of attack can be defined as $\alpha_{eff} \approx \dot{h}/U^*$. In this case, the downwash is $w^* = U^*\alpha + \dot{h}$.

Wagner's function [Wagner, 1925] represents the growth of circulation about a thin airfoil at an angle of attack starting impulsively from rest to a uniform velocity, U^*, or equivalently for a sudden increase in angle of attack [Sears, 1940; Fung, 1955]. It can be interpreted physically as being due to the diminishing influence of the starting (shedding) vortex, which induces a downward vertical velocity on the airfoil, as it is convected downstream with velocity U^*; see Figure 2.2. In this case, known as Wagner's problem, the circulatory lift, per unit span, is given by:

$$L_C(t) = \tfrac{1}{2}\rho\, U^* c 2\pi\, w^*\, \varphi(t) = \tfrac{1}{2}\rho\, U^{*2} c 2\pi\, w^*\, \varphi(t) \tag{2.3}$$

The exact form of Wagner's function can be expressed in terms of modified Bessel functions [Fung, 1955]. A widely used approximation, which offers a good compromise between simplicity and accuracy, is Jones' [1938] two-state representation[2]:

$$\varphi(t) = 1 - 0.165\, e^{-0.0455\, U^* t / b} - 0.335\, e^{-0.3 U^* t / b} \tag{2.4}$$

Note that as the distance from the airfoil to the starting vortex tends to infinity ($U^* t \to \infty$), $\varphi(t) \to 1$, such that the circulatory lift tends towards the familiar steady state expression.

---

[2] A number of authors have examined the validity of this approximation, either directly in the time domain in comparison with its exact form and with higher number of states [Dowell, 1980], or in the frequency domain with Theodorsen's function [Peterson and Crawley, 1988].

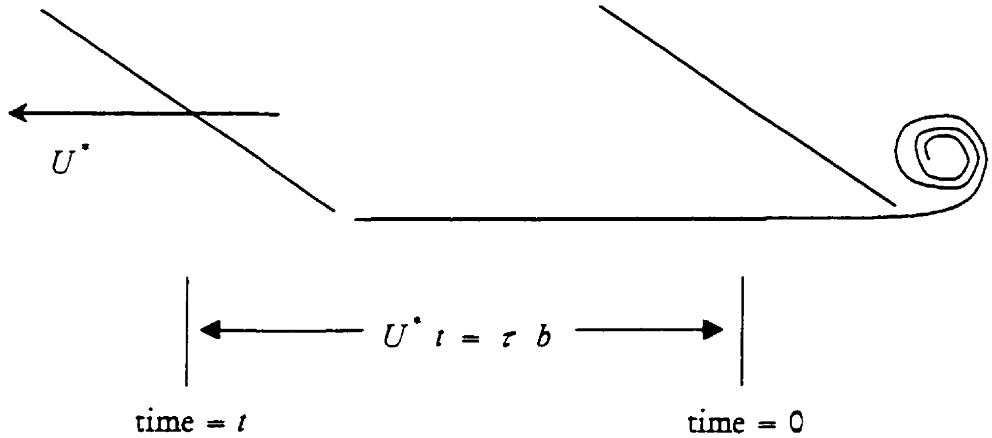

Figure 2.2 - Schematic of Wagner's problem (adapted from Fung [1955]).

The circulatory lift given by equation (2.3) for Wagner's problem can be applied to arbitrary motion, in heave and pitch, in the context of linear aerodynamics with the help of the superposition principle in the form of Duhamel's integral and the effective downwash at the three-quarter chord point. Hence, the elementary lift increment, dL, due to an elementary increment in the effective downwash at time t = 0 is

$$dL_C = \tfrac{1}{2}\rho\, U^{*} c\; 2\pi\, dw^{*}_{3/4}\; \varphi(t) \tag{2.5}$$

The circulatory lift, per unit span, for an arbitrary motion, and assuming the motion starts at time t = 0, is thus the summation of these elements:

$$L_C(t) = 1/2\,\rho U^{*} c\, 2\pi \left[w^{*}_{3/4}(0)\,\varphi(t) + \int_0^t \varphi(t\text{-}s)\,\frac{dw^{*}_{3/4}(s)}{ds}\,ds \right] \tag{2.6}$$

Similarly for the aerodynamic moment, using the fact that for the uncambered thin airfoil the moment at the aerodynamic center, located at the quarter-chord point, is zero, we have:

$$M_{E.A.}(t) = (0.5+a_h)b\; L_C(t) = (0.5+a_h)b^2 \rho U^{*}\, 2\pi \left[w^{*}_{3/4}(0)\,\varphi(t) + \int_0^t \varphi(t\text{-}s)\,\frac{dw^{*}_{3/4}(s)}{ds}\,ds \right] \tag{2.7}$$

In addition to the circulatory airloads, associated with the creation of vorticity, are apparent mass terms. Loosely speaking, these non-circulatory terms physically represent the reaction force of the air displaced by the accelerated motion of the airfoil. They have been derived by Theodorsen [1935] and are expressed for the lift and moment about the elastic axis:

$$L_{NC}(t) = \pi\rho b^2 \left[\ddot{h} + U^* \dot{\alpha} - b\, a_h\, \ddot{\alpha}\right] \tag{2.8 a}$$

$$M_{EA_{NC}}(t) = \pi \rho b^2 \left[b\, a_h\, \ddot{h} - b\,[0.5 - a_h]\, U^* \dot{\alpha} - b^2\,[a_h^2 + 1/8]\,\ddot{\alpha}\right] \tag{2.8 b}$$

For most practical purposes, except for very light structures, these terms are usually neglected as the airmass is often very small compared with the airfoil's. This is typified by the non-dimensional airfoil/air mass ratio, $\mu = m/\pi\rho b^2$, which is always much greater than one. In addition, and as pointed out by Fung [1955], and von Kármán and Sears [1938], the apparent mass terms lose their importance for small reduced frequencies. In any case, the total lift and moment for arbitrary motion are the summation of the circulatory and non-circulatory loads.

For simple harmonic motion, the circulatory loads are also given in terms of Theodorsen's function, C(k), which expresses unsteady aerodynamics for this type of motion [Theodorsen, 1935]. The relationship between the two functions was first shown by Garrick [1938] in the frequency domain, and later by Sears [1940] in the more general Laplace domain, hence the term generalized Theodorsen's function. In the frequency domain, we have:

$$\mathcal{F}[\varphi(t)] = C(k)/ik \equiv \{F(k) + iG(k)\}/ik \tag{2.9}$$

where $\mathcal{F}[\varphi(t)]$ is the Fourier transform of $\varphi(t)$, and k is the reduced frequency. In this sense, Wagner's function is sometimes referred to as a step response, whereas Theodorsen's function as an impulse response. Theodorsen's function in the Jones approximation is given as:

$$C(k) = 1 - \frac{0.165\ ik}{ik + 0.0455} - \frac{0.335\ ik}{ik + 0.3} \tag{2.10}$$

For example, the lift is:

$$L = \pi \rho b^2 \left[\ddot{h} + U^* \dot{\alpha} - b\, a_h \ddot{\alpha}\right] + 2\pi \rho U^* b\, C(k) \left[\dot{h} + U^* \alpha + b(1/2 - a_h)\, \dot{\alpha}\right] \tag{2.11}$$

Note that since $C(k)$ is a complex function, which physically introduces a lag between the motion and the lift force (and aerodynamic moment), the aerodynamic stiffness is not only composed of the displacement term, α, but of velocity terms, $\dot{h}$ and $\dot{\alpha}$, as well. Similarly, the aerodynamic damping is also a function of the displacement and velocities.

2.3.2 Unsteady aerodynamics due to vertical turbulence

Aerodynamic forces and moments are also generated by the presence of vertical turbulence, which in effect changes the local angle of attack on the airfoil. This is represented in Figure 2.3 for the case of a sharp-edged gust.

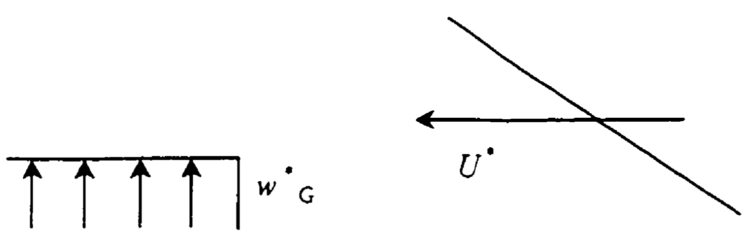

Figure 2.3 - Schematic of airfoil entering a sharp-edged vertical gust.

Due to the finite time associated with penetration of a discrete gust around the airfoil, the aerodynamics exhibit a gradual increase in magnitude. These unsteady effects are expressed in terms of $\psi(t)$, Küssner's function. This gust-penetration function represents the growth of circulation as a sharp-edged gust strikes the leading edge of the airfoil in incompressible flow [Küssner, 1936; Fung, 1955; von Kármán and Sears, 1938]. Similarly to Wagner's function, it can be expressed by a two-state representation, taken from Leishman [1994]:

$$\psi(t) = 1 - 0.5792\,e^{-0.1393\,U^{*}t/b} - 0.4208\,e^{-1.802\,U^{*}t/b} \tag{2.12}$$

The lift, per unit span, due to a sharp-edged vertical gust is given by:

$$L(t) = \tfrac{1}{2}\rho U^{*2}\, c\, 2\pi\,(w^{*}_{G}/U^{*})\ \psi(t) = \tfrac{1}{2}\rho U^{*}\ c\, 2\pi\, w^{*}_{G}\ \psi(t) \tag{2.13}$$

Both Wagner's and Küssner's functions, in their two-state representations, are shown in Figure 2.4 as a function of distance travelled in semichords, equivalent to the non-dimensional time, $\tau = U^{*}t/b$.

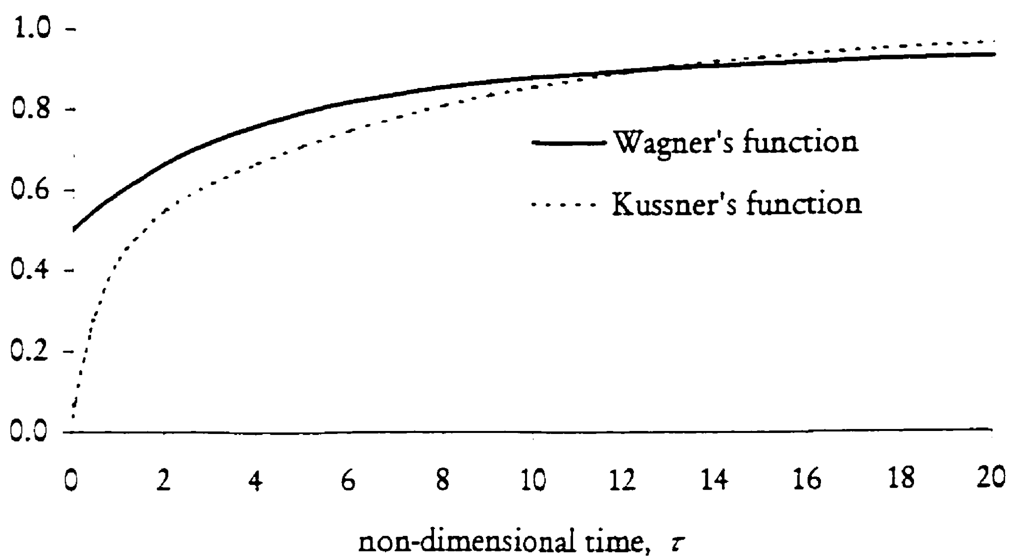

Figure 2.4 - Two-state representations of Wagner's and Küssner's functions as a function of distance travelled in semichords.

Using Duhamel's superposition integral, the force and moment due to vertical turbulence can be derived in the same manner as that used for the lift and aerodynamic moment due to arbitrary motion. Differences between the two set of expressions are the downwash at the three-quarter chord, which is replaced by the vertical turbulence (equivalent to the downwash on the airfoil in the region where the gust has penetrated), w^{*}_{T}, and the absence of apparent mass terms; i.e. no air mass is displaced by the airfoil motion in this case. In effect, Duhamel's superposition integral enables the use of Küssner's function, originally derived for a discrete gust, $w^{\bullet}_{G}$, to be employed for the problem of continuous turbulence, $w^{\bullet}_{T}$. The resulting expressions are:

$$L_{\psi}(t) = 2\ \pi \rho b U^{\bullet}\left[w^{\bullet}_{T}(0)\ \psi(t) + \int_{0}^{t} \psi(t\text{-}s)\frac{dw^{\bullet}_{T}(s)}{ds}ds \right] \tag{2.14 a}$$

$$M_{EA\ \psi}(t) = 2\ \pi \rho b^{2}\left[a_{h} + 0.5\right]U^{\bullet}\left[w^{\bullet}_{T}(0)\ \psi(t) + \int_{0}^{t} \psi(t\text{-}s)\frac{dw^{\bullet}_{T}(s)}{ds}ds \right] \tag{2.14 b}$$

Note that similarly to the arbitrary motion circulatory lift, the gust-penetration lift also acts at the quarter chord [Sears, 1938].

2.3.3 Unsteady aerodynamics due to unsteady free-stream (longitudinal turbulence)

In this thesis, arbitrary-motion theory (equations (2.6), (2.7) and (2.8)) is extended to the case of a random time-varying airspeed, $U^{\bullet}(t)$, based on relatively recent developments made in helicopter aerodynamics theory, more specifically on the works of Friedmann [Friedmann and Robinson, 1990; Dinyavari and Friedmann, 1986; Friedmann, 1987] and of van der Wall [van der Wall and Leishman; 1994; van der Wall, 1991].

Friedmann extended Greenberg's theory, originally derived to capture unsteady aerodynamics for simple harmonic motion of both the airfoil and airspeed, to the general case of arbitrary airfoil motion and time-varying velocity. He obtained an expression for the circulatory lift very similar to the one for pure arbitrary motion (equation (2.6)), except essentially for two differences. One difference is cosmetic in nature, as the latter is expressed in the traditional integro-differential form, whereas Friedmann makes use of the two-state Wagner's function to represent the circulatory lift in pure differential form, with an additional second order ODE. The equivalency between the integro-differential and differential, with augmented states, formulation will be demonstrated later in this section, and is derived in Appendix A.

The other difference is fundamental, as it accounts for fluctuations in the airspeed. Expressing Friedmann's generalized Greenberg theory for arbitrary motion of the 2D airfoil in integro-differential form gives:

$$L_C(t) = 1/2\,\rho U^*(t)\,c\,2\,\pi\left[w^*_{3/4}(0)\,\varphi(t) + \int_0^t \varphi(t\text{-}s)\frac{dw^*_{3/4}(s)}{ds}\,ds\right] \tag{2.15}$$

Notice that compared to equation (2.6), the airspeed terms are now time dependant in terms of both the present time, t, and the historical time, s, in the integral ($U^*(s)$ is hidden in $w^*_{3/4}(s)$ in the form of $U^*(s)\,\alpha\,(s)$). In other words, the circulatory lift at time, t, is a function of the instantaneous value of the airspeed and its history. Unsteady effects due to airspeed variations defined by $U^*(s)\,\alpha$ in the integral consider airspeed fluctuations at the time they occur on the airfoil.

An aspect that requires further discussion in the above model, and which is not immediately obvious, concerns the airspeed term in Wagner's function, which is assumed to be constant and set at the mean airspeed, U^*_m. In effect, this assumption defines the distance travelled by the vortices in the wake as a mean distance, $U^*_m\ t$, thus neglecting airspeed fluctuations in the trailing wake. In support of this assumption, an heritage from Greenberg's original theory, Friedmann argues that unsteady airloads are much more sensitive to the velocity of the wake vortices than their position. We are, however, more satisfied with the justifications offered by van der Wall and Leishman. They argue that for a combination of low frequency and small amplitude airspeed variations, the assumption is justified. This makes physical sense, considering that in these conditions, the distance covered by the shed vortices is determined, in large part, by the mean air flow speed.

In addition, van der Wall and Leishman offer more concrete and effective evidence to support this simplification, as well as providing comparative examples between different theories, some less exact than others. Their basis of comparison is Isaacs' theory[3] and results from a CFD Euler code. Comparison of circulatory lift values between these two models indicates no

---

3

Note that Isaacs considered only periodic fore-aft and pitch oscillations. Isaac's theory was extended by van der Wall [1991] to include heave motion as well, and can be considered exact in the sense that no simplification to a mean airspeed is made.

significant differences. They further show that circulatory lift values obtained with Greenberg's and Isaacs' theories compare very well for a harmonically oscillating flow and angle of attack, at low frequencies and amplitudes (for example, $k = 0.2$ and amplitude of flow oscillation/mean airspeed = 0.4). At higher amplitudes of airspeed oscillation differences appear between the two theories, but their behaviour remains qualitatively the same. This simplification is hence retained for this work, and is coherent with two other assumptions required for this thesis as well, namely chordwise flow uniformity, justified by an excitation spectrum concentrated in the low frequency range; and Taylor's hypothesis. These two assumptions will be discussed in detail later.

It is also relevant to note that fore-aft movement of an airfoil in an uniform stream is not physically the same as fluctuations of the free-stream velocity. This is schematized in Figure 2.5. In the first case, which is treated by Isaacs and Greenberg, the airflow is uniform along the chord, and airmass is displaced by the accelerating airfoil. On the other hand, which is the case investigated in this thesis[4], a chordwise velocity gradient exists for a varying free-stream, and similarly for vertical turbulence no airmass is displaced by the moving airfoil. Accordingly, the difference affects both the non-circulatory force and moment, as well as the bound vorticity of the circulatory terms. However, the free vortex sheet in the airfoil wake is the same in both cases.

For small reduced frequencies, van der Wall and Leishman argue that fore-aft movement aerodynamics is equivalent to the unsteady free-stream problem. Their argument is based on two facts. First, with regards to the circulatory loads, the flow velocity gradients along the chord are small for small reduced frequencies, hence a relatively chordwise uniform flow exists. Second, concerning the non-circulatory loads, as pointed out earlier [Fung, 1955; von Kármán and Sears, 1938], the apparent mass terms are significant mainly at high frequencies. The assumption of chordwise uniformity of the airflow is employed here, and is extended to the case of random fluctuations. This is supported by the longitudinal turbulence velocity spectrum being concentrated in the low frequency range.

---

[4] According to van der Wall and Leishman [1994], all theories, including Isaacs', published on the problem of a pulsating flow claim to handle unsteady free-stream, whereas strictly speaking, they should apply to the case of an airfoil moving fore and aft.

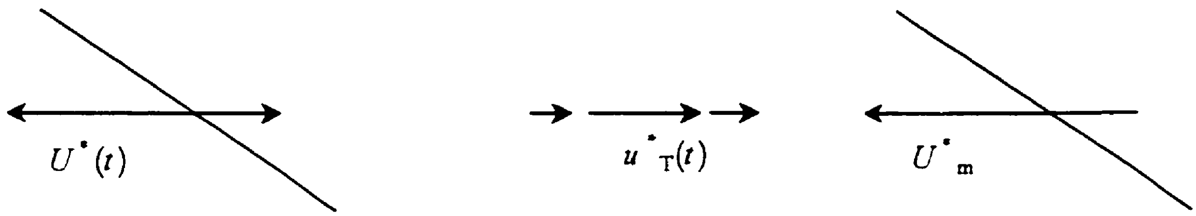

fore-aft airfoil movement unsteady free-stream

Figure 2.5 - Fore-aft airfoil movement versus unsteady free-stream aerodynamics.

Based on the above discussion, aerodynamic forces due to turbulent variations of the free-stream velocity, and accounting for arbitrary pitch and heave motions, are modelled by the following equations:

$$L_{\varphi} = \pi\rho b^2\left[\ddot{h} + U^*(t)\,\dot{\alpha} - b\,a_h\,\ddot{\alpha}\right] + 2\pi\rho b U^*(t)\left[w^*_{3/4}(t)\;\varphi(0) - \int_0^t w^*_{3/4}(s)\frac{d\varphi(t-s)}{ds}\,ds\right] \quad (2.16\text{ a})$$

$$\begin{aligned} M_{\mathrm{EA}\,\varphi} &= \pi\rho b^2\left[b\,a_h\,\ddot{h} - b\,[0.5 - a_h]\,U^*(t)\,\dot{\alpha} - b^2\,[a_h^2 + 1/8]\,\ddot{\alpha}\right] \\ &+ 2\pi\rho b^2\,[a_h + 0.5]\,U^*(t)\left[w^*_{3/4}(t)\;\varphi(0) - \int_0^t w^*_{3/4}(s)\frac{d\varphi(t-s)}{ds}\,ds\right] \end{aligned} \quad (2.16\text{ b})$$

where $$\varphi(t-s) = 1 - 0.165\,e^{-0.0455\,U^*_{\mathrm{m}}(t-s)/b} - 0.335\,e^{-0.3\,U^*_{\mathrm{m}}(t-s)/b} \quad (2.17)$$

and $$w^*_{3/4}(s) = \dot{h}(s) + U^*(s)\,\alpha(s) + b\,(0.5 - a_h)\,\dot{\alpha}(s) \quad (2.18)$$

The first terms in the lift and aerodynamic moment expressions represent the non-circulatory forces associated with the fluid inertia. Note that had we considered fore-aft movement, the additional apparent mass terms, $\pi\rho b^2\dot{U}^*\alpha$ and $-\pi\rho b^2\dot{U}^*\alpha b(\frac{1}{2}-a_h)$, would have appeared in the lift and moment expressions, respectively. The circulatory forces, given by the second terms, model the effects of the bound vorticity and the shed wake. These equations are the same as equations (2.6), (2.7) and (2.8) except that they have been integrated by parts, and more fundamentally, the airspeed is now allowed to vary in time.

To show more specifically the effect of the longitudinal excitation, the airspeed and downwash terms are expanded for the lift, which gives:

$$
\begin{aligned}
L_{\varphi} = {} & \pi \rho b^2 \left[\ddot{h} + [U^*_m + u^*_T(t)]\,\dot{\alpha} - b\, a_h\, \ddot{\alpha} \right] \\
& + 2\pi \rho b \left[[U^*_m + u^*_T(t)]\dot{h} + [U^{*2}_m + 2U^*_m u^*_T(t) + u^{*2}_T(t)]\,\alpha + b[0.5 - a_h][U^*_m + u^*_T(t)]\,\dot{\alpha} \right] \varphi(0) \qquad (2.19) \\
& - 2\pi \rho b [U^*_m + u^*_T(t)] \int_0^t \left[\dot{h} + [U^*_m + u^*_T(s)]\,\alpha + b[0.5 - a_h]\,\dot{\alpha} \right] \frac{d\varphi(t-s)}{ds}\, ds
\end{aligned}
$$

The history of the longitudinal turbulence is represented by the $u^*_T(s)$ term in the integral. By examining this equation, it is also relevant to realize that the airfoil is excited by longitudinal turbulence in more than one way. They are the $u^*_T(t)$, $u^{*2}_T(t)$ and $u^*_T(t)\ u^*_T(s)$ terms. The two nonlinear noise terms make the problem extremely difficult to resolve, if not unsolvable, analytically, but are easily handled numerically.

These expressions are very similar to the airloads developed by Bucher and Lin [1988] for the analysis of wind turbulence on bridges, with two notable exceptions. One difference is that the instantaneous airspeed, $U^*(t)$, outside the integral in equation (2.16) is taken inside their integral. This is done without justification. It can be attributed to the fact that they have introduced the airspeed fluctuations not at the source, but at the end of their derivation, essentially made under a constant airspeed assumption. This formulation is thus theoretically questionable. We have, however, in the course of this thesis run a few test cases with their model and found no important differences with ours, which indicates a certain robustness of the aerodynamic model. The second difference is that they neglected all quadratic noise terms, u^{*2}_T, in order to be able to obtain an analytical solution. An analytical solution, in the form of a stability analysis, is possible is this case given that their structural and aerodynamics models are linear.

Finally, combining the airloads due to arbitrary motion, the unsteady free-stream (longitudinal turbulence) and the vertical turbulence, the total lift and aerodynamic moment are:

$$L(t) = L_{\varphi}(t) + L_{\psi}(t) \tag{2.20 a}$$

$$M_{EA}(t) = M_{EA\varphi}(t) + M_{EA\psi}(t) \tag{2.20 b}$$

When these aerodynamic force and moment expressions are combined with the structural equations of motion, and realizing that $\theta = \alpha$, equation (2.1) becomes a set of integro-differential equations as shown in Section 2.5. The numerical integration of this system can be facilitated by transforming the integral terms into differentials with the addition of two new second-order differential equations, also shown in Section 2.5. Each additional second-order equation corresponds to two augmented states, given by z^*_1, $\dot{z}^*_1$, z^*_2 and $\dot{z}^*_2$, a consequence of the chosen two-state representation for Wagner's and Küssner's functions, respectively. This derivation is given in Appendix A. See also Edwards et al. [1979], Leishman [1994] and Friedmann [1987].

The aeroelastic system of equations becomes an 8th order random differential system which then can be expressed in state space form:

$$\{\dot{x}\} = [A(t)]\ \{x\} + [A_3]\ \{x^3\} + \{B(t)\} \tag{2.21}$$

The vector $\{x\}$ contains the four structural states and the four aerodynamic states, $\{x\} = \{\theta, h, \dot{\theta}, \dot{h}, z^*_1, \dot{z}^*_1, z^*_2, \dot{z}^*_2\}^T$. Note that the matrix $[A(t)]$ is time-varying, as it contains the longitudinal turbulence terms $u^*_T(t)$ and $u^{*2}_T(t)$. This is where the parametric excitation appears. The other matrix $[A_3]$, which defines the nonlinear structural terms, is time-invariant since the random excitation originates from the aerodynamics. Had we modelled nonlinear aerodynamic effects, this matrix would have also been time-varying. Finally, the vertical turbulence excitation appears as an external random forcing in $\{B(t)\}$. The vector $\{B\}$ and matrices $[A]$ and $[A_3]$ are developed in Appendix C in non-dimensional form.

2.4 Turbulence Model and Dynamics

In aeronautical applications, turbulence models can generally be categorized within two different approaches [Barnes, 1994]. The methods associated with a discrete gust representation are usually of a deterministic nature, such as Küssner's sharp-edged gust problem. On the other hand, continuous turbulence methods allow for a stochastic (random) treatment and perspective. Hybrid methods also exist, such as the statistical discrete gust. Each of these methods has particular advantages and disadvantages, depending on the specific requirements and nature of the problem. In the present analysis the interest lies in the effect of nonlinearities from a dynamical and theoretical perspective, as opposed to design load requirements. It thus requires a more refined model of turbulence, which is given by the random continuous approach. Nevertheless, the random treatment of turbulence still requires a number of simplifications which depend on the degree of realism one is looking for, balanced by the requirement to make the problem manageable and tractable. In the following paragraphs, the simplifications used in this work are described. Some of them are intimately linked to, and defined by, the aerodynamic model.

2.4.1 Taylor (and von Kármán)'s hypothesis, or the frozen gust assumption

This simplification has particular relevance to the analysis of moving objects, such as an airfoil, through a field of turbulent velocities. In general, turbulence is a function of both time and space. However, if a relatively large mean free-stream velocity, $\vec{V}_m$, is superimposed on the field of fluctuations, $\vec{V}_T = \{u^*_T(t), v^*_T(t), w^*_T(t)\}$, it is assumed that for a coordinate system attached to the mean free-stream velocity the temporal gradients of turbulent velocity fluctuations are small compared to the spatial gradients. Thus, temporal changes can be neglected, and turbulence is treated purely as a random field, ie $\vec{V}_T = \vec{V}_T\,(x_m, y_m, z_m)$. This is known as Taylor's hypothesis [Costello et al., 1992; Houbolt et al., 1964] or the frozen gust assumption [Dowell et al., 1978].

In this work we further assume that the airfoil is moving along the x, x_m axis with a constant velocity, which corresponds to the mean free-stream velocity, ie $\vec{V}_m = U^*_m\,\vec{\imath}$. Since temporal gradients are neglected for the reference frame fixed to the mean flow, a conversion from a spatial to a time system of coordinates is permitted through a Galilean transformation. In this sense the turbulence model is transformed from a random field to a random process, and is expressed as $\vec{V}_T = \vec{V}_T\,(x_m, y_m, z_m) = \vec{V}_T\,(x - U^*_m\,t, y, z)$ where x, y and z form the airfoil-fixed system of coordinates. Hence, at any point fixed on the airfoil, turbulence is considered as a function of time only. Note that (x, y, z) form an inertial reference frame since the fluctuations in airspeed do not originate from the airfoil but from turbulence.

2.4.2 Isotropy, homogeneity and stationarity

Another widespread simplification is to assume isotropy[5] of the turbulence field, which loosely means that its properties are independent of orientation at any point in space. The theory of isotropic stochastic continuous turbulence has been pioneered by Taylor and von Kármán [Houbolt et al., 1964; Fung, 1955]. Isotropy also implies homogeneity [Lin, 1961]. Homogeneity refers to invariance of statistical properties in space. Due to the spatial to temporal conversion discussed above, homogeneity of the random field is translated into a stationary random process, which refers to invariance of statistical properties in time. General correlation functions of turbulent velocities are hence dependant on time (or space) intervals, not on their absolute time (or location).

2.4.3 Dryden model

It is common to represent an isotropic turbulent field by its double velocity correlation matrix, where due to isotropy only the diagonal terms are non-zero [Lin, 1961; Costello et al., 1992]. In 3-D flow, the three diagonal terms represent the longitudinal and transverse (vertical and lateral) components of turbulence. From these correlation functions, power spectra can be developed as these two entities form Fourier transform pairs. In general, the spectral content of the turbulence is provided by either the von Kármán or Dryden models, which are presently the two most widely accepted models. The Dryden model is used in this work since it is easier to handle mathematically, while still retaining an appropriate degree of refinement. One important refinement is to allow a different modelling for the longitudinal and transverse components. Another refinement is that this model takes into account the non-white noise characteristic of the excitation. These factors are usually neglected in more "brute force" type analyses; see, for

---

5

Note that isotropy is a reasonable assumption for our problem since we are modelling free, as opposed to self-induced, turbulence. More specifically, self-induced turbulence is often associated with random fluctuations in the boundary layer where the flow is non-isotropic [White, 1974].

example, Prussing and Lin [1983], and Heo and Ibrahim [Heo, 1985; Ibrahim and Heo, 1987].

In terms of the temporal radian frequency, the one-sided PSD Dryden longitudinal and vertical turbulent velocity representations are given, respectively, as [Fung, 1955; Hoblit, 1988]:

$$\Phi_{LT}(\omega) = \sigma_T^{*2} \left(\frac{2L^*}{\pi U^*_m} \right) \frac{1}{1 + [L^* \omega / U^*_m]^2} \tag{2.22 a}$$

$$\Phi_{VT}(\omega) = \sigma_T^{*2} \left(\frac{L^*}{\pi U^*_m} \right) \frac{1 + 3\,[L^* \omega / U^*_m]^2}{[1 + [L^* \omega / U^*_m]^2]^2} \tag{2.22 b}$$

They are shown, in non-dimensional form, in Figure 2.6 for the range of scale of turbulence considered in this work. A first observation is that, depending on the value of L, but for the same variance, the shape and relative magnitude of the two excitations at any given frequency vary significantly. Another observation is that at low frequencies, the power spectral density of the longitudinal excitation is roughly twice as large as for the vertical excitation.

It can be shown [Houbolt et al., 1964] that the scale of turbulence, L^*, divided by the mean free-stream velocity, U^*_m, is equal to the correlation time of the longitudinal random excitation, whereas the correlation time of the vertical random excitation is half that ratio, that is ½ L^*/U^*_m. Hence, the scale of turbulence determines the spectral content of the excitation. We see from Figure 2.6 that the lower the scale of turbulence, the closer we are to the white noise idealisation.

In practice, the excitation is considered to be "white" if the system time scales are much larger than the noise correlation time, or similarly if the excitation spectrum remains relatively flat (constant) for a frequency range which encompasses the natural frequencies of the airfoil. As mentioned earlier, the white noise idealisation has been used for the most part in the analytical treatment of systems in longitudinal turbulence; rotor blades for example [Prussing and Lin, 1983]. This is mainly because it simplifies significantly the analysis, and enables closed-form solutions to be obtained (if allowed by other factors such low dimensionality and/or linearity of the problem both for the system and excitation). On the other hand, a larger value of scale of turbulence dictates the excitation to be distributed in the lower frequencies, which for aeronautical applications is often more realistic, as discussed by Hoblit [1988] for example.

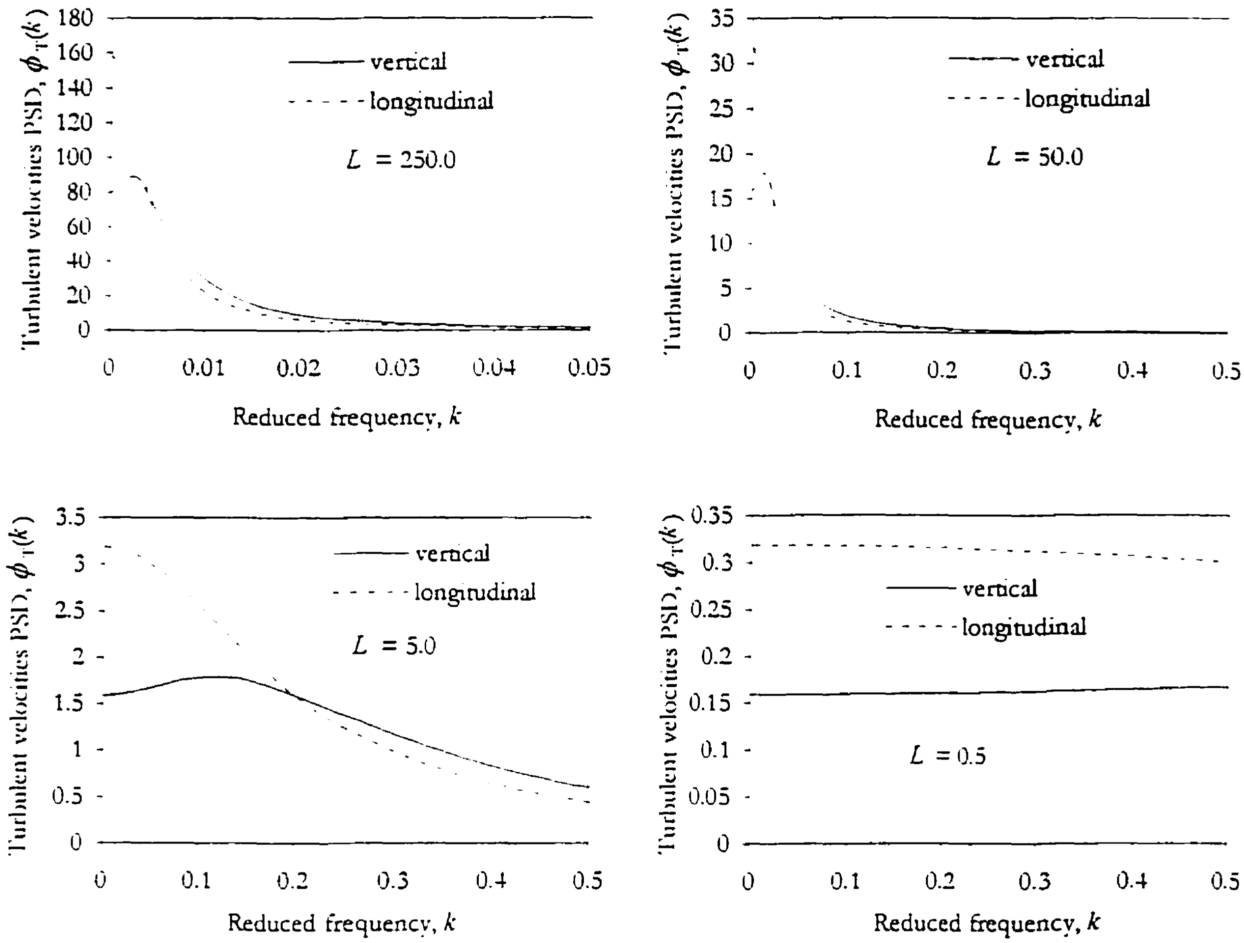

Figure 2.6 - Closed-form solution of the non-dimensional Dryden turbulence PSD for different values of scale of turbulence, L; $\sigma_T^2 = 1$.

Since the problem will be solved in the time domain, the turbulent velocity PSDs must be transformed accordingly. This is done essentially by finding an appropriate transfer function which relates a white noise process acting as an input to the Dryden turbulent velocity as the output. In addition, to satisfy the Gaussian nature of turbulence, the input white noise must also be a Gaussian distribution. The derivation is given in Appendix B, and the final expressions are shown at Section 2.5.

2.4.4 Chordwise uniformity

In the context of this work, a physical interpretation of the scale of turbulence is the "average" distance travelled by the airfoil during which the turbulent velocities can be considered as being uniform. Thus, the larger the scale of turbulence, the further, in average, the airfoil travels before experiencing a change in turbulence velocities. In this light, it may be assumed that for relatively large magnitudes of scale of turbulence the velocity over the airfoil is nearly uniform at any instant in time. Accordingly, the assumption of uniform velocity, notably chordwise, enables the circulatory aerodynamic model developed for fore-aft motion of the airfoil to be applied to the unsteady free-stream problem as discussed in Section 2.3.

Note that chordwise uniformity with regards to vertical turbulence requires a scale of turbulence twice as large as that for longitudinal turbulence, as discussed above in terms of noise correlation time. However, in fact this is not required. Variations of vertical velocities along the chord can be easily handled by Küssner's function. Spanwise uniformity is implicitly assumed due to the 2-D nature of the problem. Changes along the vertical axis are also neglected, since the amplitude of the vertical motion is considered relatively small.

2.4.5 Gaussian distribution

The final major assumption is the Gaussian distribution of the fluctuations. This is a commonly used assumption [Hoblit, 1988], supported by various experimental data [Lin, 1961]. In principle, this distribution allows extremely large deviations from the mean, but with very small probability. In other words, the larger the instantaneous value of $u^{*}_{T}(t)$ for example, the less often this particular value will appear. One significant consequence of the appearance of large deviations in the fluctuation velocities is flow reversal, for which the aerodynamic model breaks down.

In our problem, the likelihood that flow reversal occurs depends on both the mean airspeed, about which the fluctuations occur, and the variance (or its standard deviation) of $u^{*}_{T}(t)$. This is exemplified in Figure 2.7. Take the case of a mean airspeed, $U^{*}_{m} = 4$, for example. For the given turbulence variance, $\sigma^{*2}_{T} = 1$, and mean zero, flow reversal occurs for all values of the longitudinal turbulent velocity smaller than -4 (i.e. $u^{\bullet}_{T} < -4$), thus with a probability $P(u^{\bullet}_{T} < -4) = 0.00003$. If $U^{\bullet}_{m} = 3$, the probability of flow reversal is: $P(u^{\bullet}_{T} < -3) = 0.00135$. The probability of flow reversal is 0.0228 and 0.1587 for $U^{\bullet}_{m} = 2$ and 1, respectively. These probabilities are given by the area under the curve of the Gaussian probability density function as shown below for $P(u^{\bullet}_{T} < -1)$.

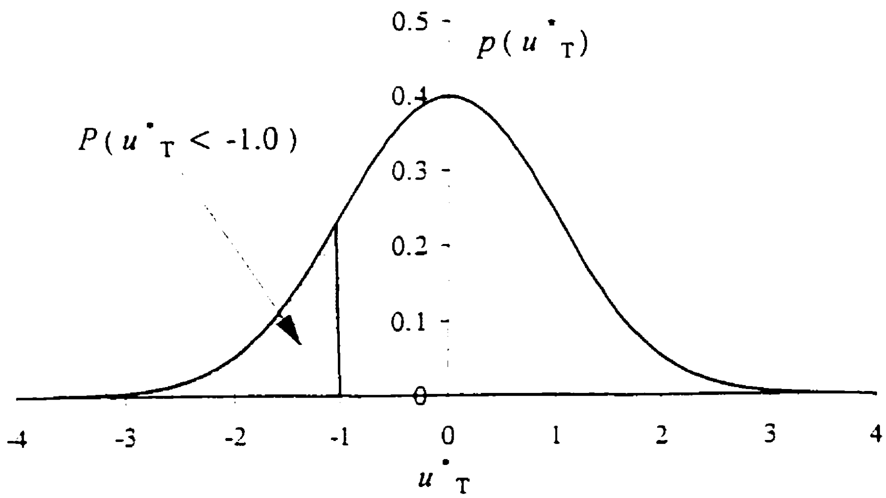

Figure 2.7 - Gaussian probability density representing $u^{\bullet}_{T}(t)$ for $\sigma^{\bullet 2}_{T} = 1$.

Thus, for mean airspeeds greater than 3, the probability of flow reversal is so low (< 0.1%) that it is a non-issue. At this particular value of turbulence variance, flow reversal starts to become an issue for airspeeds lower than 2, i.e. P(flow reversal) > 2%, but remains a secondary factor until the mean airspeed is much lower. For values of turbulence variance lower than 1, flow reversal starts to become important at even lower airspeed. Note that for the case of the quadratic noise term, $u^{\bullet 2}_{T}(t)$, its probability density function exists only for $u^{\bullet 2}_{T}(t) > 0$.

2.5 Aeroelastic-Turbulence System Equations of Motion

2.5.1 Integro-differential formulation - Dimensional form

The following equations represent the integro-differential formulation of aeroelastic-turbulence system in dimensional form. Equations (2.23 a) and (2.23 b) are the pitch and heave equations of motion, respectively. They are the combination of equations (2.1), (2.14) and (2.16).

$$I_{EA}\ddot{\theta}+m\,x_\theta b\ddot{h}+D_\theta\dot{\theta}+K_\theta\,\theta+K_3\,\theta^3=\pi\rho b^2\left[b\,a_h\ddot{h}-b(0.5-a_h)U^*\dot{\alpha}-b^2(a_h^2+1/8)\ddot{\alpha}\right]$$
$$+2\,\pi\rho b^2(a_h+0.5)U^*\left[w^*_{3/4}\,\varphi(0)-\int_0^t w^*_{3/4}(s)\frac{d\varphi(t-s)}{ds}ds\right] \quad (2.23\text{ a})$$
$$+2\,\pi\rho b^2(a_h+0.5)U^*_{\mathrm{m}}\left[w^*_{\mathrm{T}}\,\psi(0)-\int_0^t w^*_{\mathrm{T}}(s)\frac{\mathrm{d}\,\psi(t-s)}{ds}ds\right]$$

$$m\ddot{h}+m\,x_\theta b\,\ddot{\theta}+D_h\,\dot{h}+K_h\,h=-\,\pi\rho b^2\left[\ddot{h}+U^*\dot{\alpha}-b\,a_h\ddot{\alpha}\right]$$
$$-2\,\pi\rho\,\mathrm{b}U^*\left[w^*_{3/4}\,\varphi(0)-\int_0^t w^*_{3/4}(s)\frac{d\,\varphi(t-s)}{ds}ds\right] \quad (2.23\text{ b})$$
$$-2\,\pi\rho\,b\,U^*_{\mathrm{m}}\left[w^*_{\mathrm{T}}\,\psi(0)-\int_0^t w^*_{\mathrm{T}}(s)\frac{d\,\psi(t-s)}{ds}ds\right]$$

where $\varphi(t-s)=1-\ 0.165\mathrm{e}^{-0.0455\,U^*_{\mathrm{m}}(t-s)/b}-\ 0.335\mathrm{e}^{-0.3U^*_{\mathrm{m}}(t-s)/b}$

and $\psi(t-s)=1-\ 0.5792\ \mathrm{e}^{-0.1393\ U^*_{\mathrm{m}}(t-s)/b}-\ 0.4208\ \mathrm{e}^{-1.802\ U^*_{\mathrm{m}}(t-s)/b}$

Equations (2.24 a) and (2.24 b), derived in Appendix B, are the time domain equations of motion for the longitudinal and vertical turbulent velocities, respectively. G^*_{wn} represents a Gaussian distributed white noise with a power spectral density, $\Phi_{\mathrm{wn}}=1$.

$$\dot{u}^*_{\mathrm{T}}+u^*_{\mathrm{T}}\frac{U^*_{\mathrm{m}}}{L^*}=\sigma^*_{\mathrm{T}}\left(\frac{2U^*_{\mathrm{m}}}{\pi L^*}\right)^{1/2}G^*_{\mathrm{wn}} \quad (2.24\text{ a})$$

$$\dot{w}^*_{\mathrm{T}}+w^*_{\mathrm{T}}\frac{2U^*_{\mathrm{m}}}{L^*}=-\frac{U^{*2}_{\mathrm{m}}}{L^{*2}}\int_0^t w^*_{\mathrm{T}}\,dt+\sigma^*_{\mathrm{T}}\left(\frac{U^{*3}_{\mathrm{m}}}{\pi L^{*3}}\right)^{1/2}\int_0^t G^*_{\mathrm{wn}}\,dt+\sigma^*_{\mathrm{T}}\left(\frac{3U^*_{\mathrm{m}}}{\pi L^*}\right)^{1/2}G^*_{\mathrm{wn}} \quad (2.24\text{ b})$$

2.5.2 Differential formulation - Dimensional form

Transforming the pitch and heave integro-differential equations (2.23) into pure differential equations by introducing four aerodynamic states gives the following equations. The detail of the transformation is presented in Appendix A.

$$
\begin{aligned}
I_{EA}\ddot{\theta}+m x_\theta b\ddot{h}+D_\theta\dot{\theta}+K_\theta\theta+K_3\theta^3 = {} & \pi\rho b^2\left[b\, a_h \ddot{h}-b(0.5-a_h)U^*\dot{\alpha}-b^2(a_h^2+1/8)\ddot{\alpha}\right] \\
& +2\pi\rho b^2(a_h+0.5)U^*\left[w^*_{3/4}\,\phi(0)+z^*_1\bar{b}_1\bar{b}_2(A_1+A_2)+\dot{z}^*_1(A_1\bar{b}_1+A_2\bar{b}_2)\right] \\
& +2\pi\rho b^2(a_h+0.5)U^*_m\left[w^*_T\,\psi(0)+z^*_2\bar{b}_3\bar{b}_4(A_3+A_4)+\dot{z}^*_2(A_3\bar{b}_3+A_4\bar{b}_4)\right]
\end{aligned}
\tag{2.25 a}
$$

$$
\begin{aligned}
m\ddot{h}+m x_\theta b\ddot{\theta}+D_h\dot{h}+K_h h = {} & -\pi\rho b^2\left[\ddot{h}+U^*\dot{\alpha}-b\, a_h\ddot{\alpha}\right] \\
& -2\pi\rho b U^*\left[w^*_{3/4}\,\phi(0)+z^*_1\bar{b}_1\bar{b}_2(A_1+A_2)+\dot{z}^*_1(A_1\bar{b}_1+A_2\bar{b}_2)\right] \\
& -2\pi\rho b U^*_m\left[w^*_T\,\psi(0)+z^*_2\bar{b}_3\bar{b}_4(A_3+A_4)+\dot{z}^*_2(A_3\bar{b}_3+A_4\bar{b}_4)\right]
\end{aligned}
\tag{2.25 b}
$$

$$\ddot{z}^*_1+\dot{z}^*_1(\bar{b}_1+\bar{b}_2)+z^*_1\bar{b}_1\bar{b}_2 = w^*_{3/4} = \dot{h}+U^*\alpha+b(0.5-a_h)\dot{\alpha} \tag{2.26 a}$$

$$\ddot{z}^*_2+\dot{z}^*_2(\bar{b}_3+\bar{b}_4)+z_2\bar{b}_3\bar{b}_4 = w^*_T \tag{2.26 b}$$

$z^*_1, \dot{z}^*_1$ and $z^*_2, \dot{z}^*_2$ in equations (2.26 a) and (2.26 b) represent the four aerodynamic states due to the lag terms in Wagner's and Küssner's functions respectively. A_1, A_2, $\bar{b}_1$ (multiplied by b/U^*_m) and $\bar{b}_2$ (multiplied by b/U^*_m) are the coefficients in Wagner's function; Similarly, A_3, A_4, $\bar{b}_3$ (multiplied by b/U^*_m) and $\bar{b}_4$ (multiplied by b/U^*_m) are the coefficients in Küssner's function:

$A_1 = 0.165$ $\quad A_2 = 0.335$ $\quad \bar{b}_1 = b_1\, U^*_m/b = 0.0455\, U^*_m/b$ $\quad \bar{b}_2 = b_2\, U^*_m/b = 0.3\, U^*_m/b$

$A_3 = 0.5792$ $\quad A_4 = 0.4208$ $\quad \bar{b}_3 = b_3\, U^*_m/b = 0.1393\, U^*_m/b$ $\quad \bar{b}_4 = b_4\, U^*_m/b = 1.802\, U^*_m/b$

2.5.3 Matrix differential formulation - Non-dimensional form

In order to get a better physical insight into equations (2.25) and (2.26), they are expressed in matrix form, as a standard mechanical engineering problem. Also, the following non-dimensional parameters are introduced:

Heave displacement:	$\xi = h/b$
Airfoil/air mass ratio:	$\mu = m/\rho\pi b^2$
Radius of gyration (squared):	$r_\theta^2 = I_{EA}/mb^2$
Frequency ratio:	$\bar{\omega} = \omega_h/\omega_\theta$
Damping ratio in heave:	$\zeta_h = D_h/2(mK_h)^{1/2}$
Damping ratio in pitch:	$\zeta_\theta = D_\theta/2(I_{EA}K_\theta)^{1/2}$
Cubic nonlinear torsional spring coefficient:	$k_3 = K_3/K_\theta$
Scale of turbulence:	$L = L^*/b$
Variance of turbulence:	$\sigma_T^2 = \sigma^{*}{}_T^2 / b^2\omega_\theta^2$
Airspeed and velocity fluctuations:	$U_m = U^*_m/b\omega_\theta$, $u_T = u^*_T/b\omega_\theta$,
	$w_T = w^*_T/b\omega_\theta$
Time:	$\tau = U^*_m\, t/b$
Aerodynamic states (lag terms):	$z_i = z^*_i\, b^2/U^*_m$, $i = 1,2$

The first matrix is the mass matrix, $[M]$, and is time-invariant. The second matrix is the damping matrix, $[D(\tau)]$, which is time-varying due to the random airspeed fluctuations (i.e. longitudinal turbulence). Similarly with the third matrix, $[K(\tau)]$, representing the linear stiffness. The fourth matrix is the nonlinear stiffness matrix, $[K_3]$, originating from the structure of the airfoil. It is time-invariant because the turbulence acts directly on the aerodynamics, modelled as linear. The vector on the right of the equation represents the vertical turbulence, acting as a random external forcing. Accordingly, in condensed form, we have:

$$[M]\{x''\} + [D(\tau)]\{x'\} + [K(\tau)]\{x\} + [K_3]\{x^3\} = \{0, 0, 0, w_T(\tau)/U_m\}^T \qquad (2.27)$$

where $\{x\} = \{\theta, \xi, z_1, z_2\}^T$

In developed form, equation (2.27) becomes:

$$\begin{bmatrix} 1+\dfrac{a_h^2+1/8}{\mu r_\theta^2} & \dfrac{x_\theta}{r_\theta^2}-\dfrac{a_h}{\mu r_\theta^2} & 0 & 0 \\ x_\theta-\dfrac{a_h}{\mu} & 1+\dfrac{1}{\mu} & 0 & 0 \\ 0 & 0 & 1 & 0 \\ 0 & 0 & 0 & 1 \end{bmatrix} \begin{Bmatrix} \theta'' \\ \xi'' \\ z_1'' \\ z_2'' \end{Bmatrix} +$$

$$\begin{bmatrix} \dfrac{2\zeta_\theta}{U_m}+\dfrac{\mathrm{unf}(1/2-a_h)}{\mu r_\theta^2}-\dfrac{2(a_h+1/2)(1/2-a_h)\mathrm{unf}\,\varphi(0)}{\mu r_\theta^2} & -\dfrac{2(a_h+1/2)\mathrm{unf}\,\varphi(0)}{\mu r_\theta^2} & -\dfrac{2(a_h+1/2)(A_1b_1+A_2b_2)\mathrm{unf}}{\mu r_\theta^2} & -\dfrac{2(a_h+1/2)(A_3b_3+A_4b_4)}{\mu r_\theta^2} \\ \dfrac{\mathrm{unf}}{\mu}+\dfrac{2(1/2-a_h)\mathrm{unf}\,\varphi(0)}{\mu} & \dfrac{2\zeta_h\varpi}{U_m}+\dfrac{2\mathrm{unf}\,\varphi(0)}{\mu} & \dfrac{2(A_1b_1+A_2b_2)\mathrm{unf}}{\mu} & \dfrac{2(A_3b_3+A_4b_4)}{\mu} \\ -(1/2-a_h) & -1 & b_1+b_2 & 0 \\ 0 & 0 & 0 & b_3+b_4 \end{bmatrix} \begin{Bmatrix} \theta' \\ \xi' \\ z_1' \\ z_2' \end{Bmatrix} +$$

$$\begin{bmatrix} \dfrac{1}{U_m^2}-\dfrac{2(a_h+1/2)\mathrm{unsf}\;\;\varphi(0)}{\mu r_\theta^2} & 0 & -\dfrac{(a_h+1/2)\;b_1b_2\,\mathrm{unf}}{\mu r_\theta^2} & -\dfrac{2(a_h+1/2)\;b_3b_4}{\mu r_\theta^2} \\ \dfrac{2\mathrm{unsf}\;\;\varphi(0)}{\mu} & \dfrac{\varpi^2}{U_m^2} & \dfrac{b_1b_2\,\mathrm{unf}}{\mu} & \dfrac{2b_3b_4}{\mu} \\ -\;\mathrm{unf} & 0 & b_1b_2 & 0 \\ 0 & 0 & 0 & b_3b_4 \end{bmatrix} \begin{Bmatrix} \theta \\ \xi \\ z_1 \\ z_2 \end{Bmatrix} + \begin{bmatrix} \dfrac{k_3}{U_m^2} & 0 & 0 & 0 \\ 0 & 0 & 0 & 0 \\ 0 & 0 & 0 & 0 \\ 0 & 0 & 0 & 0 \end{bmatrix} \begin{Bmatrix} \theta^3 \\ \xi^3 \\ z_1^3 \\ z_2^3 \end{Bmatrix} = \begin{Bmatrix} 0 \\ 0 \\ 0 \\ \dfrac{w_T}{U_m} \end{Bmatrix} \qquad (2.28)$$

where $\quad \text{unf} = U(\tau)/U_m = 1 + u_T(\tau)/\ U_m$

and $\quad \text{unsf} = (U(\tau)/U_m)^2 = (1 + u_T(\tau)/U_m)^2 = 1 + 2u_T(\tau)/U_m + (u_T(\tau)/U_m)^2$

Also given is the non-dimensional form of the time domain turbulent velocity equations, equation (2.24). The longitudinal and vertical turbulent velocities are, respectively:

$$u_T' + u_T \frac{1}{L} = \sigma_T \left(\frac{2}{\pi L}\right)^{1/2} G_{wn}(\tau) \tag{2.29 a}$$

$$w_T' + w_T \frac{2}{L} = -\frac{1}{L^2}\int_0^{\tau} w_T \, d\tau + \sigma_T \left(\frac{1}{\pi L^3}\right)^{1/2} \int_0^{\tau} G_{wn}(\tau)\, d\tau + \sigma_T \left(\frac{3}{\pi L}\right)^{1/2} G_{wn}(\tau) \tag{2.29 b}$$

Chapter 3

MODEL SIMULATION AND ANALYSIS METHODOLOGY

This chapter is divided into two parts. In the first part, we are concerned with the numerical solution of the equations of motion, derived in Chapter 2, which generate the airfoil dynamics in terms of time series. In the second part, we deal with the transformation of these time series into functionals, such as probability density function (PDF) or power spectral density (PSD). In the context of nonlinearity and randomness these two aspects are not trivial and warrant proper attention.

No general analytical solution techniques exist for nonlinear random differential equations, particularly when the parameters are also randomly changing. There are, however, some cases where analytical solutions can be obtained. These solutions are usually expressed directly in terms of PDF, moments or stability boundaries for example. Nevertheless, their use is very limited since they are governed by a number of restrictions and simplifying assumptions. Some simplifications are, for example, small noise intensity, white noise or Gaussian response. Perhaps, the greatest restriction in the context of our problem is the requirement for a low dimensional system. From this point of view, our system, which has four structural states and four aerodynamic states, can be considered to be high dimensional.

The use of numerical integration techniques is more versatile, and has been applied successfully to a number of nonlinear random problems. Comparisons between numerical and analogue simulations, and with analytical solutions where available, are discussed in detail by Mannella [1989], Fronzoni [1989] and McClintock and Moss [1989], for example. Furthermore, according to Mannella, numerical simulation should be thought of as a theoretical tool and a natural complement of the system modelling for stochastic dynamical systems. His position is justified considering the great number of limitations imposed on currently available analytical techniques, as well as the practical difficulties in conducting experiments.

3.1 Numerical Time Domain Simulation

3.1.1 Runge-Kutta algorithm

The primary solution method for this analysis is based on the commonly used fourth-order Runge-Kutta integration scheme. The equations of motion (equations 2.27) must first be cast into a system of first-order differential equations, as given by the next equation (in non-dimensional form), and where the vector $\{B(\tau)\}$, and matrices $[A(\tau)]$ and $[A_3]$, are given in Appendix C:

$$\{x'\} = \{f(x, \tau)\} + \{B(\tau)\} = [A(\tau)]\ \{x\} + [A_3]\ \{x^3\} + \{B(\tau)\} \tag{3.1}$$

where $$\{x\} = \{\theta, \xi, \theta', \xi', z_1, z_1', z_2, z_2'\}^T. \tag{3.2}$$

The integration is then performed with the following time discretization:

$$\{x(\tau+\Delta\tau)\} = \{x(\tau)\} + (\{k1\} + 2\{k2\} + 2\{k3\} + \{k4\})\Delta\tau/6 + \Delta\tau\{B(\tau)\} \tag{3.3}$$

where $$\{k1\} = \{f(\mathrm{x}, \tau)\} \tag{3.4 a}$$

$$\{k2\} = \{f(\mathrm{x} + k1\Delta\tau/2,\ \tau + \Delta\tau/2)\} \tag{3.4 b}$$

$$\{k3\} = \{f(\mathrm{x} + k2\Delta\tau/2,\ \tau + \Delta\tau/2)\} \tag{3.4 c}$$

$$\{k4\} = \{f(\mathrm{x} + k3\Delta\tau,\ \tau + \Delta\tau)\} \tag{3.4 d}$$

The same procedure is followed at each time step for the two turbulent velocity equations (equation 2.29). These two differential equations act effectively as filters for the white noise before it enters the aeroelastic system. By raising the correlation time of the excitations, away from white noise, the turbulence sample path is smoothened. Note that the integrals in the vertical turbulent velocity differential equation (equation 2.29 (b)) are performed using a simple trapezoidal rule. To minimize round-off errors, all simulations were performed in double-precision. The algorithm for the full simulation is given in appendix D.

3.1.1.1 Time step

Because the Runge-Kutta method is explicit the time step of the integration is, in part, governed by numerical stability considerations. For an oscillator type system, the classical minimum requirement is to insure that the time step meets the following [for example, D'Souza, 1984]:

$$\Delta\tau \leq 2/k_{max} = T_{min}/\pi \tag{3.5}$$

k_{max} represents the highest undamped frequency of the linear system, or the highest aeroelastic modal frequency for a coupled aeroelatic system. In corollary, T_{min} is the shortest period.

In the more general case where nonlinearities and parametric excitation are considered, and for non-oscillator type systems such as the turbulent velocity differential equations, the concept of k_{max}, or T_{min}, must be generalized to the notion of system time scale (symbolized by T). For example in the nonlinear case, the period of the limit cycle oscillation (LCO) is a new time scale. It is generally of the same order of magnitude as one of the linear system natural periods. The parametric excitation introduces a new time scale as well which is represented by the noise correlation time. It is equivalent to the scale of turbulence in its non-dimensional representation[1]. The scale of turbulence is also generally of the same order of magnitude as the system time scales except in the limit of white noise, where it becomes relatively very small. We must also consider

1

As discussed in Chapter 2, the noise correlation time of the longitudinal turbulence, t_{cor}, is equal to the scale of turbulence divided by the mean airspeed: $t_{cor} = L^*/U^*_m$. When the non-dimensional parameters are introduced, the relation becomes: $\tau_{cor} = L$.

the noise correlation time of the vertical excitation, specifically in terms of the numerical integration of its differential equation. It is half the correlation time of the longitudinal component. According to Mannella [1989], the general stability requirement becomes:

$$\Delta\tau \ll T_{min} \tag{3.6}$$

where T_{min} represents the shortest time scale of the system.

The other requirement that the time step must meet is the accuracy of the response. A small time step insuring numerical stability does not guarantee an accurate response and may lead to important truncation errors if it is too large. For example, we have found that using a too large, but stable, time step would result in a skewed PDF of the turbulent velocities compared to the exact zero mean Gaussian shape. Accordingly, we have limited the maximum value of the time step to $1/25^{th}$ the noise correlation time of vertical turbulence, which is equal to $1/50^{th}$ the scale of turbulence. For example, we have the following conditions for L = 0.5 and 50.0:

$$\Delta\tau \le 0.01 \quad \text{for } L = 0.5 \tag{3.7 a}$$

$$\Delta\tau \le 1.0 \quad \text{for } L = 50.0 \tag{3.7 b}$$

The stability and accuracy requirements must be balanced with the need for efficiency. In our case, efficiency is dictated by the statistical and probabilistic nature of the problem, which requires a very large sample time. We have found that smoothness of the probability density distribution and convergence of the mean-square were more a function of the physical sample time, $T = N\,\Delta\tau$, rather than the number of iterations, N. For a given problem, steady state in PDF and in mean-square are reached at a smaller number of iterations for a simulation with a larger time step, compared with a smaller $\Delta\tau$. Accordingly, a simulation with a larger time step requires less iterations. This is meaningful considering that a typical run, for one set of parameter conditions, requires $N \sim 20 \times 10^6$ to 50×10^6 iterations to obtain a smooth PDF. On a 233 MHz Pentium II, with 128 Meg of RAM, it means between 6 and 15 hours real time.

For the nonlinear aeroelastic system, it has been found that numerical stability is not a concern. The choice of a time step is primarily dictated by accuracy balanced by efficiency requirements. We have taken the time step to be $1/128^{th}$ the smallest natural uncoupled period of the system. For the lower values of scale of turbulence, generally $L \leq 5.0$, the limiting criterion has been the noise correlation time, since we have used the same time step to integrate both the equations of motion of the aeroelastic system and the turbulent velocities.

On the other hand, the linear system is much more sensitive to the choice of the time step due to the parametric excitation. Furthermore, we have noted an enhanced sensitivity for large scales of turbulence and for airspeeds close to the flutter speed. We have adjusted the time step accordingly to smaller values than permitted by the nonlinear problem. Note that this problem does not occur for the linear system without longitudinal turbulence, and we repeat, nor for the nonlinear system in combined excitation.

3.1.2 Houbolt's method

The second integration method we used, essentially for validation purposes, is Houbolt's method which is an implicit scheme based on backward differences at three previous times. It was developed by Houbolt [1950] to determine the aeroelastic transient response of aircraft to (vertical) gusts. As applied to a two-dimensional nonlinear airfoil, the method is described in detail by Lee and Leblanc [1986] or Alighanbari [1995]. Note that in general, the method needs a special starting procedure since the integration requires values at three previous times. However, because we are dealing with a random process, we have chosen not to be specifically concerned by the actual sample path of the motion but by averages or functionals of its time history. This approach will be further discussed later. Consequently, for our analysis the initial conditions are not a concern. Note, as well, that this method has been applied only to the integration of the aeroelastic equations of motion, not to the turbulent velocities which we have integrated using the R-K method. The algorithm for our system is given in Appendix E.

Houbolt's method is generally considered to be more stable than the R-K method. This is so since it is an implicit scheme whereas the Runge-Kutta integration is explicit. For a linear system with constant coefficients, it is unconditionally stable, as demonstrated by Jones and Lee [1985] for example. However, it has been shown it could be unstable for some nonlinear systems, while the R-K method was stable for the same time step [D'Souza, 1984]. Since our system is nonlinear, the time step for this procedure must also consider potential numerical stability problems.

As for the R-K, the other consideration is the accuracy of the result. For a 1DOF linear system excited by simple harmonic forcing, Jones and Lee [1985] have compared the transient and steady state behaviour of numerical results from Houbolt's scheme with the exact analytical solution. They determined that the high frequency transient behaviour was accurately modelled for a time step smaller than $1/256^{th}$ the natural period of the system. An accurate steady state response required a less stringent 128 time steps per cycle. For a nonlinear aeroelastic system, Alighanbari [1995] showed that the time histories presented no differences when obtained with 256 or 512 steps/cycle, whereas the solution based on 64 steps/cycle exhibited a slight phase shift. For this thesis, since the purpose of using Houbolt's scheme is to establish a validation basis for the R-K method, the time step has been chosen to match the R-K integration which is 128 steps/cycle for most cases.

3.1.3 Gaussian distributed white random noise

We have produced Gaussian distributed white random noise according to the method used in the physics literature. This is a three-step process starting with the generation of uniformly distributed random numbers. These uniform deviates are then transformed into Gaussian numbers and cast into a time dependant form, resulting in a white noise process.

3.1.3.1 Random number generator

Throughout this research, we have been forced to change computers at a number of occasions. This has been beneficial in the sense that we have had to use different types of random number generator, thus indirectly validating our results since they proved to be independent of the origin of the pseudo-random numbers.

One generator used is taken from an International Mathematical and Statistical Library subroutine [IMSL, 1987]. It generates uniformly distributed pseudo-random numbers on the interval (0,1] based on a multiplicative congruential generator internally programmed in machine language. It produces the sequence of non-negative integers:

$$a_i = C\, a_{i-1} \bmod (M), \quad i = 1, 2, 3, \ldots \tag{3.8}$$

The sequence is initiated with a seed, a_0, chosen between 1 and the maximum value which can be generated by the generator. The maximum value of the sequence is called the period of the generator, and is determined by the combination of the modulus, M, and multiplier, C. An appropriate choice of M and C will give a maximum period equal to the modulus (also modulo[2]), thus providing a uniform distribution within the interval [1, M]. The distribution is then normalized by dividing each generated number by the modulus:

$$u_i = a_i \,/\, M, \quad i = 1, 2, 3, \ldots \tag{3.9}$$

The bigger the modulus the denser the points are in the unit interval (0, 1]; in the limit the distribution becomes continuous. Other desirable properties of this method are related to the independence between numbers and also between sequences of number. These have been shown to be potentially a problem for the congruential generator if the multiplier-modulus combination is not chosen carefully [Fishman and Moore, 1986]. In their paper, Fishman and Moore provide a detailed analysis of different multipliers used in conjunction with the multiplicative congruential generator of modulus $2^{31} - 1$. A battery of statistical tests is applied to different sequences of pseudo-random numbers, and the best multipliers are determined. For our research, M is taken as $2^{31} - 1$, and C is chosen as 950706376 which is considered the "best" multiplier according to Fishman and Moore [1986]. This multiplier also ensures a period equal to the modulus, that is ~ 2×10^9.

The same multiplier-modulus combination will always give the same sequence for similar seeds. Thus, this is obviously a deterministic process, and it is the reason why the numbers are described as pseudo-random as opposed to being truly random. The fact that the sequence of

---

[2] For the reader who is not familiar with the modulo, it generates the residue of the ratio of two integers. For example take $a = 5 \bmod 3$, the residue of $5/3$ is $a = 2$ (i.e. $5/3 = 1 + 2/3$).

numbers originates from a deterministic process is in itself not relevant. It can be argued that randomness is a way to account for variations which cannot be controlled or which we do not choose to control. In this light randomness may not have any physical basis, but this is a philosophical question. What matters is that the sequence of numbers possesses some basic statistical properties, and that the solution of the problem is independent of the origin of these random numbers.

We examined the "randomness" of the pseudo-random number sequence to ensure independence of the results with respect to the generator. For the same modulus, a multiplier of 16807 was tested in comparison with the "best" multiplier. No significant differences were noted. In addition, a shuffled version of the pseudo-random number sequence was also tested, and again no difference in the system dynamics was noticed.

The other random number generator we have used comes from Press et al. [1996], who propose several different types of random number generator. They all have the nice feature of being portable, since they are programmed in Fortran and are machine independent. We have chosen the routine RAN1 which offers a good compromise between validity and execution time. RAN1 is based on the same principle as the IMSL generator with a multiplier C = 16807 and modulus $M = 2^{31} - 1$. The output of the multiplicative congruential generator is then shuffled. The period is in the order of 10^8. According to Press et al., RAN1 passes all statistical tests, where other simpler generators fail[3]. Most results shown in this thesis are based on RAN1. Some typical results have been compared with the IMSL based routine; no differences in response mean-square, PSD or PDF have been noted.

3.1.3.2 Box-Muller algorithm

The uniform deviates are then transformed into Gaussian distributed numbers using the Box-Muller algorithm [Knuth, 1998]. According to Knuth, this technique must be credited to G. Box, M. Muller and G. Marsaglia. It takes two random numbers, u_1 and u_2 which are uniformly

[3] Note that this generator is not to be confused with another generator bearing the same name RAN1 in the previous edition of this book [Press et al., 1987]. We have tried this older generator and have observed artificial peaks in the turbulence and airfoil response PSDs. Hence, we have discarded it.

distributed on the unit interval, as input:

$$G = (- 2\sigma_G{}^2 \ln u_1)^{1/2} \cos (2\pi u_2) \tag{3.10}$$

and outputs a Gaussian sequence, whose series has a variance $\sigma_G{}^2$.

3.1.3.3 White noise process

In order to implement this algorithm into a numerical time integration scheme as a white noise process, we consider that the variance of the Gaussian numbers is equal to the area under the white noise (single sided) PSD curve:

$$\sigma_G{}^2 = \phi_{WN}\, k_{max} \tag{3.11}$$

k_{max}, which could also be referred to as the Nyquist radial frequency, since a Gaussian number is generated at each time step, $\Delta\tau$, of the numerical integration, is given by:

$$k_{max} = \pi / \Delta\tau \tag{3.12}$$

Combining equations (3.11) and (3.12) into (3.10) gives a Gaussian distributed white noise process:

$$G_{WN}(\tau) = (- 2\phi_{WN}\ \pi/ \Delta\tau \ln u_1)^{1/2} \cos (2\pi u_2) \tag{3.13}$$

whose intensity is determined by its PSD, ϕ_{WN}. This algorithm is the heart of a number of Monte Carlo simulations, white or coloured noise, in the physics literature [Sancho et al., 1982; Fox et al., 1988; Fox, 1989].

At each time step of the simulation, four statistically independent uniform deviates are produced, which in turn generate two different Gaussian white noise processes. Thus, the longitudinal and vertical turbulent velocity differential equations (equations 2.29) are each fed by different Gaussian numbers. This is justified physically by the hypothesis of isotropy of the turbulent field, which leads to a diagonal double velocity correlation matrix, hence, uncorrelated velocity components as discussed in Chapter 2. Furthermore, from a practical perspective, it was observed that using the same uniform deviates for both turbulence components lead to a skewed PDF in heave, which is not reasonable due to the symmetry of our problem. The overall simulation process is schematised in Figure 3.1.

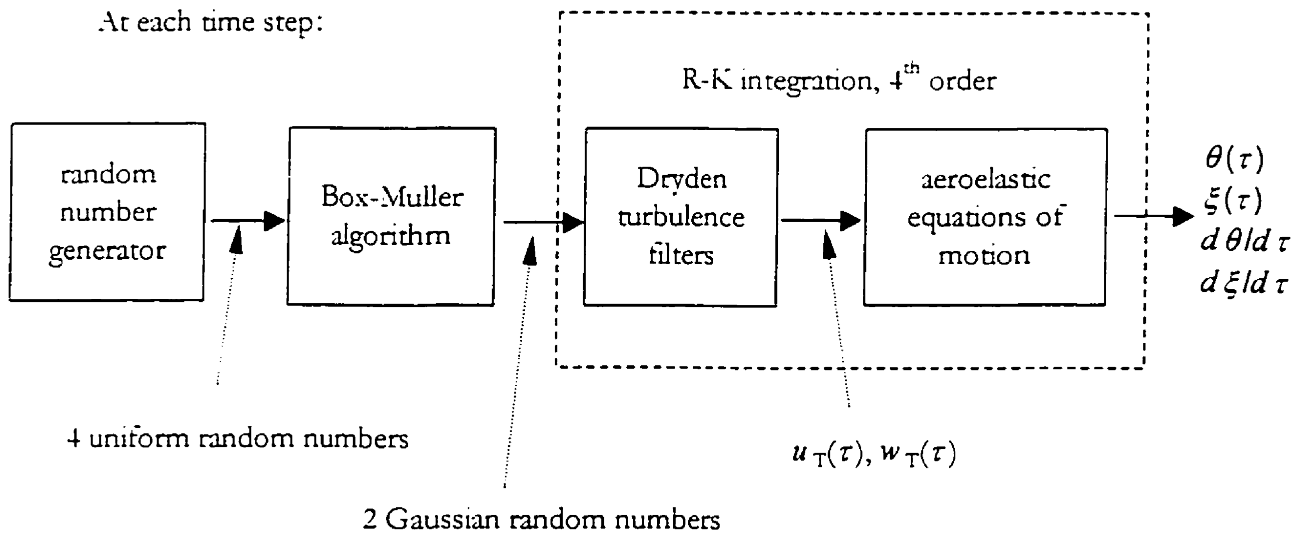

Figure 3.1 - Functional diagram of the numerical simulation.

3.1.4 Validation procedure

Numerical simulation is not without risks, specifically due to random perturbations. As pointed out by some authors [Kloeden and Platen, 1992; Mannella, 1989], the time discretization and numerical integration of stochastic differential equations must be treated with much more care than for deterministic ODEs. In this respect, two broad types of numerical integration schemes have been defined. One is called the strong approximation, and is concerned with path-wise convergence of the simulated process to the true theoretical process. The second type, referred to as the weak approximation, only requires convergence to functionals of the true solution, such as probability densities or moments; hence, it considers a global dynamics, as opposed to a local dynamics, point of view.

Intuitively, it could be advanced that the dichotomy between weak and strong approximations loses some of its relevance for coloured noise, which generally characterizes turbulence, because of its smoother sample path. However many practical applications, namely in engineering, do not necessitate close sample path approximations, as long as the weak convergence is obtained. This is the approach followed for this thesis. Only in a few instances will reference to sample paths be made. Moreover in these cases, it will be clear that the interest does not lie with the actual path-wise validity in the strong sense, but rather from a qualitative point of view and in comparison with other simulated paths. It is sound to be primarily concerned with a numerical integration scheme that meets the weak approximation criterion, but whose sample paths give a reasonable qualitative representation of the system dynamics. The validation will therefore concentrate on functionals of the sample time history response.

3.1.4.1 Validation of turbulent velocities

The validation of the numerically simulated longitudinal and vertical turbulent velocities is performed by comparing their mean, mean-square, PDF and PSD to the analytical solutions from which these numerical solutions are derived. To that effect, we choose two values of scale of turbulence which correspond to a high value, $L = 50.0$, and to a low value, $L = 0.5$, the later effectively modelling white noise, and a variance $\sigma_T^2 = 1.0$.

Longitudinal turbulence

In comparison with a unit variance, zero mean, exact Gaussian distribution, the PDFs of the longitudinal component of turbulence for the two values of scale of turbulence are shown in Figure 3.2. The numerical mean and mean-square are also given in the figure.

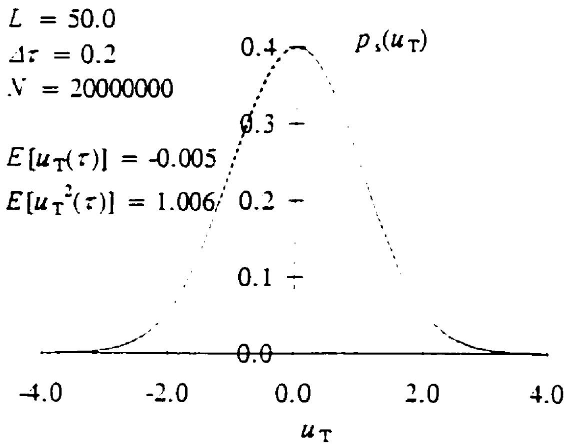

Figure 3.2 - PDF of longitudinal turbulent velocity from R-K numerical solution (—), in comparison with Gaussian curve (- - -); $\sigma_T^2 = 1.0$.

Next, the time evolution of the mean-squares is presented in Figure 3.3. Only the first 4,000,000 steady state iterations are shown. The case for L = 50.0 converges to $E[u_T^2]$ = 1.006 with an accuracy of ± 0.0005 after 20,000,000 iterations. The case for L = 0.5 converges to $E[u_T^2]$ = 0.999 with an accuracy of ± 0.0001 after 40,000,000 iterations. Note as well the two different time steps used. They are chosen in accordance with the value of scale of turbulence and in view of the requirements for the integration of the aeroelastic equations of motion, as discussed earlier.

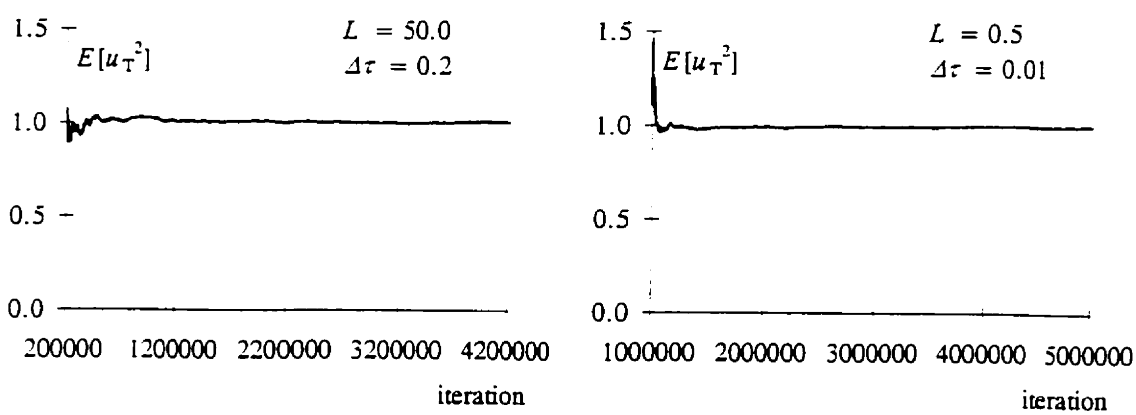

Figure 3.3 - Time (iteration) evolution of R-K simulated longitudinal turbulent velocity mean-square; $\sigma_T^2 = 1.0$.

Finally, the numerical solution PSDs of longitudinal turbulence, in comparison with the closed-form PSDs (non-dimensional), are shown in Figure 3.4.

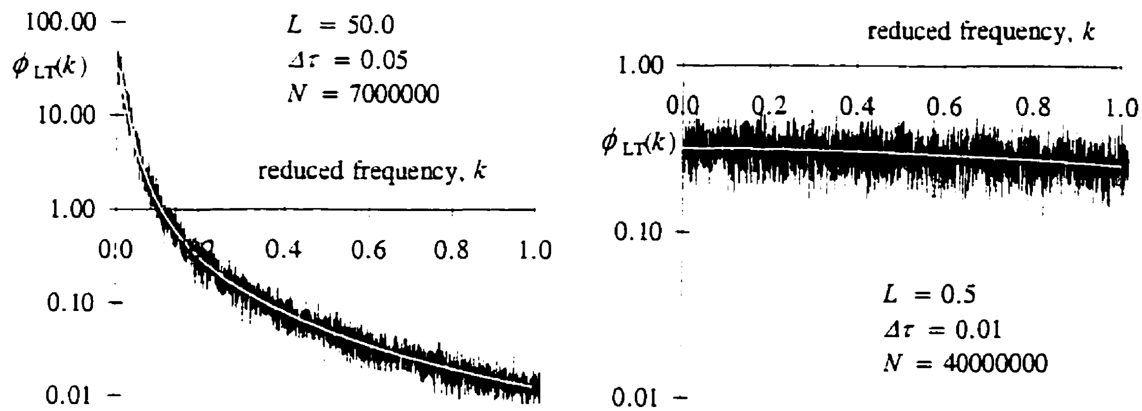

Figure 3.4 - PSD of longitudinal turbulent velocity from R-K numerical solution (—), in comparison with closed-form solution (solid white line); $\sigma_T^2 = 1.0$.

Vertical turbulence

The exact same comparisons are presented for the vertical turbulence component in Figures 3.5 to 3.7.

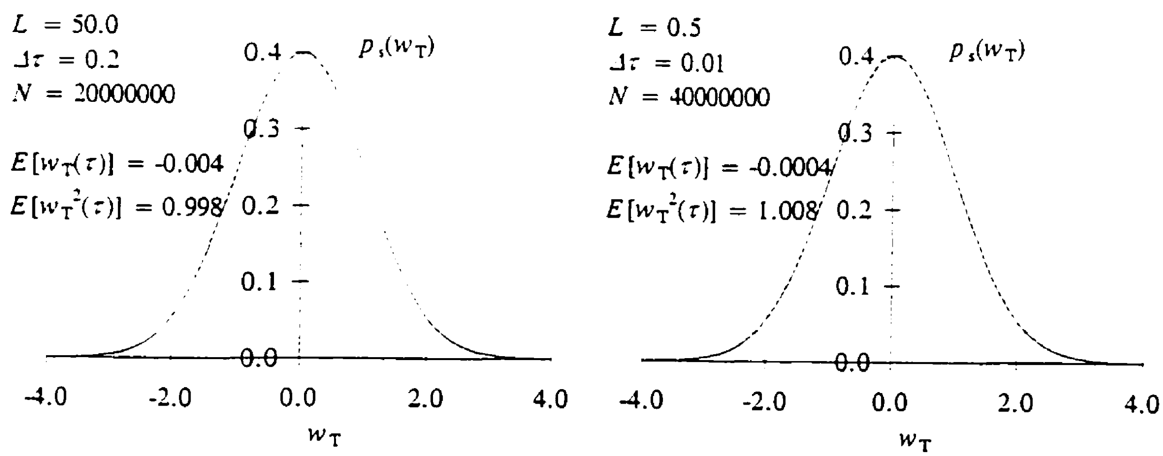

Figure 3.5 - PDD of vertical turbulent velocity from R-K numerical solution (—), in comparison with Gaussian curve (- - -); $\sigma_T^2 = 1.0$.

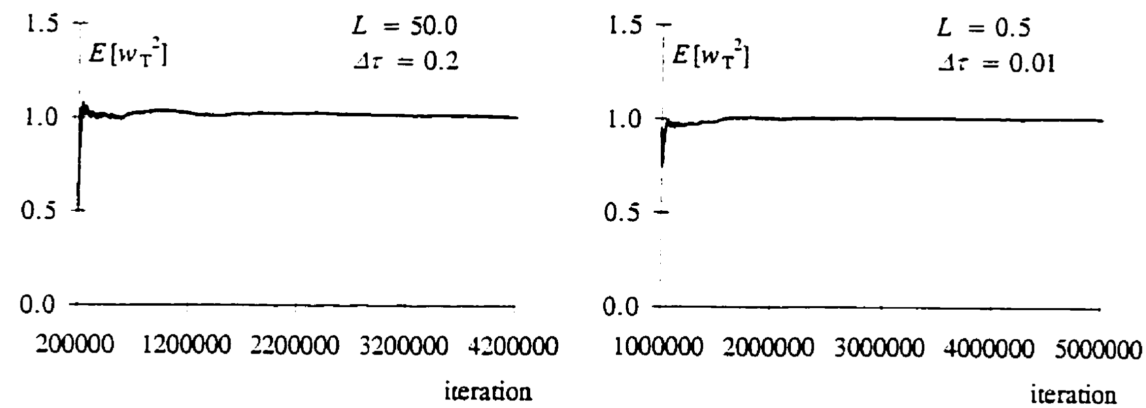

Figure 3.6 - Time (iteration) evolution of R-K simulated vertical turbulent velocity mean-square; $\sigma_T^2 = 1.0$.

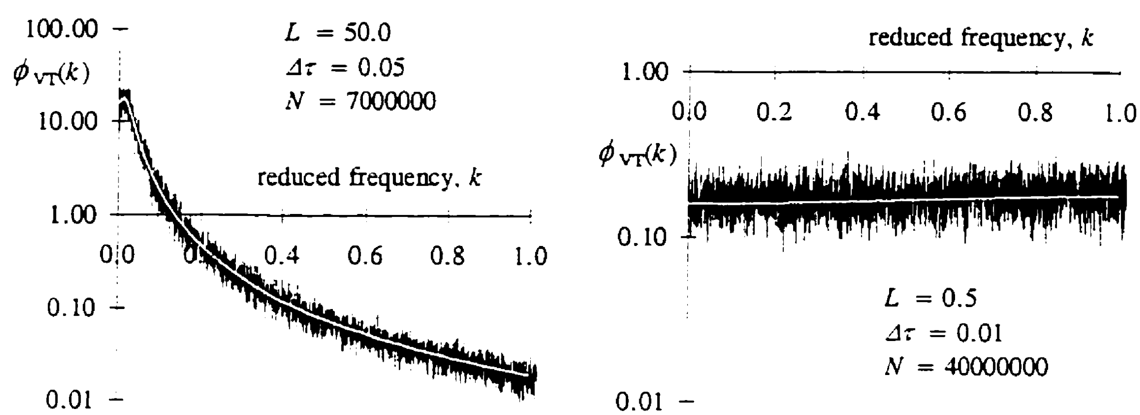

Figure 3.7 - PSD of vertical turbulent velocity from R-K numerical solution (—), in comparison with closed-form solution (solid white line); $\sigma_T^2 = 1.0$.

3.1.4.2 Validation of aeroelastic response

In contrast, the validation of the aeroelastic response cannot be done directly since we do not have an analytical solution acting as a basis of comparison. An indirect approach must be used. This is well summarized by Farmer [1982]: "For nonlinear equations that cannot be solved analytically, there is no rigorous method to make certain that a simulation is faithful to the equations. There are, however, certain indications: The behaviour of the simulated system must agree for any cases where analytical solutions are known; the behaviour of the simulation should converge as the resolution of the simulation increases; and, simulation by several different proper methods should all give similar results." We add another indication which is coherence of the results with expected behaviour dictated by either the physics of the problem, or other results for similar problems. The validation of the aeroelastic response is approached in accordance with these four principles.

Comparison with analytical solutions

Performing a standard eigenvalue problem, using routine ELMHES from Press et al. [1996], we have checked the flutter airspeed, the frequency of oscillation of the slow (unstable) mode at the neutrally stable flutter point, and the modal frequencies and damping at pre-flutter speed of the linear numerical solution. The flutter point is obtained by tracking the real part of the eigenvalues as they change with airspeed. Flutter occurs at the airspeed at which two of them, since we have a complex conjugate pair, cross the imaginary axis. At lower airspeeds, the non-excited numerical (R-K) solution displays a converging oscillation to zero. At higher speeds the numerical solution exhibits diverging oscillations.

The imaginary part of the eigenvalue gives the modal frequency. At the flutter speed, where the solution is neutrally stable, the imaginary part of the unstable pair of eigenvalues is used to check the frequency of the non-excited numerical solution once the effect of the fast (stable) mode has disappeared. The pre-flutter eigenvalues can also be used to check the modal damping and frequencies of the numerical solution. This is performed by calculating the PSD of the linear response to pure vertical turbulence. Since the damping is small, the two peak frequencies in the PSD correspond to the imaginary parts of the two conjugate pair of eigenvalues. Similarly, the damping (multiplied by the eigenfrequency) calculated from the half-power point of each mode, assuming the two modes are well separated, correspond to the real part of the eigenvalue.

The calculated PSD of the numerical linear response to pure vertical turbulence can also be checked against the frequency domain analytical solution. The closed-form PSD is obtained by multiplying the square of the norm of the transfer function, relating the linear aeroelastic system response to vertical turbulence, by the vertical turbulence PSD:

$$\begin{Bmatrix} \phi_{\theta} \\ \phi_{\xi} \end{Bmatrix} = \begin{Bmatrix} |F_{\theta}|^2 \\ |F_{\xi}|^2 \end{Bmatrix} \phi_{VT} \tag{3.14}$$

The two functions, F_{θ} and F_{ξ}, represent the aeroelastic system characteristics and the aerodynamic external moment and force, including Kussner's function. They are given in Appendix F along with their derivation. The vertical turbulence PSD, ϕ_{VT}, is given in equation (2.22 (b)) in dimensional form.

Two cases are shown, for coloured (L = 50.0) and effective white noise (L = 0.5) excitations, and at different airspeed in Figures 3.8 and 3.9, respectively. In both cases, the closed-form and numerical solution PSDs are indistinguishable, except for the higher spectral density at the peaks of the numerical based spectrum. The small difference is attributed to the discretisation process of the Fourier transform and can be diminished by taking more averages. The Fourier transform analysis is described later. Not given, but note that in both cases, the difference in pitch mean-square between the numerical and closed-form solutions is less than 1%.

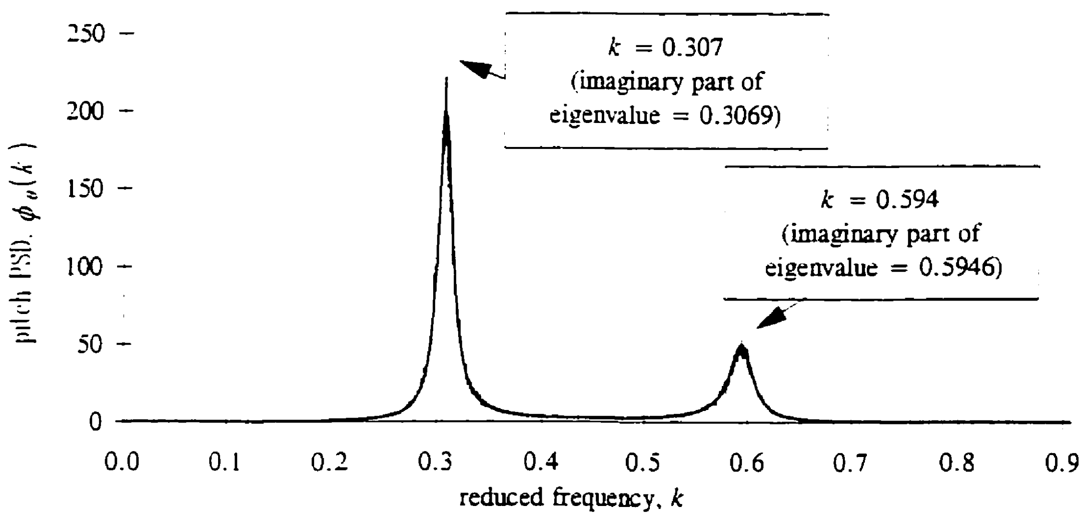

Figure 3.8 - Comparison of numerical (—) and closed-form (—) solution PSDs of pitch linear response to coloured vertical turbulence; σ_T^2 = 1.0, L = 50.0 and U = 2.0, $\bar{\omega}$ = 0.6325, x_{θ} = 0.25, r_{θ} = 0.5, μ = 100.0, a_h = -0.5, ζ_{θ} = 0.0, ζ_h = 0.0.

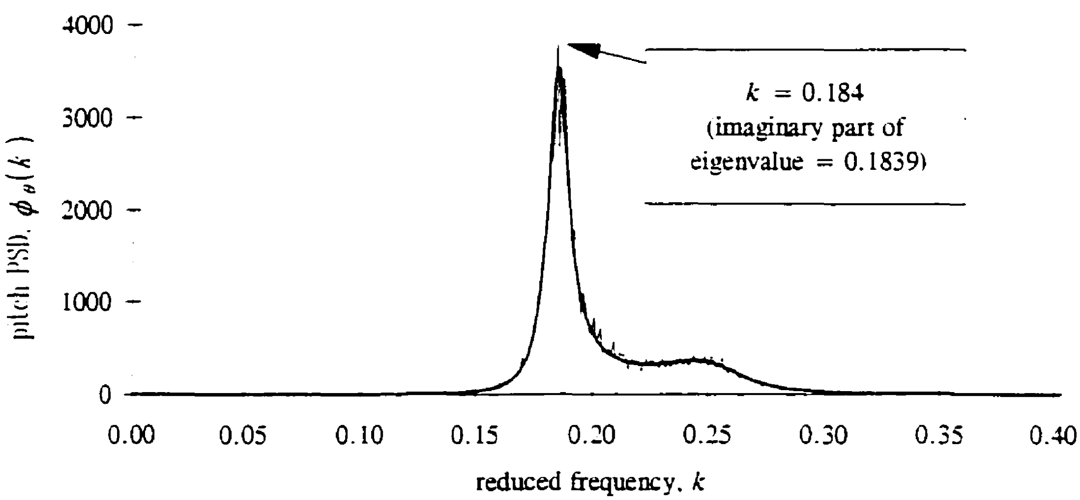

Figure 3.9 - Comparison of numerical (—) and closed-form (—) solution PSDs of pitch linear response to white vertical turbulence; $\sigma_T^2 = 1.0$, $L = 0.5$ and $U = 4.0$, $\bar{\omega} = 0.6325$, $x_\theta = 0.25$, $r_\theta = 0.5$, $\mu = 100.0$, $a_h = -0.5$, $\zeta_\theta = 0.0$, $\zeta_h = 0.0$.

Finally, we have also compared the nonlinear deterministic numerical solution with results from the describing function method; see Figure 4.2. In applying this method, the response is assumed to be simple harmonic. Furthermore for our problem where the nonlinearity is a cubic torsional stiffness, the nonlinear restoring force is expressed by this equivalent linear stiffness force:

$$k_{eq}\,\theta = k_3\, 3A^2/4\ \theta \tag{3.15}$$

where A is the amplitude of the nonlinear pitch oscillation. The equivalent linear force is then included in the original linear problem and a standard eigenvalue analysis is performed. Since A is not known, a value is assumed. With this assumed value of A, the problem is solved by iterating on the airspeed until a first set of eigenvalues experiences a change in sign in their real part. This is the airspeed corresponding to the assumed LCO amplitude, A. Its frequency is given by the imaginary part of the eigenvalue. For further details on this method, see Gelb and Vander Velde [1968].

Convergence with time step

As discussed in sub-Section 3.1.1.1, we have found that convergence of the numerical solution depends in a large part on the excited aeroelastic system being linear or nonlinear. First presented is the nonlinear case. Figure 3.10 shows the time (in terms of iteration) evolution of the pitch angle mean-square for three different time steps. For the scale of turbulence in this example, $L = 50.0$, the time step permitted by the integration of the turbulent velocity equations of motion is larger than the value used. The value of time step, $\Delta\tau = 0.2$, is chosen to meet the requirement of the aeroelastic equations of motion.

It is observed that convergence to the long term "steady state" behaviour is reached faster for the larger time steps, which indicates that it is more a property of the real time, $N\,\Delta\tau$, rather than the number of iterations, N. After 20M iterations, the difference between the three solutions fluctuates slightly, but remain between ± 0.5% of each other. Not shown, but note that changing the initial conditions, and the input noise sample by using different seeds in the random number generator do not modify the long term dynamics, in the statistical and probabilistic sense, of the system. Similar convergence is also exhibited for the pure longitudinal turbulence excited case.

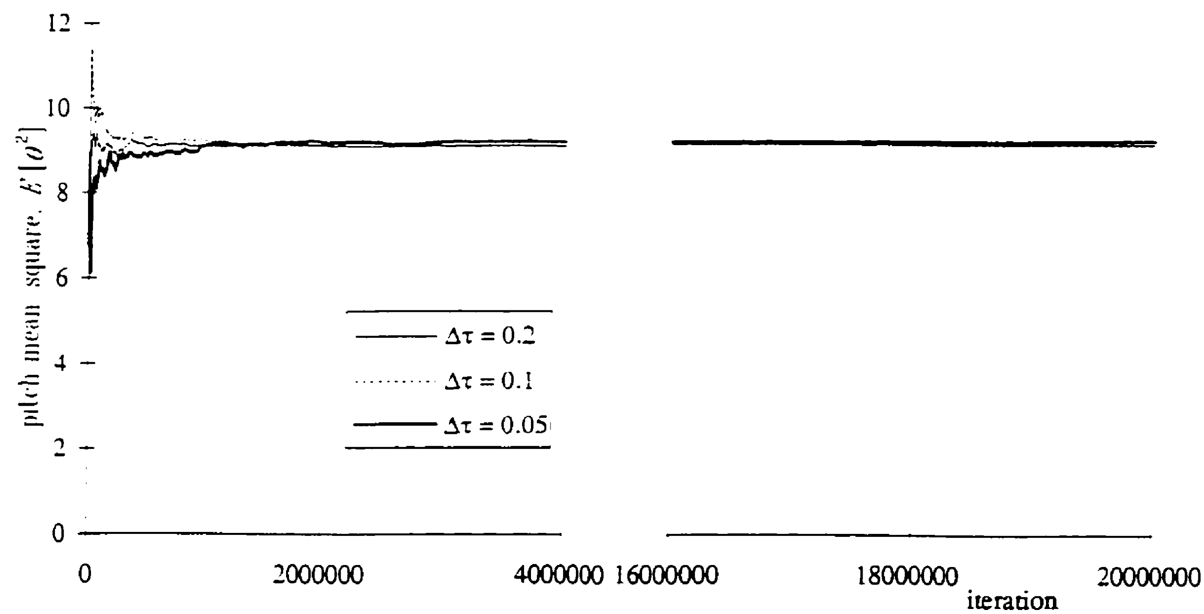

Figure 3.10 - Pitch angle mean-square iteration evolution for three different time steps; Nonlinear airfoil excited by combined turbulence; $L = 50.0$, $\sigma_T^2 = 1.0$ and $U_m = 5.0$, $\bar{\omega} = 0.6325$, $x_\theta = 0.25$, $r_\theta = 0.5$, $\mu = 100.0$, $a_h = -0.5$, $\zeta_\theta = 0.0$, $\zeta_h = 0.0$, $k_3 = 400.0$.

In comparison to the nonlinear system, convergence of the linear solution excited by both turbulence components is much slower and more sensitive to the choice of time step. This is due to the parametric excitation and can be problematic for the higher values of scale of turbulence and for airspeeds close to the flutter point. Accordingly for the linear excited airfoil, we have had to run the simulations for a larger number of iterations, as well as adjusting the time step to smaller values.

Figure 3.11 shows that convergence for the linear airfoil requires a much smaller time step, $\Delta\tau$ = 0.01, than is the case for the previously discussed nonlinear airfoil. After 30M iterations, the difference between the two solutions with time steps $\Delta\tau$ = 0.01 and $\Delta\tau$ = 0.005 remains between ± 1% of each other and converging to $E[\theta^2]$ = 10.1. For the smaller scale of turbulence, L = 0.5, at the same turbulence variance and airspeed, a similar convergence accuracy is obtained much earlier at 4M iterations.

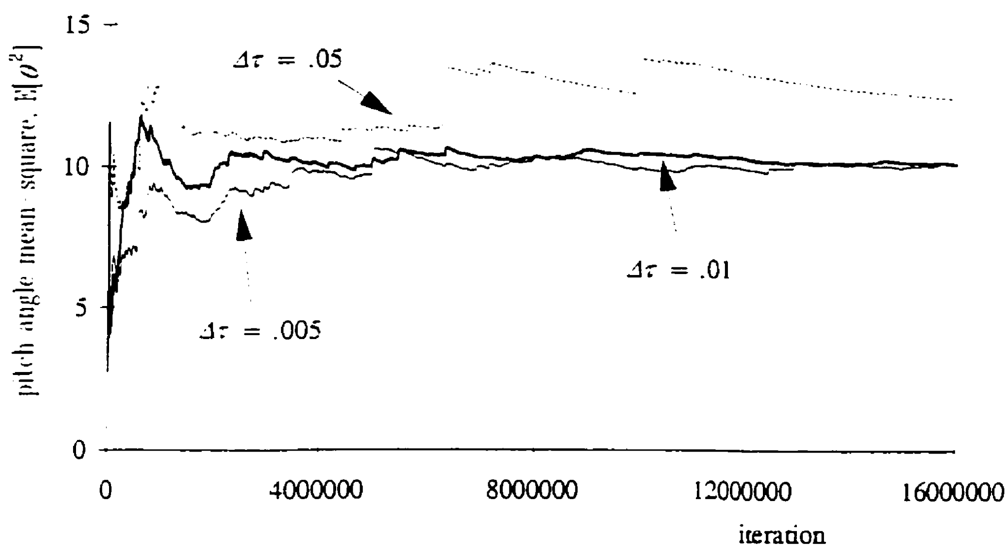

Figure 3.11 - Pitch angle mean-square iteration evolution for three different time steps; Linear airfoil excited by combined turbulence; L = 50.0, σ_T^2 = 1.0 and U_m = 2.0, $\bar{\omega}$ = 0.6325, x_θ = 0.25, r_θ = 0.5, μ = 100.0, a_h = -0.5, ζ_θ = 0.0, ζ_h = 0.0, k_3 = 0.0.

The solutions from the Runge-Kutta and Houbolt methods are nearly identical, except for the transient part, as demonstrated below. The initial differences are due to the special starting procedure required for Houbolt's method, but which have not been considered in this analysis for reasons stated earlier. The fact that convergence exists between the two solutions validates this omission. Furthermore, we observe weak and strong convergence types. The weak convergence type is displayed by the behaviour of the mean-square, for example, and is shown in Figure 3.12. At 4M iterations, the difference between the two solutions is less than 0.5%.

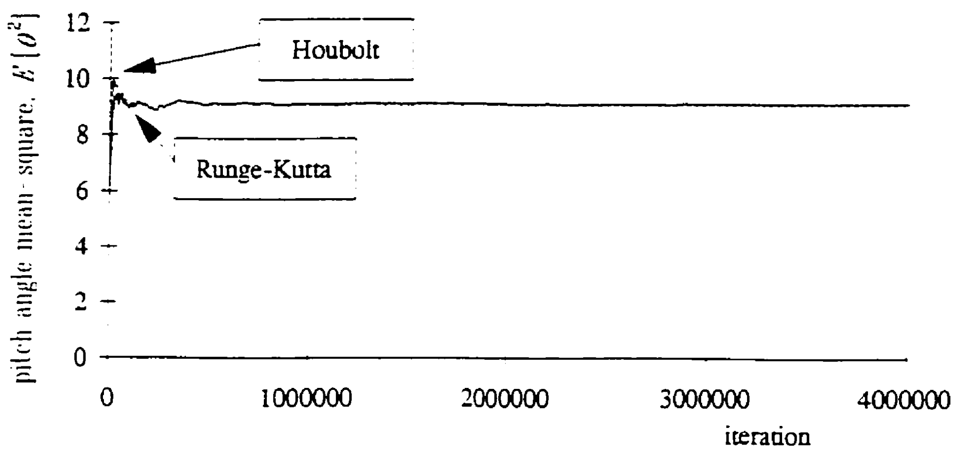

Figure 3.12 - Pitch angle mean-square iteration evolution for R-K (—) and Houbolt (- - -) methods; Nonlinear airfoil in combined turbulence; L = 50.0, σ_T^2 = 1.0, $\Delta\tau$ =0.2, and U_m = 5.0, $\bar{\omega}$ = 0.6325, x_θ = 0.25, r_θ = 0.5, μ = 100.0, a_h = -0.5, $\zeta_\theta = \zeta_h$ = 0.0, k_3 = 400.0.

As shown in Figure 3.13, a strong convergence type also exists between the solutions of the two methods since the sample time histories tend to converge as well. Although this is not of direct interest to us, since, for this thesis, we are more concerned with global aspects of the dynamics than in sample paths, it does reinforce our confidence in the simulation procedure. Note as well that the transient behaviour of the pitch time history, indicated by the difference between the Houbolt and R-K solutions, appears to die down very quickly (at about 2000 iterations). This observation supports our previous statement concerning the insignificant impact of transients and initial conditions.

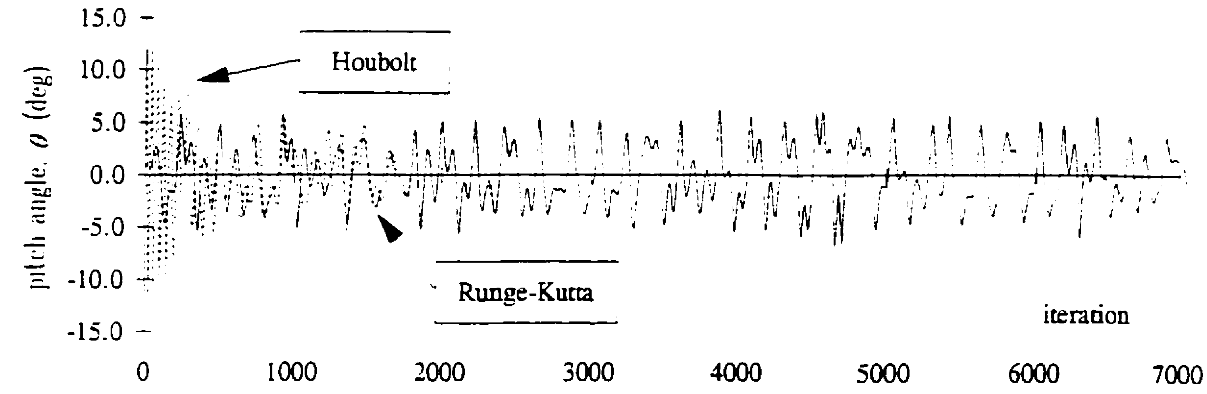

Figure 3.13 - Pitch angle time (iteration) history for Runge-Kutta (—) and Houbolt (- - -) methods; Nonlinear airfoil in combined turbulence; L = 50.0, σ_T^2 = 1.0, $\Delta\tau$ =0.2, and U_m = 5.0, $\bar{\omega}$ = 0.6325, x_θ = 0.25, r_θ = 0.5, μ = 100.0, a_h = -0.5, $\zeta_\theta = \zeta_h$ = 0.0, k_3 = 400.0..

Also shown for comparison in Figure 3.14 are the sample time histories of the turbulent velocities. Note that in the Houbolt simulation procedure, we have integrated the turbulent velocities using the R-K algorithm and the aeroelastic equations with Houbolt's method. Since we have already validated directly and explicitly the numerical turbulent velocities in comparison with their closed-form solutions, this approach permits us to focus on the numerical integration of the aeroelastic equations because they have the exact same "random" excitation input in both methods.

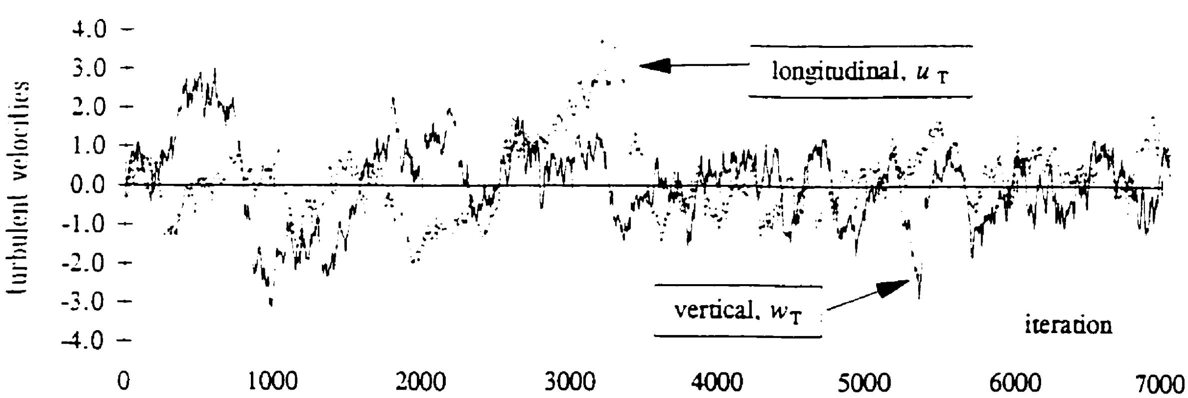

Figure 3.14 - Turbulent velocities time (iteration) history; L = 50.0, σ_T^2 = 1.0; Runge-Kutta method, $\Delta\tau$ = 0.2.

Coherence with expected results

The last element we have used to establish the validity of our numerical results is to check their coherence with expected results. In many ways this can be a tricky, subjective and intuitive process. Hence, by itself this check is not sufficient, but it solidifies the overall validation process. There are two avenues. One is concerned with the consistency (or self-consistency as used by Dowell and Ilgamov [1988]) of the results with the equations of motion. For example, does it make physical sense to have a skewed PDF when no asymmetry is modelled. The answer is not obvious and may depend on whether or not there is more than one underlying deterministic attractor.

The second avenue is to compare our results with those of similar problems. Since there are degrees of similarity, we have based the comparison on the identification of the areas where the problems differ from each other, and by searching for physical explanations for these differences. These comparisons are discussed throughout the thesis.

3.2 Time Series Analysis

The output of the numerical time integration is assumed to be ergodic, such that all the dynamic information is contained in one sample path. Ergodicity refers to the equivalency of time and ensemble averages. Specifically, it means that averaging one sample over a long period of time is equivalent to averaging many samples, with each having randomly picked initial conditions, at one point in time. In this regard, the initial conditions for this analysis will be inconsequential.

A necessary condition to ensure ergodicity is stationarity. This is a property of the turbulence model, and is also assumed to be valid for the aeroelastic response. In turn, stationarity of the signal requires that steady state, in the statistical sense, has been reached. Although we do not believe that for this analysis the transients, in the statistical sense, have any significant effect on the calculation of averaged results, such as the moments, PDF and PSD, we have not included them in the calculation of averages. The transient time was simply determined from visual inspection of the nonlinear non-excited system.

3.2.1 Probability density function

The probability density function of the system response is analysed using both the marginal and the bi-dimensional representations. The marginal PDF represents the probability density of a single variable for a multi-dimensional process. Hence, in effect it is a uni-dimensional PDF. Adapted to our problem, its theoretical definition is given by equation (3.16) for the pitch angle for example, where $p(\theta, \xi, \theta', \xi', z_1, z_1', z_2, z_2')$ is the joint probability density function. The integration is performed on all remaining seven variables, leaving θ as a free variable:

$$p(\theta) = \int_{-\infty}^{\infty} p(\theta, \xi, \theta', \xi', z_1, z_1', z_2, z_2')\, d\xi\, d\theta'\, d\xi'\, dz_1\, dz_1'\, dz_2\, dz_2' \tag{3.16}$$

In practice, the integration is carried out by first dividing the expected range of pitch angle into 101 intervals. Subsequently, the number of times the pitch angle visits each interval during a simulation is recorded. This number of intervals is chosen because it provides a good compromise between resolution of the numerical PDF and simulation time. The result is an histogram which is then normalised to provide a unit area under the PDF curve, i.e.

$$P(-\infty < \theta < \infty) = \int_{-\infty}^{\infty} p(\theta)\, d\theta = 1 \tag{3.17}$$

The bi-dimensional PDF is a joint density limited to two variables, as shown for the pitch angle and pitch rate for example:

$$p(\theta, \theta') = \int_{-\infty}^{\infty} p(\theta, \xi, \theta', \xi', z_1, z_1', z_2, z_2')\, d\xi\, d\xi'\, dz_1\, dz_1'\, dz_2\, dz_2' \tag{3.18}$$

In its implementation and due to practical considerations, we have divided the range of the free variables into 51 by 51 (= 2601) intervals, compared with the 101 for the marginal PDF. The resolution of the bi-dimensional PDF is therefore half the resolution of the marginal PDF, but its calculation takes a much longer time. The rest of the procedure is essentially the same.

3.2.2 Moments

The assumption of ergodicity enables the first two moments, respectively mean and mean-square, to be expressed as shown below:

$$E[x] \equiv \int_{-\infty}^{\infty} xp(x)dx = \bar{x}(t) = \frac{1}{T}\int_{0}^{T} x(t)dt \tag{3.19}$$

$$E[x^2] \equiv \int_{-\infty}^{\infty} x^2 p(x)dx = \overline{x^2}(t) = \frac{1}{T}\int_{0}^{T} x^2(t)dt \tag{3.20}$$

where x represents any of the system state variables. The time integral equations are then discretized and easily implemented in the numerical simulation algorithm.

3.2.3 Largest Lyapunov exponent

The largest Lyapunov exponent is numerically calculated based on the tangent space method as described in Chapter 1. With this method, the nonlinear equations of motion can be linearized by calculating the Jacobian about the reference random trajectory. Both sets of equations, nonlinear and linear, are then solved simultaneously and the norm of the linear solution is monitored. Alternatively, instead of directly linearizing the equations of motion they are solved twice with different but close initial conditions and with the same noise realisation. In this case, the Euclidian norm between the two nonlinear solutions is monitored. We have tested both techniques. They give the same value for the largest Lyapunov exponent.

An important property of the largest Lyapunov exponent is its invariance for any reference trajectory within a given attractor. In Figure 3.15 this property is verified by calculating λ_{max} for two sets of initial conditions and noise realisation. In the long term, both exponents tend towards the same value, thus confirming the invariance property. Also shown is the impact of the time step. Similarly with the mean-square, a smaller time step requires more iterations for convergence.

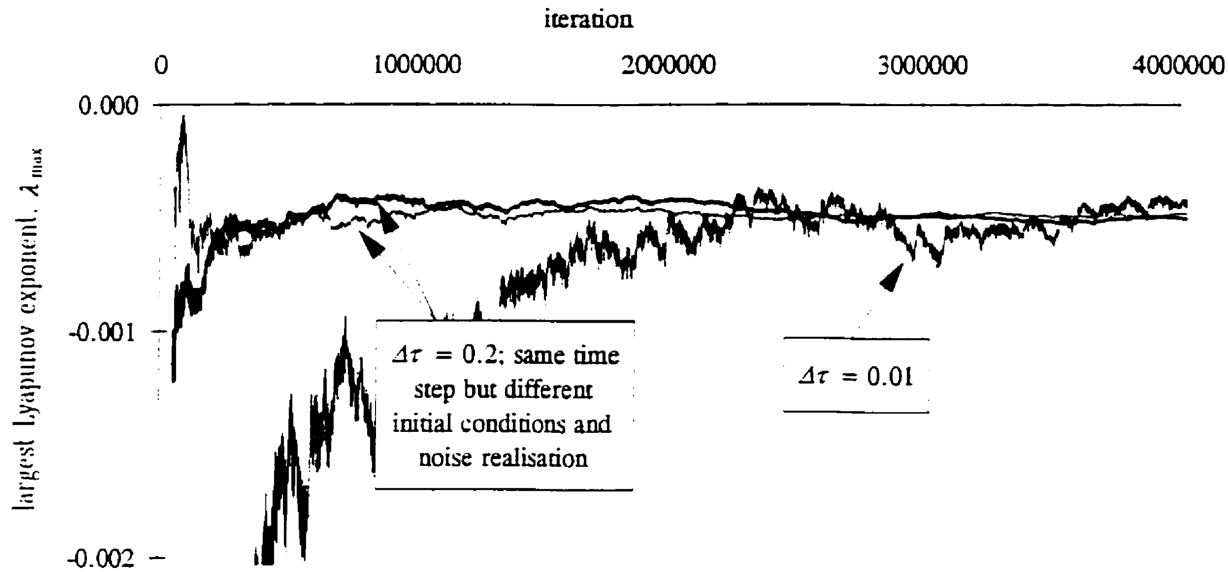

Figure 3.15 - Time evolution of the largest Lyapunov exponent for two sets of initial conditions and noise realisation, and two time steps, for nonlinear airfoil in pure longitudinal turbulence; tangent space method; U_m = 4.3, σ_T^2 = 1.0, L = 50.0, k_3 = 400.0.

For the sake of completeness, note that we have also calculated the largest Lyapunov exponent using the direct or real space method. Recall this method, applied to a problem where the equations of motion are known, gives λ_{max} by solving the nonlinear equations twice, but contrary with the tangent space method, with different noise realisations. We have noticed that in general this method does not seem to be useful since it indicates neutral convergence of the trajectories. For example, take the case where the reference trajectory is a random LCO, the Euclidean norm according to the real space method remains on average constant and fluctuates randomly about the average with the same intensity. Since the norm remains constant on average, λ_{max} tends to the trivial solution. In contrast, the tangent space method gives a non-zero λ_{max} Only for the case where the attractor is a deterministic fixed point have we found that the two methods, tangent and real space, give the same (non-zero) largest Lyapunov exponent.

3.2.4 Spectral analysis

The spectral analysis of the output data from the numerical integration is performed using a Fast Fourier Transform (FFT) algorithm [Kahaner et al., 1989]. The maximum number of data points the computer can handle at once to perform the transform is limited to $N_{FFT} = 2^{16} = 65536$. This is much smaller than the number of data points required by the PDF analysis for example. We have thus performed sequential averages of the transforms made over 65536 data points. The number of averages done were chosen based on the criticality of the problem at hand, and ranged from 20 to 150.

In performing the averages, we have also monitored the stationarity of the process and the representativeness of each 65536 data points sample by calculating the response mean-square of each sample. A stationary process implies that no evolutive trend is displayed by the sample mean-squares. Furthermore, proper estimates of the "infinitely" long process by the samples require that their mean-squares do not vary significantly in comparison to their mean value, which represents the mean-square of the full process.

In order to minimize aliasing effects, potentially causing high frequencies to appear as low frequencies, we have chosen the Nyquist frequency to be much larger than any physical frequency suspected to appear in the spectrum. The Nyquist (radial) frequency is given by $k_{Nyq.} = \pi/\Delta T$ where ΔT is the sampling time interval to perform the FFT. It is not necessarily chosen to be equal to the integration time step, $\Delta\tau$, but can be larger. Hence, the smaller the sampling time, the larger the Nyquist frequency. For most spectral analysis performed in this work, we have used a sampling time $\Delta T = 0.25$, which gives a Nyquist frequency, $k_{Nyq.} = \pi/\Delta T = \pi/0.25 = 12.6$. This is well above the frequency range where the system displays any dynamics.

Choosing a too small sampling time may however have a detrimental effect on the FFT frequency resolution $\Delta k = 2\pi/(N_{FFT}\,\Delta T) = \pi/(2^{15}\,\Delta T)$. This aspect is also considered in the choice of an appropriate sampling time. There is no exact recipe for the choice of ΔT. Per set of data, we have changed its value and examine the resulting PSDs in light of the expected physical spectral content.

We have also been concerned with potential leakage problems which may cause a broadening and flattening of the PSD peaks, or more specifically a transfer of the power at some particular frequency into nearby frequencies. This issue has been evaluated by changing the frequency resolution of the FFT and by performing data windowing. We have used the Welch window which appears to be slightly preferred by Press et al. [1996] over other commonly used window shapes. The Welch window is given by equation (3.21) and shown graphically in Figure 3.16.

$$w_j = 1 - \left(\frac{j - 0.5(N_{FFT} - 1)}{0.5(N_{FFT} + 1)} \right)^2 \qquad (3.21)$$

where $j = 0, 1, 2, \ldots 65535$, and w_j is multiplied to each value of the time series to be transformed.

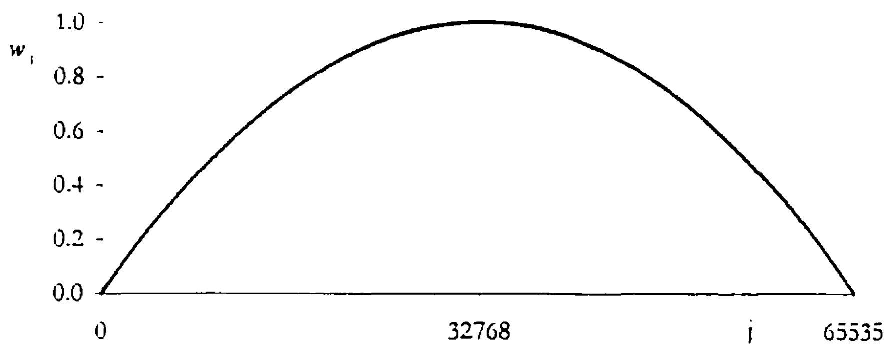

Figure 3.16 - Welch window for $N_{FFT} = 65536$.

Chapter 4

RANDOM BIFURCATION ANALYSIS

- Binary Flutter Conditions

We have two motives to study the bifurcation scenario experienced by the fluttering airfoil under turbulent excitation. First, a good appreciation of the bifurcation scenario is required to understand the airfoil stability and response characteristics. In this regard, the investigation of the random flutter/supercritical Hopf bifurcation sets the stage for the analysis of other aspects of the airfoil dynamics. Another motive to study the bifurcation scenario is grounded in a more fundamental undertaking to investigate the problem of *noise-induced transitions* or *stochastic bifurcation*.[1]

The emphasis will be put on the global (steady state in the probabilistic sense) dynamics. Some localized (in time) aspects of the dynamic behaviour will also be discussed, but no major conclusions will be drawn from them.

1

According to Arnold [1998], the qualifying term "stochastic" applies to problems where the excitation is white, whereas "random" refers to coloured noise excited problems. Because this thesis deals mainly with coloured excitation, reference to *random bifurcation* seems more appropriate. However and in the specific context of a bifurcation analysis, it appears that stochastic bifurcation is in general accepted terminology for either white or non-white excitation. Also note that the term "noisy" is sometimes used as a neutral appellation.

4.1 Deterministic Baseline

Throughout this chapter, unless otherwise stated, results are given for the following set of airfoil non-dimensional parameters: $\bar{\omega} = 0.6325$, $x_\theta = 0.25$, $r_\theta = 0.5$, $\mu = 100.0$, $a_h = -0.5$, $\zeta_\theta = 0.0$, $\zeta_h = 0.0$. The nonlinearity is a hardening torsional stiffness and has the following coefficient, $k_3 = 400.0$. With these conditions, the baseline deterministic (non-excited) bifurcation type is of the supercritical Hopf type. Using the airspeed as the control parameter, this bifurcation type is first characterized by a loss of stability of the stable fixed point which is then followed at higher airspeeds by a stable LCO centred about the unstable fixed point at the origin.

4.1.1 Binary flutter

The loss of stability of the fixed point, which is located at the origin since no bias is modelled, occurs at the flutter speed, U_f. It is solely determined by the linear system. Shown in Figure 4.1 (a) and 4.1 (b) are the real and imaginary parts of the eigenvalues, respectively.

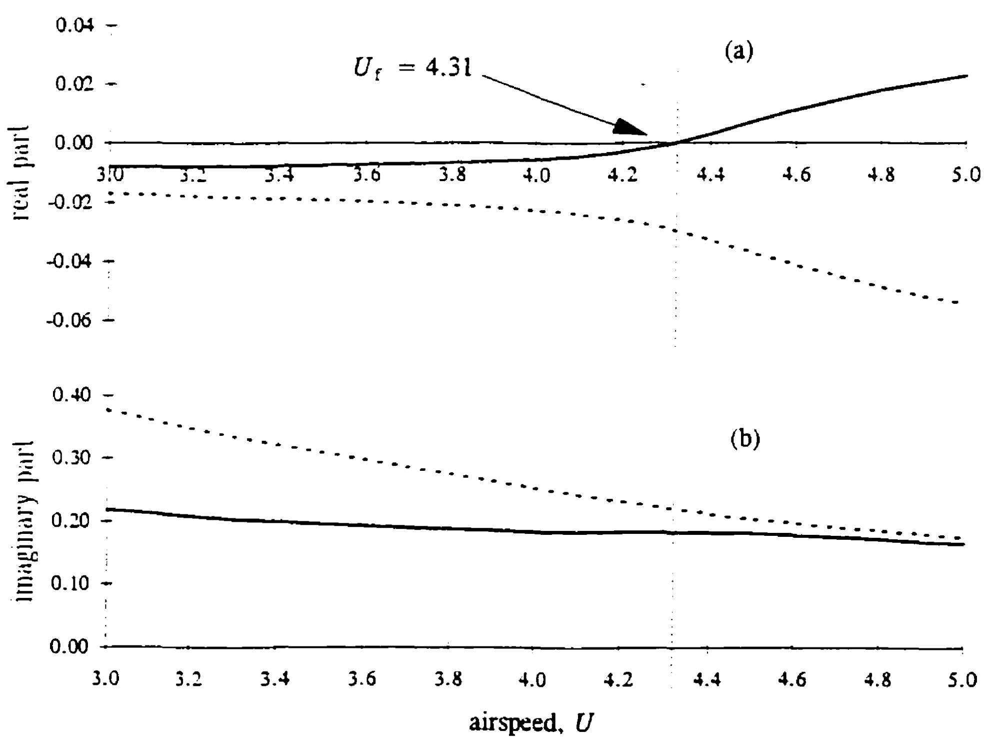

Figure 4.1 - Behaviour of (linear and non-excited) airfoil eigenvalues with airspeed; (a) real part; (b) imaginary part.

Flutter occurs at $U_f = 4.31$, as given by the real part of the complex conjugate pair which changes sign. The figure also illustrates the coalescence of the two eigenfrequencies, whose value are given by the imaginary part. The flutter frequency is $k_f = 0.182$.

4.1.2 Post-instability behaviour

For the linear airfoil and for airspeeds above the flutter speed, any disturbances on the airfoil will in theory grow to infinity. With the nonlinearity, the oscillations stabilize on a limit cycle whose steady state amplitude is independent of initial conditions. These oscillations represent a balance between the (unstable) linear forces and the restraining mechanism of the hardening spring whose effective stiffness increases with the LCO amplitude. For the post-instability airspeed range of interest, the LCO is the only stable attractor in the state space. Its amplitude in pitch as a function of airspeed is shown in Figure 4.2. Both the numerical and describing function method (DFM) solutions are given.

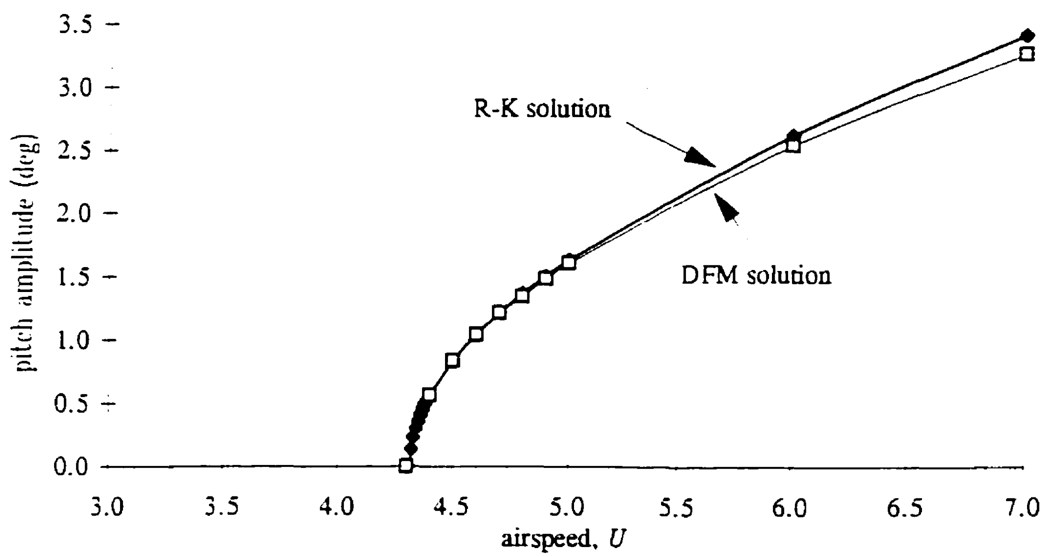

Figure 4.2 - Amplitude of the LCO as represented by the pitch motion for the non-excited nonlinear airfoil, as a function of airspeed; R-K and DFM method solutions; $k_3 = 400.0$.

As described in Chapter 3, the DFM assumes simple harmonic motion. Accordingly, the increasing difference in LCO amplitude with airspeed between the two solutions can be interpreted as an indication of the enhanced relative importance of harmonics of the fundamental frequency in the "true" numerical solution.

Also of interest is the change with airspeed of the pitch response mean-square compared with the heave response mean-square. From Figure 4.3, which compares the amplitude of oscillation and response mean-square of the pitch and heave, it is observed that the pitch dynamics remains close to the simplest expression of the Hopf normal form, which is characterised by a linear mean-square response - airspeed relationship. Indeed, the radius variable of this normal form expressed in polar coordinates, $\dot{r} = a\,r + a_3\,r^3$, is essentially characterised by two terms, a linear and a cubic term [Argyris et al., 1994]. Consequently, at steady state (i.e. $\dot{r} = 0$) the radial variable increases linearly with the square root of the control parameter a, or similarly, its mean-square is a linear function of the control parameter, ie $r^2 = -a/a_3$, where a is positive and a function of U, and a_3 is negative for the supercritical Hopf bifurcation. On the other hand, the heave dynamics departs from this behaviour very early after the flutter point. The likely physical explanation for this observation is the location of the nonlinearity, which directly affects the pitch response but only indirectly affects the heave.

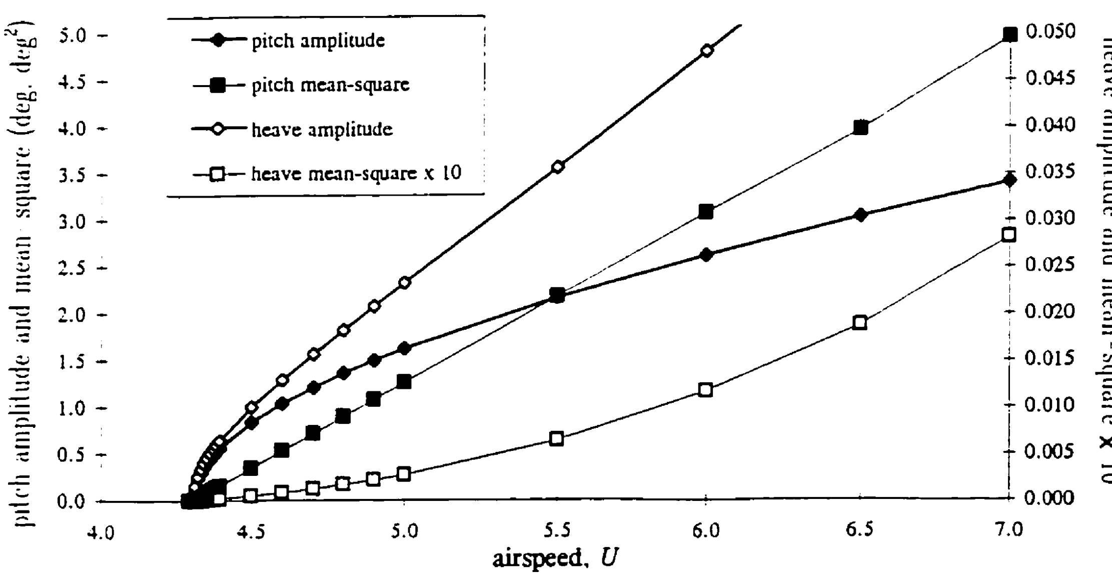

Figure 4.3 - Diagram of pitch and heave amplitude of oscillations and response mean-square of non-excited nonlinear airfoil, as a function of airspeed; $k_3 = 400.0$.

4.2 Interpretative and Practical Considerations

In the broad sense, a bifurcation means a qualitative change in the dynamic behaviour of a system as a parameter is varied. In turn, a change in behaviour implies the identification of the behaviour in question. This is a relatively easy and straightforward task for a deterministic system, whereas in the random case it is a much more complex, and equivocal, venture. We have argued in Chapter 1 that the most natural representation of the stochastic (and random) dynamics is the probability density function (PDF), where for example the peaks, or extrema, are the stochastic analogue of the deterministic amplitudes of motion. We have also argued that the PDF defines the type of dynamic behaviour. Accordingly, we consider the PDF to be an appropriate tool to identify any qualitative change in the dynamics of the random problem.

Due to practical considerations, a clarification with regard to the use of the PDF is in order. Since a bifurcation refers to a change in the dynamical behaviour of the system as a whole, a strict interpretation of the behaviour for our multi-dimensional system requires a joint PDF of at least the four dimensions associated with the structural degrees-of-freedom, ie $p_s(\theta, \theta', \xi, \xi')$. The subscript "s" represents steady-state behaviour in the statistical sense. We are, however, practically restricted to the marginal and bi-dimensional PDF projections, for example $p_s(\theta)$ or $p_s(\theta, \xi)$. This is cause for care in the interpretation of the results, and we need to define a proper terminology to differentiate between a change of behaviour of the system from that of an observed change in the marginal PDF of a state. Accordingly, in situations where we are positive that a qualitative change in the dynamical behaviour of the whole system has occurred, we will use the term ***bifurcation***. Otherwise, and until we feel reasonably confident that a bifurcation has occurred, the observation of a change in shape of a marginal PDF, for example from a uni- to a bi-modal, will bare the name ***transition***.

Having said that, based on the deterministic behaviour we expect to witness dynamic behaviour whose fundamental features can be captured by a two-dimensional picture, or a bi-dimensional PDF. For example, the essence of a deterministic LCO, being a one-dimensional object, can be seen on a phase plane. The equivalent representation of the phase plane for the random case is the bi-dimensional PDF. Both representations are shown in Figure 4.4 for the deterministic airfoil dynamics. We see that the phase plane is the projection of the bi-dimensional

PDF looking down the probability axis. In the case of the zero-dimension equilibrium point, its basic topology[2] is expected to remain unchanged in PDFs of any dimension[3].

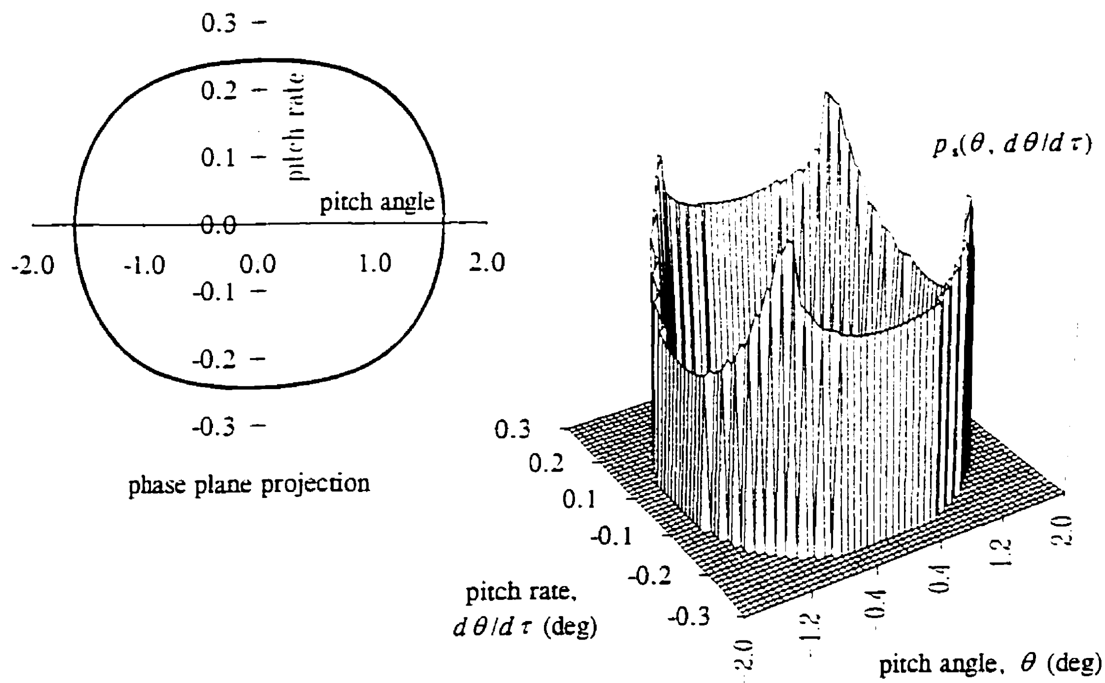

Figure 4.4 - Bi-dimensional PDF and phase plane of the pitch pitch-rate of the non-excited nonlinear airfoil at $U = 5.0$, $k_3 = 400.0$.

The representation of the dynamics in the form of the PDF leads to the concept of a P-bifurcation. We have discussed that the interpretation of the P-bifurcation as being a "real" bifurcation is a source of argument between physicists and engineers on one hand and mathematicians and dynamics theoreticians on the other. The former generally favour the P-bifurcation notion, while the latter advocate the D-bifurcation interpretation, which is associated with the concept of largest Lyapunov exponent. Thus, we also use the largest Lyapunov exponent as a measure of the dynamic behaviour, and in particular for the D-bifurcation. As well we make use of the response mean-square as an indicator of the D-bifurcation point. We have found that

[2] We borrow the very simple words of Argyris [1994] and define topology as the study of qualitative geometry.

[3] However, for higher dimensional dynamical objects such as a chaotic attractor, the phase plane projection is not sufficient. For example, the torus which represents a quasi-periodic attractor requires a 3-D state space projection. This is possible in the deterministic case, but impossible in the random case due to the need for an additional dimension representing the probability density axis.

for our nonlinear problem with pure longitudinal turbulence, the D-bifurcation point could also be identified with the (nonlinear) response mean-square.

The bifurcation scenario is discussed in three phases, according to the source of excitation. In a first analysis, the problem is analysed for pure longitudinal turbulence. This excitation source is parametric, hence, makes the mathematical model time-varying. The pure vertical turbulence excitation, acting as an external forcing, is then treated. After having broken down the nonlinear airfoil-turbulence model in its two excitation components, in the hope of obtaining a more fundamental understanding of its dynamics, a synthesis is then offered by discussing the more realistic case of combined (longitudinal and vertical) turbulence excitation.

4.3 Pure Longitudinal Turbulence Excitation

4.3.1 The two-step bifurcation

The PDF of the dynamics of the fluttering nonlinear airfoil in pure longitudinal turbulence ($u_T \neq 0$, $w_T = 0$) is presented in Figure 4.5, showing the marginal steady state density in pitch as a function of mean airspeed. Note that the PDF is multiplied by the pitch response mean-square to facilitate the visual interpretation of the dynamics. This is especially so for the equilibrium point, which for a pure PDF would otherwise be represented by a Dirac delta function centred at zero pitch angle, instead of a flat density.

Figure 4.5 typifies the dynamics of the system since the other structural states, pitch rate, heave and heave rate, also exhibit the same marginal PDF portrait characterized by two transition points. The first transition point, at U_{m1}, separates a region with a flat density from a uni-modal one; the second transition point, at U_{m2}, separates the uni-modal from a bi-modal density.

As expected, Figure 4.5 resembles the bifurcation landscape experienced by the Landau equation under multiplicative noise, as described in Chapter 1. We are cautious in this statement since we have not concluded yet that the observed behaviour indicates a bifurcation. In addition, because the Landau system is one-dimensional its bi-modal density represents a stochastic pitchfork, while we expect a Hopf bifurcation in our case. However, we are led to believe that these observed transitions are actually bifurcations since the two transition points occur at the same airspeeds for all marginal PDFs. These airspeeds are located at $U_{m1} = 3.64$ and $U_{m2} = 4.75$ for this example.

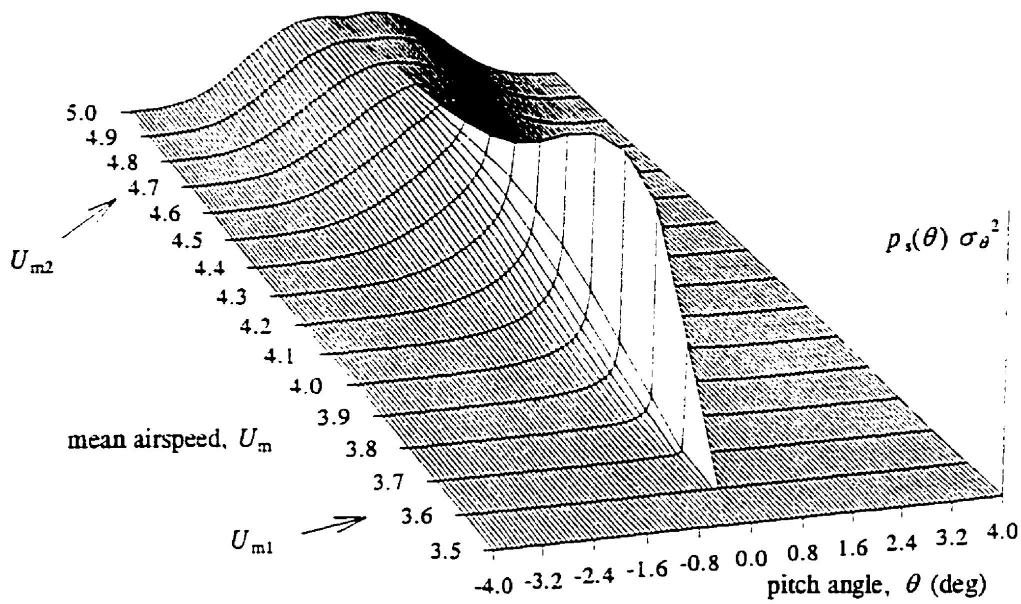

Figure 4.5 - Marginal PDF diagram of the airfoil pitch angle with pure longitudinal turbulence as a function of mean airspeed; $\sigma_T^2 = 1.0$, $L = 50.0$, $k_3 = 400.0$.

The same values of critical airspeed are also observed in the bi-dimensional PDF representation shown in Figure 4.6. U_{m1} separates a region with no dynamics from a single peaked density centred at zero, while U_{m2} separates the single peaked shape from a crater-like shaped PDF.

The double peaked shape of the marginal PDF is shown as a crater in the bi-dimensional density. This is compatible with the dynamics of a limit cycle oscillation, hence, it indicates a coherence of the results with the model. It also reconciles the observed resemblance between the one-dimensional Landau system pitchfork bifurcation with the Hopf bifurcation represented with the marginal PDF. Therefore, since we have also found that all marginal PDFs present the same double transition landscape, and that the two critical speeds are the same for all states, we conclude that a bifurcation exists. It is in fact a *two-step bifurcation* with three distinct regions of qualitatively different dynamic behaviour.

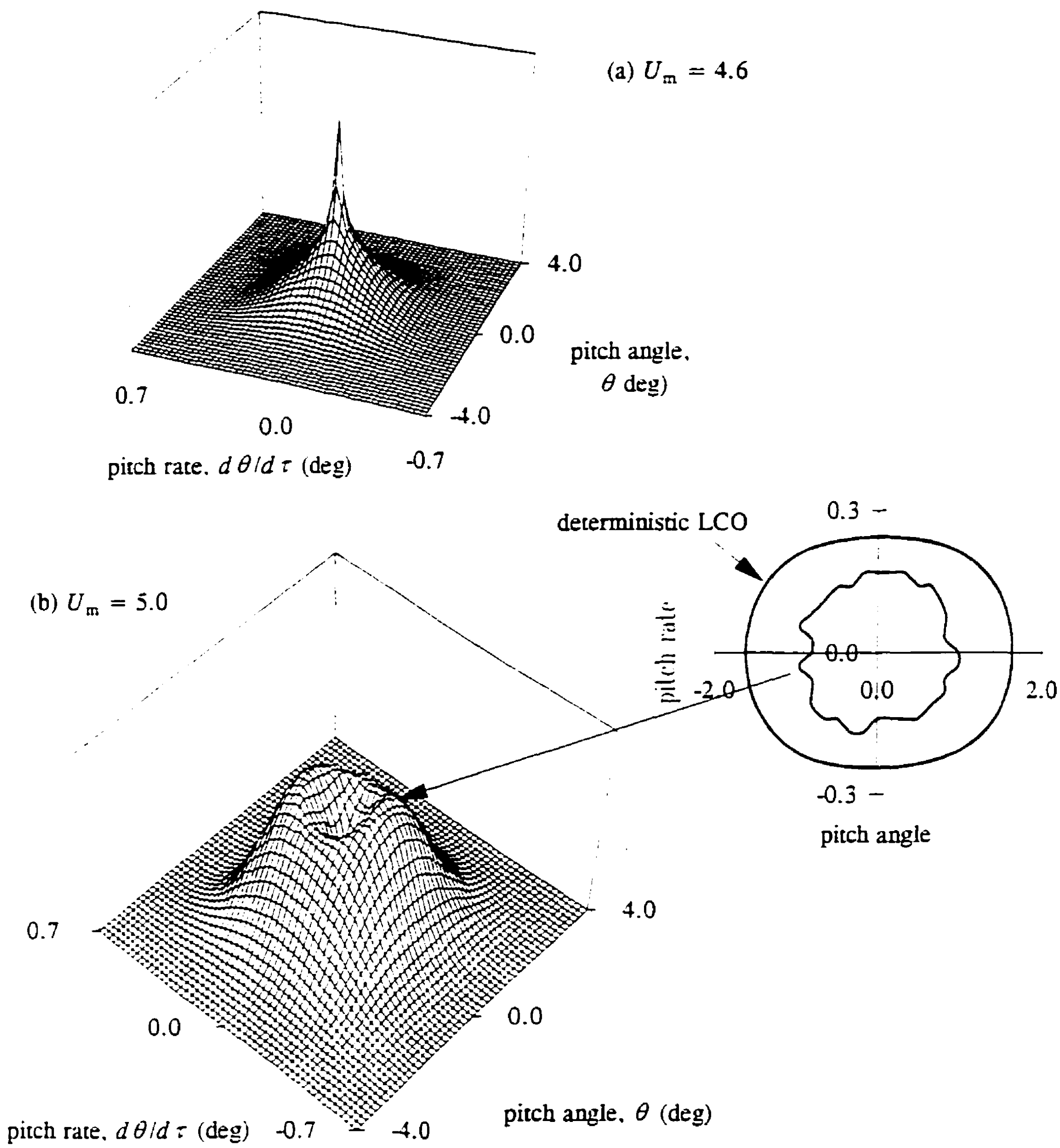

Figure 4.6 - PDFs in pitch pitch-rate with pure longitudinal turbulence; $\sigma_T^2 = 1.0$, $L = 50.0$, $k_3 = 400.0$; (a) for second region, $3.64 \le U_m \le 4.75$; (b) for third region, $4.75 \le U_m$.

4.3.2 Motion types and characteristics

The first region, $U_m \le U_{m1} = 3.64$, represents an equilibrium point in the deterministic sense, or a *deterministic fixed point* since it is characterized by a flat density, indicating no dynamics.

Not shown here, but for the pure PDF the Dirac delta function indicates that the equilibrium point is at zero pitch angle. The second region, $U_{m1} = 3.64 \leq U_m \leq U_{m2} = 4.75$, is denoted by a sharp single peaked PDF, with some diffusion about its mean which occurs at zero pitch angle. Notice that the basic topology of the single peaked dynamics remains unchanged between the marginal and bi-dimensional PDFs. Extending the notion of dimensionality of deterministic dynamic objects to random ones, the dynamics of the second region is interpreted also as an equilibrium point but in the random sense, hence a *random fixed point*.

It is only in the third region, $U_m \geq U_{m2} = 4.75$, that we recognize the double-peaked shape of the marginal PDF representation, and more specifically the crater-like shape of the bi-dimensional PDF representation, that characterizes the LCO motion. The contour of the density gives the most probable value that the system states will take during the motion. In other words, the system spends most of its time in the vicinity of the crater contour. Looking down the probability density axis of the bi-dimensional PDF, the contour is the random equivalent of the non-excited LCO in the phase plane. The apparent irregularity of the contour is due to the finite size of the sample ($N = 40{,}000{,}000$). Increasing the sample size would give a smoother contour. The third region represents a *random limit cycle oscillation.*

Time history and frequency content aspects

To gain a better physical insight the dynamics is now discussed from the perspective of a time history. It has obvious limitations for a random process, but is a more familiar conceptual tool. Also discussed is the frequency content of the response. Figure 4.7 compares the motion of the random fixed point and LCO. The data presented is for steady state motion, in the probabilistic sense.

The time history of the motion of the stochastic fixed point (shown in Figure 4.7 (a)) indicates sustained dynamic behaviour, but no fully developed oscillations. It is only in the third region, defining the random LCO (Figure 4.7 (b)), that the response demonstrates *fully developed* periodic oscillations, an expression apparently introduced by Stratonovich [1967] and later adopted by Yoon and Ibrahim [1995]. However, the distinction between the two types of oscillation is not clear in the time domain, and we must refer to the PDF for a clean demarcation.

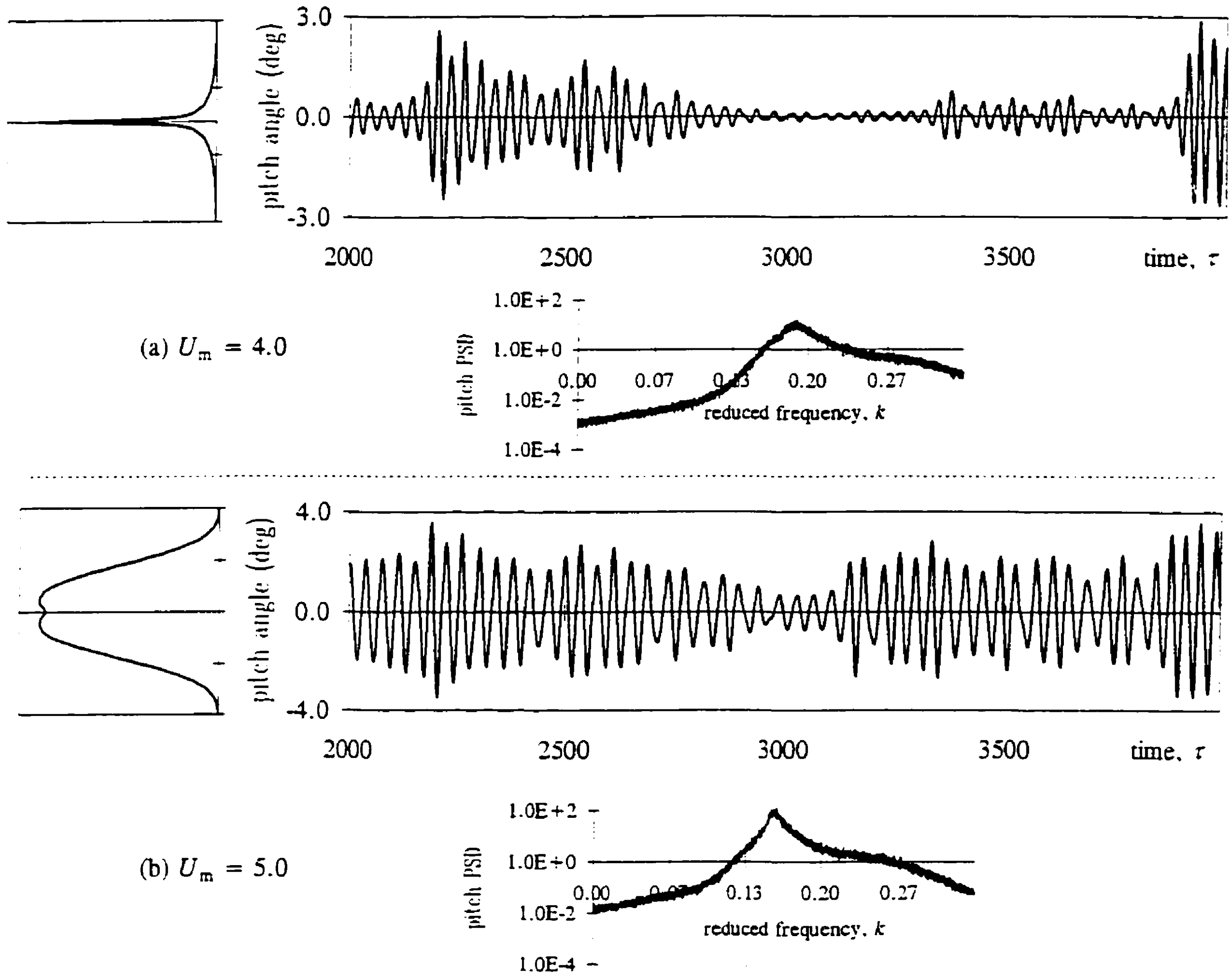

Figure 4.7 - Pitch dynamics of the nonlinear airfoil in pure longitudinal turbulence; $\sigma_T^2 = 1.0$, $L = 50.0$, $k_3 = 400.0$; (a) random fixed point, $U_{m1} < U_m < U_{m2}$; (b) random LCO, $U_m > U_{m2}$.

The description of the time history becomes even more blurry if one considers a fourth type of dynamic behaviour, introduced and labelled ***uncertain motion*** by Yoon and Ibrahim [1995][4], which appears for airspeeds very close to the first bifurcation point at U_{m1}. As they put it, the motion is characterized by an on-off intermittency type behaviour. For example, as shown in Figure 4.8 at $U_m = 3.7$ (recall $U_{m1} = 3.64$), localized bursts of relatively large amplitude arise and then die out. These are followed by long periods of no visible motion before any dynamics become visible again.

4 In their work, Yoon and Ibrahim modelled the parametric excitation as a narrow band centred at one of the system natural frequencies.

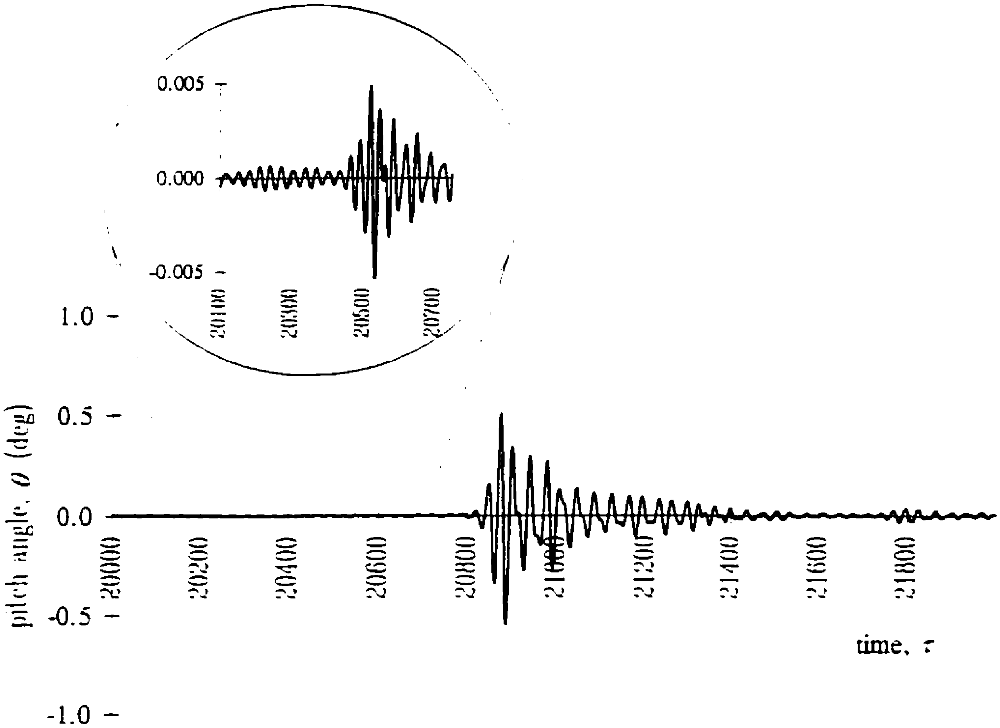

Figure 4.8 - Sample time history of the pitch motion of the nonlinear airfoil in pure longitudinal turbulence; $\sigma_T^2 = 1.0$, $L = 50.0$, $k_3 = 400.0$, $U_m = 3.7$.

The key word is "visible", since changing the scale of the amplitude axis displays dynamics, but at a different scale. In fact, this motion is not qualitatively different than the dynamics of the random fixed point, in the sense that it is represented by a sharp single peaked PDF. Essentially, the origin of this behaviour is the fluctuations in the parameters, which in the close vicinity of the bifurcation point makes the system alternate between momentary stability and instability. The same fundamental phenomenon occurs at higher mean airspeeds, but is not as preponderant. Accordingly, our results suggest that the notion of uncertain motion is questionable in the theoretical description of the system long term dynamics, although it may have some practical significance.

Another common perspective of the steady state dynamics is provided by examining the frequency content of the signal. Again, no fundamental difference is noted between the random fixed point and LCO. We note, however, a sharper peak in the PSD of the LCO, i.e. for $U_m > U_{m2}$, a sign of a more dominant periodic oscillation, as observed in the time histories. A similar observation has been noted by Fronzoni et al. [1987] for a two-dimensional system.

4.3.3 Bifurcation types

In this section, the nature of the two bifurcation points is discussed. We start with U_{m1} which separates a region with no dynamics from another region where there is sustained motion as given by the response mean-square. Figure 4.9 demonstrates that U_{m1} appears to be insensitive to the nonlinearity in the system. It then seems rational to associate U_{m1} with a *D-bifurcation.*

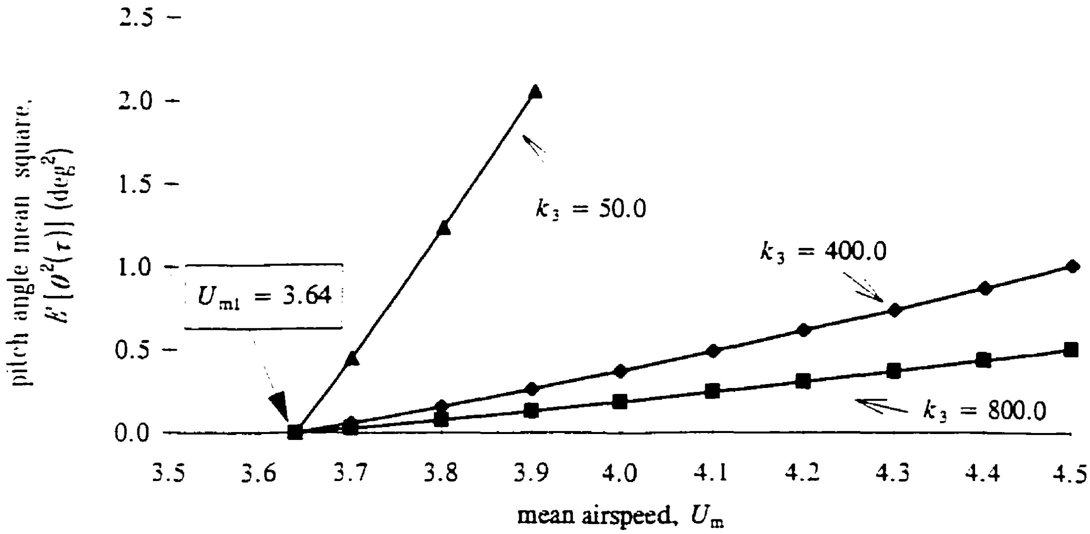

Figure 4.9 - Longitudinally excited pitch response mean-square for different magnitudes of nonlinearity of the airfoil; σ_T^2 = 1.0, L = 50.0.

This conclusion is affirmed by the largest Lyapunov exponent, which exhibits a discontinuity at U_{m1}, see Figure 4.10. Recall that the strict definition of the D-bifurcation requires a change of sign of the largest Lyapunov exponent. In Figure 4.10, there is no change of sign per se because we are calculating λ_{max} about the new stable bifurcating nonlinear solution. For the linear airfoil λ_{max} becomes positive at exactly the same airspeed, thus confirming that U_{m1} represents a D-bifurcation. Since U_{m1} is purely defined by the linearized system, and having argued earlier that flutter is a linear instability mechanism, we suggest that from an aeroelastic perspective U_{m1} may be interpreted as the *random flutter point.*

Note that the largest Lyapunov exponent has been re-normalized by multiplying it by U_m/σ_T in order to get rid of its artificial direct dependence on airspeed, a consequence of our choice of non-dimensional parameters (recall that the unit of λ_{max} is 1/time, and time in the standard non-dimensional space is $\tau = U^*_m\, t/b$). This change enables a better physical insight on the interpretation of the behaviour of λ_{max}. Automatically, the tendency of λ_{max} to go to zero at lower airspeeds appears. This is a direct consequence of neglecting structural damping. The damping is solely provided by the aerodynamics.

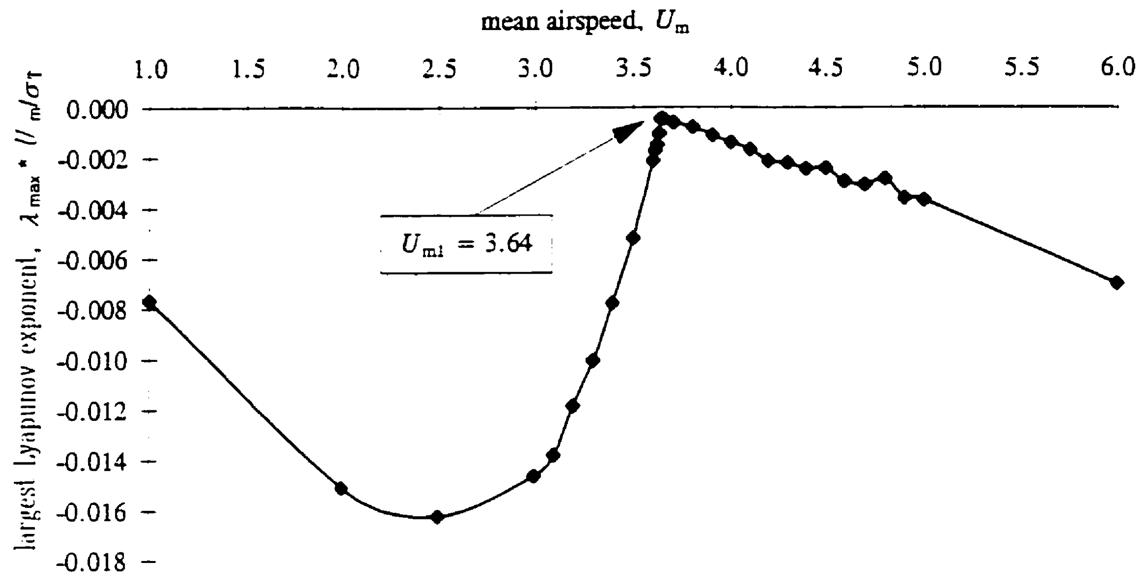

Figure 4.10 - Largest Lyapunov exponent for the longitudinally excited airfoil;
$\sigma_T^2 = 1.0$, $L = 50.0$, $k_3 = 400.0$

No discontinuity in the behaviour of the largest Lyapunov exponent is observed at U_{m2}[5]. Accordingly, we conclude that the qualitative change in dynamic behaviour observed at U_{m2}, defined by a change of shape of the PDF from uni- to bi-modal, is a *P-bifurcation*. We also define U_{m2} as the *onset of the random LCO*. Furthermore, and contrary to the D-bifurcation, the phenomenological bifurcation is a result of the interaction between the noisy and nonlinear nature of the system.

5

This non-vanishing behaviour of the largest Lyapunov exponent for the range of control parameters past the D-bifurcation has also been observed numerically by Shenck-Hoppé [1996] for the noisy Duffing-van der Pol equation in the Hopf scenario, and subsequently discussed on the theoretical and analytical level by Arnold [1998].

We must clarify this last statement since the next graph (Figure 4.11), contrary to intuition, does not indicate a dependence of the P-bifurcation point on the degree of nonlinearity. The onset of the random LCO occurs at $U_{m2} = 4.75$ for all three values of k_3 shown. It is noticed that the effect of changing the magnitude of the nonlinearity is only felt by the pitch angle at the maxima of the marginal PDF. An explanation of this behaviour is found in more simple systems where analytical solutions exist. Take the one-dimensional Landau equation under multiplicative white noise (equation 1.14), which we have generalized for any magnitude of the nonlinear coefficient, k_3:

$$\dot{x} = \lambda x - k_3 x^3 + \sigma x \xi_t \tag{4.1}$$

Following the same procedure as that presented in Chapter 1, the extrema of the steady state PDF are found to be:

$$x = 0, x = \pm\sqrt{(\lambda - \sigma^2/2)/k_3} \tag{4.2}$$

which means that the nonlinear coefficient is required for the existence of the non-zero extrema, but that its magnitude does not affect the point where these extrema first appear on the λ axis. In other words, their existence depends on the system being nonlinear, but their appearance on the control parameter axis, λ, depends only on the noise intensity as defined by $(\lambda - \sigma^2/2)$ which must be positive. The same conclusion can also be derived from a paper by Ariaratnam [1980], where a 1DOF (i.e. two-dimensional) problem is investigated.

We conclude by suggesting that the single-peaked region, between U_{m1} and U_{m2}, is more a property of the longitudinal excitation than a consequence of the nonlinearity. This idea is developed in Chapter 7 where we discuss one effect of longitudinal excitation which is to organize or force the airfoil dynamics to be centred around the origin.

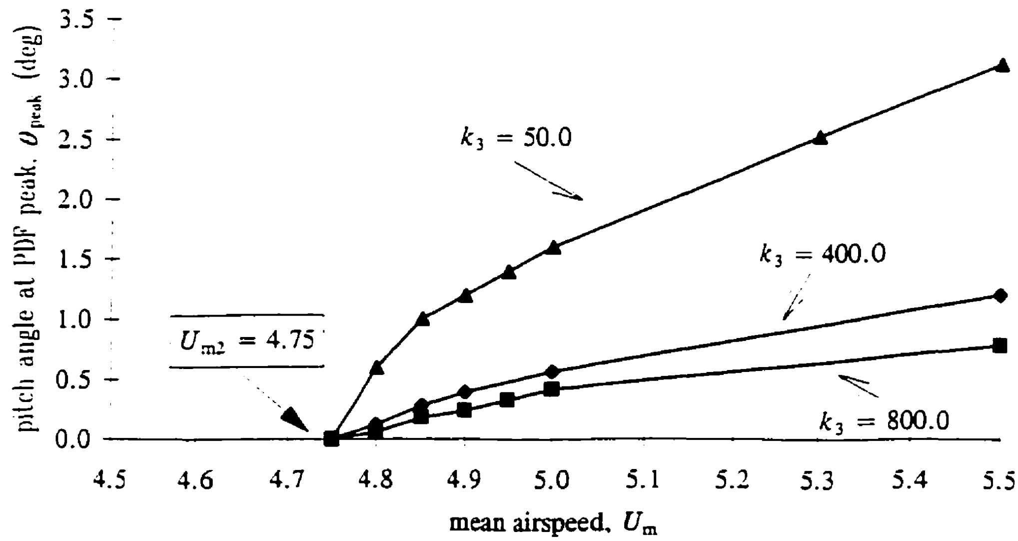

Figure 4.11 - Extrema of the pitch PDF as a function of mean airspeed axis for different magnitudes of nonlinearity of the airfoil in pure longitudinal turbulence; $\sigma_T^2 = 1.0$, $L = 50.0$.

As a last point on the discussion of the bifurcation type, we wish to mention that there does not seem to exist a consensus, yet, on the meaning of the Hopf bifurcation in the random, or stochastic, sense. For example, and symptomatic of the debate between dynamicists and physicists, the former use the term *stochastic Hopf bifurcation* to describe the complete two-step bifurcation scenario [Arnold, 1996 and 1998]. On the other hand, P-bifurcation advocates such as Levefer and Turner [1986] or Fronzoni et al. [1987] tend to use *stochastic Hopf bifurcation* to strictly define the second bifurcation (P-bif.).

4.3.4 Bifurcation shift

The bifurcation landscape can be represented in a different manner by plotting the steady state motion mean-square and the location of the peak of the marginal PDFs a function of mean airspeed, and in comparison with the unique deterministic flutter/Hopf bifurcation point at $U_f = 4.31$. We want to draw two conclusions from Figure 4.12. One is that the random flutter point is advanced with respect to the deterministic flutter speed, occurring at $U_{m1} = 3.64$ for this particular case. The second is that the onset of the random LCO is postponed, occurring at $U_{m2} = 4.75$.

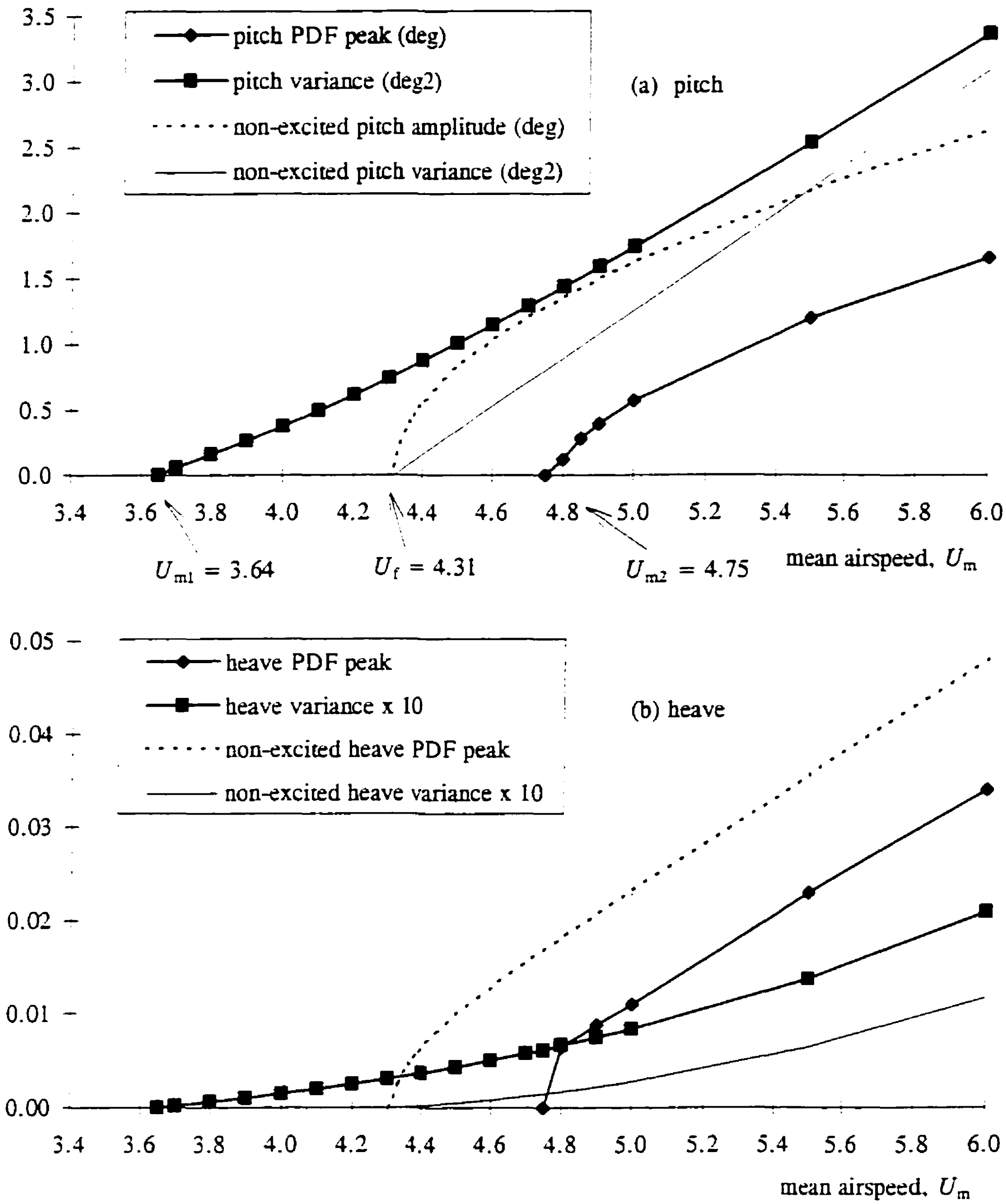

Figure 4.12 - Bifurcation diagram for the non-excited and longitudinally excited nonlinear airfoil as represented by the pitch (a) and heave (b); $\sigma_T^2 = 1.0$, $L = 50.0$, $k_3 = 400.0$.

These two conclusions are generalized to other values of turbulence characteristics. Figure 4.13 shows that regardless of the turbulence variance and scale, the flutter point is always advanced and the LCO onset is always postponed in pure longitudinal turbulence excitation. The mechanisms of the advancement of the flutter point will be discussed in Chapter 5.

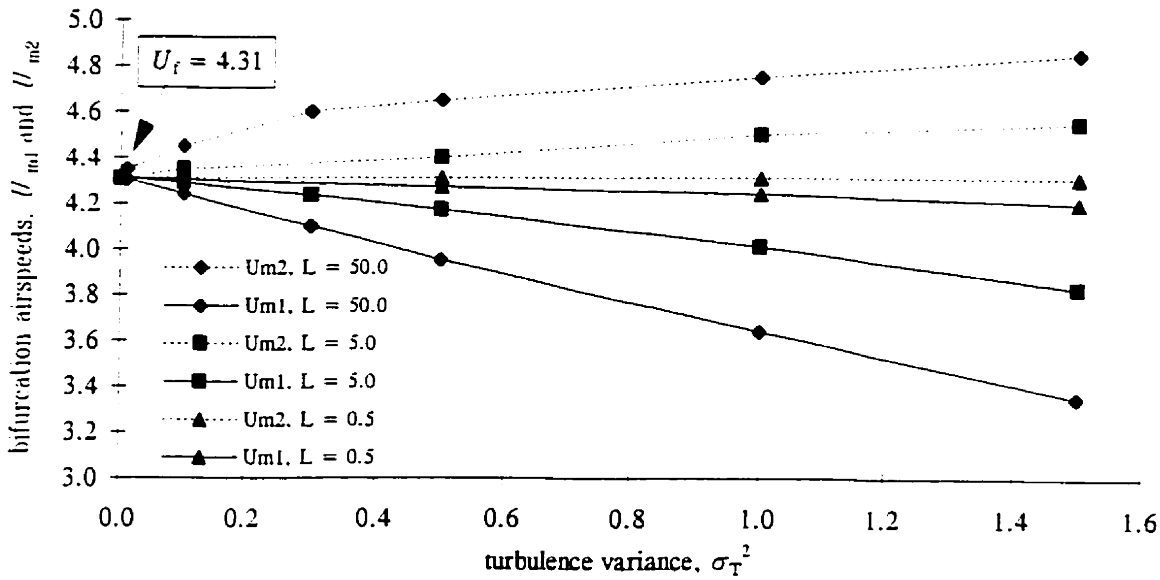

Figure 4.13 - D- and P-bifurcation airspeeds of the longitudinally excited nonlinear airfoil as a function of turbulence variance and for different values of scale of turbulence; $k_3 = 400.0$.

4.4 Pure Vertical Turbulence Excitation

In this section, we analyse the case where the vertical component of turbulence is considered and the longitudinal component is disabled, that is $w_T \neq 0$ and $u_T = 0$. The airspeed does not vary in time, hence it is kept constant. In the more general mechanical context, this problem is equivalent to an externally forced system without any parametric excitation.

4.4.1 Preamble

In contrast with the previous case, the visualisation of the PDF of the nonlinear airfoil motion excited by vertical turbulence does not provide a straightforward picture of the bifurcation scenario. The reason is that the airspeed at which a transition is observed in the PDF depends on which state(s) is considered. This is so for either the one-dimensional, marginal, PDF or the bi-dimensional projection, as exemplified by Figures 4.14 and 4.15, respectively.

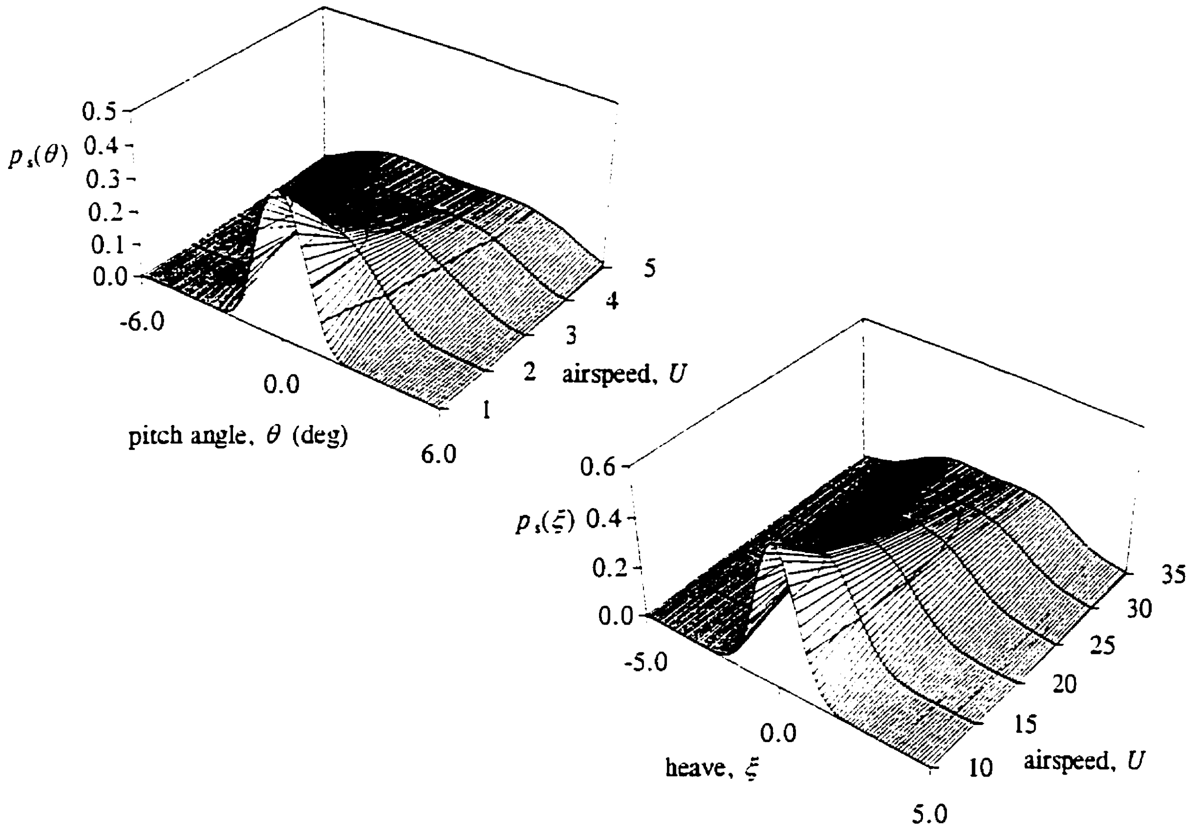

Figure 4.14 - Marginal PDF diagrams of the airfoil pitch angle and heave displacement in pure vertical turbulence, as a function of airspeed; $\sigma_T^2 = 1.0$, $L = 50.0$, $k_3 = 400.0$.

From Figure 4.14, we observe that the pitch transitions at a much lower airspeed than the heave. In fact, the pitch angle transitions from a uni- to a bi-modal PDF at $U = 3.6$, while the heave displacement experiences the same type of transition but at a much higher airspeed, given by $U = 30$. Although not shown, it should be noted that the pitch-rate and heave-rate marginal PDFs also exhibit a uni- to a bi-modal transition, and also at different airspeeds. We also retain from Figure 4.14 that, contrary to pure longitudinal turbulence, the probability density landscape exhibits only one transition point, since only two different density shapes are observed.

Similarly for the bi-dimensional PDF projection, we have noted different transition airspeeds between different states. For example, and using the same system parameter values and turbulence conditions as for Figure 4.14, we have found that the pitch pitch-rate bi-dimensional PDF transitions at $U = 4.1$, while the heave heave-rate density changes at a much higher airspeed. Figure 4.15 shows that at $U = 4.30$, an airspeed just before the deterministic flutter point, the pitch pitch-rate PDF is bi-modal, whereas the heave heave-rate has a uni-modal bell shape.

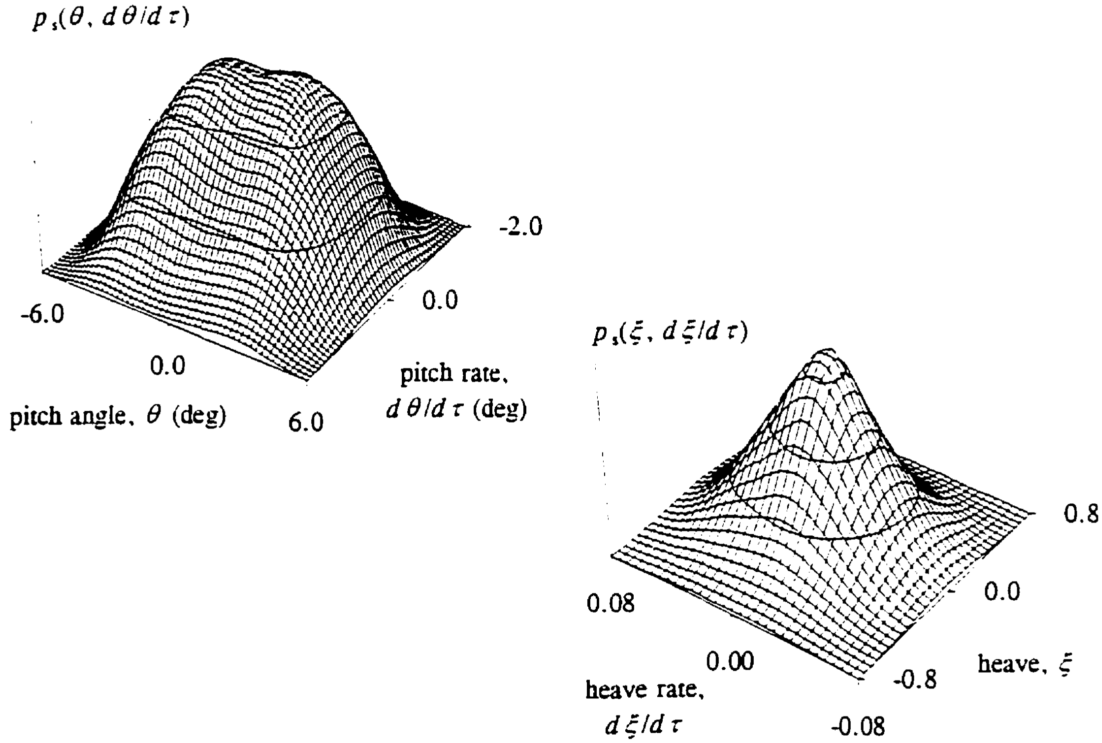

Figure 4.15 - Bi-dimensional PDF of the airfoil pitch pitch-rate and heave heave-rate in pure vertical turbulence for $U = 4.30$; $\sigma_T^2 = 1.0$, $L = 50.0$, $k_3 = 400.0$.

Since we are fundamentally restricted to a bi-dimensional PDF projection, our ability to obtain a global perspective of the airfoil dynamics as exhibited by its probability density is limited. In this respect, there is room for interpretation, especially concerning the location of bifurcation point on the airspeed axis.

Accordingly, to make the analysis tractable we have chosen to base our interpretation of the bifurcation on the dynamics of the pitch DOF. In support of this approach are the following arguments. One argument is the observation of the non-excited pitch dynamics which behaves as a function of airspeed very similarly to the radial component of the Hopf bifurcation normal form. We have attributed this behaviour to the location of the nonlinearity which acts directly on the pitch DOF. Another argument is based on the vertically excited airfoil PDFs. The densities exhibit transition in pitch and pitch-rate at values of airspeed which appear to be physically much more representative of the bifurcation point than the heave and heave-rate transition airspeeds. Consequently, we are lead to believe that the random bifurcation scenario is dictated in a large part by the pitch DOF.

Another important limitation imposed on us is the relatively fragile theoretical foundations of nonlinear dynamics when the system is subject to additive noise. This is reflected by the contradictory results found in the literature. Some of them will be discussed at the end of this section. Surprisingly, the multiplicative noise problem appears to have reached a higher level of maturity in its theoretical treatment. Nevertheless, some aspects of the bifurcation scenario can still be addressed with a degree of certainty. Speculative interpretations will be suggested for other aspects which cannot be demonstrated clearly.

Before discussing our results further, we believe it is relevant to first describe the expected dynamics. This is done in order to facilitate the analysis of the results, which, as described above, do not lend themselves to a straightforward interpretation. What we are looking for is basically a bell-shaped (Gaussian like) bi-dimensional PDF at pre-flutter airspeeds, representing a fixed point, and a crater-like shape at post-flutter airspeeds characterizing the random LCO. The equivalent representations in the marginal PDF projection are respectively uni- and bi-modal shapes.

Note from Figure 4.15 that the bell-shaped curve, shown in the heave response for example, corresponds to our expectations. We cannot say the same for the two-peaked shape displayed by the pitch pitch-rate bi-dimensional PDF, since this distribution does not correspond to either a fixed point or an LCO. We will discuss this in the next sub-section.

4.4.2 The P-bifurcation

We have found that under vertical turbulence, the bifurcation scenario depends on the turbulence level. The discussion is divided along this line. There are the low and the high turbulence level cases.

4.4.2.1 Case 1 - low turbulence level

For low values of turbulence variance, the bifurcation scenario is represented in Figure 4.16. At pre-bifurcation airspeeds, we are able to distinguish a uni-modal bell-shaped bi-dimensional PDF which bifurcates directly into a crater-like shaped density. In this example, the pitch pitch-rate bi-dimensional PDF transitions at $U = 3.9$.

The observed density shapes correspond to our expectations. First, the unequivocal uni-modal bell-shaped bi-dimensional PDF is interpreted as a *random fixed point,* since the motion is distributed about the origin. Notice however that its topology is different than for the random fixed point in longitudinal excitation, since for the latter the random fixed point has a sharp peak. The bell shape of this random fixed point is a direct contribution of the external forcing Gaussian distribution. Second, after the bifurcation point, we recognize the expected crater-shaped PDF representing a random LCO. It remains crater-like for higher airspeeds, without changing into a two-peaked shape.

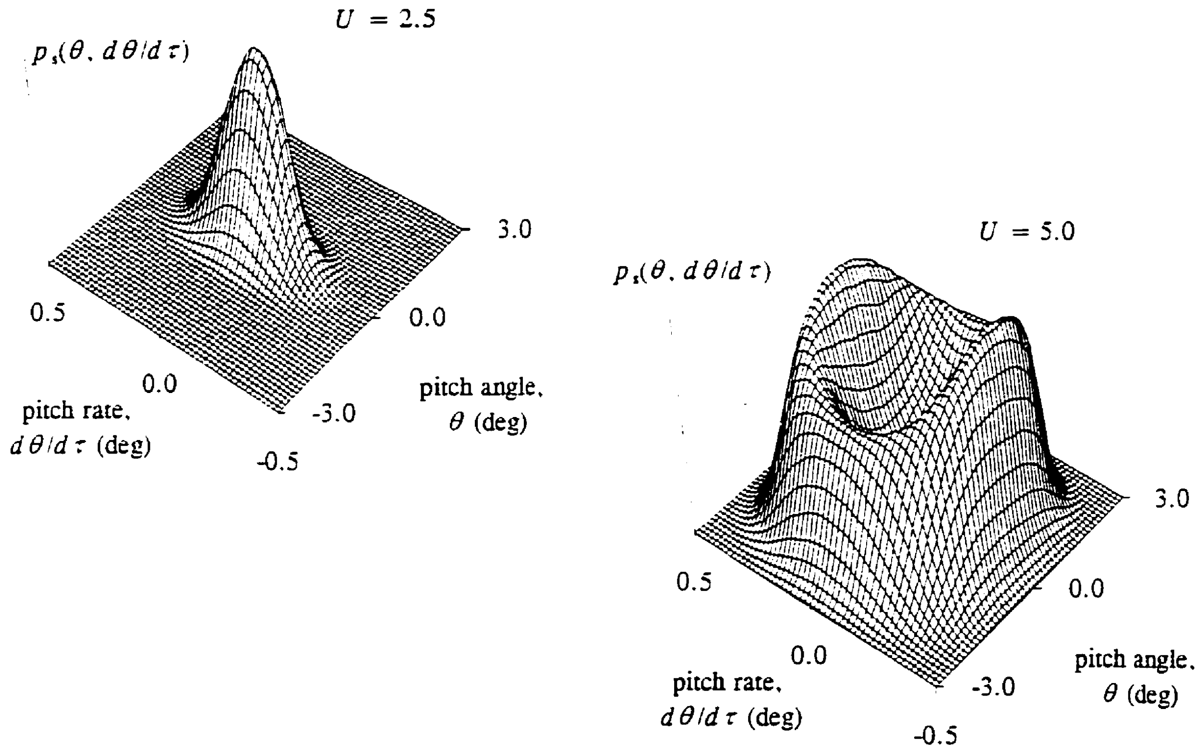

Figure 4.16 - Bi-dimensional PDF of the airfoil pitch pitch-rate in pure vertical turbulence at $U = 2.5$ and $U = 5.0$; $\sigma_T^2 = 0.01$, $L = 50.0$, $k_3 = 400.0$.

For this particular nonlinear airfoil and scale of turbulence, this bifurcation scenario is retained up to a turbulence variance, $\sigma_T^2 = 0.06$. For higher turbulence levels, the bifurcation changes to the case described in sub-section 4.4.2.2.

4.4.2.2 Case 2 - high turbulence level

The fundamental difference at high values of turbulence variance concerns the shape of the probability density at post-bifurcation airspeeds. In this case, the crater shape disappears in favour of a two-peaked bi-dimensional PDF. This is illustrated in Figure 4.17 for a turbulence variance, σ_T^2 = 0.1 and airspeed, U = 5.0. Note that the pre-bifurcation bi-dimensional PDF (shown for U = 2.5) has the expected bell shape.

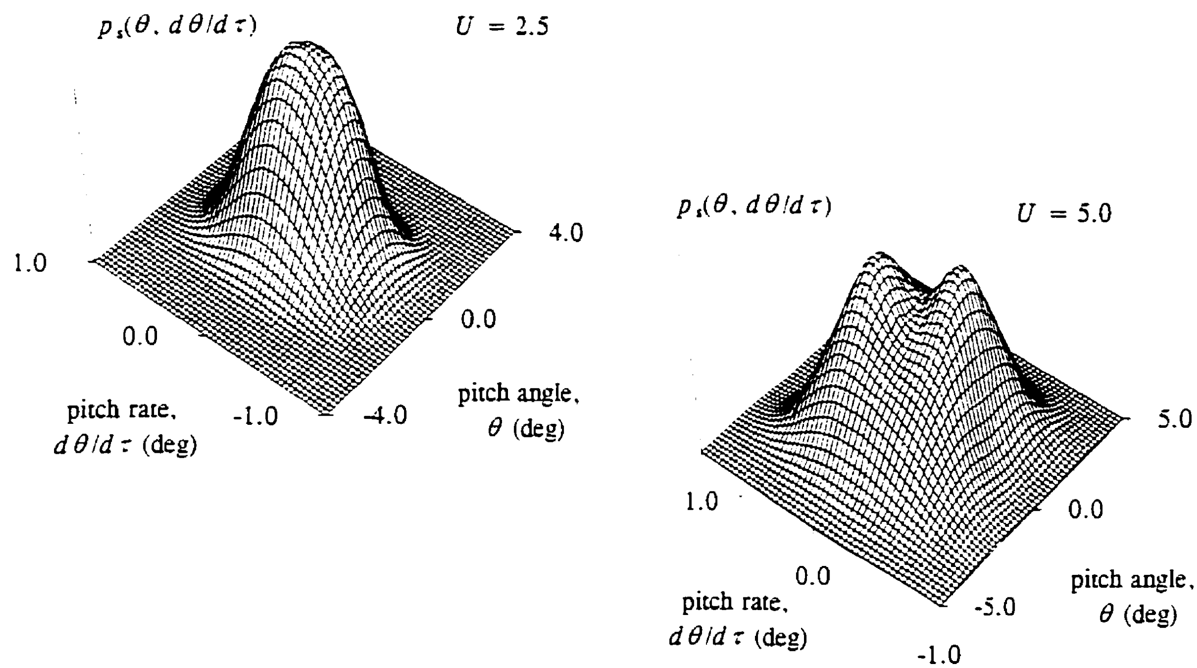

Figure 4.17 - Bi-dimensional PDF of the airfoil pitch pitch-rate in pure vertical turbulence at U = 2.5 and U = 5.0; σ_T^2 = 0.1, L = 50.0, k_3 = 400.0.

At this turbulence variance, the pitch pitch-rate PDF transitions at U = 3.0. For higher airspeeds we have tried to find a crater, indicative of an LCO in its random form, with no success. In fact, the bi-dimensional PDF exhibits a very complex picture at the higher airspeeds, which we attribute to the contamination of the expected LCO dynamics by other types of underlying deterministic dynamic behaviour. Hence, the salient features of the post-bifurcation high turbulence level dynamics, as represented by the pitch pitch-rate bi-dimensional PDF, are the two peaks, with a saddle appearing at the origin instead of the expected crater.

We further argue that for large values of excitation variance, vertical turbulence destroys the LCO. The destructive effect of turbulence is reinforced by, or associated with, a greater contribution of super-harmonics and a skewing, and deformation, of the otherwise well behaved elliptical shape of the underlying deterministic LCO. We will discuss these aspects in detail in Chapter 6 and show that this behaviour can be attributed to large nonlinear effects.

4.4.2.3 Loss of the D-bifurcation

For both cases, low and high turbulence levels, it is demonstrated that the nature of the bifurcation is of the P-type by showing that it is not of the D-type. Figure 4.18 displays no discontinuous behaviour of the largest Lyapunov exponent as a function of airspeed. Consequently, there is no dynamical bifurcation according to its definition [Arnold, 1998]. It is a *phenomenological bifurcation*. In support of this argument, we also add that some authors [Leng et al., 1992] have shown that for simple systems under external noise, a qualitative change in the PDF was not indicated by a discontinuity in the Lyapunov exponent.

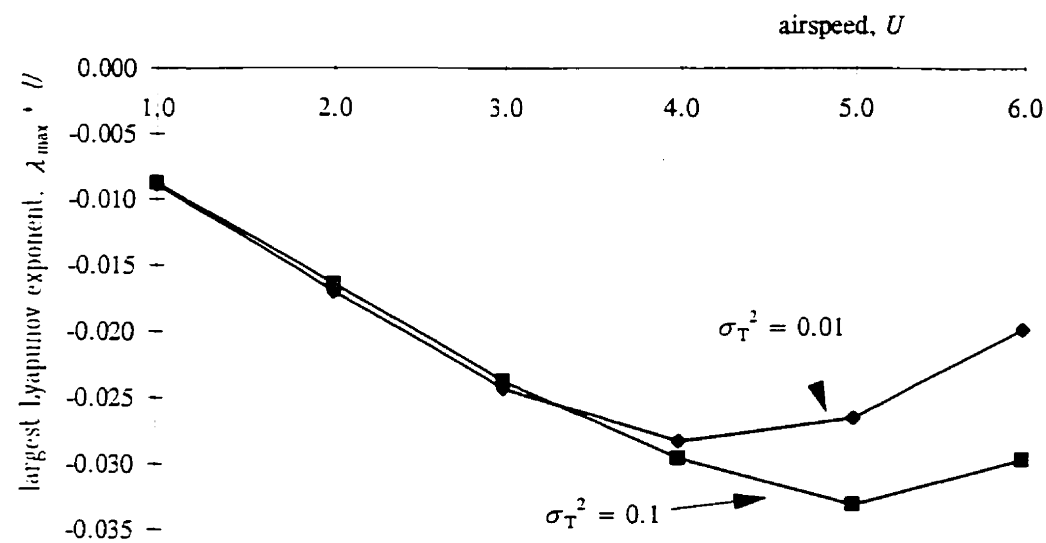

Figure 4.18 - Largest Lyapunov exponent for the vertically excited nonlinear airfoil as a function of airspeed, for two values of turbulence variance; $L = 50.0$, $k_3 = 400.0$.

We can further interpret this last observation by stating that under additive noise the D-bifurcation of the underlying deterministic system appears as a P-bifurcation. We also note that strictly speaking for a nonlinear aeroelastic system the loss of the D-bifurcation indicates that the flutter point no longer exists. This is a consequence of the combined effect of the nonlinearity and the vertical turbulence. This argument does not hold for the linear system, as will be shown in Figure 7.1, since in this case the dynamical bifurcation (D-bif.) exists.

On the question of the location of the P-bifurcation point on the airspeed axis, we can only speculate. Unfortunately, we have no means to provide any definitive remarks since the airspeed at which the pitch and heave PDFs structure changes do not coincide. Moreover, and as mentioned earlier, conflicting results appear in the literature. Nevertheless, our results based on the pitch dynamics suggest that the P-bifurcation is advanced by vertical turbulence in comparison with the non-excited flutter/Hopf bifurcation.

4.4.3 Literature survey - Contradictory results

In light of the uncertainties discussed above, we add that no fully satisfying answer can be obtained from the theoretical literature. As introduced in Chapter 1 we found contradictory results on the two issues of the location of the bifurcation point and of the type of motion (as exhibited by the PDF) after the bifurcation. For example and in partial support of our findings, Schimansky-Geier et al. [1985] and Ebeling et al. [1986] reported analytical results, verified by computer simulations, of two-dimensional nonlinear systems experiencing a Hopf bifurcation in the deterministic case. Under additive white noise excitation they observed a two-step bifurcation with three types of dynamic behaviour. For low values of the control parameter they argued that the system exhibited a single probability density maximum at the origin. At a larger value of the control parameter, but lower than for the deterministic Hopf bifurcation, the bi-dimensional PDF showed two off-centred maxima and a saddle point at the origin. For still larger values of the control parameter, greater than for the deterministic Hopf bifurcation, a crater appeared. On the contrary, Schenk-Hoppé [1996] reports only two different types of qualitative behaviour for the same type of problem. The bell-like shape of the Duffing-van der Pol equation excited by additive white noise bifurcates directly into a crater-like shape, and apparently at the same value of control parameter as the deterministic Hopf bifurcation.

Other results of simple systems which re-enforce the interpretation of an advancement of the P-bifurcation point by additive noise are the following. As mentioned in Chapter 1, Lugiato et al. [1989] have discussed the case of a one-dimensional system, excited by pure additive coloured noise, which exhibits an early transition from a uni- to bi-modal shape. In their case the shift is attributed to the colour of the noise. The physical rationale is the following. Consider the colour of the noise being related to the scale of turbulence, hence its correlation time (recall the relationship between scale of turbulence and correlation time discussed in Chapter 2), such that the larger its correlation time in comparison with the system time scales, the slower the fluctuating response returns to its deterministic stationary value. This enables the system to remain for a relatively long period of time away from its non-excited solution, say at the origin, thus giving rise to a bi-modal PDF centred at this value. Longtin et al. [1990] finds the same behaviour for a single variable delay-differential equation. A similar observation can also be deduced from the theoretical work offered by Sri Namachchivaya [1988] on the noisy Hopf bifurcation. In this last work, Sri Namachchivaya does not specifically address the bifurcation point, but shows that the extrema of the motion is not zero at values of the control parameter smaller than the deterministic point.

In contrast to the observations discussed above, with regards specifically to the influence of additive noise on the P-bifurcation are the following. Knoblock and Wiesenfiel [1983], Schumaker [1987] and Mackey et al. [1990] discuss basically the same problem of the normal form of either the pitchfork or Hopf bifurcation for a system under additive white noise. They all argue that the additive noise excitation does not shift the point on the control parameter axis where a qualitative change in PDF is observed. Their argument however is questionable in the sense that their derived normal form is expressed as a one-dimensional system, similar to the deterministic case, with an additive white noise term. Recall that we have discussed in Chapter 1 that such a system (one-dimensional under additive white noise) did not allow for a shift in bifurcation point. It then makes sense that given their derived normal form, their interpretation does not support a shift due to additive noise of a higher dimensional system. The more puzzling result, however, comes from Schenk-Hoppé [1996] which, as discussed earlier, suggests that the bell-shaped PDF bifurcates at the same point as the deterministic case. He obtains this result, not by reducing his system to its normal form, but by calculating the two-dimensional stationary Fokker-Planck equation.

With regards to the location of the P-bifurcation point, we cannot explain the contradiction between Schenk-Hoppé's [1996] result on one hand and the results from Schimansky-Geier et al. [1985], Ebeling et al. [1986], Sri Namachchivaya [1988], Lugiato et al. [1989] and Longtin et al. [1990] on the other hand. We can only say that our results seem to better match the latter.

However, in terms of the PDF shape, and specifically in reference to the works of Schimansky-Geier et al. [1985], Ebeling et al. [1986] and Schenk-Hoppé [1996], we can offer the following interpretation in light of our results. We believe that the two-step bifurcation observed by the two former works is shown in our case as a one-step bifurcation for the following reason. Consider our problem with the turbulence variance $\sigma_T^2 = 0.1$ shown in Figure 4.17. The bell-shaped PDF bifurcates directly into a two-peaked PDF, and remains two-peaked for higher airspeeds. Hence, contrary to the reference works, the two-peaked PDF does not change into a crater-like PDF as the control parameter is increased. In their case, the external forcing depends only on the noise level, which remains constant as the control parameter is varied. However, for the airfoil problem, although we keep the turbulence level constant with airspeed, the aerodynamic forcing due to vertical turbulence increases with airspeed (this will be discussed in more detail in Chapter 6). It has the effect that the two-peaked PDF cannot transform into a crater-like shape at higher airspeeds.

We also believe that in light of our results, the results of Schimansky-Geier et al. [1985] and Ebeling et al. [1986] on one hand, and Schenk-Hoppé [1996] on the other, can be reconciled, in so far as the PDF shape is concerned. We argue that it is likely that the latter could have exhibited a two-peaked PDF instead of a crater-like PDF given a larger noise level.

4.5 Combined (Vertical and Longitudinal) Turbulence Excitation

In discussing the combined turbulence excitation problem ($w_T \neq 0$, $u_T \neq 0$), we intend to show that the bifurcation scenario of the nonlinear airfoil is largely determined by the vertical component of turbulence. This is the main result of this section. It enables us to draw a number of conclusions regarding the bifurcation in combined turbulence, from the analysis of the pure vertical excitation. Hence, we cannot interpret the behaviour of the combined model as the simple addition (qualitative or quantitative) of the contribution of the two separate excitations. One rationale is that the principle of superposition (used in a conceptual sense) does not hold for this problem. It does not hold for two reasons. One, is that the system is nonlinear, and secondly, one of the excitation is parametric. Another rationale is that the two turbulence components act on the airfoil in two fundamentally different ways. The vertical component acts as an external forcing, hence it directly affects the response of the airfoil, while the longitudinal components acts on its parameters, hence, affecting its stability. With this aim in mind, we proceed by simply comparing the PDFs and the behaviour of the largest Lyapunov exponent for the three cases of excitation.

4.5.1 PDF representation

The marginal PDF in pitch for the combined turbulence case is shown in Figure 4.19.

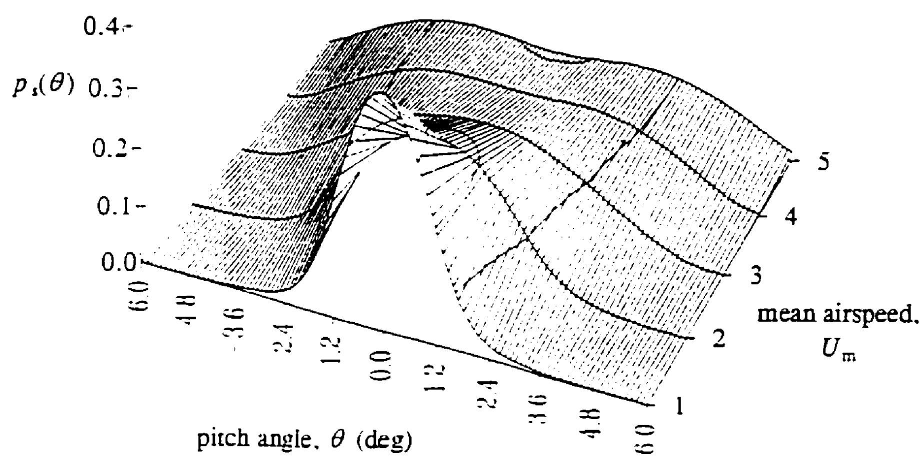

Figure 4.19 - Marginal PDF diagram of the pitch angle for combined turbulence excitation, as a function of airspeed; $\sigma_T^2 = 1.0$, $L = 50.0$, $k_3 = 400.0$.

Comparing Figure 4.19 with Figure 4.5, for pure longitudinal turbulence, and Figure 4.14, for pure vertical turbulence, it is clear that the pure vertical and the combined turbulence excitation cases have the same qualitative behaviour. We have noted the same similarity for the other airfoil states, as well as with the bi-dimensional PDF projection.

From this point of view, the only difference between the pure vertical and combined excitation is quantitative. As we will discuss in more detail in Chapter 7, the combined excitation displays a shift in airspeed of the transition from a uni- to a bi-modal PDF compared with the pure vertical turbulence excitation problem. We attribute the shift to a destabilisation effect of longitudinal turbulence. The logic is the following. A decrease in the stability of the airfoil induces a greater response to the vertical excitation, which in turn puts a greater demand on the nonlinearity, thus a shift in transition airspeed.

4.5.2 Largest Lyapunov exponent

The other important measure for the bifurcation is the largest Lyapunov exponent. It is shown in Figure 4.20 for three cases of excitation and for the non-excited airfoil.

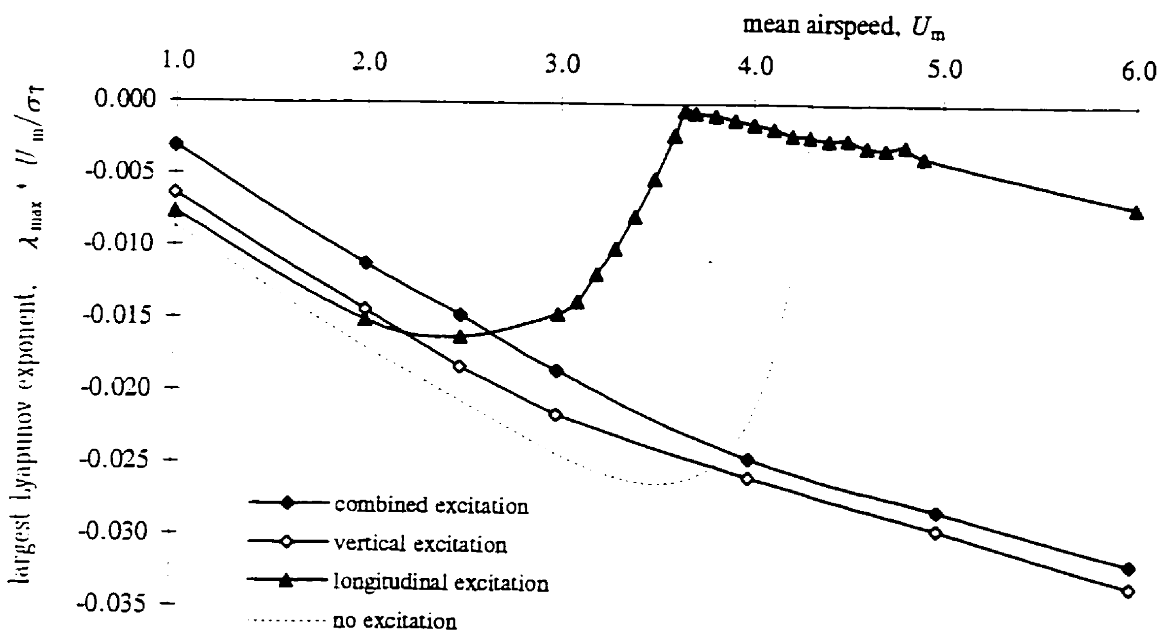

Figure 4.20 - Largest Lyapunov exponent for pure longitudinal, pure vertical and combined turbulence, and non-excited cases, as a function of airspeed; $\sigma_T^2 = 1.0$, $L = 50.0$, $k_3 = 400.0$.

We notice that the D-bifurcation that exists for the pure longitudinal case and for the non-excited problem, does not appear when vertical turbulence is considered. From this point of view, the only difference between the pure vertical and combined turbulence excitation is also quantitative. The dynamics of the nonlinear airfoil in combined turbulent excitation exhibits a largest Lyapunov exponent closer to the zero axis, hence a decrease in stability due to its longitudinal component. From these two series of observations, we conclude that for the nonlinear airfoil the effect of the longitudinal component is relatively minor, whereas the dominant behaviour is determined by the vertical component.

Accordingly, we can summarize the current discussion by stating that our results suggest that the P-bifurcation landscape of the fluttering nonlinear airfoil excited by (combined) turbulence depends on the turbulence level. It is characterized by a bell-shaped PDF representing a random fixed point, bifurcating into either a crater-like PDF for low turbulence variance, or into a two-peaked PDF for high turbulence variance. This is schematized in Figure 4.21.

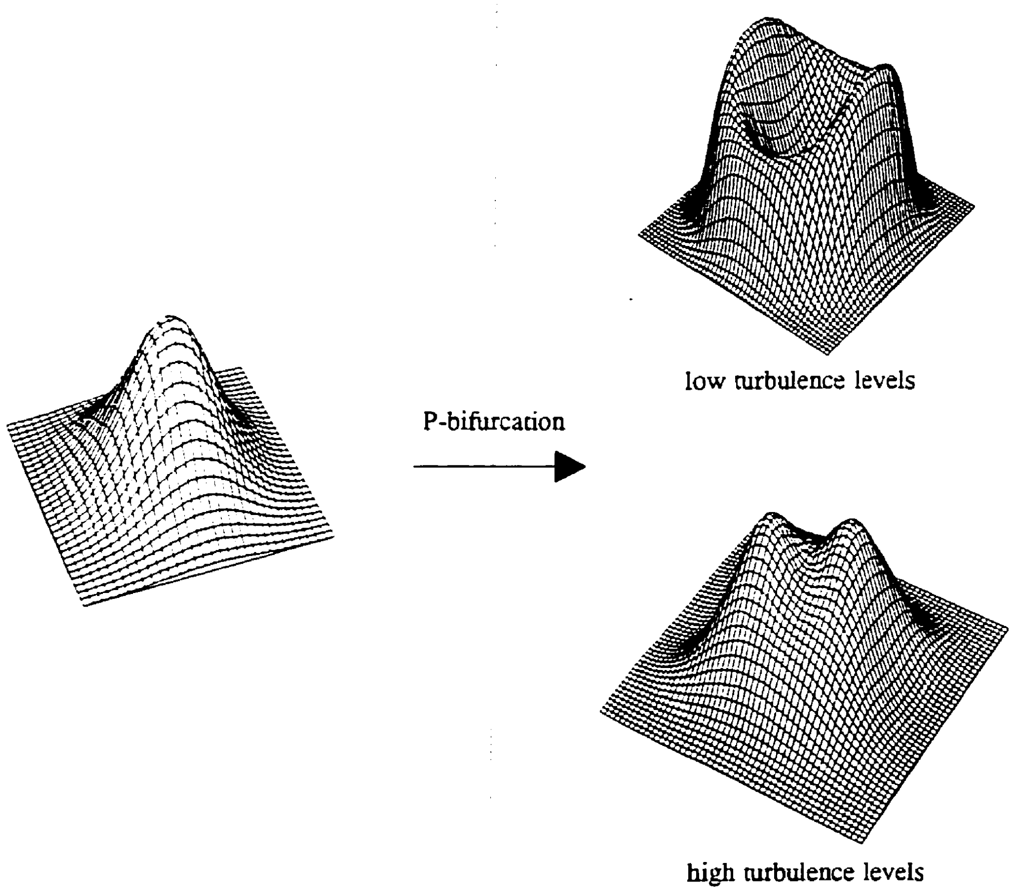

Figure 4.21 - Schematic of bifurcation scenario for nonlinear airfoil in combined turbulence.

4.6 Concluding Remarks

From the preceding analysis, we retain a number of points with regards to the bifurcation scenario of the nonlinear airfoil under (combined) turbulent excitation:

1. The dominant features of the random flutter/Hopf bifurcation scenario are essentially dictated by the vertical component of turbulence, whereas the effect of the longitudinal component appears to be relatively minor in that it decreases the stability of the airfoil, hence, possibly affecting the location of the bifurcation point.

2. Secondly, the bifurcation scenario is characterized by a qualitative change in the PDF, while no discontinuity in the largest Lyapunov exponent is observed. In this sense, the D-bifurcation obtained for the deterministic nonlinear airfoil appears to be transformed into a P-bifurcation. This is a consequence of the vertical component of turbulence. Furthermore, we say that turbulence destroys the D-bifurcation such, that strictly speaking the flutter point no longer exists. This does not apply to the linear airfoil.

3. On the topic of a shift of the P-bifurcation point due to turbulence, we can only speculate. It appears that the P-bifurcation may be advanced. First, with regard to the effect of the vertical turbulence we believe that the early transition of the pitch pitch-rate bi-dimensional PDF represents an advancement of the bifurcation point. This speculative argument is based mainly on the assumption that the bifurcation is determined by the pitch DOF, since this is where the nonlinearity is acting directly, and not on the heave DOF which transitions much later. With regard to the effect of the longitudinal component, the rationale supporting an advancement of the P-bifurcation is a de-stabilisation of the airfoil, which in turn induces larger nonlinear effects. This aspect will be discussed in Chapter 7.

4. The P-bifurcation scenario depends on the turbulence level. It is characterized by a bell-shaped, or uni-modal, PDF transforming into a crater-like shape PDF for low values of turbulence. For higher turbulence levels, the bell-shaped bi-dimensional PDF bifurcates into a two-peaked density, with a saddle at the origin. Furthermore, we say that turbulence

tends to destroy the underlying structure of the deterministic LCO in favour of a new type of motion. This will be discussed in Chapter 6.

With regards specifically to the bifurcation scenario in pure longitudinal turbulence, which is not without significance, we retain three points:

1. The random bifurcation is a two-step bifurcation characterized by, first, a D-bifurcation followed by a P-bifurcation. The dynamic response at airspeeds between the D- and P-bifurcations displays a uni-modal PDF with a sharp peak centred at zero. At post-P-bifurcation airspeeds, the LCO structure is observed via a crater-like shape of the pitch pitch-rate bi-dimensional PDF.

2. The flutter point (D-bifurcation) is advanced, and more generally the stability of the airfoil is decreased. This aspect will be discussed in more detail in Chapter 5 for the flutter point, and in Chapter 7 for the general destabilisation.

3. Longitudinal turbulence has a tendency to force the dynamics to be centred around the origin. This aspect will be discussed in Chapter 7 as an organising effect.

As a last remark, we generalize our findings to a more universal randomly excited nonlinear dynamical system. Since we have determined that the bifurcation scenario of the turbulent excited airfoil is essentially dictated by the vertical component of turbulence, and since in any real system, both multiplicative and additive noise are present, we question the robustness of the bifurcation scenario under pure multiplicative noise. We are then tempted to extend the concept of bifurcation robustness and structural stability applied to deterministic systems (see for example Guckenheimer and Holmes [1990] or Argyris et al. [1994]), and propose that, because both multiplicative and additive noise are present in reality, the bifurcation scenario generally observed for pure multiplicative noise is qualitatively not robust. We go further and argue that this applies regardless of the relative intensity of both noise components, since any small amount of additive noise should destroy the D-bifurcation.

Chapter 5

DYNAMIC INSTABILITY MECHANISM(BINARY FLUTTER)

This discussion is in part complementary to the works of Lin et al. [Bucher and Lin, 1988, 1988, 1989; Lin and Li, 1993; Li and Lin, 1995; Lin, 1996] on bridges. The vast majority of their work on stochastic (and random) aeroelastic bridge instabilities has concentrated on the analytical treatment of single-degree-of-freedom type instabilities, mainly negative damping flutter. They found that longitudinal turbulence is generally destabilizing on the basis of a single-degree-of-freedom model, whereas it could have a stabilizing effect if coupling with additional modes of vibration is introduced. We have found only one clear instance where the coalescence (binary or two-mode) flutter is treated [Bucher and Lin, 1988], albeit very superficially. Their analysis showed a destabilizing effect, in the mean-square sense, of longitudinal turbulence on this type of flutter. Furthermore, the degree of destabilisation appears to be essentially proportional to the excitation spectral density.

The present work also complements the work on helicopter rotor blades of Lin et al. [Lin et al, 1979; Fujimori et al, 1979; Prussing and Lin, 1982, 1983], where different types of blade dynamics have been considered. Of particular interest is the torsion-flap problem, which is similar to the binary flutter experienced in this thesis [Done, 1996] except for the added periodic parametric excitation originating from forward flight [Fujimori et al, 1979]. Considering the excitation as white noise, modelling the aerodynamics as quasi-steady and neglecting the quadratic noise component, u_T^2, it was also found by Fujimori et al [1979] that in-plane turbulence had a destabilizing effect, also in the mean-square sense, on this type of flutter.

Our discussion also adds to the work of Ibrahim et al. [1990, 1991] on stochastic panel (two-mode) flutter. Using a structural model with two or three modes, assuming quasi-steady supersonic aerodynamics, and considering a parametric white noise excitation originating from structural in-plane loads and only acting on the stiffness terms, they found that the parametric excitation was always destabilizing in the mean-square sense. Their work is similar to ours in so far as the nature of the deterministic flutter mechanism is concerned. It is different because their model is not the same, and because their analysis did not address specifically the topics discussed later in this chapter. In summary, the effect of longitudinal turbulence on binary flutter remains, for a large part, an open question.

Stability criteria

The identification process of the random instability (flutter) point is implemented practically using the mean-square response of the nonlinear airfoil in pure longitudinal turbulence. We have also monitored the behaviour of the largest Lyapunov exponent for some representative cases, and found that both criteria, nonlinear mean-square response and largest Lyapunov exponent, gave the same flutter speed. See for example Figures 4.9 and 4.10 discussed earlier. In this sense, the numerically calculated flutter speed can be considered to correspond to the concept of sample stability. It thus follows the strict definition of the D-bifurcation.

5.1 Aspects of Frequency Coalescence

In this section we aim specifically to determine if the phenomenon of frequency coalescence plays a role in the advancement of the random flutter point, more particularly if the longitudinal excitation modifies the coalescence.

5.1.1 Modification of modal frequencies

5.1.1.1 Nonlinear airfoil

For the nonlinear baseline airfoil in pure longitudinal turbulence we have observed, for airspeeds close to the random flutter point, a shift of the dominant peak in the response PSD towards higher frequencies. The dominant peak represents the mode losing stability in the linear regime, and which coalesces with the second linear mode at a higher frequency. A shift of the first modal frequency, induced by the longitudinal turbulence, towards the second modal frequency suggests an advancement of the coalescence phenomenon. This is presented in Figure 5.1 for one particular airspeed, $U_m = 3.8$. We observe that the PSD peak is located at $k_p = 0.196$, compared with $k_1 = 0.187$, which is the first modal frequency of the non-excited linear airfoil at the same airspeed.

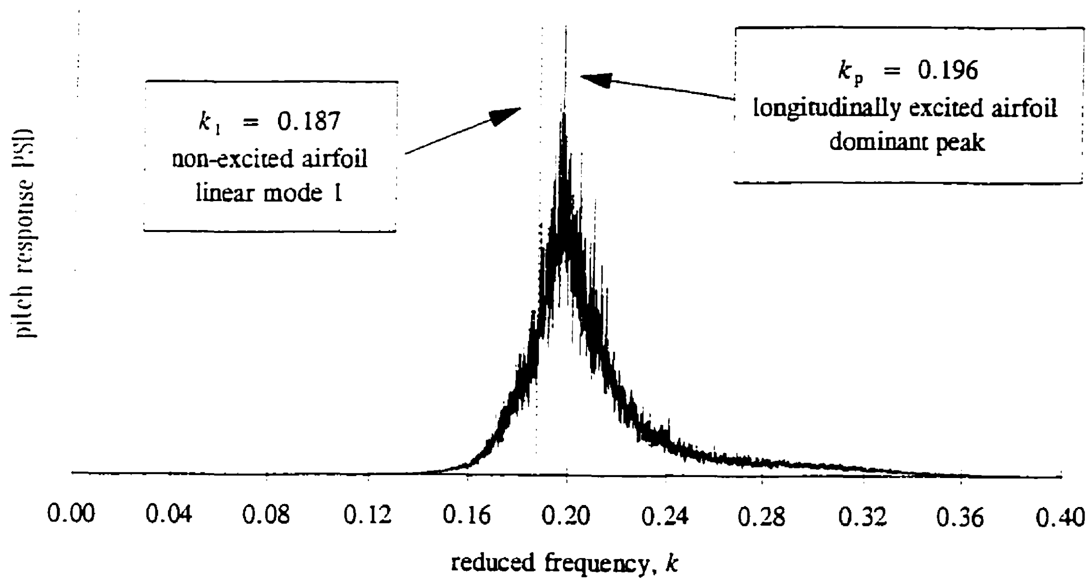

Figure 5.1 - PSD of the nonlinear airfoil pitch response in pure longitudinal turbulence, at $U_m = 3.8$; $\sigma_T^2 = 1.0$, $L = 50.0$, $k_3 = 400.0$.

In Figure 5.2, this result is generalized to other airspeeds. It shows the location of the dominant PSD peak as a function of mean airspeed. Note that the example chosen has a random flutter speed at $U_{mt} = 3.64$. Also notice that the frequency has been re-normalized to get rid of the artificial dependence on mean airspeed, as was done for the largest Lyapunov exponent. In this manner, the frequency coalescence is more clearly observed.

It can be noted that for airspeeds approximately above the deterministic flutter speed, U_f, the reverse situation exists. At these higher airspeeds the frequency of the random response is lower than both the non-excited first modal frequency and the more physically relevant LCO frequency. We have observed the same tendency (shift of frequency towards smaller values) for the nonlinear airfoil in combined excitation (see for example Figure 6.26), which we have attributed to the nonlinear-random interaction. It may be that this nonlinear-random effect is also present for pure longitudinal turbulence and becomes important at higher airspeeds where the response is larger. For airspeeds closer to the random flutter point, U_{m1} = 3.64, the airfoil response mean-square is relatively small. In this case, nonlinear effects are less important such that the dominant peak, k_p, is mainly determined by the effect of the longitudinal excitation.

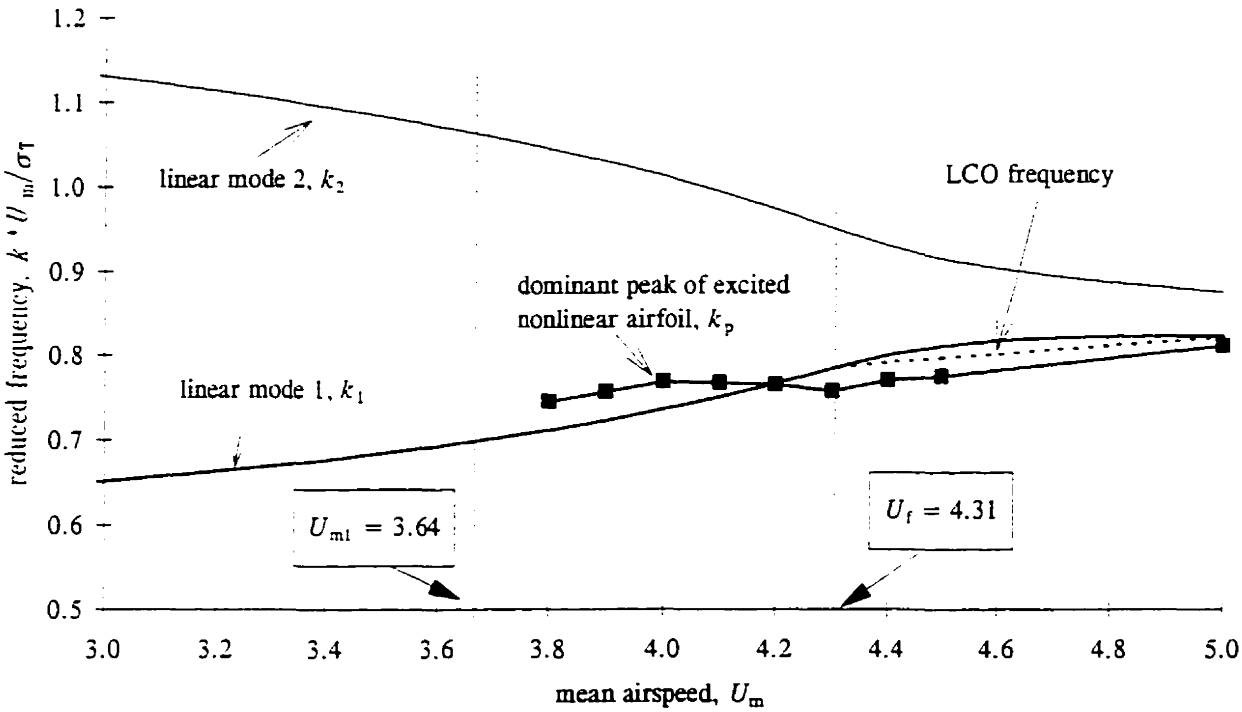

Figure 5.2 - Dominant PSD peak of the nonlinear airfoil pitch response in pure longitudinal turbulence in comparison with the two linear deterministic modal (eigen) frequencies and LCO frequency, as a function of mean airspeed; σ_T^2 = 1.0, L = 50.0, k_3 = 400.0.

5.1.1.2 Linear airfoil

The observed PSD signal shown in Figures 5.1 and 5.2 is fundamentally nonlinear, since the system is operating at post-random flutter airspeeds. In order to verify the hypothesis of an advancement of the coalescence we want to ensure that the random modal frequency is not corrupted by the nonlinearity, thus we need to investigate the linear dynamics. This approach, however, has two drawbacks. It limits the range of investigation to pre-random flutter airspeeds, where the coalescence is not yet fully active as can be seen for example in Figure 5.2 for the deterministic eigenfrequencies. Second, the linear airfoil cannot have sustained behaviour unless it is excited by an external forcing.

Accordingly, we now consider the system with vertical turbulent excitation, not to investigate the effect of vertical turbulence but as a means to excite the system and probe its dynamics, and in particular its random eigenfrequencies which we are trying to capture. In using the term random eigenfrequency, we are making reference to its companion in the eigenvalue duo which is expressed by the Lyapunov exponent, i.e. the real part of the eigenvalue. Since the concept of Lyapunov exponent has a meaning in the random (and stochastic) sense, it is likely that the notion of random eigenfrequency also has some significance. In fact, the notion of an eigenfrequency, in the random sense, bears the name ***rotation number*** in the theory of random dynamical systems [Arnold, 1998]. It has been predicted theoretically that multiplicative noise modifies the value of the eigenfrequencies [Sri Namachchivaya and Van Roessel, 1993].

The use of vertical turbulence to excite the modal frequencies has its own limitations for airspeeds close to the flutter point. Since the system is very lightly damped in this region it responds with a large amplitude, hence violating the linear aerodynamic assumption. However, since the specific interest of this discussion is the possible shift in modal frequency, the response amplitude should not be an immediate concern. More importantly, the response amplitude of the linear airfoil does not modify its modal characteristics[1].

1

This is exemplified by the behaviour of the largest Lyapunov exponent (representing the real part of the eigenvalue for mode 1) which is independent of the vertical excitation for the linear problem. Analytically, it is explained by realizing that for the linear airfoil the variational equation (equation 1.26) used for the calculation of λ_{max} does not depend on the response or reference trajectory, $x_r(t)$, but only on the state transition matrix, $[A(t)]$, which is time-varying in our case due to the longitudinal excitation.

To demonstrate the shift in modal frequencies of the linear airfoil in combined turbulent excitation we choose an example which has a random flutter speed at U_{m1} = 4.25. We first examine the pitch response PSD for an airspeed, U_m = 4.0, shown in Figure 5.3. In comparison with pure vertical excitation, as represented by the closed-form solution, we observe a narrowing of the dominant mode accompanied by an increase in its peak frequency, hence towards the second mode. This dominant mode represents the slow linear mode (mode 1). We add that for this example the shift in frequency is small, which we attribute to the smallness of the shift in flutter speed (from U_f = 4.31 to U_{m1} = 4.25) for this particular set of turbulence conditions. Also shown is the width of the dominant mode at the half-power point, which will be discussed later.

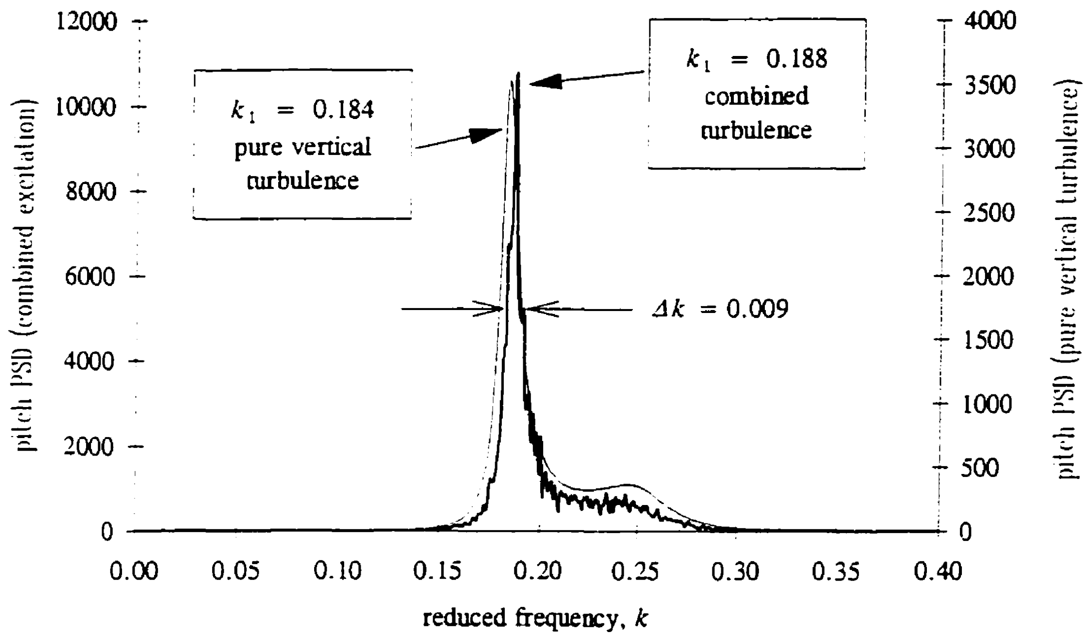

Figure 5.3 - PSD plot of the linear airfoil pitch response to combined excitation turbulence (numerical solution, —) and pure vertical turbulence (closed-form solution, —) at U_m = 4.0; σ_T^2 = 1.0, L = 0.5, k_3 = 0.0.

Furthermore, Figure 5.3 hints at a shift towards lower frequencies of the faster mode (mode 2), hence towards coalescence. We do not think, however, that this is convincing since at this airspeed the PSD is dominated largely by the mode losing stability. To that effect, Figure 5.4 is presented showing the same information as Figure 5.3, but for a lower mean airspeed, U_m =

3.5. In comparison with the PSD of the response to pure vertical turbulence, we observe a narrowing of the second mode and a shift of its peak frequency towards lower frequencies, hence towards coalescence. Note as well the narrowing of the first mode and its shift to the right.

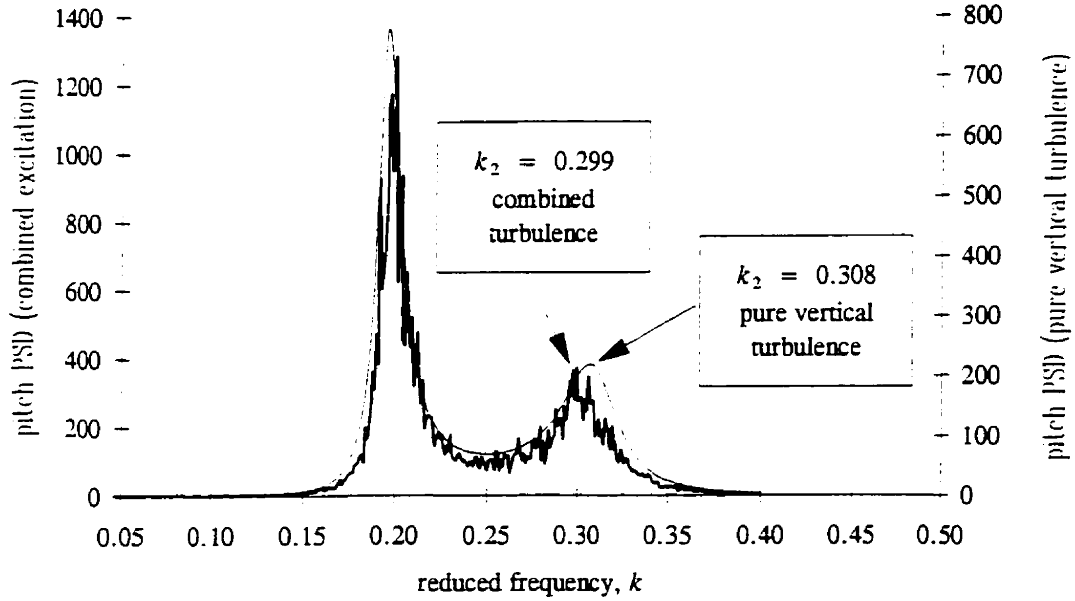

Figure 5.4 - PSD plot of the linear airfoil pitch response to combined excitation turbulence (numerical solution, —) and pure vertical turbulence (closed-form solution, —) at $U_m = 3.5$; $\sigma_T^2 = 1.0$, $L = 0.5$, $k_3 = 0.0$.

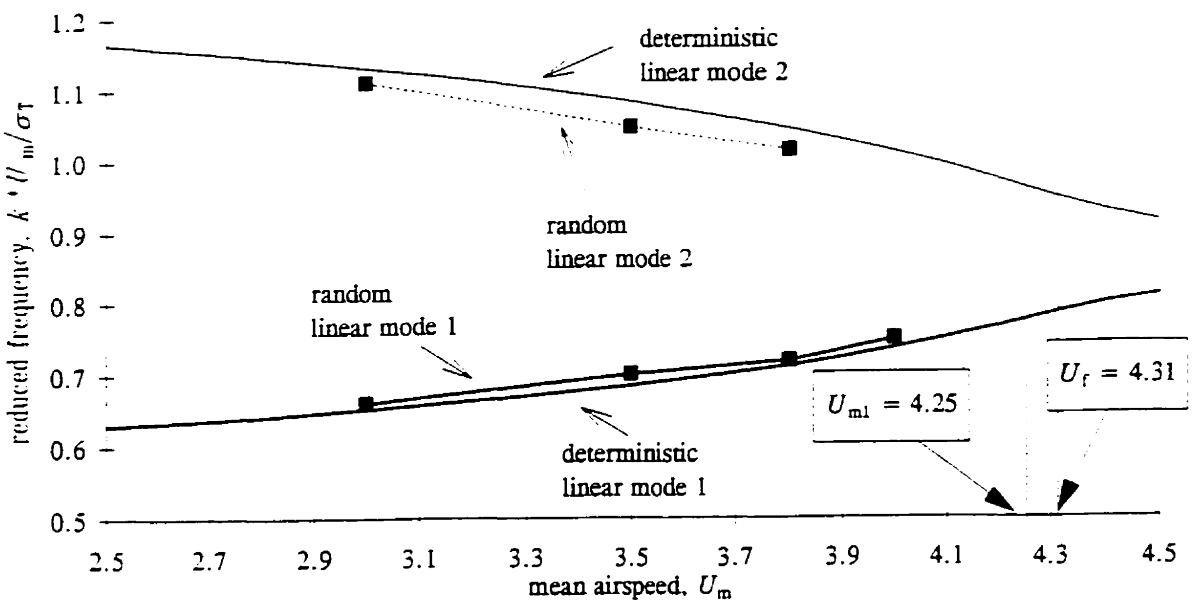

Figure 5.5 - Deterministic and random modal frequencies for linear airfoil; $\sigma_T^2 = 1.0$, $L = 0.5$.

Figure 5.5 summarizes our findings on this topic for the linear airfoil. We conclude by arguing that the observed increase of the first modal frequency combined with a decrease of the second modal frequency is an indication that longitudinal turbulence advances the frequency coalescence. We can also interpret this observation in the sense that longitudinal turbulence increases the coupling between the pitch and heave motion.

Random eigenvalues

The PSD of the linear response to combined turbulence excitation contains not only information on the system natural frequencies, but also on its modal damping. By visual inspection we note that the width of the dominant mode (i.e. mode 1) in Figures 5.3 and 5.4 is smaller for combined excitation compared with pure vertical turbulence, thus indicating a lower damping ratio for the former excitation which characterizes a closer distance to the instability point. More precisely, using the half-power point method for the dominant mode in Figure 5.3, we calculate the equivalent of the real part of the eigenvalue of random mode 1 to be:

$$-\zeta_1 k_1 = -\Delta k_{1/2\,\mathrm{PSD}} / 2 = -0.009 / 2 = -0.0045 \tag{5.1}$$

This value is compared with the largest Laypunov exponent at the same speed, λ_{max} ($U_m = 4.0$) $= -0.0047$, thus showing excellent agreement. See Figure 5.6. It demonstrates a level of coherence between the two sets of results, and provides a physical meaning to the concept of the largest Lyapunov exponent in the context of longitudinal excitation. Note, that the real part of the equivalent deterministic eigenvalue is calculated to be $\lambda_1 = -0.0055$, thus indicating more damping for the non-excited airfoil.

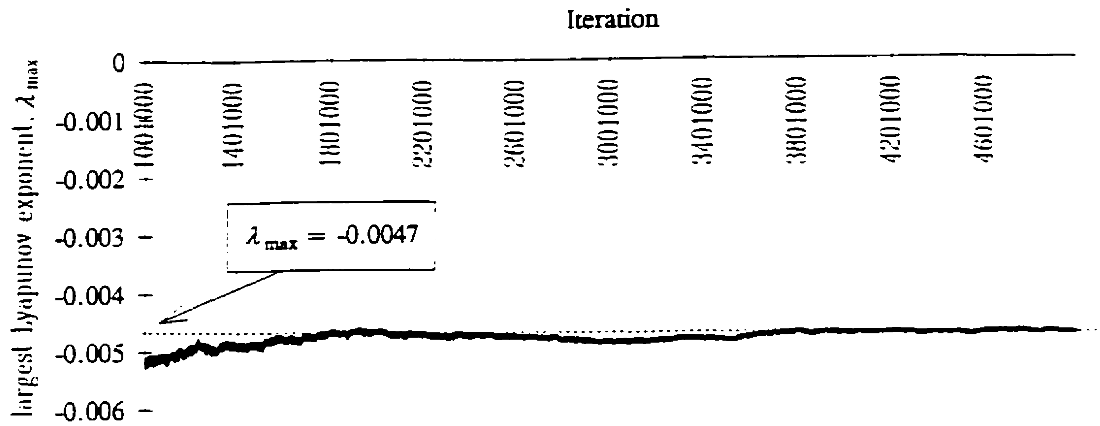

Figure 5.6 - Time (iteration) evolution of the largest Lyapunov exponent of the linear airfoil in combined excitation turbulence at $U_m = 4.0$; $\sigma_T^2 = 1.0$, $L = 0.5$, $k_3 = 0.0$.

5.1.2 Sensitivity to random stiffness and damping terms

In an attempt to further elucidate the frequency coalescence question, we try another route by examining the sensitivity of the advancement of the flutter point to the random stiffness terms, and in corollary to the random damping terms. Due to the inherent stiffness-controlled nature of the frequency coalescence phenomenon associated with classical binary flutter, it is anticipated that the random stiffness terms will prove to be essential contributing factors, whereas the latter are not expected to significantly influence the shift of the flutter point.

As opposed to quasi-steady aerodynamics[2], the concept of aerodynamic stiffness and damping is not immediately evident in the context of unsteady aerodynamics in arbitrary motion. Physically this is due to the lag introduced by unsteady effects, and is especially problematic according to the integro-differential formulation (see equation 2.23). However, in the differential formulation (see equations 2.25 and 2.26) the replacement of the integral by two new state variables, z^*_1 and $\dot{z}^*_1$, enables one to obtain aerodynamic damping and stiffness terms. In spirit, this is the interpretation used when analysing bridge flutter [Dowell, 1978], and single-degree-of-

[2] This is the modelling used by Ibrahim et al. [1990] and in spirit by Ibrahim and Heo [1987].

freedom torsional flutter[3].

The problem is approached by considering the nonlinear airfoil in pure longitudinal turbulence, and using the response mean-square as an indicator of the flutter point. In a first test, all the random terms in the damping matrix (equations 2.27 or 2.28) are disabled. Specifically the "unf" terms in matrix $[D(\tau)]$ are set to one (1), such that the damping matrix becomes time-invariant, i.e. $[D]$[4]. For the particular example chosen, the flutter speed is then found to be U_m = 3.85.

In the second test, the random terms in the stiffness matrix, "unf" and "unsf", are now set to one (1), i.e. $[K(\tau)]$ becomes $[K]$. In this case, the flutter speed becomes U_m = 4.27. Comparing these speeds with the actual random and deterministic flutter speeds, U_{m1} = 3.64 and U_f = 4.31, respectively, it is clear that the random terms in the aeroelastic system stiffness matrix have much more impact on the advancement of the flutter speed than the random damping terms. This is best shown in Figure 5.7.

We conclude by arguing that this observation confirms the nature of the shift in flutter speed to be stiffness controlled, as is the case for the deterministic part. In this sense, this is an indirect indication of an advancement of the frequency coalescence. As a final point, Ibrahim and Heo [1987] have also noted a predominant effect of random stiffness terms over random damping terms on the response of their system. However, they have not discussed their relative influence on the stability, which we have done.

---

3 See also the discussion in Chapter 2 with regards to the harmonic motion aerodynamics in terms of Theodorsen's function.

4 Recall unf is defined as unf $\equiv U/U_m = (U_m + u_T)/U_m = 1 + u_T/U_m$. Similarly, unsf $\equiv (U/U_m)^2 = 1 + 2u_T/U_m + (u_T/U_m)^2$

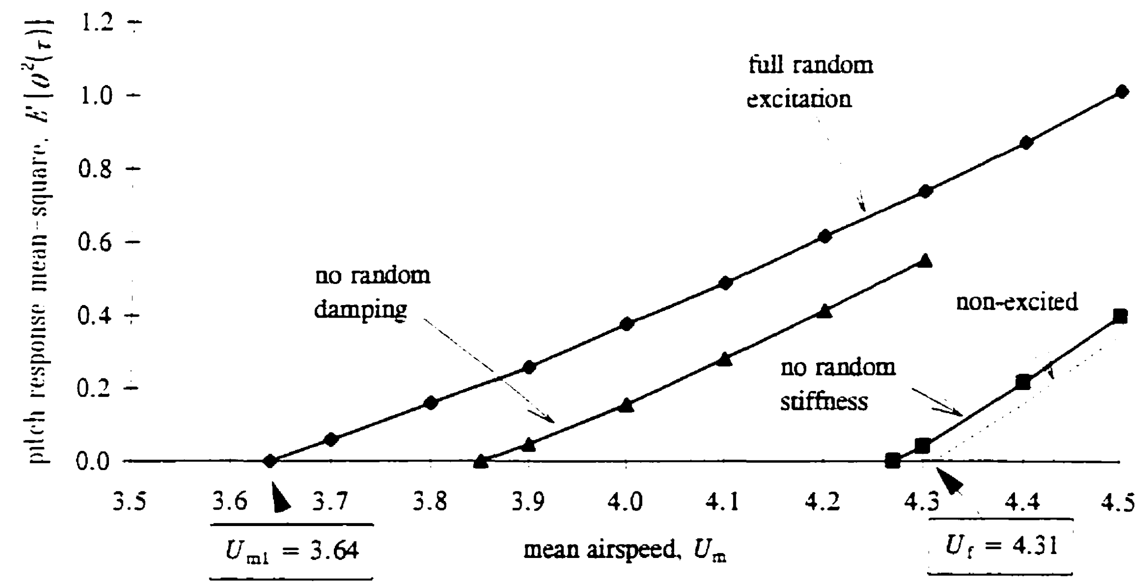

Figure 5.7 - Longitudinally excited pitch response mean-square of the nonlinear airfoil, with random damping and stiffness terms switched on and off; $\sigma_T^2 = 1.0$, $L = 50.0$, $k_3 = 400.0$

5.1.3 Sensitivity to airfoil parameters

In this section, we show that changing the airfoil parameters does not affect the advancement of the binary flutter point by longitudinal turbulence, nor the advancement of the frequency coalescence. In Figure 5.8, the random and deterministic (flutter) stability boundaries are compared for varying frequency ratio, $\bar{\omega}$, static unbalance, x_θ, and distance between the mid-chord and elastic axis, a_h, respectively. The rest of the parameters remains as per the baseline values given in Chapter 4.

From Figure 5.8, it is observed that the flutter point is advanced by the random excitation for all combinations of parameters analysed. We have also confirmed that the advancement of the frequency coalescence is present for other values of frequency ratio, namely for the case where the heave is stiffer than the pitch ($\bar{\omega} > 1.0$). For example, as opposed to the baseline airfoil ($\bar{\omega} = 0.6325$) which loses stability via mode 1, the mode losing stability for the airfoil with $\bar{\omega} = 1.4$ is the second mode. In this case as indicated by the PSD of the linear airfoil response in combined turbulence excitation, mode 2 is shifted toward smaller frequencies, hence toward coalescence.

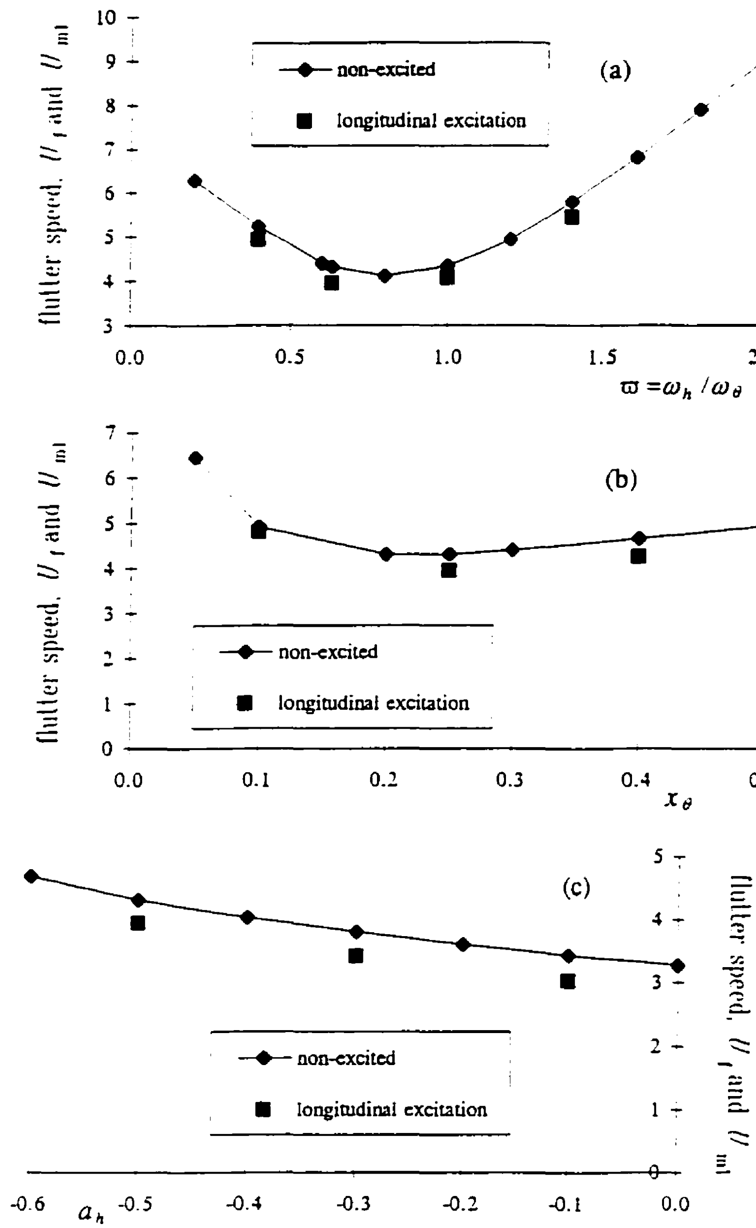

Figure 5.8 - Comparison of deterministic and random flutter boundaries for different combinations of airfoil parameters; L = 50.0, σ_T^2 = 0.5, r_θ = 0.5, μ = 100.0, ζ_θ = 0.0, ζ_h = 0.0; (a) x_θ = 0.25, a_h = -0.5; (b) $\bar{\omega}$ = 0.6325, a_h = -0.5; (c) x_θ = 0.25, $\bar{\omega}$ = 0.6325.

5.2 Influence of Dryden Turbulence Level and Spectral Content

Another relevant problem is the influence of the turbulence level as defined by its variance, and spectral content as defined by its scale. A preliminary overview of their effect on the flutter point was discussed in Chapter 4 and shown in Figure 4.13.

5.2.1 Effect of turbulence level

Focussing first on the effect of turbulence variance, Figure 4.13 suggests that a linear relationship generally exists between the advancement of the flutter point and turbulence variance (see also Figure 5.9). We can observe, however, a slight departure from linearity for the larger values of scale of turbulence, i.e. away from the white noise idealisation, which we will attribute to a non-uniform excitation spectral content.

Based on an analytical approach, the rudimentary results on bridge binary flutter from Bucher and Lin [1988] seem to indicate a linear relationship as well. Notable differences between their analysis and ours, however, are that, in addition to treating a different aeroelastic application, their parametric noise excitation is purely linear, i.e. the u_T^2 terms have been neglected. Furthermore, their excitation is modelled as white noise while we modelled coloured noise.

One consequence of considering a white noise excitation instead of coloured noise is that the turbulence level in the context of white noise is defined by its (uniform) power spectral density, ϕ_{wn}, whereas it is defined by its variance, σ_T^2, for the latter. White noise, as an idealised mathematical notion, has an infinite variance since its spectral density is uniform:

$$\sigma_{wn}^2 = \int_0^\infty \phi_{wn} dk = \phi_{wn} \int_0^\infty dk \to \infty \tag{5.2}$$

In practice, however, the system does not resonate to the full frequency spectrum, such that the excitation can be limited to a broad band with a cut-off frequency, say k_c, which is much larger than the system natural frequencies. The system "sees" white noise as long as the power spectral density is uniform over the range of frequencies to which it is sensitive. The variance of the "physical" white noise is effectively finite:

$$\sigma_T^2 = \int_0^{k_c} \phi_{wn} dk = \phi_{wn} \int_0^{k_c} dk = \phi_{wn} k_c \tag{5.3}$$

Since the variance of the "physical" white noise is directly proportional to its power spectral density, an observed linear relationship between advancement of flutter speed and turbulence power spectral density is equivalent to a linear relationship with turbulence variance. This discussion shows that our results are coherent with those of Bucher and Lin [1988].

To explain the slight departure from the linear relationship for the higher values of scale of turbulence, it must be kept in mind that the system natural frequencies, along with combination frequencies which are important for parametric resonance, change with airspeed. Accordingly, the more the flutter speed is advanced, the more the frequencies at the flutter speed change. In conjunction to changing frequencies it must also be realized that the excitation spectral content is not uniform for coloured noise. In effect this means that for a given flutter speed, the excitation at any particular critical frequency is different than that for another flutter speed since this critical frequency is changed.

This behaviour is amplified for large scales of turbulence since the shift in flutter speed is the largest and the excitation PSD changes rapidly with frequency (see Figure 2.6). In the case of white noise, a change in the system frequencies makes no difference since the excitation is uniform over all frequencies (of interest).

The role of the quadratic turbulent term, u_T^2

With regards to the influence of the quadratic noise term, u_T^2, we argue that it plays a secondary role in the advancement of the flutter point. One argument is based on the observation that the same trend in flutter speed advancement is displayed by Bucher and Lin's [1988] results and ours. This is especially so considering that even for relatively high turbulence levels (for example at $\sigma_T^2 = 1.0$ which is equivalent to an intensity, $T_u = 23\%$, when normalised with the deterministic flutter speed), the linear relationship is maintained for the case with a low value of scale of turbulence which effectively models white noise (see Figure 4.13 or Figure 5.9 for $L = 0.5$). This term was neglected by Bucher and Lin on the basis of low turbulence intensity.

Pursuing this argument, we have neutralized this term in our model by dropping it from the quadratic airspeed term, i.e. we have set unsf = $1 + 2u_T/U_m$, hence, dropping $(u_T/U_m)^2$ in equation (2.28). To generalize our interpretation to larger scales of turbulence, we have chosen the following set of turbulence conditions, $L = 50.0$ and $\sigma_T^2 = 1.0$. We have found that the flutter speed increased from $U_{m1} = 3.64$ to $U_{m1} = 3.7$. In this specific case, it then shows that u_T^2 accounts for approximately 8% of the shift in flutter speed from the deterministic problem, $U_f = 4.31$.

At first glance, it may appear surprising that the quadratic noise term plays a secondary role in the advancement of flutter at high turbulence intensity, especially considering that it acts on the stiffness terms which, as we have discussed, are the dominant factors for the stability. An order of magnitude analysis demonstrates that the calculated 8% contribution in flutter shift is compatible with its relative importance in the quadratic airspeed, U^2. Hence, taking the square of the airspeed:

$$U^2 = (U_m + u_T)^2 = U_m^2 + 2U_m u_T + u_T^2 \tag{5.4}$$

We want to compare the two random terms, $2U_m u_T$ and u_T^2. Since u_T is random, we need to find an appropriate equivalent deterministic basis of comparison. The mean is not adequate since it cancels the linear noise contribution. Accordingly, we take the root-mean-square of these two terms, which gives for the linear noise and quadratic noise terms respectively:

$$2U_m \sqrt{E[u_T^2]} = 2U_m \sqrt{\sigma_T^2} = 2U_m\ \sigma_T \tag{5.5}$$

and

$$\sqrt{E[(u_T^2)^2]} = \sqrt{E[u_T^4]} \tag{5.6}$$

Knowing the probability density function of u_T, which is Gaussian, $E[u_T^4]$ can be derived:

$$E[u_T^4] = \int_{-\infty}^{\infty} u_T^4\ p(u_T)\, du_T = \int_{-\infty}^{\infty} u_T^4 \frac{e^{-\frac{u_T^2}{2\sigma_T^2}}}{\sqrt{2\pi\sigma_T^2}} du_T \tag{5.7}$$

For the turbulence variance level used, $\sigma_T^2 = 1.0$, we find that $E[u_T^4] = 3.0$. Finally, using a mean airspeed equal to the flutter speed, $U_m = 4.31$, the relative contribution of these two terms is approximated to be the ratio of equations (5.6) over (5.5):

$$\sqrt{E[u_T^4]} \,/\, (2U_m\,\sigma_T) = \sqrt{3} \,/\, (2 \times 4.31 \times 1) = 1.73 \,/\, 8.62 = 20\% \tag{5.8}$$

According to this simple estimate, the linear noise term in the quadratic airspeed is five times more important than the quadratic noise term for a turbulence intensity, $T_u = 23\%$.

Effective variance

Investigating Figure 4.13 in more detail, which is reproduced in Figure 5.9 for the D-bifurcation only and with added information, we are looking for a better understanding of the rapport between turbulence level and spectral content, and the advancement of the flutter speed. We choose a given random flutter speed, say $U_{ml} = 3.85$, and examine the turbulence characteristics which correspond to this advancement.

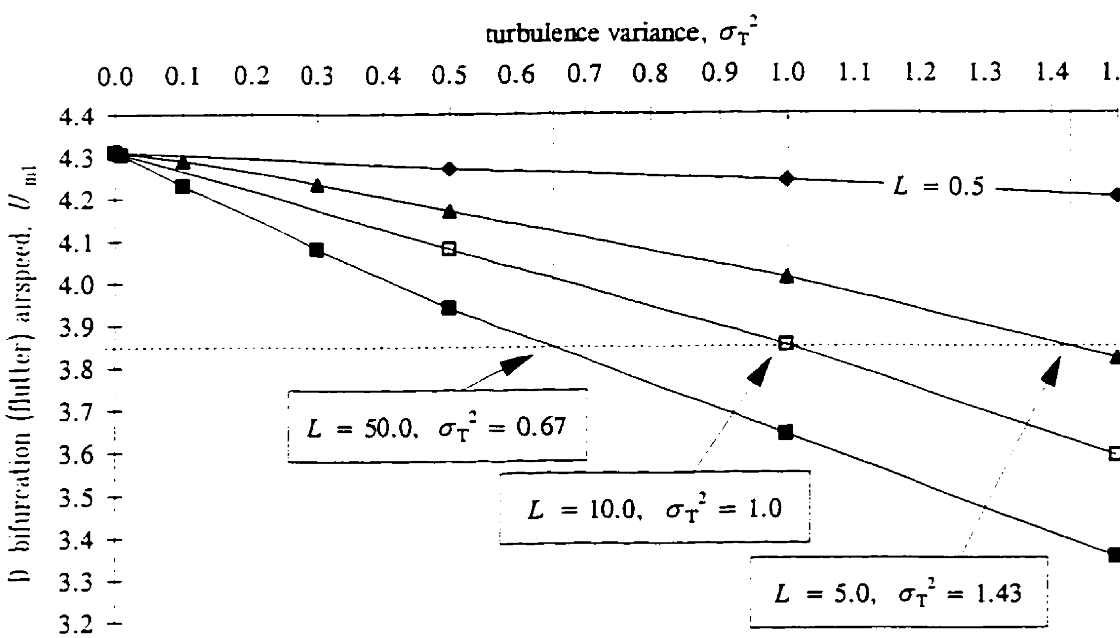

Figure 5.9 - Turbulence conditions corresponding to a flutter airspeed, $U_{ml} = 3.85$, for the longitudinally excited airfoil.

Drawing a horizontal line at that particular speed across the figure indicates that this flutter speed is obtained for either of these sets of conditions:

$$(\sigma_T^2 = 0.67, L = 50.0)$$
$$(\sigma_T^2 = 1.0, L = 10.0)$$
$$(\sigma_T^2 = 1.43, L = 5.0)$$

Not shown but the following conditions, ($\sigma_T^2 = 0.76$, $L = 25.0$), also advances the flutter point to $U_{m1} = 3.85$. We have found that the commonality between these four sets of turbulence conditions was not the value of the excitation density at some particular frequency, but the cumulated power under the excitation PSD curve up to a frequency close to the deterministic flutter frequency (recall $k_f = 0.182$). The cumulated power may be interpreted as an effective turbulence variance, defined by equation (5.9).

$$\sigma_{eff}^2(k) = \int_0^k \phi_{LT}(\kappa)\,d\kappa \tag{5.9}$$

This effective variance is exemplified in Figure 5.10 for the second set of turbulence conditions discussed above ($\sigma_T^2 = 1.0$, $L = 10.0$) with $k \approx 0.17$. The four turbulence excitations giving a random flutter speed, $U_{m1} = 3.85$, have approximately the same effective variance, $\sigma_{eff}^2 \approx 0.7$, at this frequency.

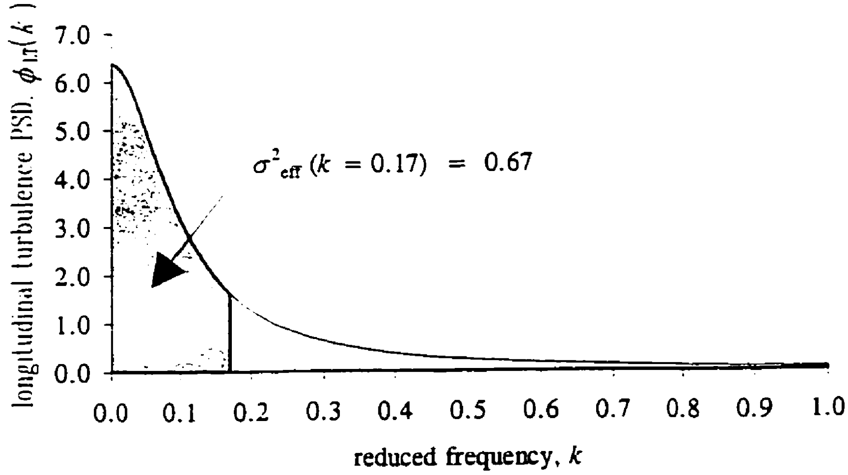

Figure 5.10 - Closed-form solution of the non-dimensional Dryden longitudinal turbulence PSD and effective variance for $k = 0.17$; $\sigma_T^2 = 1.0$, $L = 10.0$.

The same analysis done for other random flutter speeds also exhibits an approximate meeting point of the four cumulated power curves. Not surprisingly, this meeting point corresponds to a different value of effective variance, a lower variance for a smaller shift in flutter speed for example. Perhaps not so obvious is the observation that the frequency at which the cumulated power curves meet is also slightly different, but remains close to the flutter frequency.

There is, however, one notable exception to these observations and interpretations. It is for the smaller scale of turbulence, $L = 0.5$, which acts effectively as a white noise excitation. In this case, the previous discussion does not hold. For this scale of turbulence, the same effective variance as for the larger scales is reached at a much higher frequency, thus hinting to a sensitivity of the airfoil to a broader range of frequencies past the flutter frequency.

In summary for this discussion, we say that the advancement in flutter speed is approximately proportional to the area under the longitudinal excitation PSD curve up to the flutter frequency. This is so for a realistic turbulence spectrum, i.e. away from the white noise idealisation. Nonetheless, we want to stress that the proposed analysis is relatively crude as it treats the influence of the turbulent excitation via an effective variance. This approach does not consider per se the excitation spectral density at specific critical frequencies, but as a lumped continuous band. A more profound understanding can be obtained by investigating the sensitivity of the linear stability to a narrow band parametric excitation. This will be the subject of the discussion on parametric resonance.

5.2.2 Effect of spectral content

Figure 5.9 can be turned around to show the effect of scale of turbulence more clearly. In this regard, Figure 5.11 indicates an asymptotic behaviour of the advancement in flutter speed as the scale of turbulence is increased past $L = 50.0$. At this value of scale of turbulence, 95% of the turbulence power is located at frequencies lower than $k = 0.18$, which is the flutter frequency. Again, the deterministic flutter frequency appears to act as a useful reference frequency in terms of defining the region for very low frequencies that affect the stability.

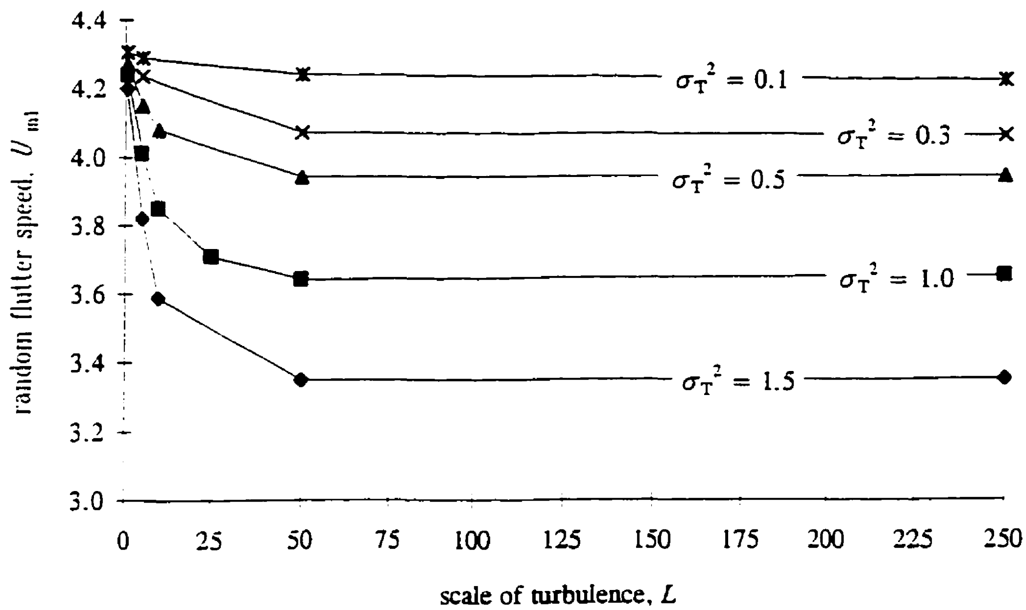

Figure 5.11 - D-bifurcation (flutter) airspeeds of the longitudinally excited airfoil as a function of scale of turbulence and for different values of turbulence variance.

The observation that the very low frequencies of longitudinal turbulence govern the stability of the airfoil is contrary to the effect of turbulence on the response of the airfoil where mid-range frequencies of the vertical excitation, generally in the vicinity of the flutter frequency, are important. We thus put our findings in contrast to Hoblit's [1988], who mentions that the exact shape of the excitation spectrum in the very low frequencies is not important since the aircraft does not respond to them. This is true for the response to turbulence, but not for its effect on stability.

A physical explanation of the enhanced sensitivity of the airfoil to low frequency parametric excitation is as follows. At large values of scale of turbulence, for which most of the excitation power is located in the low frequency range, and which is equivalent to a large noise correlation time in comparison with the system time scales, the system has more time to react and adjust to the excitation. In other words, the excitation is temporarily frozen in time for the airfoil. Conversely, for small values of scale of turbulence the white noise idealization is approached. In this case, the noise varies so quickly that the system has no time to adjust, hence it is less affected by it.

Lastly on the effect of the Dryden turbulence scale and variance, the following table showing the percentage shift in flutter speed for different values of turbulence conditions is presented. For the coloured excitation the decrease in flutter speed starts to become significant (i.e. ≥ 10%) for a turbulence variance, $\sigma_T^2 = 0.5$, which corresponds to a turbulence intensity $T_{u,Uf}$ = 16%. For the effective white noise, the shift in flutter speed is not significant for the turbulence levels examined. In this case, a large part of the excitation energy is located at high frequencies which do not influence the stability of the airfoil.

$(U_{m1}-U_f)/U_f$	$\sigma_T^2 = 0.01$ $T_{u,Uf} = 2\%$	$\sigma_T^2 = 0.1$ $T_{u,Uf} = 7\%$	$\sigma_T^2 = 0.5$ $T_{u,Uf} = 16\%$	$\sigma_T^2 = 1.0$ $T_{u,Uf} = 23\%$
$L = 50.0$	- 0.1 %	- 2 %	- 9 %	- 15 %
$L = 0.5$	-	-0.1 %	- 1.0 %	- 1.6 %

Table 5.1 - Percentage shift in flutter airspeed for different values of turbulence variance.

We will see in Chapter 7 that the percentage shift in flutter speed due to the longitudinal component of turbulence does not reflect fully the effect of this instability on the airfoil. When vertical turbulence is considered, the loss of stability associated with the advancement in flutter speed induces a much larger percentage increase in response mean-square than in flutter speed.

5.3 Parametric Resonance

The specific spectrum of the Dryden turbulence model does not allow for a targeted analysis of the system sensitivity to a particular frequency band. It is essentially a low band excitation. In order to excite specific frequencies, we have removed the Dryden turbulence spectrum in favour of the following narrow band model for the longitudinal excitation. Its analytical expression is given by the following equation: D controls the intensity (for a given ζ and r), ζ defines the width of the excitation band (for a given r), and the peak frequency is denoted by r.

$$\phi_T(k) = \frac{D}{(r^2 - k^2)^2 + (2\zeta r k)^2} \qquad (5.10)$$

where [Newland, 1975]:

$$D = \frac{2\zeta r^3}{\pi}\sigma_T^2 \qquad (5.11)$$

The time domain solution is derived in Appendix B. Equation (5.10) is represented graphically in Figure 5.12.

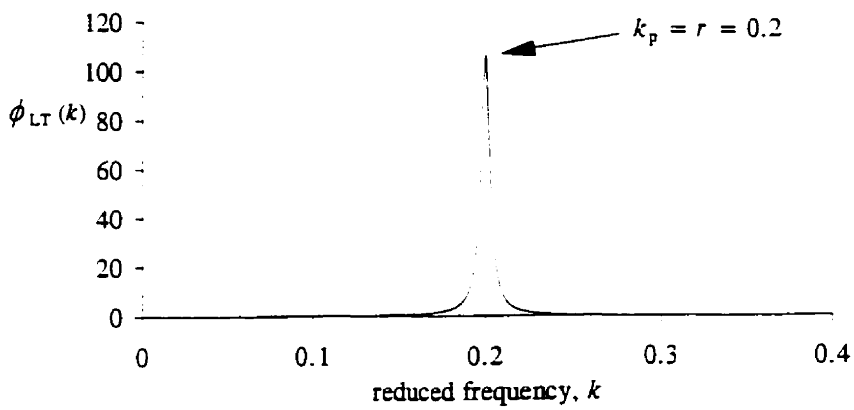

Figure 5.12 - Closed-form solution of the narrow band excitation PSD;

$\zeta = 0.015, r = 0.2, \sigma_T^2 = 1.0.$

For an excitation variance, $\sigma_T^2 = 1.0$, while keeping the band width constant at $\Delta k = 2\zeta r = .005$ defined at the half-power point, the peak frequency, r, is swept from 0.01 to 0.60. The sensitivity of the system stability to this excitation is shown in Figure 5.13.

Before discussing the results it is relevant to point out the potential parametric resonance conditions. Based on the deterministic flutter frequencies ($k_f \equiv k_1 = 0.182$, $k_2 = 0.221$), we are searching primarily for the following resonances. Note, a general observation is that the principal resonances are more likely to be present than the secondary resonances, and so on [Ibrahim, 1985; Cartmell, 1990; Lin, 1996].

Principal parametric resonances, $(k_i \pm k_j)/m$ where i, j =1, 2 and $m = 1$:

$r = 2\,k_1 \sim 0.36$

$r = 2\,k_2 \sim 0.44$

$r = k_2 + k_1 \sim 0.40$ (combination addition type)

$r = k_2 - k_1 \sim 0.04$ (combination difference type)

Secondary parametric resonances, $(k_i \pm k_j)/m$ where i, j =1, 2 and m = 2:

$$r = k_1 \sim 0.18$$

$$r = k_2 \sim 0.22$$

$$r = (k_2 + k_1)/2 \sim 0.20 \quad \text{(combination addition type)}$$

$$r = (k_2 - k_1)/2 \sim 0.02 \quad \text{(combination difference type)}$$

In light of these potential resonance conditions we examine Figure 5.13 shown below. Note that the solid thick line separates the stable region below the curve from the unstable airspeeds above it. In reference to the deterministic flutter speed, $U_f = 4.31$, we denote essentially six regions of particular sensitivity. They are discussed as follows.

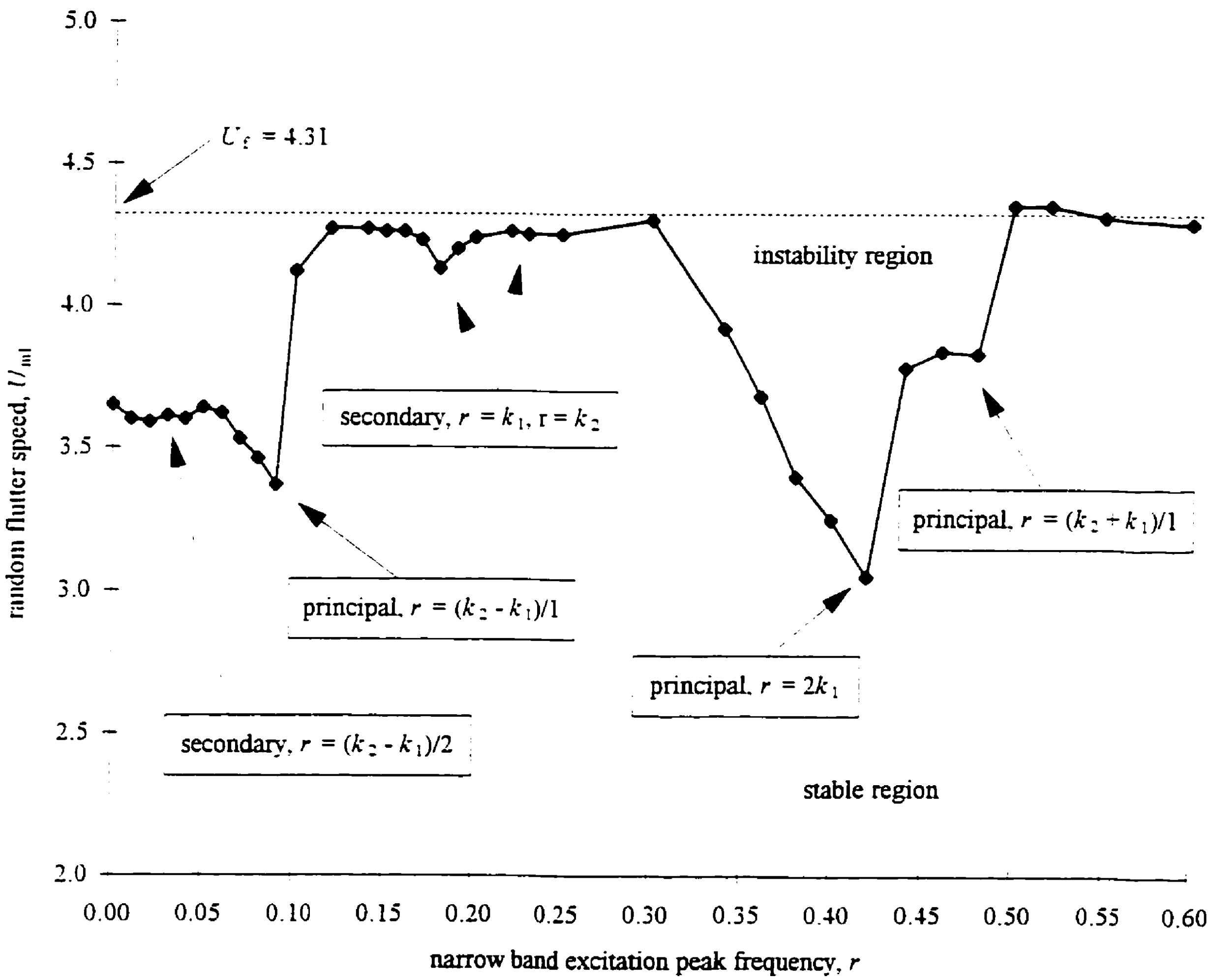

Figure 5.13 - Flutter boundary of the parametrically excited airfoil as a function of narrow band excitation peak frequency; $\sigma_T^2 = 1.0$.

Principal parametric resonance, $2k_1$

The largest advancement in flutter speed occurs at $r \approx 0.42$. This excitation frequency appears to correspond to approximately twice the frequency of the second mode, $2k_2 \approx 0.44$. However, the value for k_2 in the above potential resonances is taken at the deterministic flutter speed, $U_f = 4.31$. At the random flutter speed, $U_{m1} = 3.1$, its value has changed to $k_2 \approx 0.36$, while $k_1 \approx 0.21$. Accordingly, this resonance is more likely due to twice the frequency of the first mode, $2k_1 \approx 0.42$.

This excitation at $2k_1$ meets the condition of principal parametric resonance with the natural frequency of the flutter mode. It is the main cause of the sensitivity of the system to high excitation frequencies or why the system is effectively excited by "physical" white noise, $L = 0.5$, which we discussed earlier. For the larger values of scale of turbulence, this condition of principal parametric resonance still exists, but is much less dominant since the PSD of the excitation at this frequency ($k \approx 0.42$) is relatively small compared with the excitation spectral density in the low frequencies.

Principal parametric resonance, combination addition type, $(k_1 + k_2)/1$

For frequencies slightly greater than $r = 0.42$ another region of particular sensitivity appears to be centred around $r \approx 0.47$. At this particular flutter speed ($U_{m1} = 3.8$), the possible principal resonances are: $r = 2k_2 = 2 \times 0.275 = .55$ and $r = k_2 + k_1 = 0.275 + .187 = 0.462$. Consequently, the loss of stability in this region is more likely due to the principal parametric combination (addition type) resonance.

It is possible that the other principal resonance condition at $2k_2$ is also affecting the stability, but we believe its effect is so small compared to the other principal resonances at $2k_1$ and $k_2 + k_1$ that it is hidden within that large instability region centred around $r \approx 0.42$.

Principal parametric resonance, combination difference type, $(k_2 - k_1)/1$

At r = 0.09, another strong resonance occurs. This is also a condition of principal parametric excitation, but a combination difference type, $(k_2 - k_1)/1$. As for the resonance at r = 0.42, interpreting this result as being related to the difference of the two eigenfrequencies, it should be realised that their value is more likely to be determined by the random flutter speed than the deterministic one. At U_{m1} = 3.35, the difference between the deterministic eigenfrequencies is: $k_2 - k_1 = 0.325 - 0.20 = 0.125$ compared with 0.04 at the $U_f = 4.31$.

Secondary parametric resonances, $2k_1/2$ and $2k_2/2$

Turning our attention to the secondary parametric excitation frequencies, we note a small region of destabilization centred at r = 0.18, and to its right, a hint of resonance at r = 0.22. These conditions correspond to the two secondary (non-combination) parametric resonances. It is not surprising that their strengths are smaller than the principal parametric resonance discussed earlier. In support of this point, Ibrahim [1985] discusses the problem of a single-degree-of-freedom system in conditions of random parametric excitation, where the loss of stability for the principal parametric resonance, $\omega_{par.\ exc.} = 2\omega_n$, is much more important than for the secondary parametric condition, $\omega_{par.\ exc.} = \omega_n$. In our case, and comparing these two secondary resonances, we point out that the strongest of the two appears at k_1 which is the flutter frequency.

Secondary parametric resonance, combination difference type, $(k_2 - k_1)/2$

The last region of sensitivity is relatively broad and covers the range of very small frequencies. Its existence can be explained by two causes. There exists a condition of secondary combination difference resonance, which based on the random flutter speed, U_{m1} = 3.6, gives $(k_2 - k_1)/2 \approx (0.29 - 0.19)/2 = 0.05$. The other cause is the value of the spectral density at zero frequency. It has been shown analytically that this condition is a determinant in the stability of a single-degree-of-freedom system [Lin, 1996; Ariaratnam and Tam, 1979]. However, it was also shown that the loss of stability at this condition originated from the random damping term. In our case, since we have discussed that the damping terms have a secondary effect in the random flutter mechanism, the first cause may be the more important.

We also note a relatively small region of stabilization at $r \approx 0.50$. It cannot be associated with any natural frequencies or combination types. Such behaviour has been reported by Lin and Li [1993], Li and Lin [1995] and Lin [1996], but for the single-degree-of-freedom negative damping type instability of a bridge section. They showed that the stabilizing effect was greatest for a narrow-band detuned excitation. For a turbulence intensity, $T_{u,Uf} = 23\%$, chosen to correspond to our example shown in Figure 5.13, they obtained a 3% postponement in flutter speed for an excitation frequency centred slightly greater than the principal parametric resonance. Stabilisation due to longitudinal turbulence also occurred for a wide-band spectrum, but to a smaller degree. It was thus considered negligibly small by Lin and Li. For the narrow-band detuned excitation Lin and Li's results are similar to ours except for the even smaller magnitude of stabilization that we have in our problem. On the other hand, for the wide-band excitation our results and theirs totally differ. In our case, we lose the stabilization effect of the detuned narrow-band as the excitation band is widened (as shown for example in Figure 5.9 for $L = 0.5$, which represents effectively white noise).

For the wide-band (effective white noise) excitation, although the reported stabilisation by Lin and Li [Lin and Li, 1993; Li and Lin, 1995; Lin, 1996] and the observed destabilisation that we have observed for the airfoil are both small in magnitude, the qualitative difference between the two sets of result warrants an explanation in light of the two different types of flutter. First we consider coalescence flutter. The inherent nature of coalescence flutter is to have two closely spaced frequencies, i.e. $k_2 \approx k_1$ ($k_1 \equiv k_t$). One important consequence for parametric resonance is that the conditions of principal parametric resonance at $2k_1$, $2k_2$ and $k_2 + k_1$, are therefore in close proximity to each other (the other principal parametric resonance at $k_2 - k_1$ is close to zero for coalescence flutter). In effect and as shown in Figure 5.13, these conditions combine to form a large region of destabilization due to principal parametric resonance. We believe that this large region of destabilization undermines any stabilizing effect introduced by other (detuned) excitation frequencies when a wide-band is considered.

In the case of single-degree-of-freedom flutter reported by Lin and Li, there is no frequency coalescence. For this instability type there exists only one condition of principal parametric resonance at $2k_1$, or possibly at $2k_2$, and combination resonances, if a coupling is introduced with another degree-of-freedom. Since there is no coalescence, the frequencies are in general well separated and the region(s) of principal parametric resonance is(are) narrow. For a 2DOF analysis, results from Lin and Li indicate a narrow unstable region centred at $2k_1$, none at $2k_2$, and a relatively smaller unstable region at $k_1 - k_2$. Their results also suggest a light principal parametric combination (addition type) resonance, $k_2 + k_1$.

In summary, we have shown that the spectral content of the excitation for small and very small frequencies are important contributors to the advancement of the flutter point under parametric random excitation. This has a particular significance for the coalescence flutter mechanism where the excitation originates from turbulence, since these two specific elements (difference combination resonance of two closely spaced frequencies and large excitation in the small frequencies) combine to essentially determine the magnitude of the advancement. We have also shown that in the idealized white noise excitation, the conditions of principal parametric resonance, $2\,k_1$ and $k_2 + k_1$, also become determining factors of destabilization. Furthermore, this more refined treatment of the coalescence flutter problem (i.e. from the perspective of parametric resonance and narrow band excitation) explains the results previously obtained from the coarser approach, but more realistic Dryden turbulence model, of the preceding discussion.

5.4 Nonlinearity and Vertical Turbulence Considerations

The following discussion puts the question of the advancement of the flutter point in the context of the more general nonlinear problem in combined turbulence. This is an issue for the following reason. We have argued in Chapter 4 that the cubic nonlinearity plays no role in the shift in flutter airspeed. However, this statement implicitly assumed that the flutter point exists. It does exist when pure longitudinal turbulence is considered for a linear or a nonlinear airfoil. It also exists when combined turbulence is considered, but only for a linear airfoil. Recall that in the linear case the vertical turbulence plays no role in the advancement of the flutter point.

When nonlinear effects <u>and</u> combined turbulence excitation are considered, a strict interpretation of flutter (and its post-instability behaviour) as being a D-bifurcation leads to the conclusion that the flutter point disappears (see discussion in Chapter 4). This is so since the D-bifurcation (recall this concept is directly related to a crossing of the origin of the largest Lyapunov exponent) is lost. In this situation, the airfoil experiences a decrease of stability over a broad range of airspeed, which can be interpreted as a legacy of the advancement of the flutter point. The decrease in stability, due to longitudinal turbulence, is expressed as an increased response mean-square to vertical turbulence and by a higher value (less negative) of the largest Lyapunov exponent (see Figure 4.20 for example). The general destabilizing effect of the longitudinal component of turbulence will be treated in more detail in Chapter 7.

5.5 Concluding Remarks

The following conclusions are retained with regards to the analysis of the binary flutter problem:

1. It appears that the modal frequencies of the airfoil, strictly speaking the aeroelastic system, are modified by the longitudinal turbulence in such a way that the frequency coalescence is advanced, producing flutter at lower airspeeds.

2. The advancement of the flutter point is determined essentially by the random aerodynamic stiffness, not the damping terms. The nature of the shift of the flutter point is thus stiffness related, typical of the deterministic classical binary flutter problem.

3. The quadratic noise term, u_T^2, plays a secondary role in the shift in flutter point. Accordingly, the linear noise terms (in the stiffness matrix), u_T, are the principal cause of loss of stability.

4. The relationship between flutter speed and turbulence level (as defined by its variance) is linear for the "physical" white noise excitation, and approximately linear for the coloured spectra.

5. For a realistic turbulence spectrum, i.e. away from the white noise idealisation, the advancement in flutter speed is approximately proportional to the area under the longitudinal excitation PSD curve up to the flutter frequency.

6. More precisely, the value of the parametric excitation PSD at frequencies corresponding to the principal, $k_2 - k_1$, and secondary, $(k_2 - k_1)/2$, combination difference type parametric resonances are critical. This has a particular significance for the coalescence flutter mechanism where the excitation originates from turbulence, since these two specific elements (difference combination resonance of two close frequencies and large excitation in the small frequencies) combine to essentially determine the magnitude of the advancement. For the "physical" white noise spectrum, the two parametric resonance conditions at $2k_1$ and $k_2 + k_1$ also become important.

Chapter 6

NONLINEAR AIRFOIL RESPONSE ANALYSIS

- Binary Flutter Conditions

The response of the nonlinear airfoil to combined turbulence is analysed next. The dynamic response is examined according to different points of view in order to present a global perspective. First, the mean-square response is discussed. Observations and analyses are relatively straightforward. A discussion on the probability structure of the response follows. From this point of view, unexpected behaviour is exhibited and interpreted. This forms the most significant part of this chapter. Finally, the frequency content of the response is treated. Its main purpose is to provide information in support of the interpretation of the PDF response. It is also shown that turbulence when interacting with the nonlinearity, induces noise-controlled time scales.

It is stressed that in this section turbulence is treated in its more realistic, combined representation. Hence, the relative effects of each of its two components are not considered explicitly. However as discussed in Chapter 4, and subsequently in Chapter 7, we point out that the nonlinear response, in all of its forms whether mean-square, PDF, PSD, phase plane or time history, is determined mainly by the vertical component of turbulence. On the other hand, note that for the linear airfoil, longitudinal turbulence has a much more significant impact. This is also discussed in Chapter 7.

6.1 Mean-Square Response Analysis

6.1.1 General trends and effect of turbulence variance

In establishing general trends of the mean-square response, we retain two observations from Figure 6.1, which shows the mean-square of the pitch response for five values of turbulence variance as a function of mean airspeed and in comparison with the non-excited airfoil. One general observation is that the response increases with airspeed. We also note that the rate of increase with airspeed tends to stabilize on a constant value.

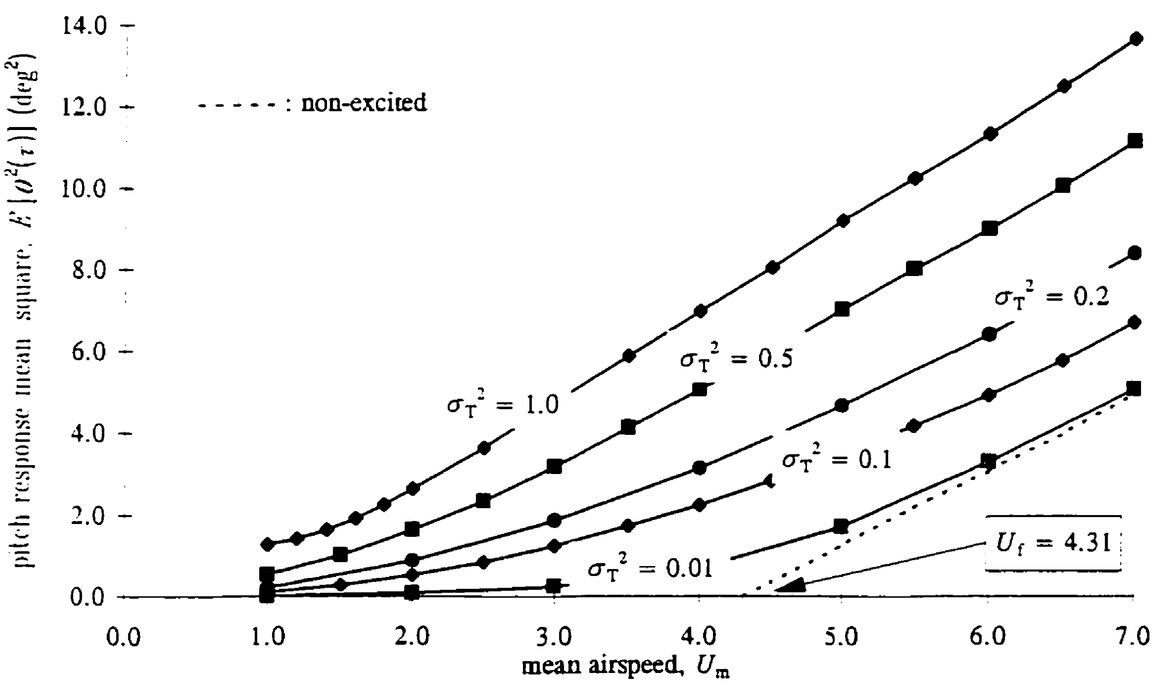

Figure 6.1 - Mean-square pitch response of the nonlinear airfoil in combined excitation for different values of turbulence variance, as a function of airspeed; L = 50.0, k_3 = 400.0.

Two important factors exist that contribute to the increasing mean-square response with increasing airspeed. One is the aerodynamic external force, due to vertical turbulence. This influence is in one way counter intuitive considering that the effective angle of attack due to a vertical gust or turbulence, w^*_T/U^*, given here in dimensional form, (which could be conceptually represented as σ^*_T/U^*_m in the random turbulence context) decreases with airspeed since the turbulence variance is kept constant. The effective angle of attack is schematized in Figure 6.2. However, this effect is more than balanced by an increase in dynamic pressure, $\frac{1}{2}\rho U^{*2}_m$, which multiplies the effective angle of attack, and other terms, to give the actual aerodynamic force due to vertical turbulence. Recall the expression of the incompressible lift (equation 2.13) in dimensional form, per unit span, due to a sharp edged (vertical) gust, w^*_G, as it strikes the leading edge of the airfoil, expressed in terms of Kussner's function:

$$L(t) = \tfrac{1}{2}\rho U^{*2}\, c\, 2\pi\, (w^*_G/U^*)\ \psi(t) = \rho U^*\ c\, 2\pi\, w^*_G\ \psi(\tau) \qquad (2.13)$$

Although this equation is only strictly valid for a gust, it serves to demonstrate the proportional dependence between airspeed and turbulence. In other words, turbulence with a constant strength sees its effect amplified with airspeed. This factor applies to both pre- and post-flutter airspeeds.

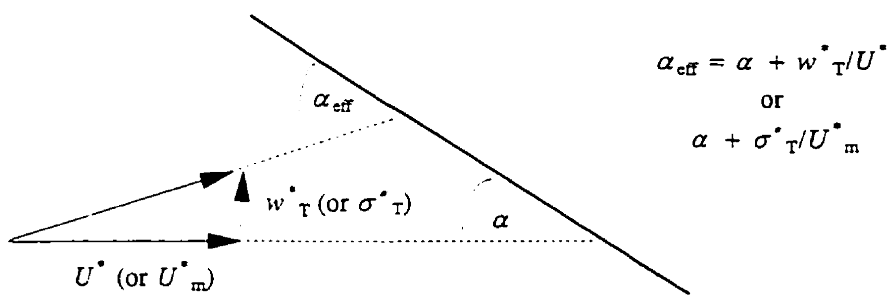

Figure 6.2 - Schematic of effective angle of attack due to vertical turbulence.

The other factor which has a direct influence on the increasing response is the underlying deterministic LCO. At post-flutter airspeeds, the stable LCO attracts the flow. Since its amplitude increases with airspeed, it forces the random response to increase as well. This behaviour is re-enforced by the repelling action of the unstable fixed point at the origin.

Related to the presence of the underlying deterministic LCO is the second general trend retained from Figure 6.1. The relationship between the pitch response mean-square and airspeed in the post-flutter region tends to be linear, a direct consequence of the underlying deterministic LCO. We have seen that the pitch bifurcation landscape for the deterministic non-excited problem remains close to the simplest expression of the Hopf normal form, which we attributed to the location of the nonlinearity in the pitch DOF. This is characterised by a linear mean square response - airspeed relationship. For the excited airfoil, it is then relevant to point out that this relationship is also maintained.

Not shown, but we have noted the same resemblance in the heave behaviour between the excited and non-excited responses. In this case, however, the rate of increase of the excited and non-excited responses mean-square with airspeed is not linear, but behaves like a quadratic. The difference between the heave and pitch responses is also attributed to the location of the nonlinearity. The pitch and heave non-excited responses mean-square are compared in Figure 4.3.

Effect of turbulence variance

Also of interest is the magnitude of the slope of the response which increases with increasing turbulence variance. For the lower values of turbulence variance, the rate of increase of the response tends to follow the non-excited slope. Past a certain turbulence level, however, $\sigma_T^2 = 0.2$ in this example, the slope becomes larger than the deterministic case such that the turbulent response diverges from the non-excited case. This level of turbulence indicates a permutation of strength between two opposing mechanisms, external random excitation and restraining nonlinearity. Take for example the turbulence variance, $\sigma_T^2 = 0.5$, the mean-square response is interpreted as an indicator that of these two mechanisms, the turbulence induced aerodynamics forcing is the strongest. In the second next topic, and in line with this discussion, we show that changing the magnitude of the nonlinearity has an influence on this pivotal value of turbulence level.

Structural damping considerations

It is noted that for the higher values of turbulence variance, the mean-square response does not tend to zero as the airspeed is decreased. This is unexpected since the aerodynamic external forcing decreases proportionally with airspeed as discussed earlier. This behaviour is attributed to the presence of the longitudinal component of turbulence, whose effect becomes relatively more important as the nonlinearity loses its influence.

More specifically, the presence of longitudinal turbulence is combined with the lack of structural damping which at low speeds becomes an important consideration. As the airspeed decreases past $U_m \approx 2.5$ (see Figure 4.10 for example and the related discussion on the largest Lyapunov exponent), the aerodynamic damping decreases as well and tends to zero, hence the airfoil becomes much more sensitive to perturbations. This is true for both the vertically and combined excited cases. For the latter, however, one may interpret the Lyapunov exponent as a mean damping since the aerodynamic damping terms fluctuate according to a Gaussian distribution due to the longitudinal excitation. In this sense, it is conceivable that temporarily (locally in time) the damping becomes zero or negative as the ratio U_m/σ_T goes to zero, such that the response to a decreasing external forcing with airspeed may still increase.

In reality, structural damping would be present and the response would not increase at such a rate as the airspeed is decreased to zero. This is confirmed by introducing a small amount of pitch structural damping. As shown in Figure 6.3, the two pitch mean-square responses start to diverge significantly for low airspeeds, hence as structural damping becomes relatively more important.

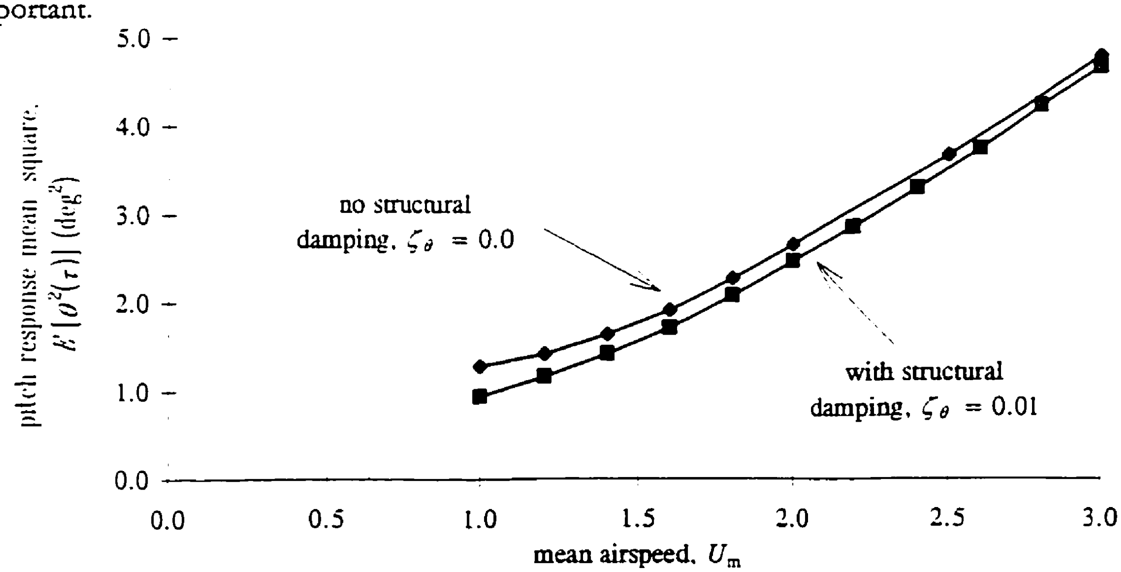

Figure 6.3 - Mean-square of the airfoil pitch response for the combined excitation case, with and without structural damping; $\sigma_T^2 = 1.0$, $L = 50.0$, $k_3 = 400.0$.

6.1.2 Effect of scale of turbulence

We remain on the topic of the effect of the turbulence, but now concentrate on the effect of its spectral shape or content as determined by the scale of turbulence. This is shown in Figure 6.4 for three values of scale of turbulence. Here again, all cases present either a linear rate of increase of the response, or tending to, for the higher speeds. The specific interest lies in the different overall response levels and rates of increase. The origin of these two observations is the same. It is essentially due to the turbulence PSD level at any given (external) resonant frequency which differ from one scale of turbulence to another.

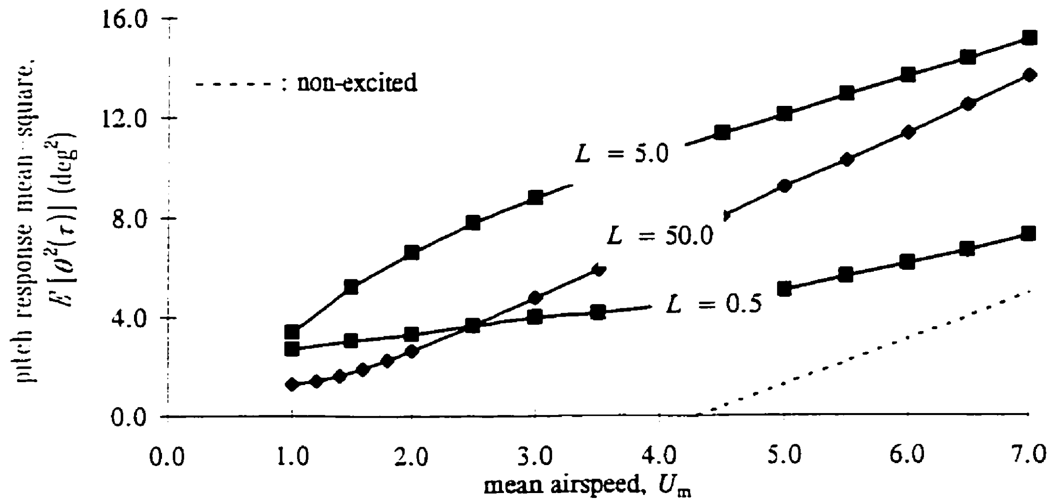

Figure 6.4 - Mean-square pitch response of nonlinear airfoil in combined excitation for different values of scale of turbulence, as a function of airspeed; $\sigma_T^2 = 1.0$, $k_3 = 400.0$.

Consider for example the case at $U_m = 5.0$. Since this is a post-flutter airspeed, the dynamics must be considered as being fundamentally nonlinear. In this case, the (external) resonant frequency is taken as the LCO frequency, $k \approx 0.16$. The vertical turbulence spectral densities at this frequency are:

	$\phi_{VT}(k \approx 0.16)$
$L = 0.5$	0.16
L = 5.0	1.73
$L = 50.0$	0.73

The vertical turbulence with a scale of turbulence, L = 5.0, provides the greatest excitation. The next greater excitation is given by the turbulence with L = 50.0, followed by the case with L = 0.5. The immediate conclusion is that the relative magnitudes of these excitation spectral densities are reflected by the mean-square responses, since for example the response mean-square at U_m = 5.0 for L = 5.0 is the largest.

We have followed the same process for the smaller airspeeds, namely in the pre-flutter regime, and found the same correspondence between response level and excitation PSD at resonant frequencies. However, at these airspeeds and for small response levels, we may assume that the airfoil responds approximately as a linear system. Accordingly, the resonant frequencies are determined by both natural (aeroelastic) frequencies.

With respect to the different rates of increase in the response with airspeed, this is explained by the combined effect of the airfoil frequencies (natural and LCO) changing with airspeed, and the non-uniform shape of the vertical turbulence spectral density. In Chapter 4, we have seen that the (reduced) frequency, k, of both the eigenfrequencies and limit cycle decrease with airspeed. For example, they range from $k \approx 0.3$ and 0.6 at U_m = 2.0 to $k \approx 0.16$ at U_m = 5.0. Furthermore as shown in Figure 6.5, the rate of increase in the excitation spectral density as the frequency is decreased appears to dictate the rate of increase of the response with airspeed.

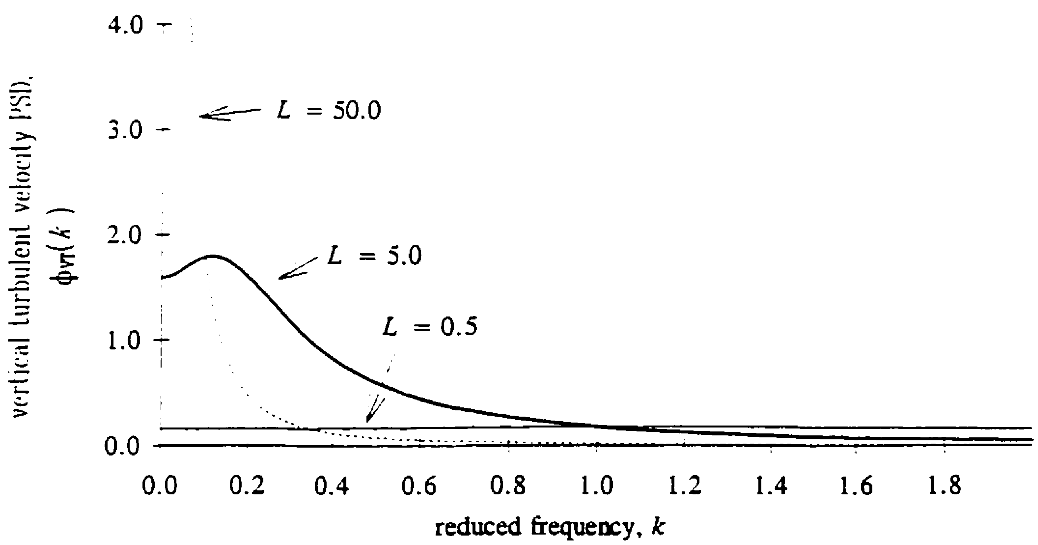

Figure 6.5 - Closed-form solution of the non-dimensional vertical turbulence PSD for three values of scale of turbulence; $\sigma_T^2 = 1.0$.

6.1.3 Effect of nonlinearity

Varying the magnitude of the nonlinear coefficient, k_3, has an important and direct effect on the response level as is shown in Figure 6.6. As expected, the larger this coefficient is, the smaller the mean-square pitch response. Similarly, the rate of change of the response mean-square with airspeed decreases as k_3 is increased.

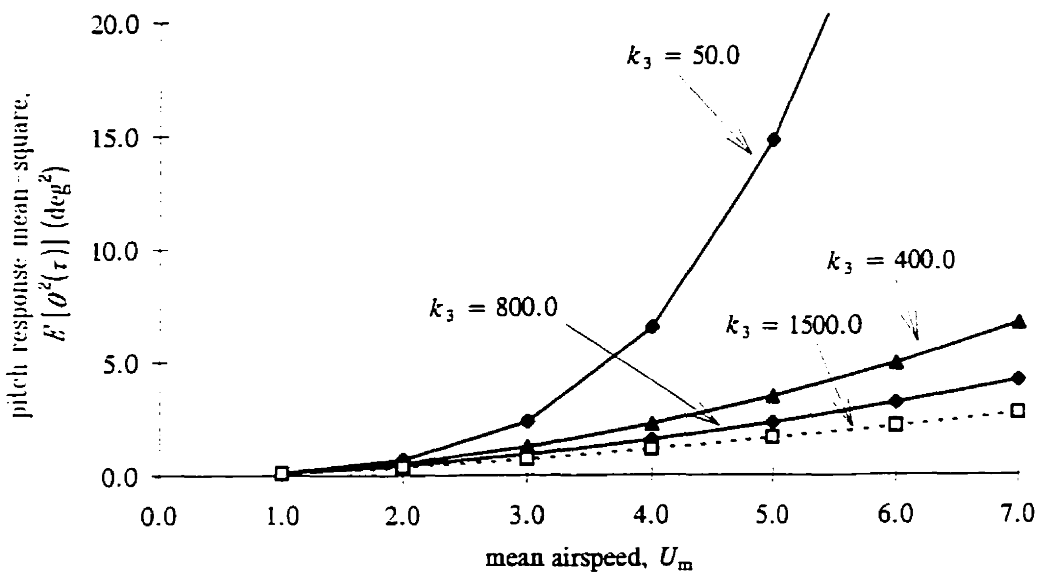

Figure 6.6 - Pitch response mean-squares of the nonlinear airfoil in combined excitation for different values of the nonlinear coefficient, as a function of airspeed; $\sigma_T^2 = 0.1$, $L = 50.0$.

The effect of the nonlinearity can also be examined by comparing the excited and non-excited responses. From this perspective, we are not concerned with the absolute value of the response to turbulent excitation, but by its relative value compared with the non-excited response for different strengths of the nonlinearity. We expect to see the excited mean-square pitch response converging to the non-excited response as the magnitude of the nonlinearity is increased while maintaining the same level of turbulence at $\sigma_T^2 = 0.1$. However, as illustrated in Figure 6.7 for four different magnitudes of the nonlinear torsional stiffness coefficient, k_3, the reverse is observed. The excited mean-square pitch response tends to diverge from the non-excited value as the nonlinearity is increased. More specifically for this example, for values of the nonlinear coefficient ≤ 400.0, the excited response tends to the non-excited response as the airspeed is increased. For $k_3 \geq 800.0$, the excited response diverges from the non-excited response. This is similar to the effect of turbulence variance discussed earlier where, depending on its magnitude, convergence or divergence of the excited response to or from the non-excited response could be observed as the airspeed is increased.

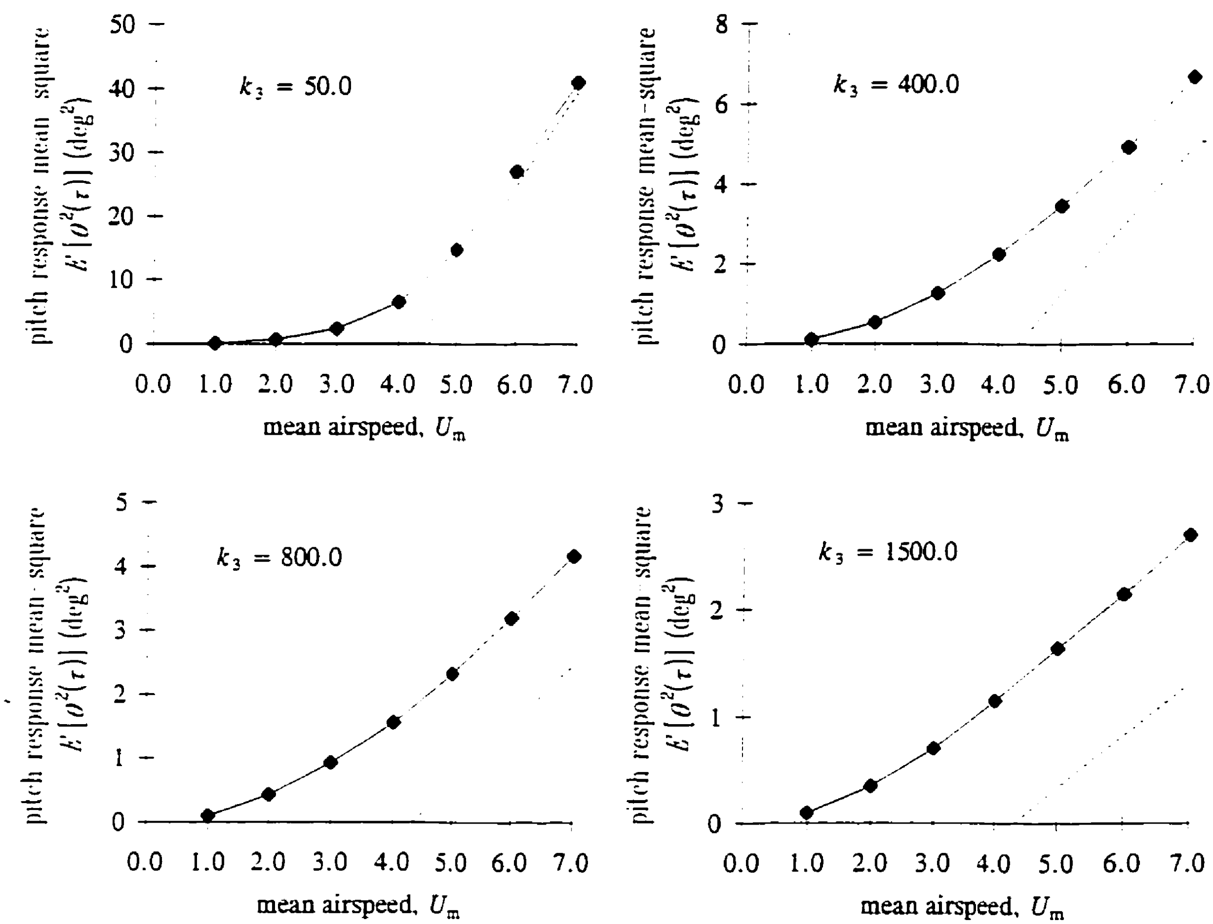

Figure 6.7 - Mean-square pitch responses of the non-excited nonlinear airfoil (---) and in combined excitation (-◆-) for four values of the nonlinear coefficient, as a function of airspeed; $\sigma_T^2 = 0.1$, $L = 50.0$.

The following explanation to this observation is provided. Consider the smaller nonlinearity, $k_3 = 50.0$, where a convergence of the excited and non-excited responses with airspeed is observed. The smaller nonlinearity does in fact induce a smaller restraining mechanism since the absolute response level is the highest. However, the excitation has also an influence on the nonlinear restraining force. Due to the nature of the hardening cubic stiffness nonlinearity, a larger response to the excitation, permitted by the smaller nonlinear coefficient $k_3 = 50.0$, produces in turn a much greater restoring force. To make the explanation clear, we call upon the concept of an effective linear stiffness introduced in Chapter 1. Without a loss of the fundamentals, assume a 1DOF system with the following stiffness terms:

$$k_{\text{linear}}\,\theta + k_3\,\theta^3\,, \tag{6.1}$$

and rewritten as

$$(k_{\text{linear}} + k_3\,\theta^2)\,\theta. \tag{6.2}$$

In the random case, θ^2 is always varying. Assume that we can obtain a deterministic representation of this stiffness force by using the mean-square of the pitch response. We get:

$$(k_{\text{linear}} + k_3\,\overline{\theta^2})\,\theta. \tag{6.3}$$

The second term in brackets may be interpreted as an effective linear stiffness coefficient. Hence, we see that although the nonlinear coefficient, k_3, has an impact on the restoring force, a large response via the $\overline{\theta^2}$ term has an even bigger impact. In other words, the smaller k_3 is, the larger $\overline{\theta^2}$ becomes and the final outcome is a larger effective stiffness, $k_3\,\overline{\theta^2}$. This is why a smaller nonlinear coefficient enables a larger absolute response but a smaller relative response in comparison with the non-excited case, and conversely for a larger nonlinear coefficient.

In summary, two effects from the nonlinearity on the mean-square response are retained. An increase in the nonlinear coefficient decreases the absolute value of the excited mean-square response, and rate of increase with airspeed, but increases their relative value compared with the non-excited response.

6.2 Probability Structure of the Response

The probability structure of the aeroelastic response displays perhaps a more interesting and perplexing behaviour than its mean-square. We have seen in Chapter 4 that the basic shapes exhibited by the one-dimensional marginal PDFs projection appeared to be either uni-modal at low speeds, or bi-modal at high speeds. However, looking more closely into the behaviour, we can denote variations in these two basic shapes. Furthermore, we find that the nature of the observed bi-modality is not unique and depends strongly on the turbulence level.

Similarly, the bi-dimensional PDF projection exhibits complex behaviour. It also provides some answers to the intricacies of the uni-dimensional marginal PDF. In the following discussion, both projections are examined and interpretations of the airfoil dynamic behaviour are also proposed.

6.2.1 General characteristics and effects of turbulence variance

6.2.1.1 Uni-dimensional, marginal, PDD projection

To investigate this aspect we have loosely defined three levels of turbulence variance as discussed below.

Case 1 - low level turbulence

For low level turbulence, defined approximately by the following range of turbulence variance $0.0 \leq \sigma_T^2 \leq 0.02$ for this particular nonlinear airfoil, the change in the pitch marginal PDD (multiplied by the pitch response variance) with airspeed is represented by the case $\sigma_T^2 =$ 0.01, shown in Figure 6.8. Also shown is the more traditional perspective, similar to a bifurcation diagram, where only the peaks of the probability density are displayed as a function of airspeed. This is illustrated in Figure 6.9.

We observe the expected uni-modal to bi-modal transition, followed by the appearance of a third peak at higher airspeeds, shown here at $U_m = 7.0$. This third peak located at zero pitch angle is a direct consequence of the shape of the underlying deterministic LCO, which deforms significantly with airspeed. (The underlying deterministic LCO will be discussed in more detail from the point of view of the bi-dimensional projection.) The deterministic LCO marginal PDF is illustrated in the inset of Figure 6.8 for an airspeed $U = 7.0$, where the third peak is shown. Note that the relative importance of this third peak is enhanced by the turbulence, but remains a second order effect.

Consider as well the distribution at U_m = 5.0. Its basic shape is strictly bi-modal and is thus qualitatively similar to the non-excited PDF, also shown in the inset of Figure 6.8. For this case of low level turbulence, the pitch dynamics is thus interpreted as being defined basically by the underlying deterministic LCO about which random motion appears as a secondary effect.

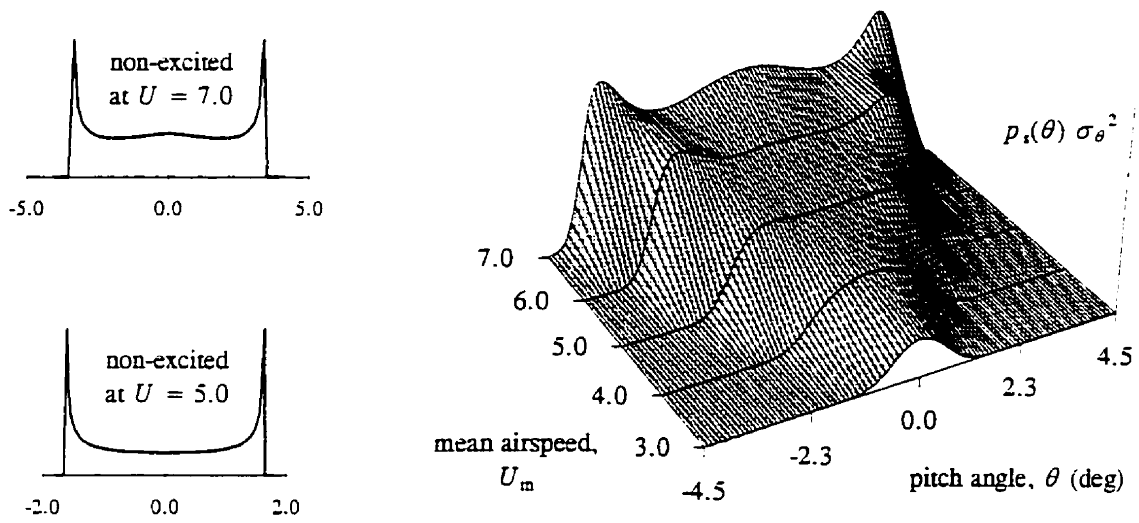

Figure 6.8 - Marginal PDF diagram of the nonlinear airfoil pitch angle, in combined turbulence, as a function of mean airspeed; σ_T^2 = 0.01, L = 50.0, k_3 = 400.0.

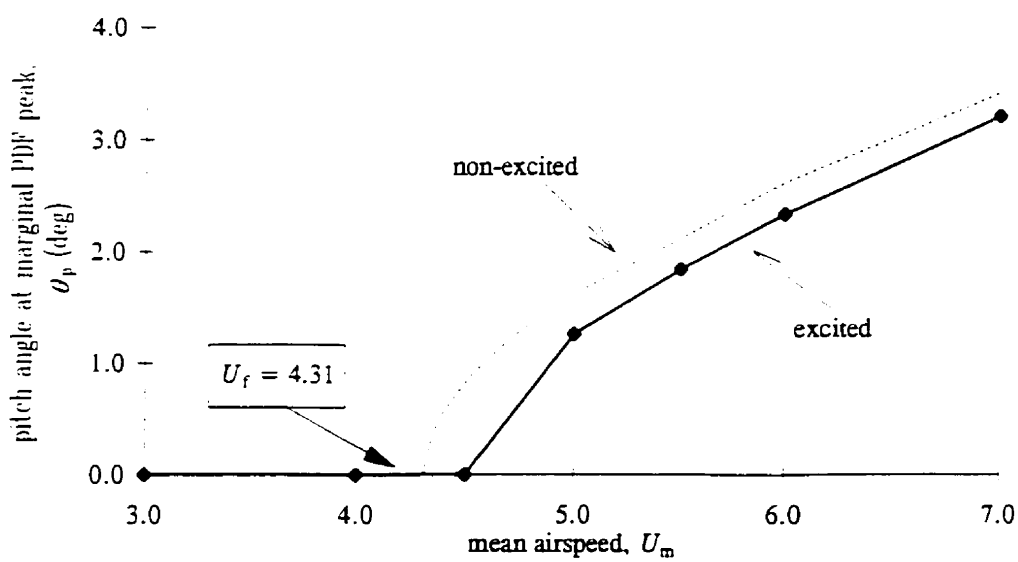

Figure 6.9 - Diagram of the peaks of the nonlinear airfoil pitch angle marginal PDF, in combined turbulence, as a function of mean airspeed; σ_T^2 = 0.01, L = 50.0, k_3 = 400.0.

In the intermediate range of turbulence variance, $0.02 \leq \sigma_T^2 \leq 0.2$, another behaviour is observed. It takes the form of a double bi-modal density at the higher airspeeds. This is illustrated in Figures 6.10 and 6.11 for a turbulence level, $\sigma_T^2 = 0.05$. All other parameters remain the same as for case 1. What we have in this case is a competition between the underlying deterministic LCO and higher order effects of the noise, in combination with the nonlinearity, which starts to become dominant. For example, again consider the probability density at $U_m = 7.0$, the mode at the origin (i.e. third peak located at zero pitch angle) has become dominant and is starting to split into two *inner* modes. Note, as well, the distribution at $U_m = 5.0$ which is now uni-modal, as opposed to the previous case which exhibits a strictly bi-modal shape. This is an indication that the underlying deterministic LCO is starting to become overwhelmed by the turbulence. The primary contribution of the LCO is displayed mainly by the two humps at low speeds, or *outer* modes at high speeds. It is the turbulence which is the direct cause of the inner bi-modal distribution. In this regard, it will be shown later that as turbulence variance is increased, the subsequent increase in response level enhances nonlinear effects, which in turn deforms the basic structure of the LCO.

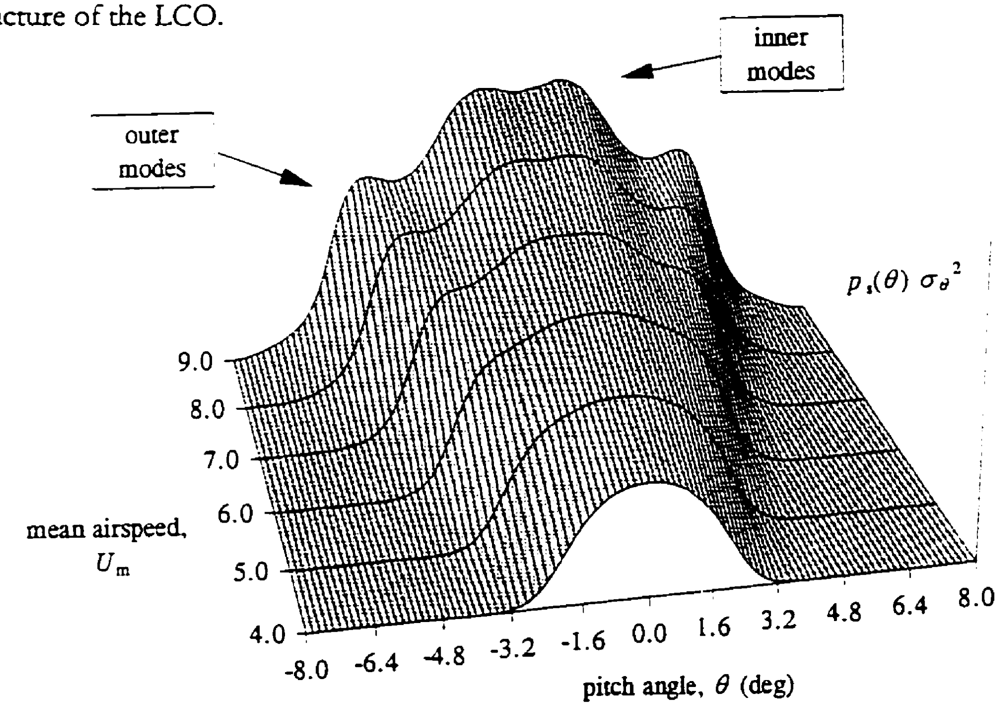

Figure 6.10 - Marginal PDF diagram of the nonlinear airfoil pitch angle, in combined turbulence, as a function of mean airspeed; $\sigma_T^2 = 0.05$, $L = 50.0$, $k_3 = 400.0$.

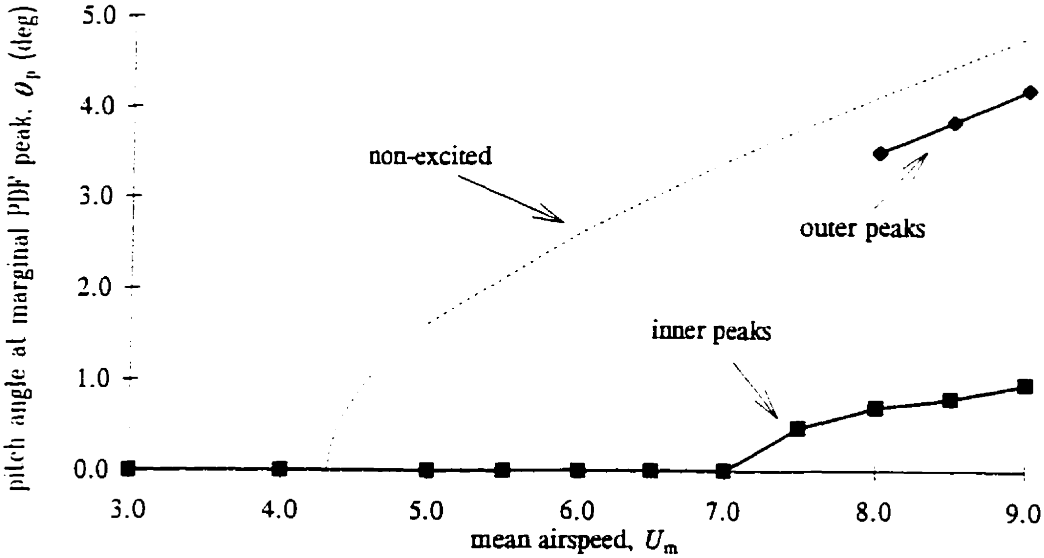

Figure 6.11 - Diagram of the peaks of the nonlinear airfoil pitch angle marginal PDF, in combined turbulence, as a function of mean airspeed; $\sigma_T^2 = 0.05$, $L = 50.0$, $k_3 = 400.0$.

Case 3 - high level turbulence

The direct influence of the underlying deterministic LCO is lost at the higher turbulence levels, $0.2 \leq \sigma_T^2$, as shown in Figure 6.12.

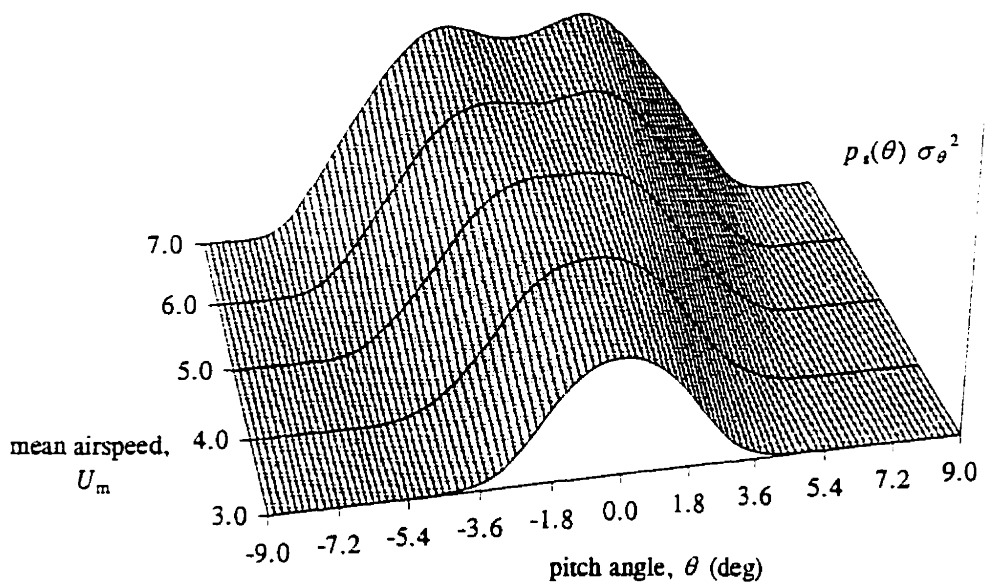

Figure 6.12 - Marginal PDF diagram of the airfoil pitch angle, in combined turbulence, as a function of mean airspeed; $\sigma_T^2 = 0.3$, $L = 50.0$, $k_3 = 400.0$.

The two outer peaks (modes) exhibited for intermediate turbulence variances have disappeared. The noise is essentially dictating the shape of the density, whose main feature is again characterized by the simple bi-modality. From this point of view, the pitch PDF of the low and the high turbulence levels are similar. However, this is a superficial observation since the fundamental origin of the bi-modality is different for both cases. It will be explained with the bi-dimensional projection.

As a summary on the effect of the turbulence variance on the pitch marginal PDF, Figure 6.13 presents the density at an airspeed, U_m = 7.0, for four values of turbulence variance in addition to the non-excited case, which defines the underlying structure of the deterministic LCO. From this point of view, the change in the origin of the bi-modality of the probability density is evidenced by the two peaks due to the LCO which fade away and tend towards lower values of pitch angle as the turbulence variance is increased from 0 to 0.05. Simultaneously, the peak at the origin gets stronger and splits into two as the turbulence variance is increased through 0.05. At this point, the two new peaks move further apart, as exemplified by the density for turbulence variances, $\sigma_T^2 = 0.1$ and $\sigma_T^2 = 1.0$.

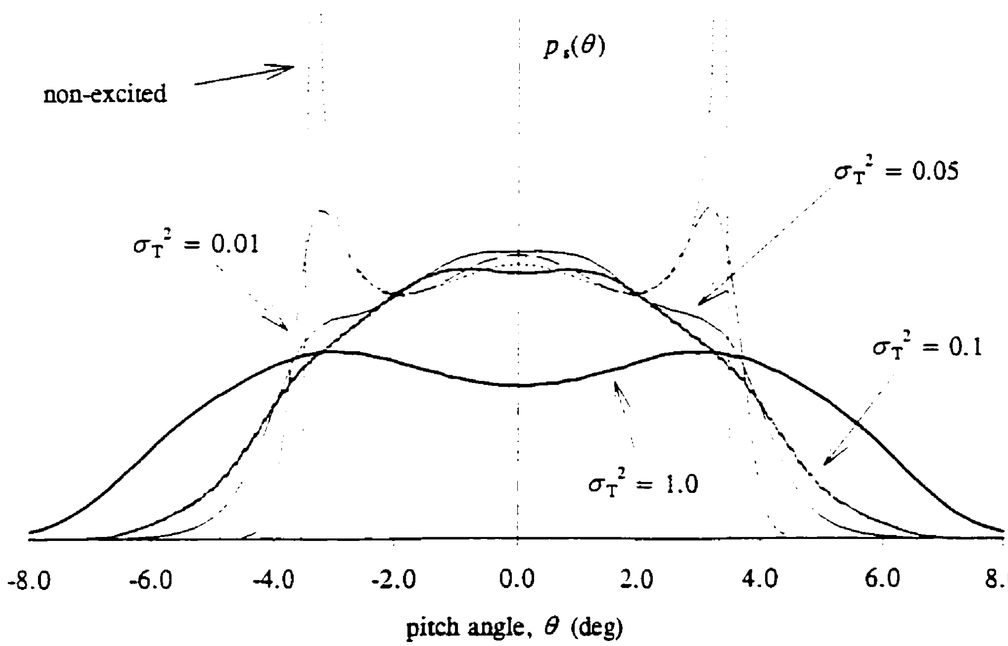

Figure 6.13 - Marginal PDF of the nonlinear airfoil pitch angle, in combined turbulence, at U_m = 7.0 and for different values of turbulence variance; L = 50.0, k_3 = 400.0.

Also acting as a summarizing picture is Figure 6.14 showing a diagram of the peaks of the pitch marginal PDF for the nonlinear fluttering airfoil, where the control parameter is now the turbulence variance instead of the usual (mean) airspeed. Here, the mean airspeed is set at U_m = 7.0.

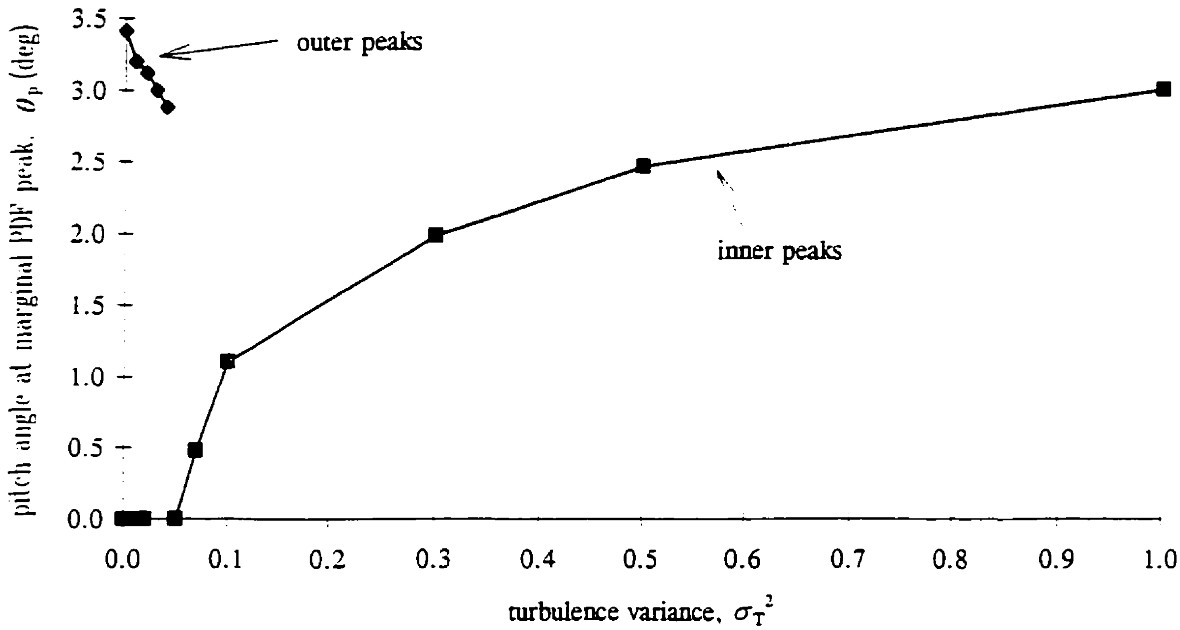

Figure 6.14 - Diagram of the peaks of the nonlinear airfoil pitch angle marginal PDF, in combined turbulence, as a function of turbulence variance; U_m = 7.0, L = 50.0, k_3 = 400.0.

The same types of probability density have been observed for the other system states, but not necessarily at the same airspeed. In other words, the pitch could be bi-modal while the heave uni-modal at the same airspeed. This aspect is shown with more focus in Figure 6.15. Presented is the transition airspeed (from uni- to bi-modal marginal PDF) for all four structural states as a function of turbulence variance, and for one particular scale of turbulence. Under each curve, the density is uni-modal, and it is bi-modal (or double bi-modal around the kink) above the curve.

From Figure 6.15, it is first observed that none of the states transition at the same airspeed, except of course for zero turbulence variance where the deterministic flutter/Hopf bifurcation occurs. Secondly, it is observed that both pitch states, displacement and rate, transition at a smaller airspeed than both heave states for all values of turbulence variance. Furthermore, the transitions of the heave states are delayed significantly with respect to the deterministic bifurcation airspeed. We believe that this is a direct consequence of the location of the nonlinearity. Since the nonlinearity is located on the torsional spring, the pitch DOF feels the nonlinearity more strongly than the heave. In corollary, the Gaussian-like density of the heave is preserved for a longer range of airspeeds. See for example Figure 4.14, where the heave probability density of the excited airfoil appears Gaussian-like at $U = 10.0$, a post-flutter airspeed (recall $U_f = 4.31$).

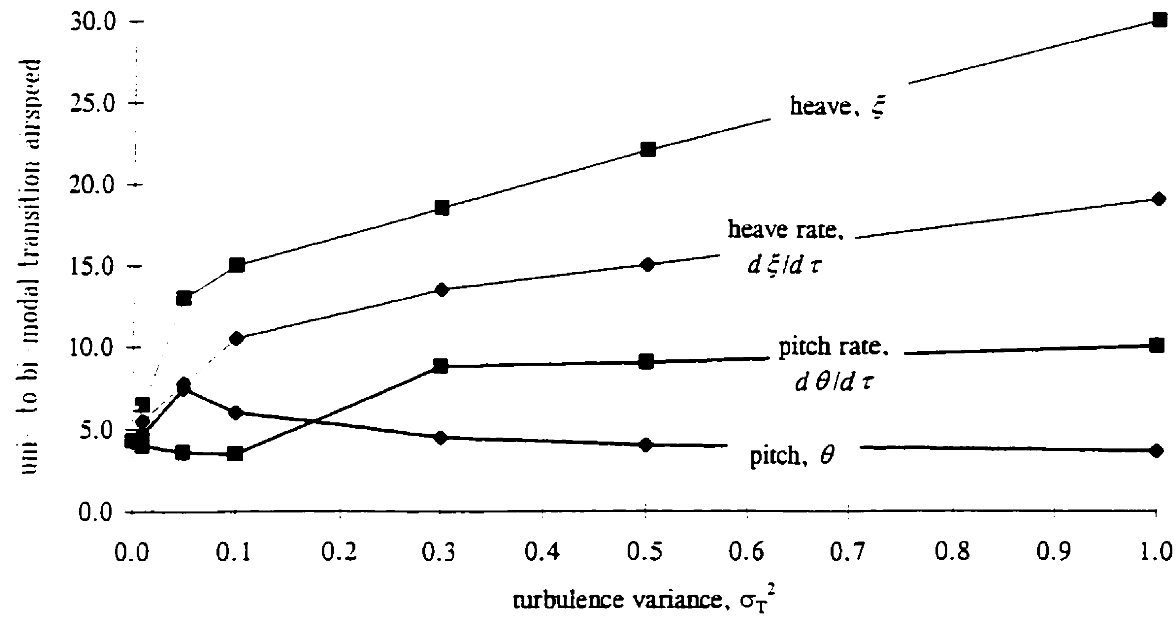

Figure 6.15 - Diagram of transition airspeed of structural state marginal PDFs as a function of turbulence variance; nonlinear airfoil in combined excitation; $L = 50.0$, $k_3 = 400.0$.

Most interesting is the third observation which concerns the non-monotonic behaviour of the transition airspeeds of the pitch states in comparison with the monotonic increase of the heave states. Note that in comparison with the deterministic flutter speed ($U_f = 4.31$), there is a postponement in pitch angle transition airspeed for low turbulence levels, changing into advancement for the larger values of turbulence variance. The initial postponement corresponds to the fading away of the underlying structure of the deterministic LCO, which is then supplanted by the other type of bi-modality originating from the more dominant turbulence effects.

Moreover, the change in transition airspeed of the pitch angle appears to be tied to the transition airspeed of the pitch rate in such a way that one is roughly the mirror image of the other. As will be shown later in Figures 6.20 to 6.22, this apparent interdependence between pitch angle and pitch rate transition airspeeds, hence between their respective marginal PDFs, is reflected on the pitch pitch-rate bi-dimensional PDF by a rotation of the density about its probability axis as the turbulence variance is varied.

6.2.2.2 Bi-dimensional PDF projection

The analysis of the bi-dimensional PDFD is very revealing and instructive in some of the elusive questions raised from the investigation of the marginal PDF projection. Hence, the following discussion is in part an attempt to provide an explanation for the behaviour of the pitch angle and pitch rate transition airspeeds with turbulence variance, as well as elucidating the nature of the second type of bi-modality observed for the higher turbulence levels. Our argumentation and reasoning are based in part on a qualitative description and analysis of the observed dynamics. This is supplemented by the knowledge of the non-excited, deterministic, dynamics which we have found provides important physical clues as well. We start by proposing a non-traditional perspective of the deterministic dynamics.

Probability structure and phase plane of the non-excited airfoil

Take the non-excited airfoil at an airspeed of $U = 5.0$. Its phase plane and bi-dimensional PDF, for pitch and pitch rate, are shown in Figure 6.16. The phase plane is evidence of a well defined ellipse, which is indicative of limit cycle with one frequency [Argyris, 1994]. In this regard, the presence of super-harmonics, which one would expect to exist for a nonlinear response, does not appear to have much significance on the pitch response at that airspeed. The presence of super-harmonics is a large deflection phenomena, and at that airspeed the response amplitude is relatively low such that the motion is essentially simple harmonic. Note that the same conclusion can be deduced from a comparison of the numerically simulated response with the analytical solution obtained via the describing function method. Hence, as mentioned by Alighanbari [1995], a departure of the analytical solution from the numerical solution as the airspeed is increased can be attributed to the increasing effect of the nonlinearity. More precisely, the describing function method assumes simple harmonic motion which is valid for a small nonlinearity, thus small deflections.

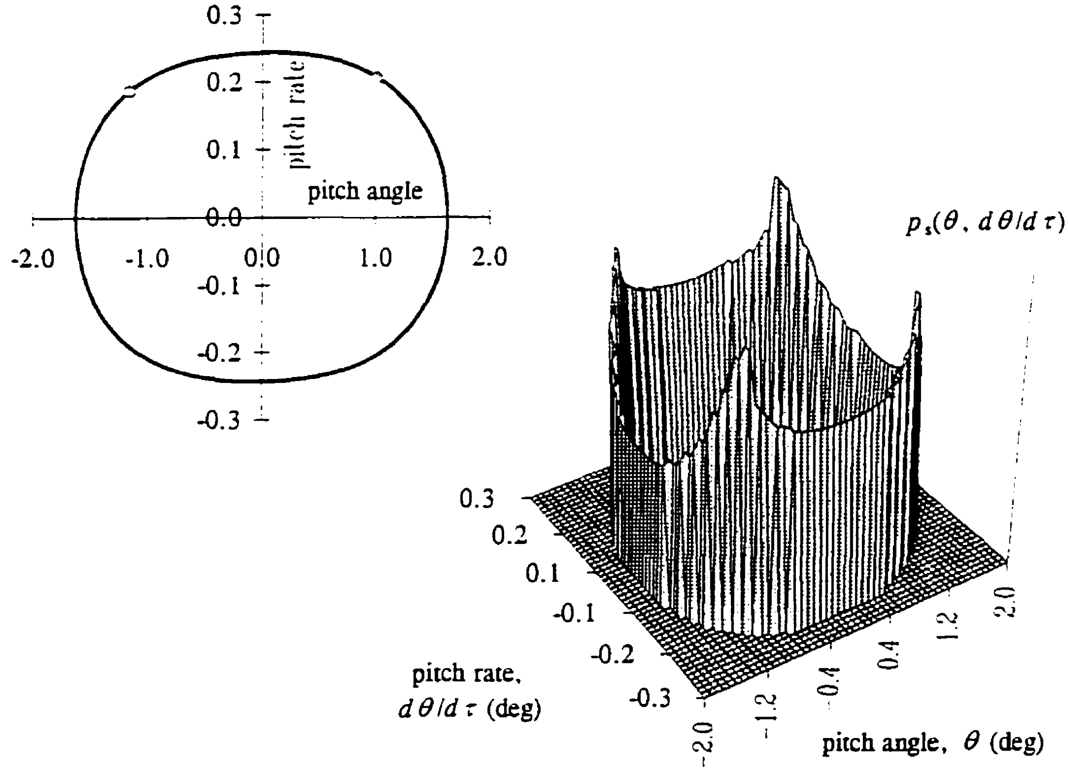

Figure 6.16 - Bi-dimensional PDF and phase plane

of the non-excited nonlinear airfoil pitch pitch-rate for $U = 5.0$; $k_3 = 400.0$

The bi-dimensional PDF representation of the deterministic response at $U = 5.0$ provides more information. Contrary to the marginal PDFs, where the two peaks are located at the maximum amplitude of pitch, and pitch rate, the bi-dimensional PDF exhibits four peaks (two of them are shown with ○ and ● on the phase plane). These peaks are located at intermediate values of pitch and pitch rate, and have approximately the same level of probability density. They represent the system states, in pitch and pitch rate, where the airfoil spends the most time. Notice also the slightly higher level of probability density at zero pitch angle compared with the density at zero pitch rate. Except for a small asymmetry, the general features of this probability density shape are representative of simple harmonic motion.

In the next two figures, Figures 6.17 and 6.18, the same two projections are presented for higher airspeeds, namely $U = 7.0$ and 9.0 respectively. At this point we remark that for this discussion, the value of the airspeed is of no direct consequence. It serves to enable conditions where the transfer of energy from the airflow to the airfoil can be modified. Accordingly, the main interest is in the increase of the response amplitude, and thus on the increasing influence of the nonlinearity and its effect on the probability density function.

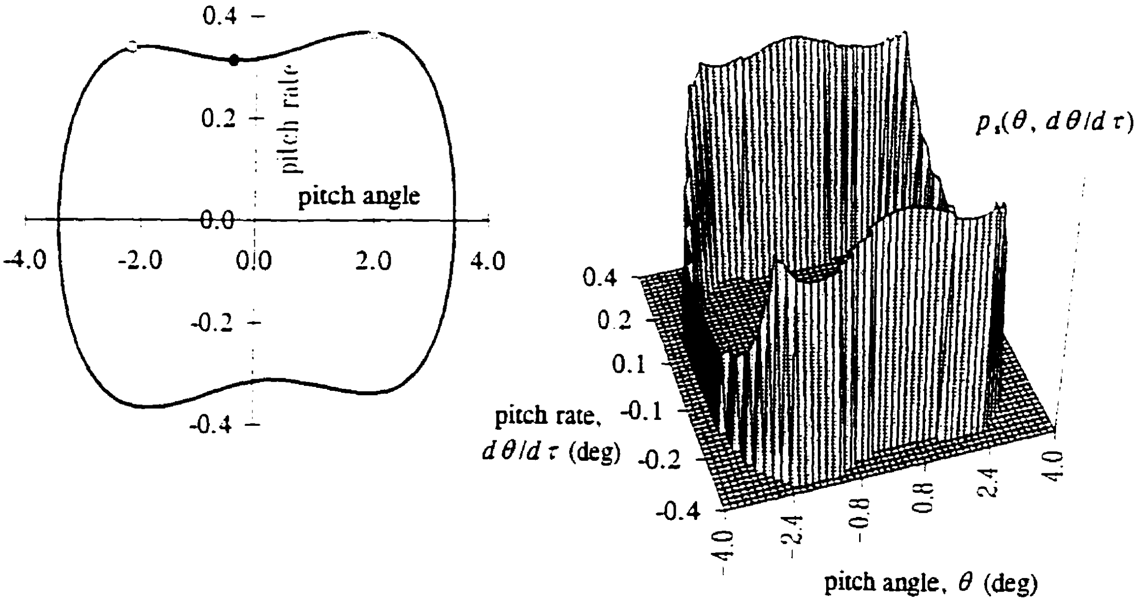

Figure 6.17 - Bi-dimensional PDF and phase plane
of the non-excited nonlinear airfoil pitch pitch-rate for $U = 7.0$; $k_3 = 400.0$.

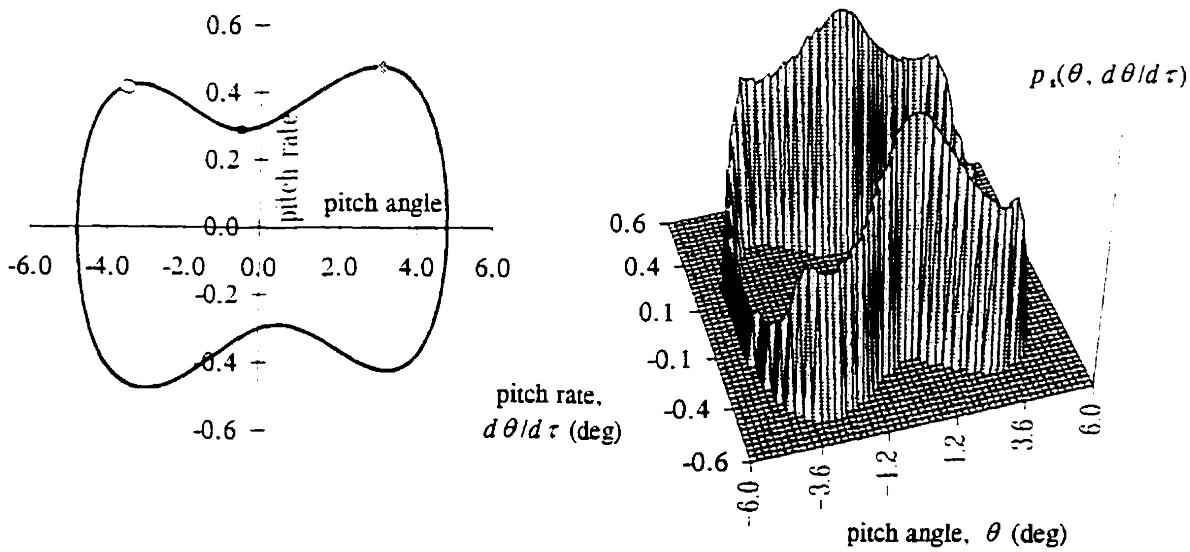

Figure 6.18 - Bi-dimensional PDF and phase plane
of the non-excited nonlinear airfoil pitch pitch-rate for $U = 9.0$; $k_3 = 400.0$.

From the more familiar phase plane projection, it is seen that the LCO has lost its elliptical shape. This is an indication of stronger nonlinear effects, directly due to the greater response. Consequently at these higher airspeeds, compared with $U = 5.0$, we expect a greater contribution of super-harmonics, as discussed by Argyris for the more general problem of the Duffing equation [1994]. We note as well a skewing of the response.

Looking now at the bi-dimensional PDFs, another set of peaks appear located at relatively low values of pitch and high values of pitch rate. They are an extension of the slight increase in probability density identified at zero pitch angle for $U = 5.0$. At $U = 7.0$, this new set of peaks starts to dominate the four other peaks. On the phase plane plots, they correspond to the two kinks. Only one is identified by •. We believe they are directly related to the appearance of the super-harmonics and the stronger effects of the nonlinearity. At $U = 9.0$, these peaks in the PDF are even more dominant.

Of interest is also the movement of the bi-dimensional PDF peaks as the airspeed is increased. This is shown in Figure 6.19 using the phase plane projection of the these three airspeeds, in addition to $U = 12.0$, superimposed on each other.

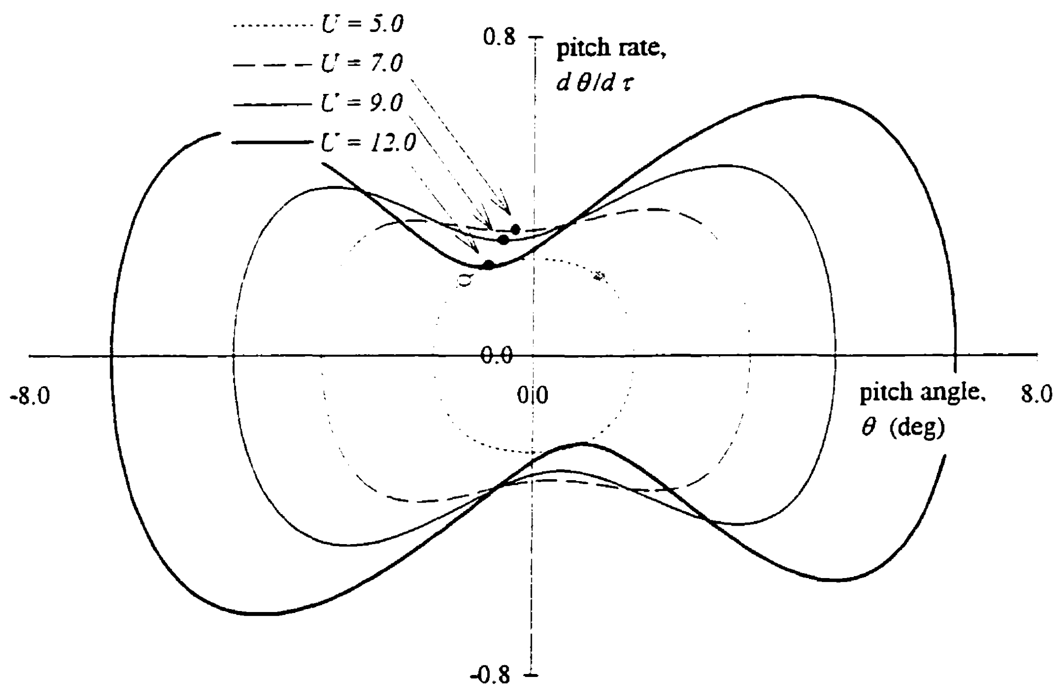

Figure 6.19 - Phase plane plots and location of the bi-dimensional PDF dominant peaks of the non-excited nonlinear airfoil pitch pitch-rate for $U = 5.0$, 7.0, 9.0 and 12.0; $k_3 = 400.0$.

Although each bi-dimensional PDF displays more than one set of peaks, or most probable value, only the dominant set is shown. First illustrated in this figure is the appearance of the new set peaks, in combination with the fact that the four other peaks are fading away relatively, as the airspeed is increased from $U = 5.0$ to $U = 7.0$. In other words, the large nonlinear effects impose a change in the hierarchy of the dominant peaks due to the creation of a new set initially located close to the pitch rate axis. This is followed by a counter clockwise rotation, i.e. away from the pitch rate axis, of the new set of dominant peaks for a further increase in airspeed to $U = 9.0$ and subsequently to $U = 12.0$.

Probability structure and random phase plane of the excited airfoil

The change of behaviour of the non-excited airfoil with airspeed is significant in terms of explaining the effect of turbulence. From the knowledge of the dynamics as a function of one control parameter, namely U, the dynamics as a function of another control parameter, σ_T^2, is interpreted. In support of this approach, it is argued that it is not the control parameter, U or σ_T^2, which directly determines the dynamics we are trying to elucidate, but the nonlinear effects. The effects of the nonlinearity are stimulated by either airspeed or turbulence. In this light, Figures 6.20, 6.21 and 6.22 present the same representations of the dynamics as was shown in Figures 6.16, 6.17 and 6.18, where the dependence was on airspeed, whereas the dependence is now on turbulence variance. This is done at one particular airspeed, $U_m = 5.0$, and for turbulence variance, $\sigma_T^2 = 0.01$, 0.1 and 1.0. Note that the lines shown in the random phase planes represent lines of equal probability density.

As introduced in Chapter 4 in terms of the bifurcation scenario, the obvious behaviour observed from these figures is the transition from a crater-like shape for $\sigma_T^2 = 0.01$ (see Figure 6.20) to a two-peaked shape, and a saddle at the origin, for the two other turbulence levels (Figures 6.21 and 6.22). In this sense, these two last bi-dimensional PDFs are qualitatively similar, and they are different from the first. However, for this discussion the interest lies in an additional aspect of the dynamics, namely the deformation and skewing of the probability structure due to important nonlinear effects.

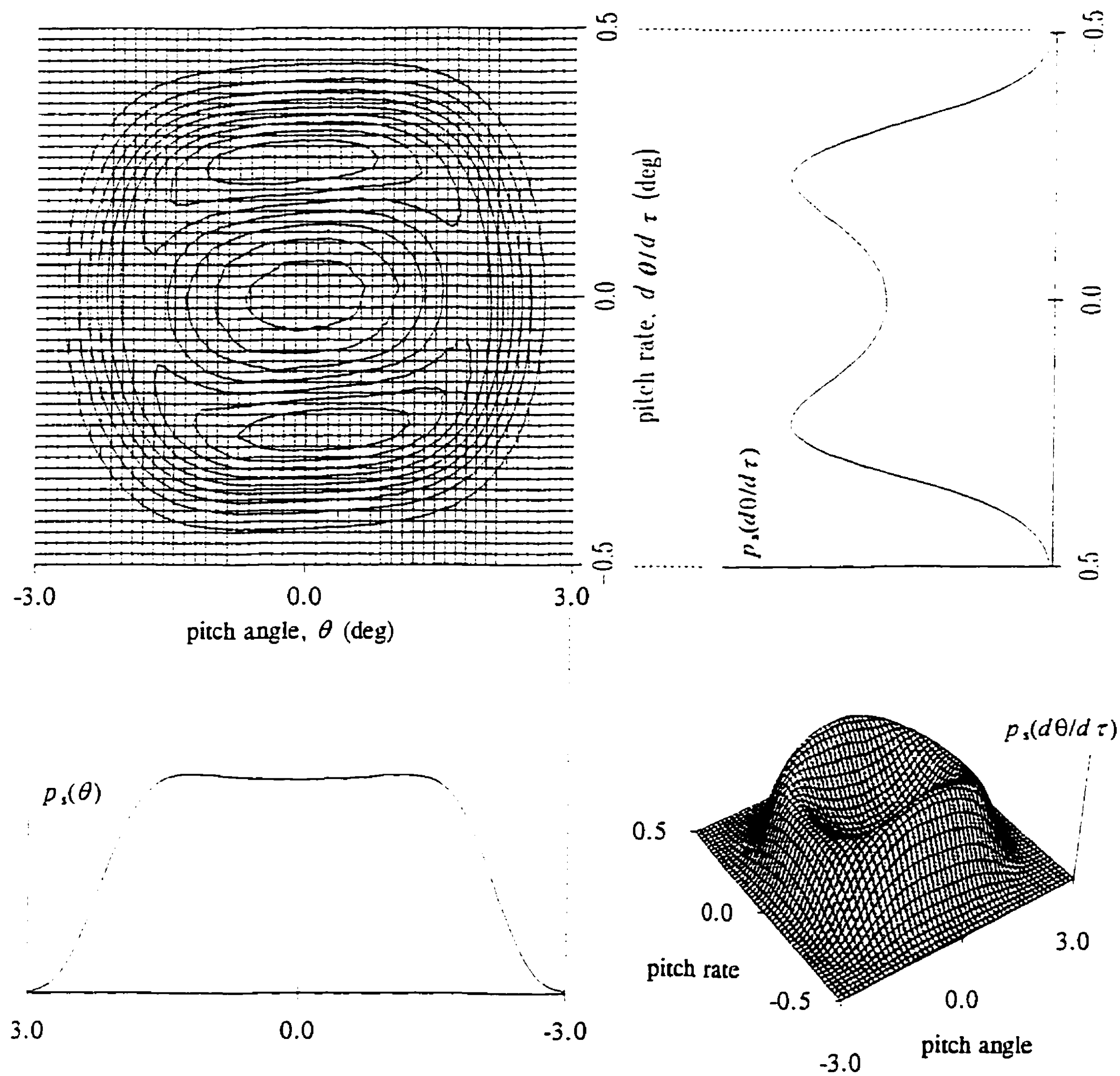

Figure 6.20 - Marginal and bi-dimensional PDFs, and random phase plane, of the nonlinear airfoil pitch pitch-rate in combined turbulence for $U_m = 5.0$; $\sigma_T^2 = 0.01$, $L = 50.0$, $k_3 = 400.0$.

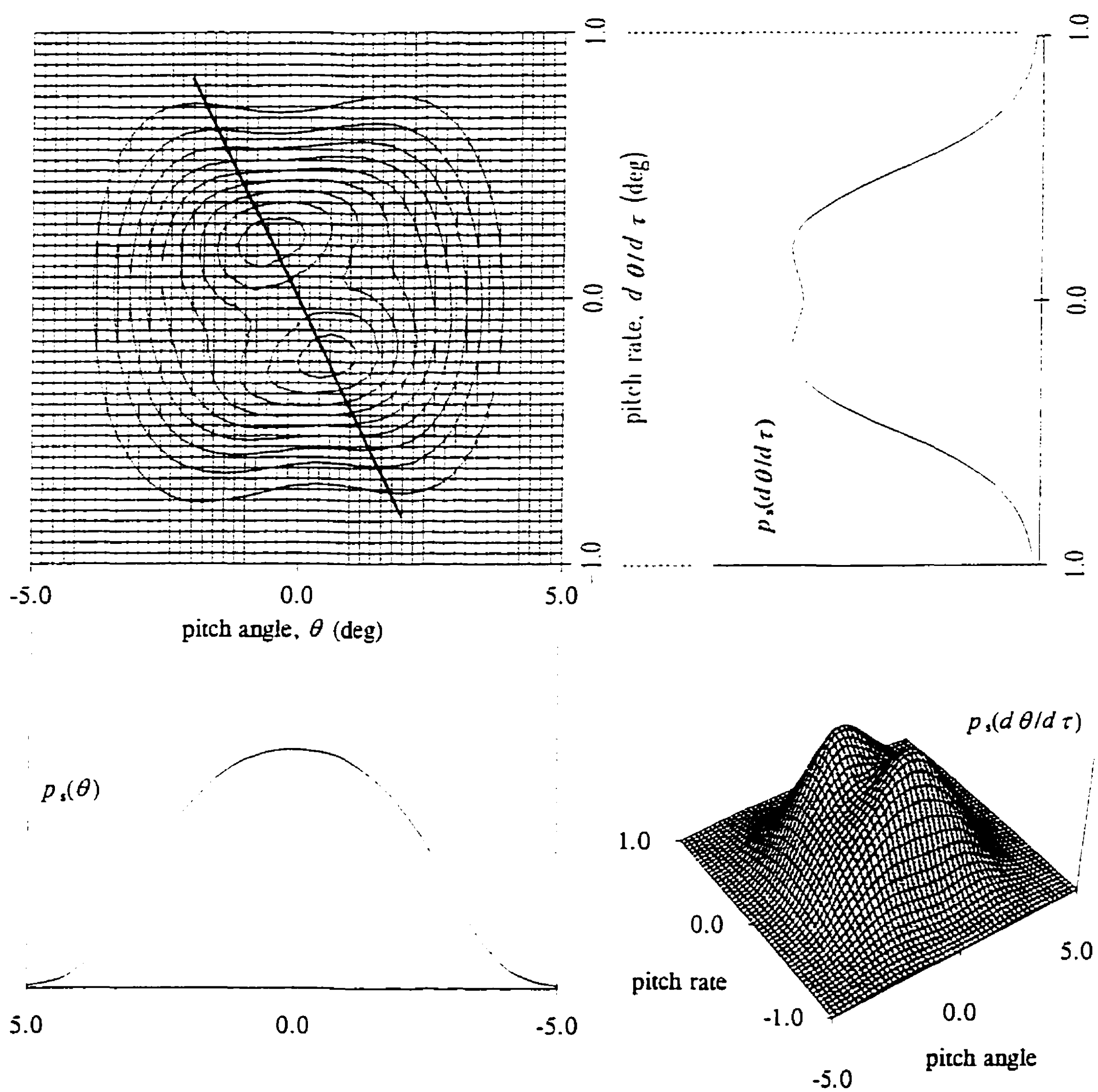

Figure 6.21 - Marginal and bi-dimensional PDFs, and random phase plane, of the nonlinear airfoil pitch pitch-rate in combined turbulence for $U_m = 5.0$; $\sigma_T^2 = 0.1$, $L = 50.0$, $k_3 = 400.0$.

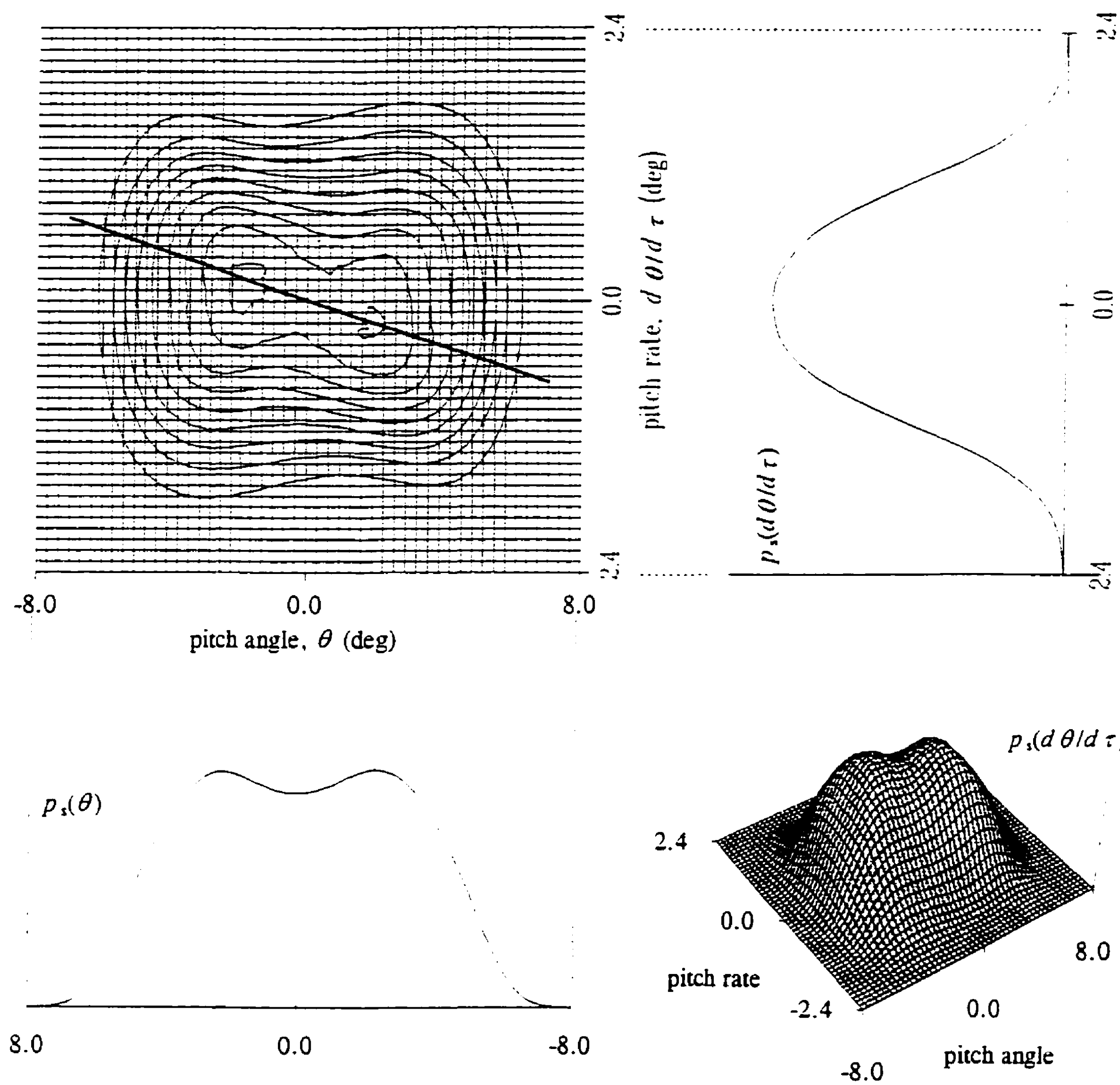

Figure 6.22 - Marginal and bi-dimensional PDFs, and random phase plane, of the nonlinear airfoil pitch pitch-rate in combined turbulence for $U_m = 5.0$; $\sigma_T^2 = 1.0$, $L = 50.0$, $k_3 = 400.0$

To understand the change in the probability structure as the turbulence variance is varied, we must refer to the probability structure of the non-excited response as airspeed is raised, since, as stated earlier, it is the increasing nonlinear effects which dictate the shape of the distribution. In order to make the process clear, we have divided the sequence of events according to three levels of turbulence as exemplified in Figures 6.20, 6.21 and 6.22. Note that these three levels do not correspond exactly to the levels defined for the pitch angle marginal density, since for the bi-dimensional representation the pitch rate variable is also considered.

Case 1 - low level turbulence

The low level turbulence is exemplified by Figure 6.20, where the variance is $\sigma_T^2 = 0.01$. The bi-dimensional PDF displays a crater-like shape. We define the crater-like shape as being a first order effect of the nonlinearity since it is also the main feature of the non-excited LCO at this same airspeed, see Figure 6.16. However, contrary to the deterministic LCO at this airspeed, $U_m = 5.0$, there is a well defined build-up of probability located at low values of pitch angle and high values of pitch rate. The origin of this build-up of probability can be deduced from the observation of the deterministic LCO at a higher airspeed, $U = 7.0$, shown in Figure 6.17. It is due to larger nonlinear effects which are enabled by the turbulent excitation. This is accompanied by the disappearance of the four original peaks of the underlying deterministic LCO which are smoothed by the noise[1]. At this level of turbulence, we define this specific feature in the PDF as a second order effect of the nonlinearity.

In terms of the marginal PDFs, the result is a bi-modal marginal PDF in both pitch and pitch rate. We qualify the bi-modality of the pitch angle PDF as weak, since its two peaks are not high compared with the probability density at the origin. It is an indication that the transition airspeed from uni- to bi-modal has just occurred. The transition in pitch occurs at $U_m = 4.6$. On the contrary the pitch rate bi-modality is strong. Its transition airspeed is located further away, at $U_m = 4.0$.

1

All other effects remaining the same, it is a general property of (external) noise to smooth the dynamics, as pointed out by Eckmann and Ruelle [1985] for example. This property can also be exemplified by the behaviour of the largest Lyapunov exponent which does not exhibit any discontinuity when vertical turbulence is considered, see Figure 4.18.

Case 2 - intermediate level turbulence

At an intermediate level of turbulence excitation, shown in Figure 6.21 for $\sigma_T^2 = 0.1$, the topology of the bi-dimensional PDF is fundamentally transformed. It displays a two-peaked shape whose peaks are located at low values of pitch angle and high values of pitch rate. Although it is difficult to pinpoint graphically the exact value of turbulence variance at which this change in shape occurs, it is found that it happens in the vicinity of $\sigma_T^2 = 0.06$.

The turbulent excitation has destroyed the crater-like shape in two ways. Firstly, it has forced some of the dynamics to occur near the origin, thus in effect filling the probability crater. This is sometimes referred to as plane- or phase-filling [Grassberger and Procaccia, 1983]. Secondly, by inducing larger nonlinear effects, the turbulent excitation has enhanced the relative importance of the two inner peaks. It is then said that the second order effect of the nonlinearity becomes dominant due to the turbulent excitation. This second aspect can be understood by again referring back to the deterministic LCO as the airspeed is raised from $U = 5.0$ to 7.0 and 9.0, and where the inner peaks become stronger in comparison with the original four. At $\sigma_T^2 = 0.1$, the combined result is still a uni-modal marginal PDF in pitch and a bi-modal marginal PDF in pitch rate.

Case 3 - high level turbulence

The destruction of the LCO structure is accompanied by another type of re-distribution of the probability density between the pitch and pitch rate. At the previous value of turbulence variance, $\sigma_T^2 = 0.1$, the two peaks tend to be aligned with the pitch rate axis. As the turbulence variance is further increased, for example to $\sigma_T^2 = 1.0$, as shown in Figure 6.22, the alignment moves toward the pitch angle axis. In other words, the basic shape of the bi-dimensional PDF does not change but it is effectively rotated about the probability axis. This rotation is better seen on the random phase plane where the contours represent lines of equal probability density. Again, this is also a general observation of the non-excited case as shown in Figure 6.19 as the airspeed is raised from $U = 7.0$ to 9.0 and 12.0. The counter clockwise rotation of the two peaks towards higher values of pitch angle and lower values of pitch rate results in a bi-modal marginal PDF in pitch and a uni-modal marginal PDF in pitch rate. This is an opposite result from the lower turbulence level, and explains the observed interdependence and mirroring movement of the pitch and pitch rate marginal PDF transition airspeed shown in Figure 6.15.

In summary, a smoothing of the underlying deterministic LCO structure accompanied by a transfer of probability to two new regions in the state space have been noted as immediate consequences of turbulent excitation. These are followed by a general skewing of the bi-dimensional PDF, and random phase plane, and the counter clockwise rotation of the two new peaks as the turbulence variance is further increased. The practical result is postponement of the pitch angle and advancement of the pitch rate at low values of turbulence variance, and conversely for high turbulence level.

We have explained and interpreted the initial probability transfer, followed by a general skewing and rotation, with the following rational. Similar to the effect of changing the airspeed, which enables a greater transfer of energy from the airflow to the airfoil and hence a greater demand on the nonlinearity as observed from the deterministic behaviour, the increase in turbulence variance also enhances nonlinear effects. In turn, the greater demand on the nonlinearity should be reproduced by the response spectral content. Hence, parallelling the effect of the nonlinearity on the PDF and phase plane for the non-excited airfoil as the airspeed is raised, we have also observed an increase in the contribution of the super-harmonics with turbulence variance. The spectral response will be discussed in more detail in Section 6.3.

In attempting to provide an explanation of the probability structure of the response, the problem has been simplified by focussing on the dynamics of the pitch DOF. In this line, the analysis is pursued and other influential factors, such as scale of turbulence and nonlinear torsional stiffness, are examined as experienced by the pitch marginal PDF transition airspeed.

6.2.2 Effects of nonlinear torsional stiffness

This next topic briefly considers the effect of varying the nonlinear torsional stiffness coefficient, k_3, on the transition airspeed of the pitch marginal PDF. Figure 6.23 shows the transition airspeed boundary for three values of turbulence variance, $\sigma_T^2 = 0.01, 0.1$ and 1.0. Each data point is identified according to the nature of the pitch uni-modal to bi-modal transition. The description *outer*, identified by the unfilled symbols □, ◇ and △, refers to the appearance of the LCO displayed by the PDF in the case where the turbulence level is considered to be low. The other description *inner*, identified by the filled symbols ■, ◆ and ▲, refers to the case described earlier as the high level turbulence, where the basic structure of the LCO is lost in favour of the appearance of inner peaks close to the origin. The two data points labelled as *inner* but where the *outer* transition airspeed is also shown in parenthesis refer to the intermediate level turbulence. In this case, there is a double bi-modality where transition of the outer peaks occurs earlier than the inner peaks, but it is the inner peaks which are dominant.

Some observations and interpretations are the following. For the *outer* uni- to bi-modal transition type, an increase in nonlinear coefficient delays the transition to higher airspeeds. A further increase in k_3 changes the nature of the bi-modality. At this point, there is a range of coefficient values where the basic structure of the LCO is competing with the inner peak(s) which are getting stronger. At still larger values of the nonlinear coefficient, the post-transition PDFs are back to being purely bi-modal, but their nature is different from the one at small values of k_3. This is referred to as the *inner* type bi-modality. Further increases in k_3 have the opposite effect which is the advancement of the transition airspeed.

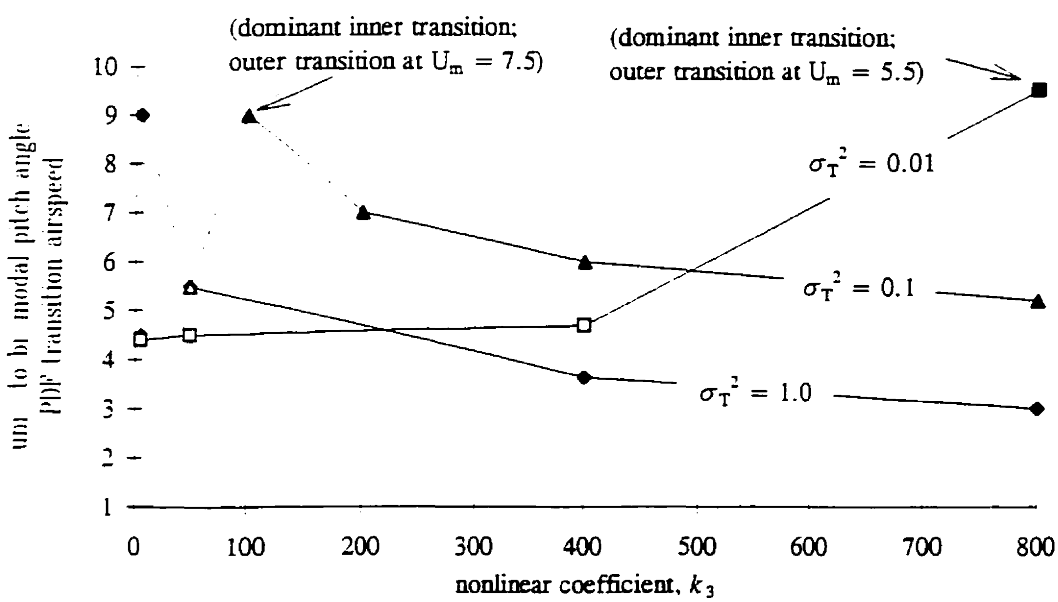

Figure 6.23 - Transition airspeed of pitch marginal PDF of nonlinear airfoil in combined excitation, for different turbulence variances, as a function of the nonlinear coefficient; L = 50.0; □, ◇ and △ : outer mode transition; ■, ◆ and ▲ : inner mode transition.

6.2.3 Effects of scale of turbulence

Figure 6.24 presents the pitch marginal PDD transition airspeed as a function of turbulence variance for three different scales of turbulence, one of which, L = 50.0, is reproduced from Figure 6.15. The overall behaviour for the three cases is the same. There is postponement of the transition airspeed at low values of turbulence variance, changing into advancement at high values. Not shown but note that the case with L = 0.5 changes to advancement for a turbulence variance, σ_T^2 = 15.0. In all cases, the region where the largest postponement airspeeds occur corresponds to the conversion zone where the nature of the bi-modality is changing as described earlier. The nomenclature for the data points is the same as defined for the previous figure.

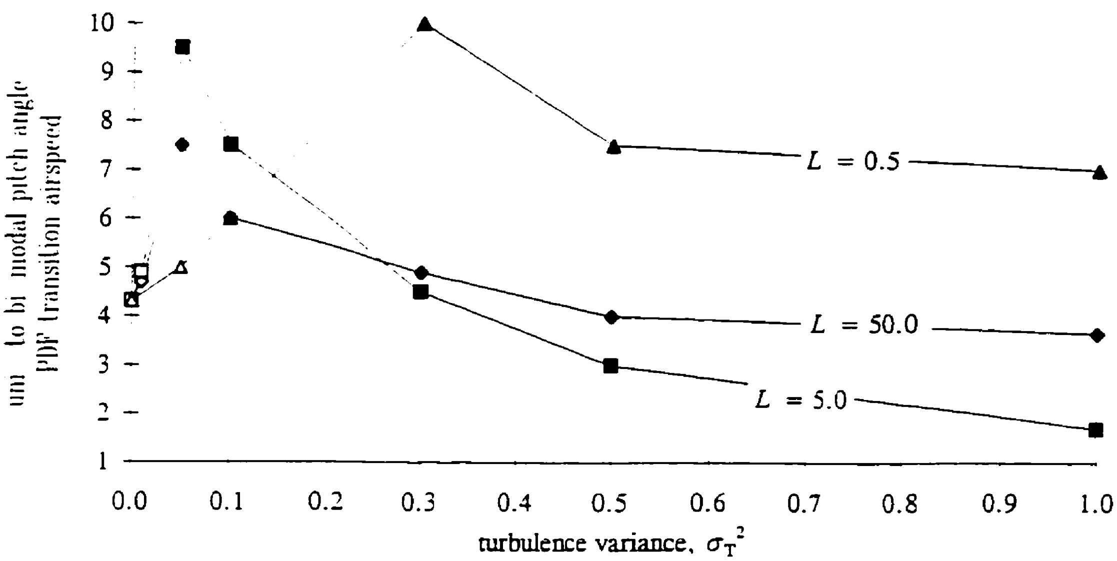

Figure 6.24 - Transition airspeed of pitch marginal PDD of nonlinear airfoil in combined excitation, for different values of scale of turbulence, as a function of turbulence variance; k_3 = 400.0; ▫, ◇ and △ : outer mode transition; ▪, ♦ and ▲ : inner mode transition.

With regards to the quantitative differences, it is believed that they are mainly dictated by the value of the excitation PSD at some critical (external) resonant frequencies, which have a direct effect on the mean-square response. For example, examine Figure 6.4 which shows the pitch response mean-square for the same three values of scale of turbulence, as a function of airspeed. The response mean-square generally indicates that the scale of turbulence, L = 5.0 case, responds the greatest, followed by the case of L = 50.0, and thirdly by the effective white noise case (L = 0.5). Realising that the excitation variance level (σ_T^2 = 1.0) used to produce the data for Figure 6.4 corresponds to the series of results on the far right of Figure 6.24, it is noted that this hierarchy of response is reproduced by the same hierarchy in transition airspeed.

The observed relationship between response mean-square and transition airspeed makes physical sense since an overall larger response level will induce a greater demand on the nonlinearity. Furthermore, the turbulence level for this example corresponds to post-transition motions characterised by the two-peaked bi-dimensional PDF. We have seen that in this case, larger nonlinear effects are associated with a counter clockwise rotation of the probability density about its axis, which tends to separate the peaks in the one-dimensional pitch marginal PDF, hence an earlier transition airspeed in pitch. In this sense, the relationship between transition airspeed and nonlinear coefficient is the same as the one with turbulence variance which in effect enhances nonlinear effects.

6.3 Frequency Content of the Response

6.3.1 Importance of super-harmonic peaks

The main relevance of presenting the spectral content of the response is in support of the previous discussion concerning the deformation and skewing of the bi-dimensional PDF due to enhanced nonlinear effects with turbulence variance (Section 6.2.1). In doing so, it will be demonstrated that the relative importance of the super-harmonics is accrued as the turbulence variance is raised.

To that effect Figure 6.25 compares the pitch PSD for three values of turbulence variance. It is observed that in addition to an overall increase in power spectral density with turbulence variance, the third and fifth harmonics become stronger in comparison with the fundamental frequency. This observation accounts for the departure of the basic LCO structure in the bi-dimensional PDF representation with increased turbulence variance, and echoes the increasing relative importance of the super-harmonics of the deterministic response with airspeed.

The appearance of an additional feature, not directly accounted for by the deterministic airfoil, is also shown in Figure 6.25. It is discussed in the sub-Section 6.3.2.2.

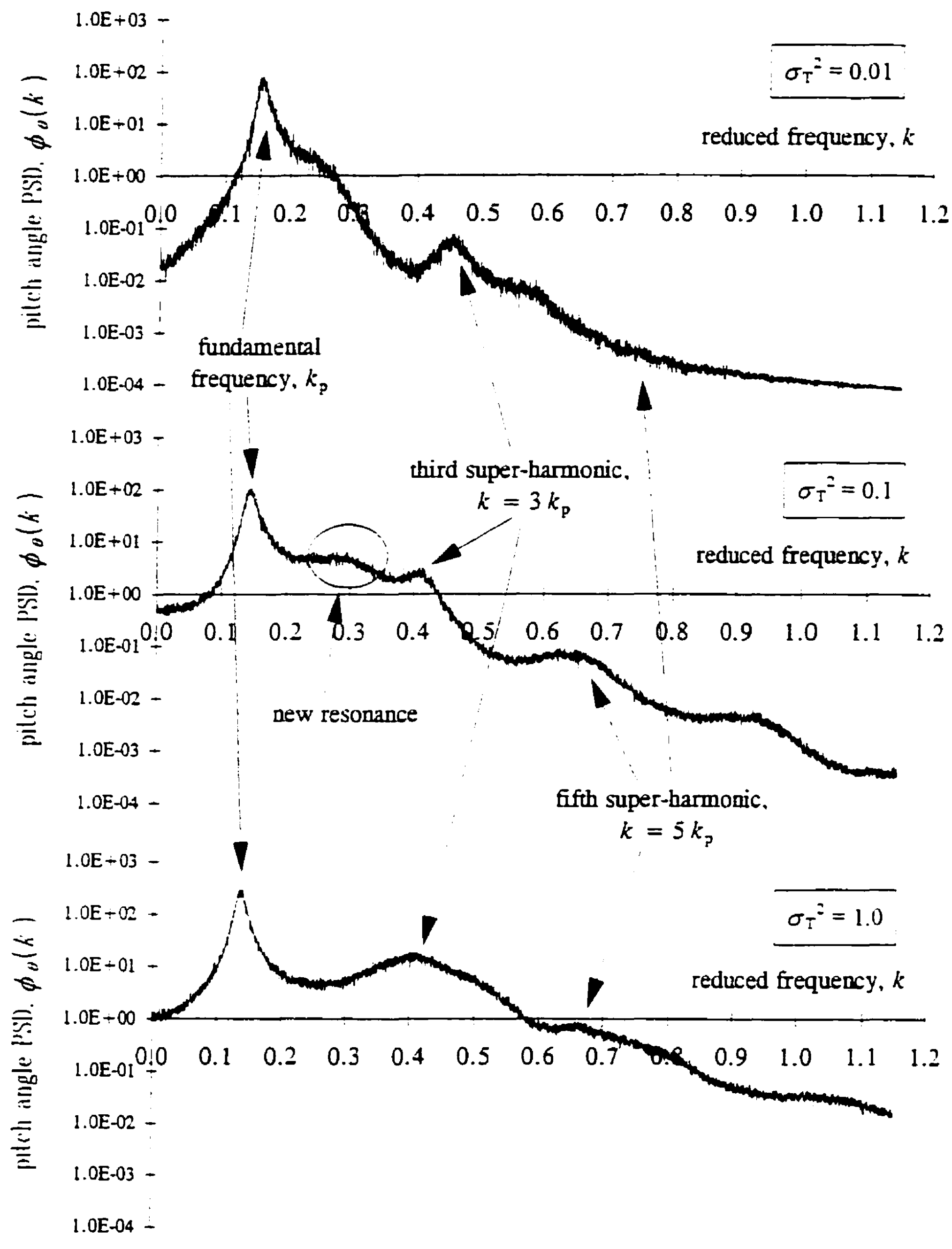

Figure 6.25 - PSD of nonlinear pitch response to combined excitation at $U_m = 5.0$, for three values of turbulence variance; $L = 50.0$, $k_3 = 400.0$.

6.3.2 Other distinctive spectral features

Other distinctive, and unexpected features are displayed by the spectrum. They are pure products of the interplay between the nonlinearity and random excitation, since they do not appear when either of these two ingredients are missing. To do full justice to these observed phenomena would require a much more in-depth analysis. In this regards, we will not attempt such an endeavour and restrict ourselves to briefly describe our observations and propose some directions for further study.

6.3.2.1 Shift of the fundamental resonant frequency

The first aspect concerns the dominant peak, which represents the fundamental harmonic of the random LCO. At pre-flutter speeds, it represents the slow mode or the mode losing stability. We have observed that it is shifted to a smaller frequency compared with the deterministic value which is at $k_{LCO} = 0.164$ for $U = 5.0$. Furthermore, the magnitude of the shift depends on the turbulence variance; see Figure 6.26.

Although we cannot provide any rational explanation for this shift in frequency, we can say it is not due to the longitudinal component of turbulence. We have shown and discussed in Chapter 4 that the longitudinal component of turbulence has an opposite effect on this mode when nonlinear effects are either small or not considered at all. Moreover, we have run tests without the longitudinal component. No change in the location of the dominant peak in the PSD was noted. Consequently, we believe the shift in frequency, in comparison with the non-excited airfoil LCO frequency, is a consequence of the combined effect of turbulence (mainly vertical) and of the nonlinearity.

A shift in frequency is by itself not totally unexpected since the nonlinearity is acting on a stiffness term. In this case and as pointed out by Cai and Lin [1997], the natural period of the system is not constant but changes with the amplitude of the motion. Note, however, that this interpretation is usually associated with a broadening of the peaks. Hence, a nonlinear stiffness oscillator is disposed to a shift in frequency. This was also noted by Roy and Spanos [1993]. In contrast, Roy and Spanos have also discussed the case of the van der Pol oscillator externally excited by noise where no shift in the resonant peak is observed. The surprise in our results comes from the observation that the shift is toward the lower frequencies, considering that nonlinear effects (due to a hardening spring) are usually accompanied by an increase in the resonant frequencies of a system. For example, both the Duffing equation, with a hardening spring, externally forced by a harmonic excitation [Nayfeh and Mook, 1979], and a coupled 2DOF system with a hardening cubic stiffness nonlinearity also excited by a harmonic forcing [Lee et al., 1997], present a resonance curve tilted to the right.

Nevertheless, and in support of our observation, we mention that an experimental manifestation of a shift towards smaller frequencies has been reported in the physics literature for simple nonlinear systems driven by additive noise [Dykman and McClintock, 1992]. In addition, these cases have been shown to exhibit what is called ***noise-induced narrowing***, as defined for example by the diminishing ratio of the bandwidth at the half power point over the peak power, which is in total contrast with the more familiar broadening observation. Dykman and McClintock seem to suggest that noise-induced narrowing is a large noise phenomena since it is preceded by a peak broadening at smaller noise intensity. Our results, presented in Figure 6.25 do in fact exhibit a narrowing of the fundamental frequency peak. This is better seen on a linear scale in Figure 6.26, which also includes the frequency response for two additional turbulence excitation variances.

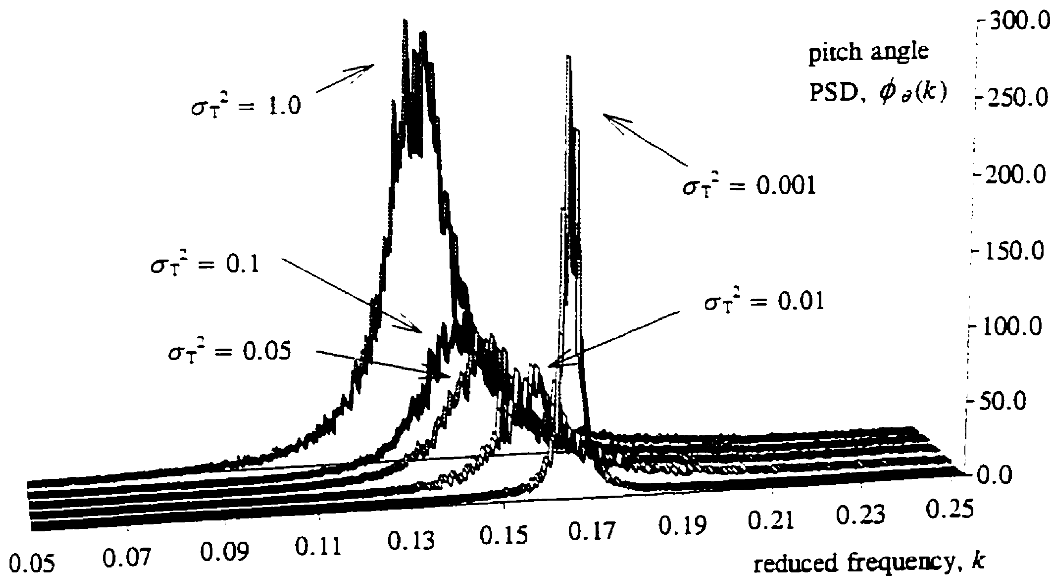

Figure 6.26 - PSD of nonlinear pitch response to combined excitation for five values of turbulence variance; U_m = 5.0, L = 50.0, k_3 = 400.0.

Note that a broadening of the peak occurs as the turbulence variance is varied from σ_T^2 = 0.001 to 0.01. Further increases of the turbulence variance, to σ_T^2 = 0.05, 0.1 and 1.0, induce a reverse trend, hence a peak narrowing. We note that the value of turbulence variance at which this reversal in trend is observed, 0.01 < σ_T^2, seems to correspond approximately to the variance at which the inner peaks in the pitch marginal PDF starts to become dominant.

6.3.2.2 New resonant peak

A totally new time scale, not present in the deterministic problem, is observed in the spectrum. In Figure 6.25, it is best seen for the case with turbulence variance, $\sigma_T^2 = 0.1$, where it appears as a broad band peak centred at $k \approx 0.3$. For the two other turbulence variances, σ_T^2 = 0.01 and σ_T^2 = 1.0, this new resonance appears as a hump in the vicinity of $k \approx 0.25$ and $k \approx$ 0.5, respectively.

The appearance of a new peak in the spectrum is a known peculiarity of nonlinear noisy systems, but for which there is a bi-stability. In the bi-stable case, the physical grounds for a new time scale can be easily understood since the noise triggers jumps between two stable attractors. At a certain value of noise intensity, coherent oscillations, in the probabilistic sense, occur between the two states. We have no such bi-stability in our case. Accordingly, this explanation does not seem to apply.

From Figure 6.25, we notice that the location of this new peak appears to be turbulence variance dependent, and occurs at higher frequencies for larger excitation levels. The same observation is retained from Figure 6.27, which compares the spectral responses of the airfoil for pure vertical and combined turbulence excitation. A shift of the new resonant peak towards higher frequencies for combined turbulence is noted as well. Both cases are responding to the same value of turbulence variance, but their mean-square responses are different, the latter being larger. This greater response to vertical turbulence is enabled by the longitudinal component of turbulence which has a destabilising effect, as will be discussed in Chapter 7. For this case, there is a 12% increase in mean-square pitch response due to longitudinal turbulence. Note as well that no fundamental differences are noticed between the spectral responses of Figures 6.25 and 6.27 which correspond to post-instability and pre-instability regimes, respectively.

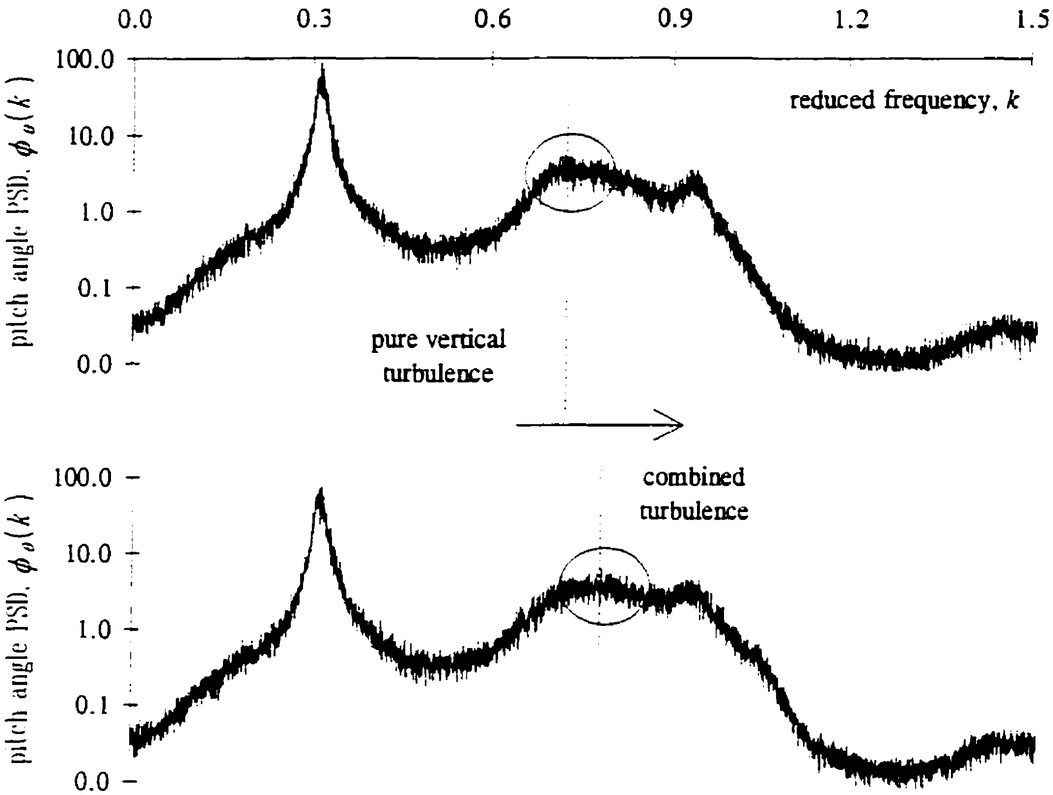

Figure 6.27 - PSD of the nonlinear pitch response to pure vertical and combined turbulence, at $U_m = 2.0$; $L = 50.0$, $\sigma_T^2 = 1.0$, $k_3 = 400.0$.

Hence, it is believed that the location of the peak is not directly due to the turbulence level, but to the airfoil mean-square response. In this light, we are tempted to propose a simplistic phenomenological interpretation in the form of an effective stiffness. Recall equation (6.3) where this concept is defined more explicitly in the context of a 1DOF system with a cubic stiffness nonlinearity:

$$(k_{linear} + k_3\,\overline{\theta}^{\,2})\,\theta. \tag{6.3}$$

In an analogy to the linear system, the term $k_3\,\overline{\theta}^{\,2}$ represents effectively a stiffness coefficient. In this sense, a larger mean-square response, $\overline{\theta}^{\,2}$, corresponds to a stiffer system, hence a displacement of this effective stiffness peak towards a higher frequency on the response spectrum. The concept of an effective linear stiffness has been shown to have merit in the context of predicting the mean-square response of noisy nonlinear systems. This is usually formalised under the approach of equivalent linearization, and has for its deterministic counterpart the describing function method. However, the use of an effective stiffness in the context of the frequency response is probably more equivocal.

Finally, we add that since it is a general observation that nonlinear random dynamical systems which possess a noise-controlled time scale are susceptible to exhibit stochastic resonance [Silchenko et al., 1999; Anishchenko and Neiman, 1997], it is likely that these two observations in our aeroelastic system are associated with an increase in the signal-to-noise ratio at some optimal value of turbulence variance[2].

6.4 Concluding Remarks

The response of the nonlinear airfoil to turbulent flow (longitudinal and vertical) takes different forms. We have chosen to concentrate on the mean-square and probability density density representations, and touch upon some aspects of the frequency response. The main points we retain are:

1. The excited response mean-square increases with airspeed. This is mainly attributed to the combined influence of an increasing aerodynamic forcing and growing amplitude of the underlying deterministic LCO.

2. Depending on turbulence variance and magnitude of the nonlinear stiffness coefficient, the excited mean-square response may tend to or diverge from the non-excited, deterministic response as the airspeed is raised. In this regard, increasing the turbulence variance or the nonlinear coefficient have the same effect in that the excited response tends to depart from the non-excited one.

2

Although stochastic resonance is usually identified with the amplification of a weak external periodic forcing, similar amplification observations have been reported where the periodic signal is not external but originates from the system itself in the form of a limit cycle [Ditzinger et al., 1994]. In this case, it is termed *stochastic resonance without external periodic force*. It corresponds to our problem.

3. As introduced in Chapter 4, the transitions in the marginal PDFs occur at smaller airspeeds for the pitch and pitch rate as compared to both heave states. We have attributed this behaviour to the location of the nonlinearity which acts directly on the pitch stiffness. Moreover, the transition airspeeds in the heave and heave rates are always delayed with respect to the reference non-excited flutter/Hopf bifurcation point, and increase monotonously with airspeed.

4. On the contrary, the transition airspeeds of the pitch states display a non-monotonic behaviour. In comparison with the deterministic flutter/Hopf bifurcation airspeed, the transition airspeeds are initially (i.e. for small values of turbulence variance) postponed in pitch angle and advanced in pitch rate. As the turbulence level is increased, the trend is inverted such that the pitch angle transitions at a smaller airspeed and the pitch rate at a larger airspeed.

5. The initial postponement in pitch angle transition airspeed, from uni- to bi-modal, corresponds to the fading away of the underlying structure of the deterministic LCO. At intermediate levels of turbulence, a competition occurs between the LCO structure and more dominant turbulence effects interacting with the non-linearity. The result is a double bi-modality of the pitch marginal PDF where the outer peaks correspond to the underlying deterministic LCO and the inner peaks to the latter effects. A further increase in turbulence variance destroys completely the LCO structure. This is represented in the pitch marginal PDF by another type of bi-modality. Accordingly, the nature of the bi-modality of the marginal PDF projection is not unique.

6. The nature of the bi-modality depends on turbulence level, and on the magnitude of the nonlinear coefficient as well. The dependence is the same for both. For example, a small turbulence variance or small nonlinear coefficient correspond to the LCO based bi-modality.

7. Associated with the destruction of the basic LCO structure, and the appearance of the inner peaks in the marginal PDFs, is the increased contribution of the super-harmonics relative to the fundamental frequency. It is a manifestation of the enhanced nonlinear

effects induced by the turbulence, and parallels the change in the dynamics of the non-excited airfoil with airspeed.

8. Finally, the interaction of the turbulent excitation with the nonlinear torsional stiffness induces two noise-controlled time scales. One is a shift towards smaller frequencies and narrowing of the dominant fundamental frequency peak. The second is the appearance of a new resonant peak, located in the intermediate frequency range.

Chapter 7

CONTRIBUTION OF LONGITUDINAL TURBULENCE EXCITATION - Binary Flutter Conditions

Specifically in response to the second objective of this thesis, which is to articulate a detailed and comprehensive picture of the contribution of the longitudinal component of turbulence as experienced by the airfoil, we examine its effects mainly from the point of view of its relative importance in the overall, more realistic, combined turbulence problem. Recall that in the introductory chapter, we mentioned that no systematic and rational investigation could be found in the literature concerning this question, for the linear nor the nonlinear airfoil. This discussion intends to bridge that gap.

During the course of this research, we have found that longitudinal turbulence has essentially two effects of a seemingly opposite nature. One is destabilising, and the other is organising. By organising, we mean a tendency to force the dynamics to be centred around the origin, as manifested by a sharpening of the response probability density. These two effects are discussed in the following sections, first separately and then in combination. They are also discussed from the point of view of their overall contribution relative to the importance of the vertical component of turbulence.

7.1 Destabilisation

The effect on stability has been discussed in part in Chapter 5 with regards to the advancement of the flutter point. The other facet of the destabilising role of the longitudinal component of turbulence has a more global effect since it affects more than the immediate region of the flutter point. This global consequence of destabilisation is the enhanced sensitivity of the airfoil to external excitations. It has been introduced in Chapter 4, for example Figure 4.20 which shows that the dynamics of the nonlinear airfoil in combined turbulent excitation exhibits a largest Lyapunov exponent closer to the zero axis compared with pure vertical turbulence, thus indicating a decrease in stability due to longitudinal turbulence.

Expressed tangibly by the response mean-square, the decrease in stability due to the longitudinal component of turbulence affects both the fixed point and the LCO which respond with more vigour to vertical turbulence. We examine this question for the nonlinear and linear airfoil (only the stable fixed point in this case), and use the response mean-square, more precisely the difference between the combined and pure vertical turbulence excitation, and the largest Lyapunov exponent as the main measures.

7.1.1 Linear airfoil

The destabilisation of the linear airfoil, strictly speaking the equilibrium point, is considered. Figure 7.1 compares both the largest Lyapunov exponent and pitch response mean-square as a function of mean airspeed for combined and pure vertical coloured turbulence. Note that in examining the linear airfoil, we are restricted to pre-flutter airspeeds, as defined by the random flutter speeds given in Chapter 5. For the case shown below, the random flutter speed is $U_{ml} = 3.95$.

From Figure 7.1 (a), it is observed that in addition to the advancement of the flutter point, the largest Lyapunov exponent is, for all airspeeds, closer to the neutral stability axis due to longitudinal turbulence in comparison with the non-excited case given by the real part of the eigenvalue of the slow mode. If we consider the interpretation that the magnitude of the largest Lyapunov exponent is an expression of the degree of stability of trajectories, we may say that longitudinal excitation decreases the stability of the system, strictly speaking the fixed point, on two accounts. Not only does it advance the flutter point, it also decreases the damping or the strength of the attraction, hence a longer time to reach steady state, in the probabilistic sense. On the other hand, we note that the loss of damping associated with the approach of the flutter speed is slightly more gradual and less explosive with longitudinal turbulence than without.

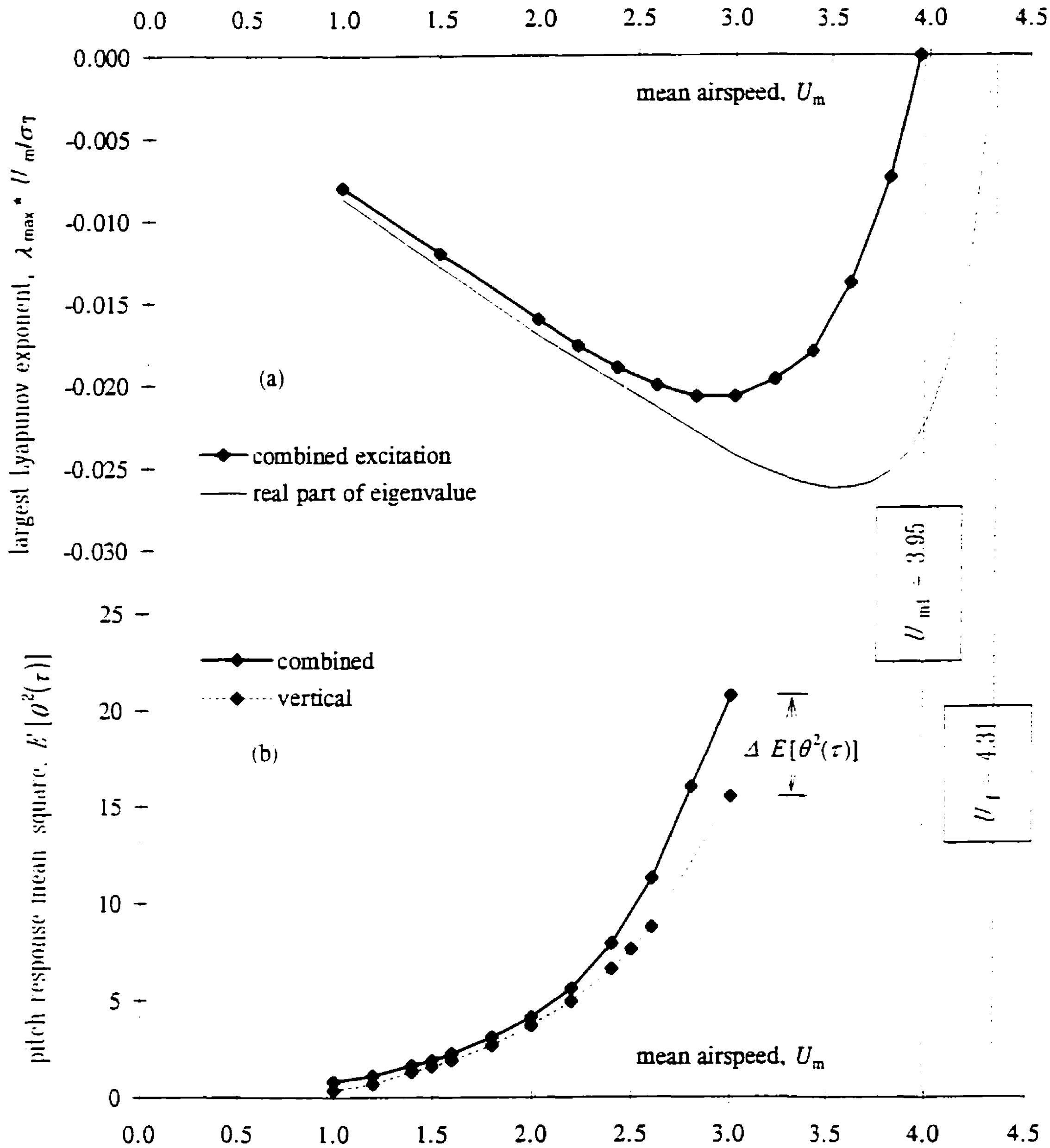

Figure 7.1 - Comparison of the largest Lyapunov exponent (a), and pitch response mean-square (b), of linear airfoil for combined and pure vertical turbulence, as a function of airspeed; $\sigma_T^2 = 0.5$, $L = 50.0$, $k_3 = 0.0$.

It is also observed that the difference between the excited and non-excited cases is significant in the vicinity of the flutter point, which we attribute to the direct consequence of its shift in airspeed. The difference then diminishes with decreasing airspeed up until it reaches approximately $U_m \approx 2.5$. For airspeeds below $U_m \approx 2.5$, the difference in the value of λ_{max} remains relatively small and constant. We interpret this range of airspeed as being no longer influenced by the shift in flutter point, but rather by a more general destabilising effect of longitudinal turbulence. In this respect, the shift in flutter speed seems to have an effect on the response for a relatively large airspeed range, $2.5 \leq U_m < U_{m1} = 3.95$.

The same trends are observed for the pitch response mean-square shown in Figure 7.1 (b). The delta response due to the presence of longitudinal turbulence (i.e. the difference in response between the combined and pure vertical excitation cases) increases with increasing airspeed for $U_m \geq 2.5$, hence as the instability point is approached. On the other hand, the delta response stays relatively constant at the lower speeds, i.e. away from the flutter point.

Another observation is that the increase in response mean-square due to longitudinal turbulence appears to be more significant than the shift in flutter point. In other words, the longitudinal component of turbulence appears to have relatively more influence on the response mean-square than on the shift in flutter speed even for airspeeds well ahead of the flutter point, as shown for example for $U_m = 3.0$ in Figure 7.1. These general statements are given a more exact meaning in the Table 7.1, where the percentage difference (increase) in response mean-square for two typical airspeeds are compared. Also presented are results for other turbulence levels, as well as the percentage shift in flutter speed as reproduced from Table 5.1.

In order to establish a meaningful description, and comparison, of the response mean-squares, the two typical values of airspeed are defined in accordance with an operational point of view. One corresponds to an *operational design airspeed*, U_D, and the other to a *limit airspeed*, U_L. In the establishment of an operational usage envelope, it is a common design practice to use a 1.2 safety factor for flutter. In other words, U_L is typically defined according to $U_f = 1.2\ U_L$, thus in our case $U_L = 4.31/1.2 \approx 3.5$. On the other hand, the definition of the design airspeed (i.e. the airspeed at which the system is normally used) does not usually follow a similar universal standard, but is lower than U_L. We choose a factor of safety in the order of 2, which translates into $U_D \approx 2.0$.

We can also attach to these two airspeeds another interpretation. We consider the design airspeed, $U_D = 2.0$, to be representative of the response level associated with the general destabilising effect of the longitudinal component of turbulence and where the shift in flutter speed has lost its influence. On the other hand, we consider the limit airspeed, $U_L = 3.5$ to be representative of the response level associated directly, and specifically, with the advancement of the flutter point.

To each value of turbulence variance, we have associated turbulent intensities based on the limit and deterministic flutter speeds. This provides a basis of comparison with a real life environment. For example, the lower turbulence variance corresponds roughly to atmospheric conditions. Houbolt et al. [1964] have given RMS turbulence velocities ranging from 2 m/sec for clear air, to 6 m/s in cumulus clouds and 12 m/sec in severe weather. Assuming a typical aircraft flutter speed of 250 m/sec, turbulence intensities based on that airspeed value range from 1%, 2% to 5%, respectively.

The two larger values of turbulence variance may correspond to a turbulent environment created by flow separation in the wake of a body as pointed out, for example, by Fujimori et al. [1979] in the context of rotor blades. As remarked in Chapter 1, the higher turbulence level may represent the case of leading edge vortex breakdown of fighter aircraft at high angle of attack.

	$\sigma_T^2 = 0.01$ $T_{u,Uf} = 2\%$ $T_{u,UL} = 3\%$	$\sigma_T^2 = 0.1$ $T_{u,Uf} = 7\%$ $T_{u,UL} = 9\%$	$\sigma_T^2 = 0.5$ $T_{u,Uf} = 16\%$ $T_{u,UL} = 20\%$	$\sigma_T^2 = 1.0$ $T_{u,Uf} = 23\%$ $T_{u,UL} = 28\%$
$(U_{m1}-U_f)/U_f$	- 0.1 %	- 2 %	- 9 %	- 15 %
$(\overline{\theta^2}_{CT} - \overline{\theta^2}_{VT})/\overline{\theta^2}_{VT}$ at U_D=2.	0.1 %	2 %	13 %	39 %
$(\overline{\theta^2}_{CT} - \overline{\theta^2}_{VT})/\overline{\theta^2}_{VT}$ at U_L=3.5	2 %	15 %	> 1000 %	> 1000%

Table 7.1 - Percentage shift in flutter airspeed and percentage increase in linear pitch response mean-square; CT: combined turbulence, VT: pure vertical turbulence; $L = 50.0$, $k_3 = 0.0$.

From Table 7.1, and supplemented by the previous discussion, we retain three observations and conclusions. They are briefly discussed.

Relative importance of longitudinal turbulence as a function of airspeed

First, it is retained that for all turbulence levels presented, the response mean-square is much more sensitive to the presence of longitudinal turbulence at $U_L = 3.5$ than at $U_D = 2$. That is, as the airspeed is increased and the flutter point is approached, the decrease in stability due to longitudinal turbulence becomes more pronounced.

Effect of turbulence level

We also note that the percentage difference in response mean-square, $(\overline{\theta^2}_{CT} - \overline{\theta^2}_{VT})/\overline{\theta^2}_{VT}$, increases with turbulence variance. This means that from a response mean-square point of view, the relative contribution of longitudinal turbulence increases with turbulence level. This trend follows the percentage shift in flutter speed.

The rational for this behaviour is the sensitivity of the airfoil to vertical turbulence which is increased as the turbulence variance is raised. We clarify this statement by mentioning that augmenting the turbulence level does two things. One, it increases the magnitude of the external forcing (i.e. the vertical excitation). This applies to both the combined turbulence and pure vertical turbulence problems. Second, it increases the destabilising effect of longitudinal turbulence. Of course, this only applies to the combined excitation problem, hence the larger percentage difference in response mean-square.

Increase in response level versus advancement of flutter speed

Thirdly, we note that although the shift in flutter speed becomes significant for turbulence variances ≥ 0.5, the impact of the longitudinal excitation on the response mean-square may be important at lower turbulence levels, i.e. $\sigma_T^2 \geq 0.1$. The percentage difference in response mean-square is in general more significant than the percentage difference in flutter speed. This is especially so at the limit airspeed, $U_L = 3.5$, which is defined in principle to prevent, with a reasonable degree of confidence, any non-intentional usage in the unstable region[1]. From a design point of view in the case where the main limiting aspect is due to turbulence, the limit airspeed should not only be defined in accordance with the advancement in flutter airspeed, but perhaps more significantly considering the increase in response level.

To make the relevance of this point clear, it must be realized that investigating the question of the shift in flutter airspeed, in isolation from the presence of the vertical component of turbulence, although a valid exercise, gives only a partial picture of the situation of the more general combined turbulence problem. As opposed to a generic parametric excitation, this is a particularity of the turbulence excitation because its longitudinal and vertical components, although in general statistically uncorrelated, must in a final analysis be considered together since one does not come without the other. In contrast, given the case for example where the parametric excitation would originate primarily from the airfoil structural support[2], whereas the external excitation would be due to low intensity turbulence, this immediate discussion would lose its applicability.

Effect of turbulence spectral content and "physical" white noise excitation

We now turn our attention to a second set of results shown in Figure 7.2 and subsequently in Table 7.2, which models the excitation effectively as a wide-band (physical white noise) excitation. We notice that the relative impact of the longitudinal component of turbulence on the response mean-square is in general less important than for the former case. This difference is explained by a change of shape of the excitation spectrum for both turbulence components.

---

1 Non-intentional operation of the airfoil in post-instability conditions may be due to bad design or manufacture, non-compliance with operational procedures or an uncontrolled operational environment, i.e. gust or turbulence.

2 This is the case studied by Ibrahim et al. [1990, 1991] on panel flutter.

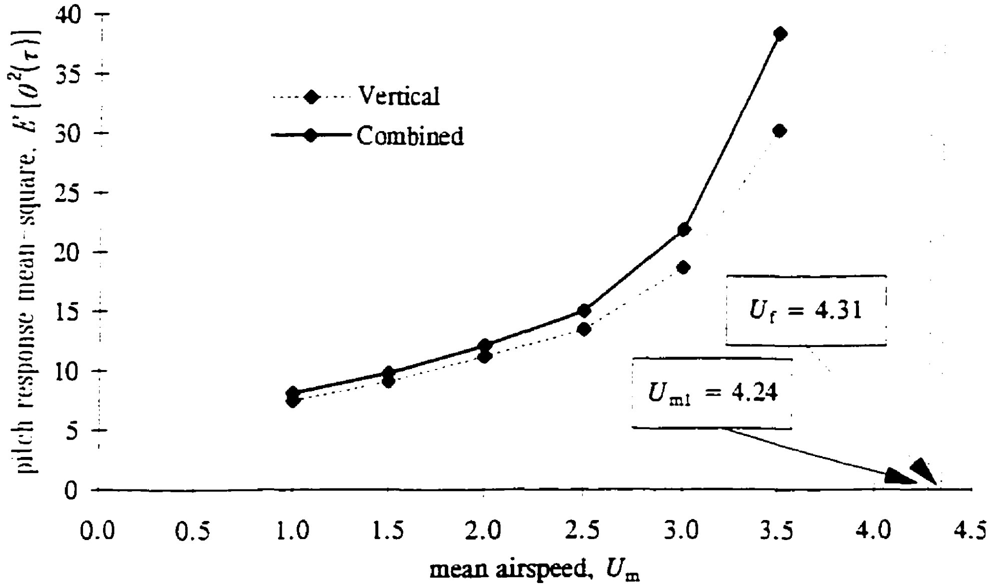

Figure 7.2 - Pitch response mean-square of the linear airfoil in pure vertical and combined turbulence excitation, as a function of airspeed; $\sigma_T^2 = 1.0$, $L = 0.5$, $k_3 = 0.0$.

	$\sigma_T^2 = 0.1$ $T_{u,Uf} = 7\%$ $T_{u,UL} = 9\%$	$\sigma_T^2 = 0.5$ $T_{u,Uf} = 16\%$ $T_{u,UL} = 20\%$	$\sigma_T^2 = 1.0$ $T_{u,Uf} = 23\%$ $T_{u,UL} = 28\%$
$(U_{m1}-U_f)/U_f$	-0.1 %	-1.0 %	-1.6 %
$(\overline{\theta^2}_{CT} - \overline{\theta^2}_{VT})/\overline{\theta^2}_{VT}$ at U_D=2.	4 %	7 %	8 %
$(\overline{\theta^2}_{CT} - \overline{\theta^2}_{VT})/\overline{\theta^2}_{VT}$ at U_L=3.5	5 %	14 %	27 %

Table 7.2 - Percentage shift in flutter airspeed and percentage increase in linear pitch response mean-square; $L = 0.5$, $k_3 = 0.0$.

At this small value of scale of turbulence, $L = 0.5$, the energy in the excitation is distributed equally amongst all resonant (parametric and external) frequencies. Accordingly, given a specific turbulence variance, the high energy which was located in the low frequency range for the former case, $L = 50.0$, has been redistributed in part to the high frequency range for $L = 0.5$. A schematic of the redistribution in excitation frequencies from a large to a small value of scale of turbulence is presented in Figure 7.3 (see also Figure 2.6).

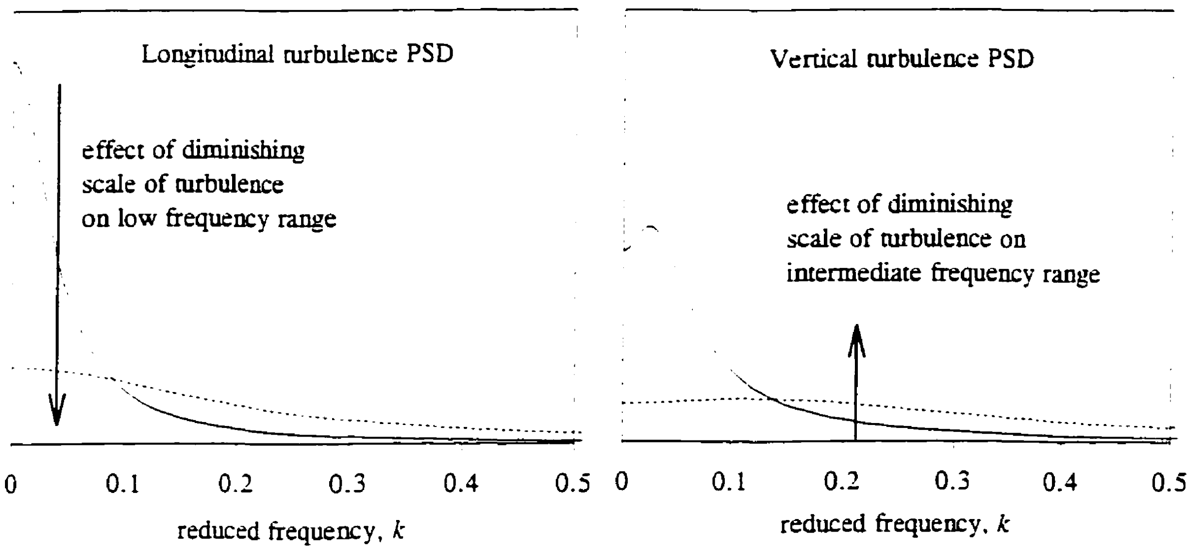

Figure 7.3 - Schematic of change in shape of longitudinal and vertical turbulence spectra from a large (—) to a small (---) value of scale of turbulence.

This redistribution has two cumulative effects. Due to the decrease in the excitation level of the low and very low frequencies, specifically for the longitudinal turbulence spectrum, overall the parametric resonances lose their strength. As a consequence, the stability of the airfoil is increased relative to the case $L = 50.0$ as directly expressed by the smaller percentage shift in flutter speed. The second effect concerns the external resonances, which are strengthened by the increase of the excitation level in the intermediate and higher frequency band, specifically for the vertical turbulence spectrum. These two effects, smaller decrease of stability and increased external forcing, when combined together diminish the relative contribution of the longitudinal component of turbulence as the scale of turbulence tends to zero.

7.1.2 Nonlinear airfoil

When the nonlinearity is introduced, sustained stable motion is exhibited past the flutter point. The restraining mechanism of the nonlinearity applies to the response to vertical turbulence whether or not longitudinal turbulence is modelled. This is shown in Figure 7.4, where both the pitch response mean-square and largest Lyapunov exponent for combined turbulence excitation and pure vertical turbulence, as a function of mean airspeed, are compared. The principal difference is quantitative, and generally small. The response mean-square for the combined excitation curve is always larger than for the pure vertical turbulence excitation. Similarly, λ_{max} for combined turbulence is closer to the no damping axis.

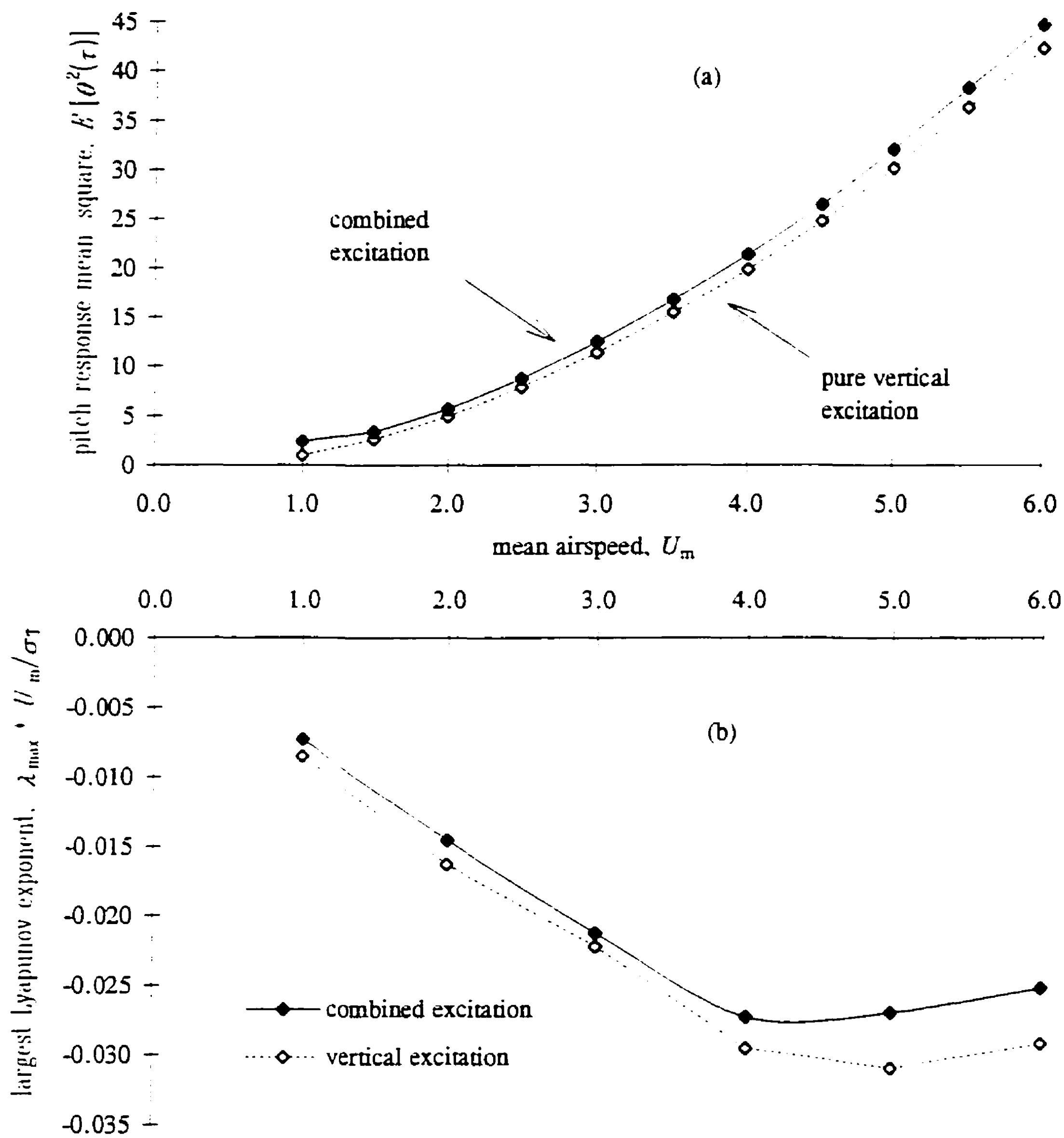

Figure 7.4 - Comparison of the pitch response mean-square (a), and largest Lyapunov exponent (b), of nonlinear airfoil for combined and pure vertical turbulence, as a function of airspeed; $\sigma_T^2 = 1.0$, $L = 50.0$, $k_3 = 50.0$.

It is also noticed from Figure 7.4 that the delta response (i.e. the difference in response between the combined and the pure vertical excitation cases) increases slowly as the airspeed is increased through the flutter point, given by $U_f = 4.31$. Relating the delta response to the destabilizing effect of longitudinal turbulence, the same conclusion can be inferred from the examination of the behaviour of the largest Lyapunov exponent as a function of airspeed since the difference between the two exponents increases as well.

In respect of the particular behaviour in the very low airspeeds, namely for $U_m \leq 1.5$, where the mean-square of the response to combined turbulence appears to diverge from the pure vertical turbulence case, we attribute this observation to the lack of structural damping which starts to become apparent for airspeeds close to zero. This was shown in Chapter 6.

Effect of the nonlinear torsional stiffness coefficient

We have observed that increasing the magnitude of the nonlinear coefficient, k_3, has for effect that the response mean-square for combined turbulence tends to the response to pure vertical excitation. We interpret this tendency as a decrease of the influence of the longitudinal turbulence with increasing nonlinearity.

Table 7.3 compares the percentage difference in pitch response mean-square for the linear and nonlinear airfoil, for two values of k_3, at three different airspeeds. In addition to the two typical airspeeds used for the linear case, a post-flutter airspeed is used as well.

	$k_3 = 0.0$	$k_3 = 50.0$	$k_3 = 400.0$
$(\overline{\theta^2}_{CT} - \overline{\theta^2}_{VT})/\overline{\theta^2}_{VT}$ at $U_D=2$	39 %	15 %	12 %
$(\overline{\theta^2}_{CT} - \overline{\theta^2}_{VT})/\overline{\theta^2}_{VT}$ at $U_L=3.5$	> 1000 %	9 %	4 %
$(\overline{\theta^2}_{CT} - \overline{\theta^2}_{VT})/\overline{\theta^2}_{VT}$ at $U=5.0$	–	6 %	2 %

Table 7.3 - Percentage increase in pitch response mean-square for different values of the nonlinear pitch cubic stiffness coefficient; $L = 50.0$, $\sigma_T^2 = 1.0$ ($T_{U=5} = 20$ %).

From this table, it is also deduced that the relative effect of longitudinal turbulence diminishes with airspeed. This is contrary to the linear case, and can be related to the fact that strictly speaking the flutter point no longer exists when both combined turbulence and nonlinearity are considered, as discussed in Chapter 4. What remains is a general destabilisation due to longitudinal turbulence. Furthermore, for small magnitudes of nonlinearity, the difference can be relatively important. It, however, diminishes as the magnitude of the nonlinearity increases.

Effect of turbulence variance

The larger relative influence of longitudinal turbulence on the response mean-square which has been observed for the linear airfoil as the turbulence level is increased, see Tables 7.1 and 7.2, is also noticed for the nonlinear airfoil. As shown in Table 7.4, an increase in turbulence variance is associated with an increase in the percentage difference in response mean-square for all airspeeds examined.

	$\sigma_T^2 = 0.1$	$\sigma_T^2 = 0.5$	$\sigma_T^2 = 1.0$
$(\overline{\theta^2}_{CT} - \overline{\theta^2}_{VT})/\overline{\theta^2}_{VT}$ at U_D=2	2 %	8 %	15 %
$(\overline{\theta^2}_{CT} - \overline{\theta^2}_{VT})/\overline{\theta^2}_{VT}$ at U_L=3.5	< 2 %	5 %	9 %
$(\overline{\theta^2}_{CT} - \overline{\theta^2}_{VT})/\overline{\theta^2}_{VT}$ at U=5.0	< 2 %	4 %	6 %

Table 7.4 - Percentage increase in the nonlinear pitch response mean-square for different values of turbulence variance; L = 50.0, k_3 = 50.0.

In closing this discussion we mention that although the longitudinal component of turbulence destabilises the airfoil, hence enhances its sensitivity to external excitations, the nonlinear response mean-square is overall governed by the vertical component of turbulence. Accordingly, we say that, in general, longitudinal turbulence plays a secondary role in terms of the system response level.

We add that this general observation has also been noted by Heo [1985] but for a more generic problem. Furthermore, and in contrast to our analysis, he considered white noise excitation only and apparently observed the dynamics away from the (stochastic) instability point.

In this respect, these results add to Heo's analysis as we have shown that the degree of the relative influence of the parametric excitation, namely longitudinal turbulence, depends on a variety of parameters which include turbulence variance and scale, airspeed and magnitude of nonlinearity.

7.2 Organisation

We change perspective and address a seemingly opposite consequence of longitudinal turbulence which is revealed by the probability structure of the response. This organizing effect is addressed by first considering the nonlinear airfoil excited by pure longitudinal turbulence.

7.2.1 Nonlinear airfoil (in pure longitudinal turbulence)

Recall we have observed a region of dynamical behaviour characterized by a single peaked density centred at the origin, and located at airspeeds between the random flutter and LCO onset airspeeds (for example see Figures 4.5 and 4.6). We have labelled this behaviour as being a random fixed point. The organising effect is expressed by the tendency of the longitudinal turbulence to force the dynamics to occur in the vicinity of the origin. It becomes apparent by comparing the PDF of the longitudinally excited airfoil with the non-excited case at an airspeed above the deterministic flutter/Hopf bifurcation speed ($U_f = 4.31$) but below the random LCO onset, as shown in the inset of Figure 7.5 for $U_m = 4.4$.

This effect can also be represented by the probability of exceedance of the pitch angle, in other words the probability that the absolute value of the pitch angle exceeds a specific value. It is a cumulative distribution and is expressed mathematically as:

$$P(\text{pitchangle}>|\theta|) \equiv P(\theta) = 1 - \int_{-\theta}^{\theta} p_s(\alpha)\, d\alpha \tag{7.1}$$

In Figure 7.5, a comparison is shown between the probability of exceedance of the pitch angle for the deterministic and pure longitudinally excited nonlinear airfoil at the same airspeed, $U_m = 4.4$.

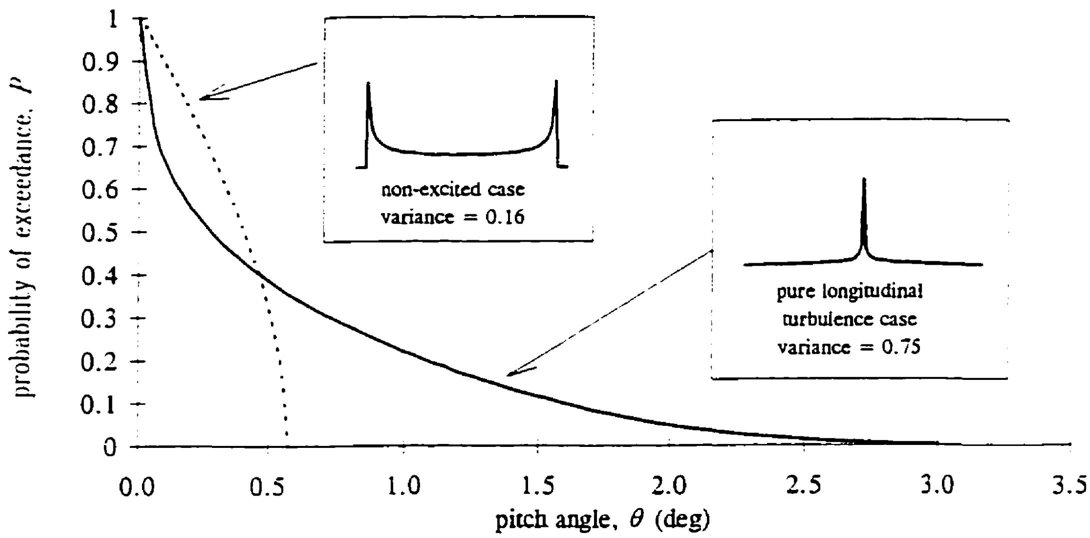

Figure 7.5 - Probability of exceedance of pitch angle of nonlinear airfoil with pure longitudinal turbulence at $U_m = 4.4$; $\sigma_T^2 = 1.0$, $L = 250.0$, $k_3 = 400.0$.

We note that although the variance of the response is larger for the excited case compared with the non-excited case, a consequence of the destabilizing effect, most of the dynamics is concentrated about the zero pitch angle which we consider to be an organizing effect. In this example, for pitch angles below 0.5 degrees, the probability of exceedance of any of these angles is smaller for the excited airfoil.

For a set of nonlinear coupled oscillators excited by parametric noise, Yoon and Ibrahim [1995] have also observed a sharpening of the PDF in comparison with the Gaussian nature of the excitation. They attributed this behaviour to the system nonlinearity. However, our results suggest, and we believe that it is the case for any general system, that the sharpening of the probability density is more a consequence of the parametric excitation than of the nonlinearity.

In support of this argument, recall our discussion in Chapter 4 where we showed that the nonlinearity is required to enable the existence of the dynamical region located between the random flutter point and the random LCO onset. However, we further showed and argued that the magnitude of the nonlinearity plays no part in determining the range of airspeed for which the PDF displays a sharp single-peaked shape, labelled as a random fixed point. The size of this region is determined by the longitudinal turbulence conditions, for example its variance. For the problem where the excitation is purely parametric, the nonlinearity is therefore required to enable sustained motion past the (random) instability point, but its role in defining the shape of the PDF is mainly supportive.

7.2.2 Linear airfoil

The investigation of the linear airfoil requires that vertical turbulence be also considered, in addition to longitudinal turbulence, since without an external forcing no steady state dynamics (for airspeeds below the flutter point) is possible. The influence of the longitudinal component of turbulence can be inferred by plotting the PDF of the response to combined turbulence against the corresponding Gaussian curve. This is shown in Figure 7.6 which compares the pitch angle marginal PDF of the linear airfoil in combined turbulent excitation with a Gaussian curve having the same variance. We observe a (small) sharper density function for the excited airfoil response.

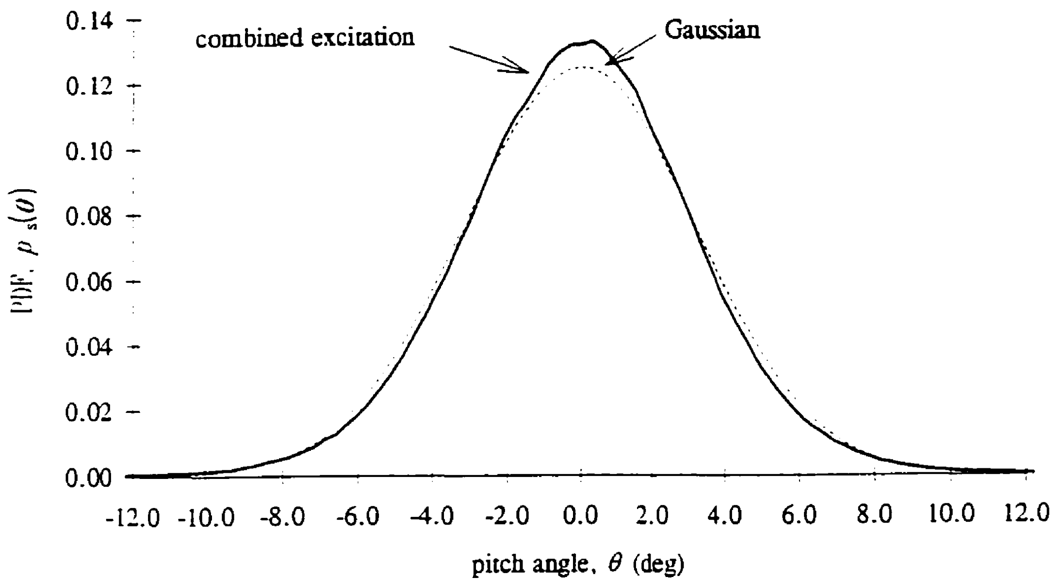

Figure 7.6 - Marginal PDF of the linear airfoil pitch response to combined turbulence in comparison with a Gaussian density; $U_m = 2.0$, $\sigma_T^2 = 1.0$, $L = 50.0$, $k_3 = 0.0$.

The Gaussian curve used as a basis of comparison typifies the PDF of the airfoil linear response to pure vertical excitation since the excitation is Gaussian distributed. It is therefore relevant to point out that in choosing the variance of the Gaussian curve to be equal to the mean-square of the response to combined turbulence, instead of the mean-square of the response to pure vertical turbulence, we have tried to isolate the probability structure from any effect other than organizing. In this regard, it is tempting to interpret the sharpening of the PDF shown in Figure 7.6 as a (small) organizing effect of longitudinal turbulence on the linear airfoil. However, this organizing effect on the linear airfoil may only be apparent, since, as we will discuss in Section 7.3.1, larger deviations from the origin are the overall consequence of longitudinal turbulence, due to its dominant destabilisation effect.

Effect of scale of turbulence and mean airspeed

Not shown but we have observed a stronger departure from normality (Gaussian shape) for larger scales of turbulence. This result appears to be coherent with the pure longitudinally excited nonlinear airfoil dynamics, for which we have observed a larger range of airspeed exhibiting a single-peaked PDF with increasing scale of turbulence (see Figure 4.13). Note as well that we have also observed a sharpening of the probability density with increasing airspeed, that is as the flutter speed is approached.

7.3 Destabilisation Versus Organisation

In the previous two sections, we have analysed these two seemingly opposite effects in isolation from each other. In doing so, we have obtained an understanding of each mechanism, thus giving us the tools to better grasp the overall influence of the longitudinal component of turbulence. In this section we consider the combination of these two effects. This topic is first treated without considering the nonlinearity. The effect of the nonlinearity will be added next.

7.3.1 Linear airfoil

The approach taken is to examine both the measures of destabilisation and of organisation, respectively, the response mean-square and PDF, with one unique projection that represents both effects. This is possible by plotting the same data shown in Figure 7.6 against a Gaussian curve which has a variance equal to the response mean-square to pure vertical turbulence. In other words, we compare the marginal PDF of the responses to combined excitation and to pure vertical excitation. This projection enables us to compare the relative strength of both effects, that is organising and destabilising.

This is shown in Figure 7.7. The predominant effect of destabilisation, over organisation, is clearly demonstrated by the flatter density of the combined excitation. A flatter density, hence a stronger diffusion about its mean, is indicative of a more important destabilizing effect since a relatively important part of the dynamics occurs at high amplitude.

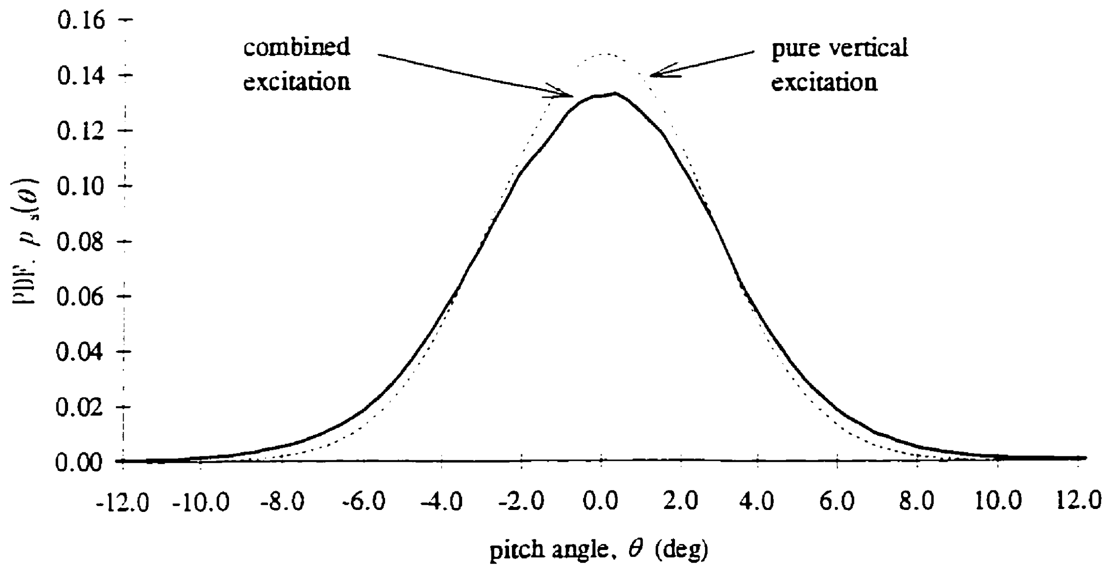

Figure 7.7 - Comparison of the marginal PDF of the linear airfoil pitch response to combined and pure vertical turbulence; $U_m = 2.0$, $\sigma_T^2 = 1.0$, $L = 50.0$, $k_3 = 0.0$.

7.3.2 Nonlinear airfoil

The question of the destabilising versus organising effects of longitudinal turbulence in the context of the nonlinear airfoil in combined turbulence can be partially represented by the transition point from a uni- to bi-modal marginal PDF in pitch angle, as shown in Figure 7.8. The position of the extrema of the marginal pitch PDF are displayed as a function of airspeed for the two cases of combined and pure vertical excitation. The difference between the two behaviours shows the contribution of the longitudinal component of turbulence, and displays an early transition point.

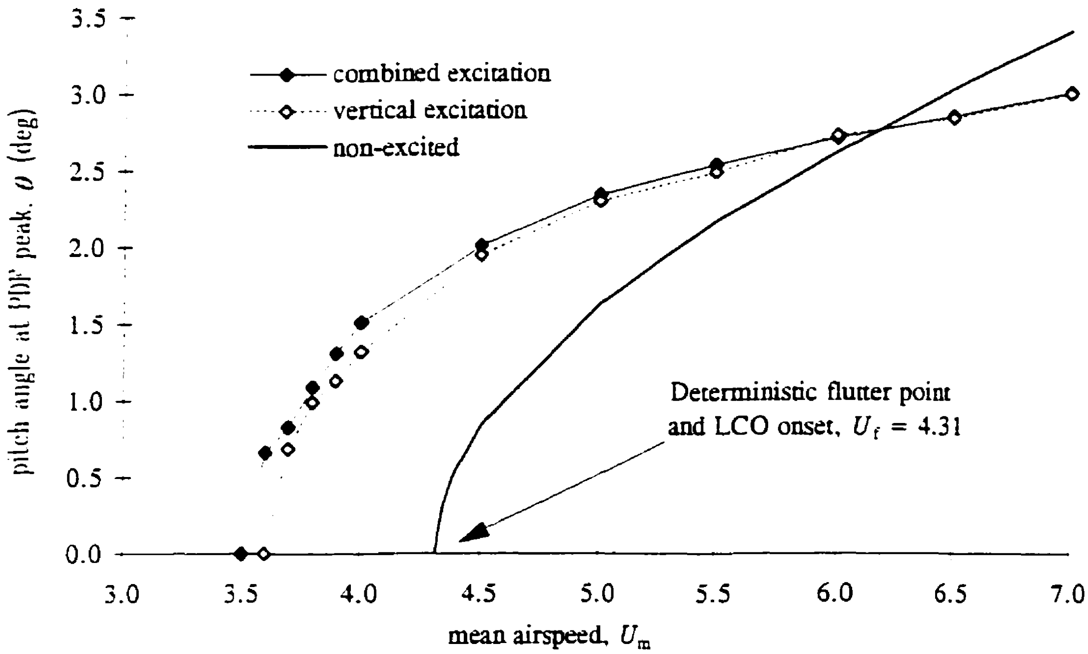

Figure 7.8 - Transition diagram (location of the marginal PDF maxima) of the pitch angle for pure vertical and combined turbulence; $\sigma_T^2 = 1.0$, $L = 50.0$, $k_3 = 400.0$.

Not shown, but longitudinal turbulence (with same variance and scale) has the opposite effect on the pitch rate marginal PDF since the transition point is delayed compared with pure vertical turbulence. Although apparently contradictory results, these two observations are coherent with the discussion in Chapter 6 concerning the probabilistic structure of the nonlinear response to (combined) turbulence. In particular, Figure 6.15 displays, for $L = 50.0$ and $\sigma_T^2 = 1.0$, an advancing transition airspeed in pitch and a retarding transition in pitch rate with increasing turbulence variance. Accordingly, we argue that by destabilising the airfoil, longitudinal excitation induces a greater response to vertical turbulence, which in turn puts a greater demand on the nonlinearity. The final effect on the probabilistic structure of the response is the same as obtained from an increased turbulence variance.

In corollary to this observation is the realisation that the airspeed at which the PDF transitions is largely determined by the vertical excitation. As exemplified by Figure 7.8, longitudinal turbulence plays a minor role. This is consistent with our observations of the response mean-square. We have found the same observation for most cases investigated, such that, in general, the shift in transition airspeed is experimentally difficult to identify due to the requirement to have very smooth PDFs, hence the need for a very large sample size.

7.4 Concluding Remarks

In summary, we have the following remarks. The first set are in regard to the effects of longitudinal turbulence, without considering the relative importance of longitudinal turbulence in comparison with vertical turbulence. Accordingly, we have found:

1. Longitudinal turbulence has two effects of a seemingly different nature, which we have interpreted as being destabilising and organising. We have interpreted the tendency of longitudinal turbulence to force the dynamics to occur about the origin as an organizing effect. It is characterised by a sharpening of the marginal PDF about its mean. This organizing effect is clearly exhibited by the nonlinear airfoil in pure longitudinal turbulence for the range of airspeed between the deterministic and random LCO onsets. For the linear airfoil, this effect is questionable.

2. In opposition to organisation is destabilisation, which in turn is characterized also by two effects. One is an advancement of the flutter point, strictly speaking experienced only by the linear airfoil. More general is the second effect which is an enhanced sensitivity to external excitation, specifically vertical turbulence in our case. This last effect translates into a larger response mean-square at any airspeed. For the linear airfoil, the percentage increase in response mean-square is generally more important than the percentage shift in flutter speed. This is particularly relevant for airspeeds relatively close to the flutter point.

3. Of these two competing effects in the presence of vertical turbulence, destabilisation, which induces a diffusion of the dynamics about the origin, is felt much more strongly by the airfoil, linear and nonlinear, than the organisation, whose result is opposite.

Now, concerning the relative influence of the longitudinal component of turbulence in the overall combined excitation problem, we have found:

1. The relative importance of longitudinal turbulence in the combined excitation problem depends in part on the magnitude of the nonlinearity. Where nonlinear effects are

important, longitudinal turbulence becomes less significant. Along this line, and as a general rule for the nonlinear airfoil, longitudinal turbulence is more of a concern at pre-flutter airspeeds than in the post-flutter region. We then say that the response of the turbulent excited airfoil is dominated in the low speed range (pre-flutter airspeeds) by the combined effect of longitudinal and vertical turbulence, whereas at high speeds (post-flutter) the contribution of longitudinal turbulence makes way to a greater influence of the nonlinearity.

2. For the linear airfoil, the relative importance of longitudinal turbulence can be significant for low airspeeds, depending on the turbulence variance and scale, but more so for high airspeeds as flutter is approached.

3. The relative importance of longitudinal turbulence in the combined excitation problem depends also, in part, on the overall turbulence characteristics, namely its intensity and spectral content. For low turbulence variance levels, as defined in the context of this thesis (for example of atmospheric origin), its impact does not appear to be significant. It becomes important, relative to the vertical component, for higher turbulence levels related to flow separation and vortex breakdown for example. With regards to the influence of the spectral content, the higher the scale of turbulence (i.e. spectrum concentrated in the low frequencies) the more important is the relative contribution of longitudinal turbulence. This is due to parametric resonance conditions (with longitudinal turbulence) which are the strongest at small frequencies, whereas the airfoil resonates (externally) to vertical turbulence at higher frequencies.

4. Overall we have found that the dynamics of the airfoil is mainly governed by vertical turbulence. Longitudinal turbulence generally plays a minor role, although it may be significant depending on turbulence variance and scale, magnitude of nonlinearity and closeness of flutter point (strictly for the linear airfoil).

Chapter 8

ASPECTS OF NONLINEAR RANDOM DIVERGENCE

In many regards, the dynamics of a diverging nonlinear airfoil in turbulent flow is different than for flutter. Under turbulent excitation, the main potential sources of difference between these two instability types are as follows. For a hardening nonlinear spring, the fixed point of the diverging airfoil bifurcates into two new stable fixed points. This bi-stability leads to basin hopping under the influence of turbulence. Furthermore, contrary to the Hopf bifurcation, the pitchfork bifurcation is not a structurally[1] stable bifurcation. As discussed in Chapter 1, any small external bias stops the fixed point from bifurcating, and an additional saddle-node bifurcation appears. Thirdly, deterministic divergence (and pitchfork) is a static problem. Its nature changes, however, as it becomes a dynamic problem due to the influence of turbulence.

In comparison to the non-excited case, the complexity of the behaviour introduced by turbulent excitation renders the investigation of nonlinear divergence complicated and its outcome much richer. For those reasons and for sake of succinctness, we cannot treat this problem at the same depth and as systematically as we have done for nonlinear flutter.

[1] The term *structurally* is taken here in the context of bifurcation theory. It does not refer to the structure of the airfoil.

Accordingly, we restrict ourselves to some aspects of random nonlinear divergence. The analysis is mainly descriptive; however, in some cases a physical explanation is given for the airfoil's behaviour. In many ways, this chapter opens the door for further research.

8.1 Deterministic Baseline

Contrary to flutter, divergence of the non-excited airfoil is a 1DOF static instability. It is solely determined by the pitch DOF, and specifically its torsional (structural and aerodynamic) stiffness properties. Keeping only the linear stiffness terms, the divergence condition is obtained from equations (2.25 a) and (2.26 a). At the divergence airspeed, U_d, the stable structural stiffness moment is equal to the destabilizing aerodynamic stiffness moment as shown in equation (8.1). The divergence airspeed is given in dimensional and non-dimensional forms in equations (8.2 a) and (8.2 b), respectively.

$$\theta K_\theta = 2\pi\rho b^2(a_h + .5)U^{*2}_d\,\theta \tag{8.1}$$

thus

$$U^*_d = \sqrt{\frac{K_\theta}{2\pi\rho b^2(a_h + .5)}} \tag{8.2 a}$$

$$U_d = \sqrt{\frac{\mu r_\theta^2}{2(a_h + .5)}} \tag{8.2 b}$$

A necessary condition for divergence to occur is that a negative aerodynamic stiffness exists. The elastic axis must then be aft of the aerodynamic centre, or $a_h > -0.5$ (since the AC is located at the quarter chord point for the airfoil in incompressible flow). For airspeeds below U_d, the total stiffness is weakened by the negative aerodynamic stiffness, but the fixed point, located at the origin when no bias is considered, is stable. For airspeeds above U_d, the magnitude of the negative aerodynamic stiffness is greater than the structural stiffness resulting in the fixed point being unstable.

Note that since U_d is solely dependent on the structural and aerodynamic stiffness properties in pitch, other parameters such as static unbalance or frequency ratio have no influence.

In the post-instability regime, the flow is attracted to two new stable fixed points. Their location is determined by a new balance of moments which include the nonlinear restoring moment, $\theta^3 K_3$, as given by equation (8.3).

$$\theta K_\theta + \theta^3 K_3 = 2\pi\rho b^2 (a_h + .5) U^{*}{}_d^2\, \theta \tag{8.3}$$

The location in pitch of the two fixed points is then given by equation (8.4) in non-dimensional form. Similarly, their location in heave is obtained by solely considering the stiffness terms in the heave equation of motion (equations 2.25 b and 2.26 a). The non-dimensional heave is given by equation (8.5). The heave rate and pitch rate are zero.

$$\theta = \pm\sqrt{-\frac{1}{k_3} + \frac{2(a_h + .5)U^2}{k_3 \mu r_\theta^2}} \qquad , U > U_d \tag{8.4}$$

$$\xi = -\frac{\theta\, 2U^2}{\mu \overline{\omega}^2} \qquad , U > U_d \tag{8.5}$$

The supercritical pitchfork bifurcation is shown in Figure 8.1 as represented by the pitch and heave. Only one of the two post-instability fixed points is illustrated. The chosen airfoil baseline parameters for this analysis are as follows: $k_3 = 400.0$, $\omega_h/\omega_\theta = 0.6325$, $x_\theta = -0.25$, $r_\theta = 0.5$, $\mu = 100.0$, $a_h = 0.0$, and no structural damping Note that the divergence airspeed occurs at $U_d = 5.00$.

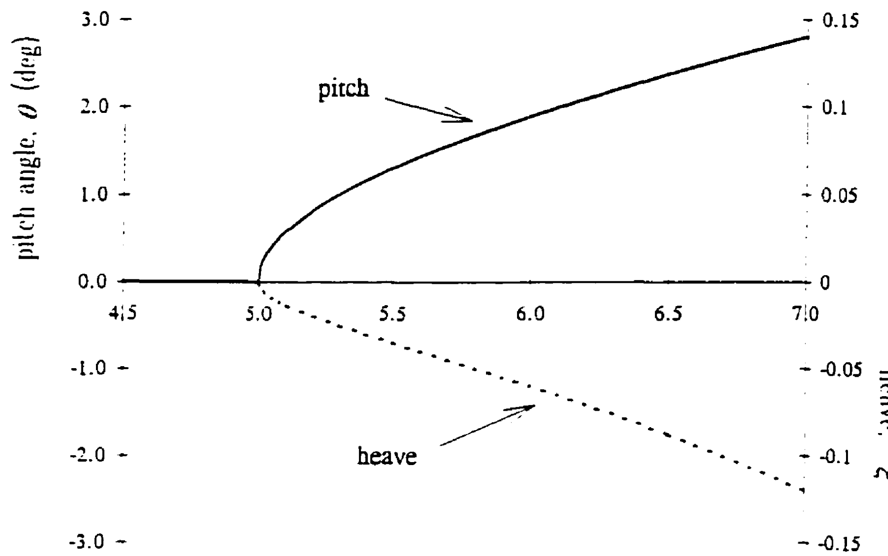

Figure 8.1 - Supercritical pitchfork bifurcation of the non-excited nonlinear airfoil as represented by the pitch and heave.

8.2 Random Bifurcation

8.2.1 Pure longitudinal turbulence excitation

Shown in Figure 8.2 is the steady state marginal PDF (multiplied by the pitch variance) of the pitch angle in pure longitudinal turbulence (L = 50.0 and σ_T^2 = 0.5) as the mean airspeed is swept slowly through divergence. Not shown, the heave displays the same portrait, whereas the pitch rate and heave rate marginal PDFs exhibit a single sharp peak centred around the origin.

Of specific interest is the region of tri-modality located between U_{m2} and U_{m3}, i.e. for 5.5 $\leq U_m \leq$ 6.4, since it is different from the flutter case and is not predicted by the theoretical analysis of the Landau equation under multiplicative white noise given in Chapter 1 (see Figure 1.5). This type of behaviour has been obtained, numerically or analytically, by Sancho et al. [1982], Stocks et al. [1989] and Horsthemke and Lefever [1984]. It has been attributed by these authors to the colour of the multiplicative noise since in the limit to white noise, they observed that the central peak disappeared in favour of the off-centred peaks.

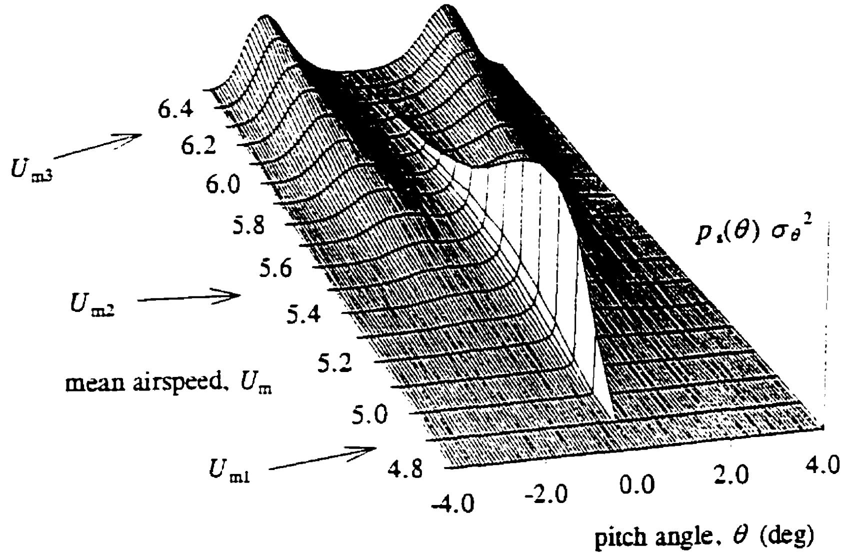

Figure 8.2 - Steady state marginal PDF diagram of the nonlinear airfoil pitch angle in pure longitudinal turbulence as a function of mean airspeed; $\sigma_T^2 = 0.5$, $L = 50.0$, $k_3 = 400.0$; $N = 10{,}000{,}000$, $\Delta\tau = 0.2$.

We have verified this interpretation for our system and found that for a smaller scale of turbulence, $L = 5.0$, a tri-modal PDF is also displayed, but for a shorter range of airspeed. At $L = 0.5$ which is very close to the white noise limit relative to the system time scales, the tri-modal density has totally disappeared.

We conclude that the existence of the tri-modal density is caused by the slowness (large noise correlation time) of turbulence. We also conclude that the (steady state) bifurcation of the diverging airfoil in pure longitudinal (coloured) turbulence is a three-step bifurcation. It is characterized by first a D-bifurcation, shown as U_{m1} in Figure 8.2, which we associate to the *random divergence airspeed.* This is followed by two P-type bifurcations separating a single-peaked from a triple-peaked region and the triple-peaked from a double-peaked PDF, represented in Figure 8.2 as U_{m2} and U_{m3}, respectively. Not shown, but in support of this conclusion we have observed that the largest Lyapunov exponent exhibits a discontinuity at U_{m1}, but remains continuous through U_{m2} and U_{m3}.

Due to the bi-stability of the problem, the transient dynamics may be significant in that the motion may be caught within one potential well for a relative long time before it jumps into the other well. Hence, under certain conditions the transient PDF representing the motion within one well, i.e. intra-well motion, may have time to reach some type of steady state[2] before basin hopping occurs. We have observed "steady state" intra-well motion for low turbulence variance and/or for high airspeeds.

Figure 8.3 shows the pitch PDF at three different times (given in terms of number of iterations) for a turbulence variance $\sigma_T^2 = 0.1$ and airspeed $U_m = 5.25$. It is observed that after 5,000,000 iterations the motion has evolved within only one well, and that the probability density appears to have nearly reached intra-well "steady state". After 20,000,000 iterations, inter-well motion has occurred, but probably relatively scarcely since steady state has not been reached.

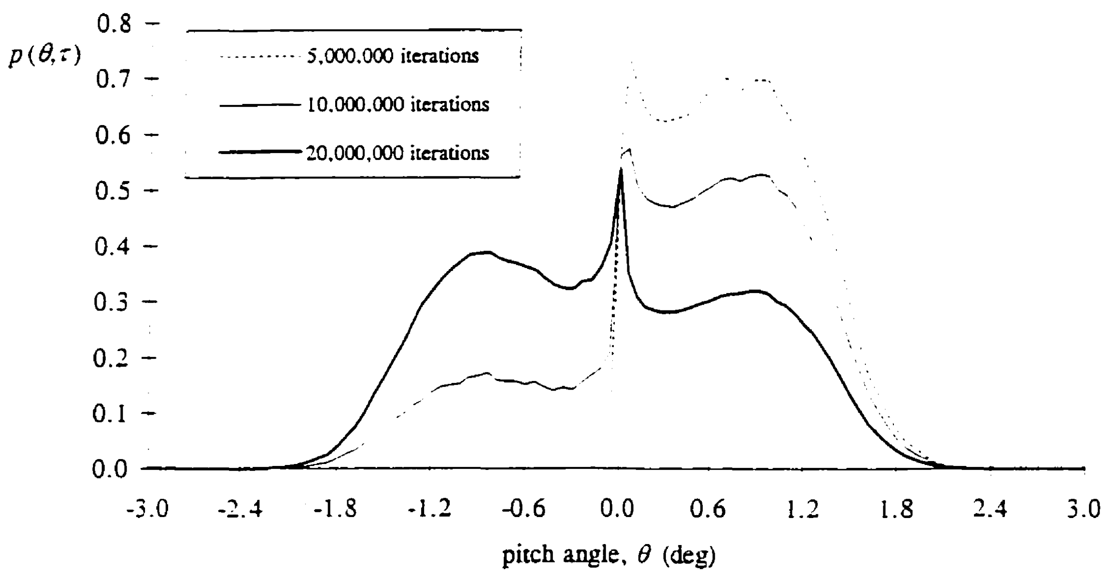

Figure 8.3 - Pitch marginal PDF of nonlinear airfoil in pure longitudinal turbulence at three different times; $U_m = 5.25$, $L = 50.0$, $\sigma_T^2 = 0.1$, $k_3 = 400.0$; $\Delta\tau = 0.2$.

[2] Steady state of the PDF is defined when its shape does not change and becomes smooth with time.

Of particular interest is the observation that there is a build-up of probability at zero pitch angle for the long term inter-well case as well as for the pure intra-well motion. For this reason, this peak cannot be attributed to basin hopping. We then believe that the origin of the peak at zero pitch angle for pure intra-well motion is the same as of the central peak of the tri-modal PDF shown in Figures 8.3 and 8.2 for a higher level turbulence. It is due to longitudinal turbulence and its tendency to organize (force) the dynamics at the origin.

Note also that in comparison with Figure 8.3, the density shown in Figure 8.2 is, for all practical purposes, symmetric. This is due to the higher turbulence level ($\sigma_T^2 = 0.5$) which forces the motion to jump more frequently between the two wells. In this case, inter-well steady state is reached after 10,000,000 iterations.

8.2.2 Combined (and pure vertical) turbulence excitation

When vertical turbulence is considered, with or without the longitudinal component, the three-step bifurcation for pure longitudinal turbulence does not appear. Instead, a single P-bifurcation is observed. Not shown but similarly with the flutter problem, the D-bifurcation is lost as corroborated by the behaviour of the largest Lyapunov exponent, which does not exhibit a discontinuity.

The P-bifurcation is represented in Figure 8.4 by the pitch marginal PDF transition diagram. It is observed that a uni-modal Gaussian-like density, which represents the random fixed point at the origin, transitions into a bi-modal density, which represents the two nonlinear random fixed points. Note that the heave displays also the same transition, uni- to bi-modal, but at higher airspeed.

On the other hand, the heave rate and pitch rate stay uni-modal and centred at zero. This observation is coherent with the interpretation that the dynamics is represented by a random fixed point (or two in the post-bifurcation regime). A zero mean uni-modal pitch rate probability density is the random equivalent of a zero pitch rate for the non-excited airfoil; similarly for the heave rate.

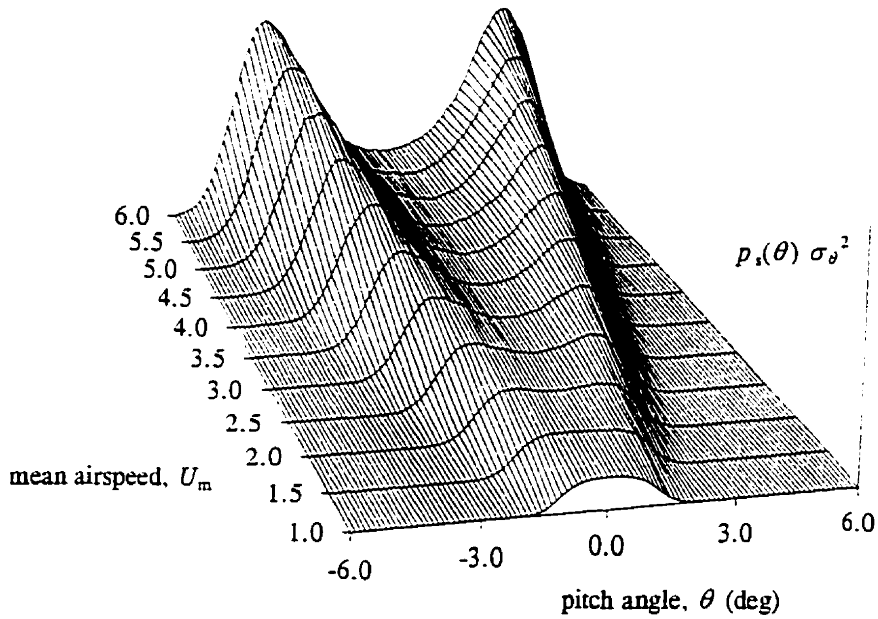

Figure 8.4 - Steady state marginal PDF diagram of the nonlinear airfoil pitch angle in combined turbulence, as a function of mean airspeed; $\sigma_T^2 = 0.1$, $L = 50.0$, $k_3 = 400.0$; $N = 5{,}000{,}000$, $\Delta\tau = 0.1$.

The bi-dimensional PDF of the pitch-heave displays also a uni- to bi-modal transition, as schematized in the inset of Figure 8.5 for pre- (below the curve) and post-bifurcation (above the curve) regimes. Note their elongated S-like shape. Assuming that the peaks in the pitch-heave probability space correspond to the *random fixed points*, it follows rationally that the P-bifurcation point should correspond to the airspeed at which the bi-dimensional PDF transitions. According to this interpretation, Figure 8.5 suggests that the P-bifurcation, which corresponds to the divergence/pitchfork bifurcation in the deterministic case, is advanced by turbulence, namely its vertical component.

We have observed the same pre- and post-bifurcation motion for other turbulence variances and scales. Therefore, contrary to the flutter/Hopf bifurcation in turbulent flow, the bifurcation scenario of the turbulence excited divergence/pitchfork appears to be the same for all turbulence conditions. It is emphasized that this conclusion is only true when vertical turbulence is considered. As discussed earlier in Section 8.2.1, the divergence/pitchfork bifurcation in pure longitudinal turbulence depends on the scale of turbulence.

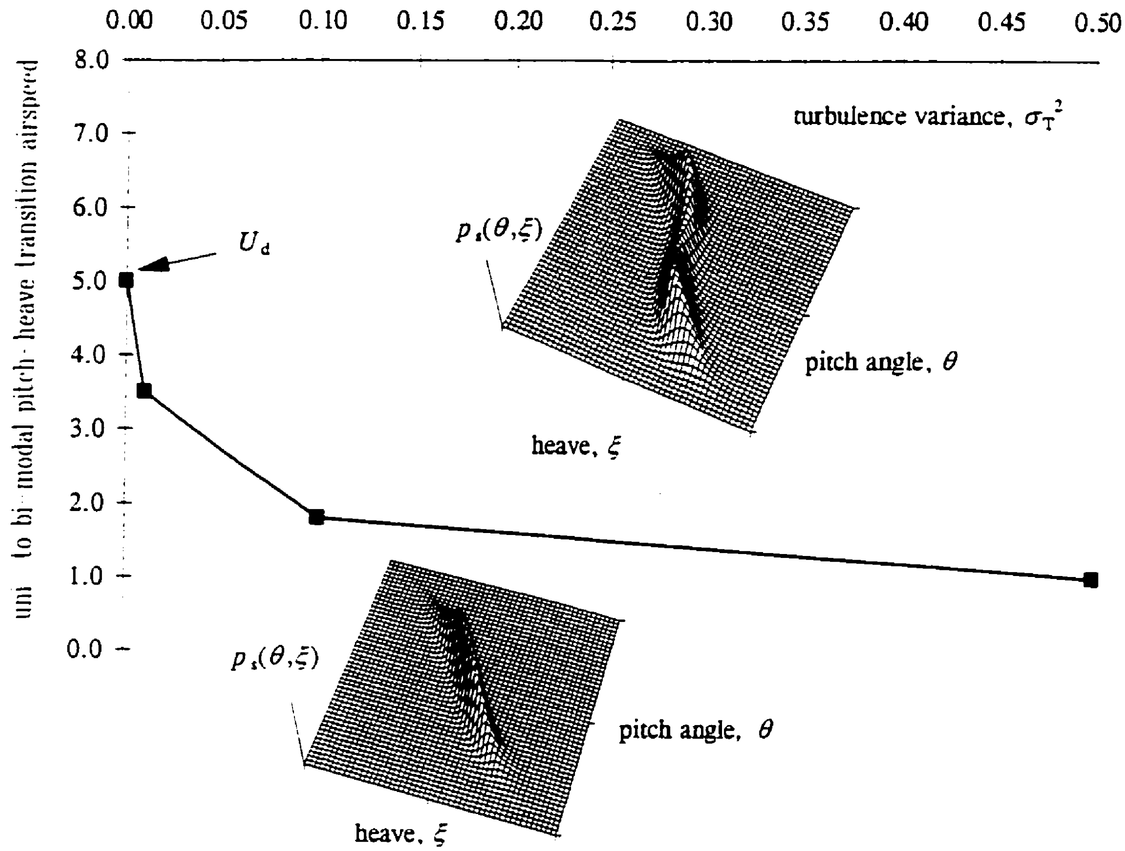

Figure 8.5 - Uni- to bi-modal transition mean airspeed of steady state bi-dimensional PDF in pitch-heave of nonlinear airfoil in combined turbulence, as a function of turbulence variance; L = 50.0, k_3 = 400.0.

Contribution of longitudinal turbulence

Similarly with the Hopf bifurcation in combined turbulence, the longitudinal component of turbulence does not change the random bifurcation which is essentially determined by the vertical component. We have made a number of simulations with and without longitudinal turbulence and confirmed that its effect on the bifurcation is basically quantitative.

Furthermore, our results have shown a small but systematic delay of the pitch PDF transition airspeed for combined turbulence in comparison with pure vertical turbulence. It is speculated that this observation may be related to an organizing effect of longitudinal turbulence, which is clearly exhibited for pure longitudinal turbulence via the appearance of the central peak in the response PDF (see Figure 8.2 and Figure 8.3).

8.3 Divergence Instability

In this section, it is shown that contrary to random flutter, the random divergence airspeed, U_{m1}, is not always advanced by longitudinal turbulence. It may also be postponed. It is also shown that the ratio of heave to pitch frequencies (frequency ratio, $\bar{\omega} = \omega_h / \omega_\theta$), which has no influence on divergence of the deterministic airfoil, plays a role in the shift of the random instability. Finally, our results indicate that, in general, turbulence has a much smaller impact on the shift in divergence airspeed than is experienced for flutter.

8.3.1 Influence of turbulence parameters

The divergence airspeed is illustrated in Figure 8.6 for different turbulence conditions.

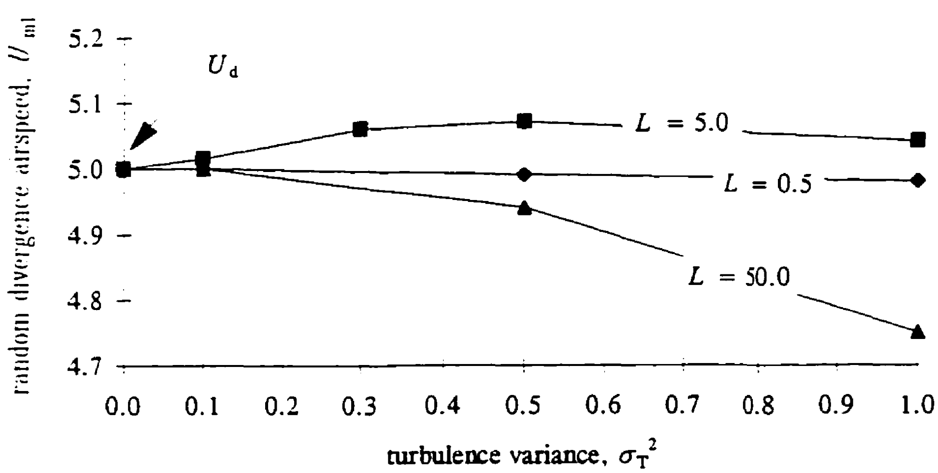

Figure 8.6 - Divergence airspeed as a function of turbulence variance and for different scales of turbulence.

These results indicate that for the small and large scales of turbulence, longitudinal turbulence is destabilizing, whereas it is stabilizing for L = 5.0. Furthermore, the relationship between divergence airspeed and turbulence variance does not appear to be as straightforward as is the case for the binary flutter instability. From a quantitative point of view, the advancement or postponement of the divergence airspeed is small even at the higher turbulence variance. Consider the case for L = 50.0 and σ_T^2 = 1.0, which corresponds to a turbulence intensity $T_{u,Ud}$ = 1.0/5.0 = 20 %, divergence is advanced by 5 %.

Figure 8.7, which shows the effect of scale of turbulence, also suggests a complex dependance of the divergence airspeed on (longitudinal) turbulence spectral content. The magnitude of the shift is also small.

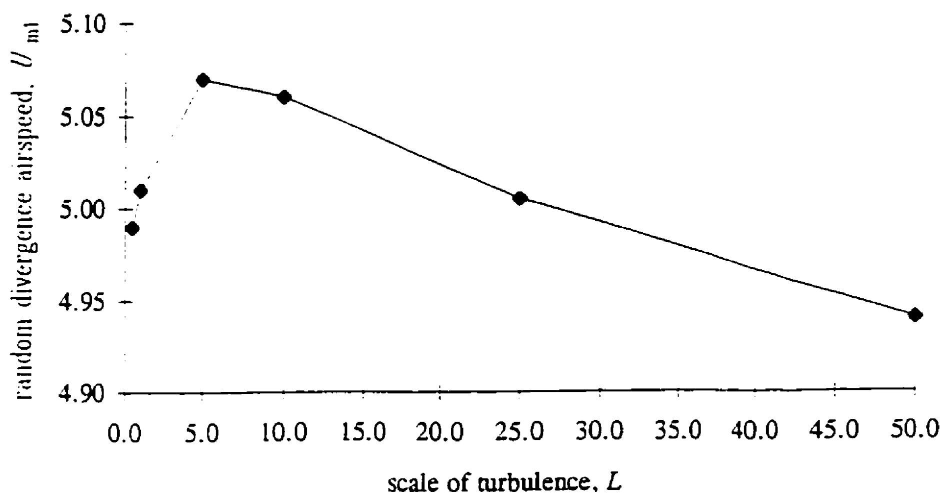

Figure 8.7 - Divergence airspeed of airfoil as a function of scale of turbulence; σ_T^2 = 0.5.

8.3.2 Influence of airfoil parameters

The airspeed at which divergence occurs is also dependent on the airfoil parameters. Equation (8.1) shows that for the non-excited case, U^*_d depends on the airfoil linear torsional stiffness coefficient, the distance between the EA and the AC and on the semi-chord. For the longitudinally excited airfoil, we observe an additional dependance on the frequency ratio, $\bar{\omega}$ = ω_h/ω_θ, as shown in Figure 8.8.

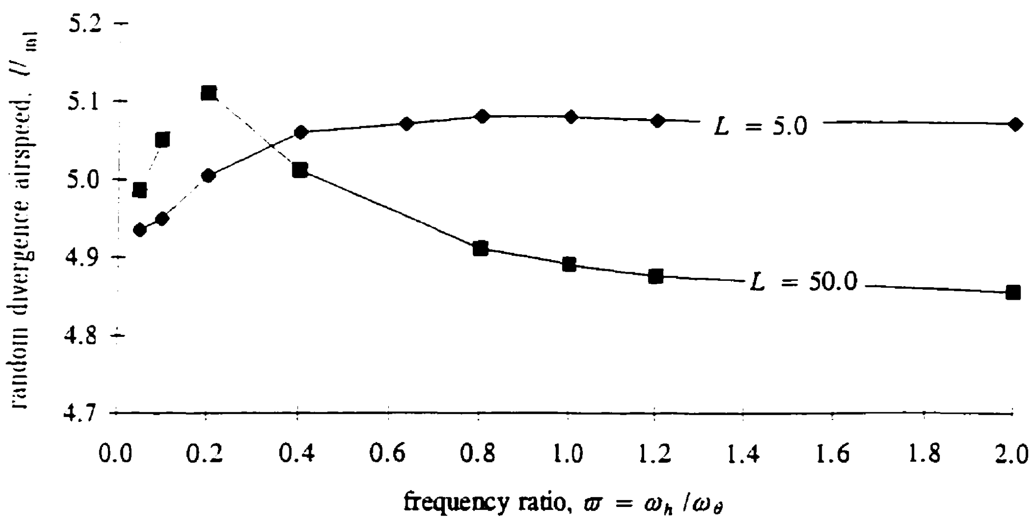

Figure 8.8 - Divergence airspeed as a function of frequency ratio; $\sigma_T^2 = 0.5$.

Figure 8.8 indicates a particular sensitivity of U_{m1} on $\bar{\omega}$ for small values (of frequency ratio), i.e. when the pitch is stiffer than the heave. For large frequency ratios, the rate of change of U_{m1} with $\bar{\omega}$ is small. Furthermore, for large values of $\bar{\omega}$ the system tends to the single DOF dynamics. Hence, in the limit of a large frequency ratio, the heave is so stiff that the pitch dynamics is effectively decoupled from the heave. As we can deduce from Figure 8.8 a decoupling of the pitch DOF from the heave can be stabilizing or destabilizing, depending on scale of turbulence and on the frequency ratio of the original coupled (2DOF) system. Our results are put in contrast with the results from Bucher and Lin [1988; 1988; 1989] and Lin [1996] for single-degree-of-freedom negative damping flutter; Bucher and Lin argued that although longitudinal turbulence may destabilize individual modes acting separately, introducing a coupling with other modes helps in transferring the energy from the least stable to the more stable modes, thus stabilizing the overall system. For divergence, our findings show that it is not necessarily the case.

For our baseline 2DOF airfoil (i.e. with $\omega_h/\omega_\theta = 0.6325$), Figure 8.9 shows that decoupling the heave from the pitch is destabilizing since the divergence airspeed of the pitch 1DOF system is smaller than for the 2DOF system for all turbulence conditions shown. However, we want to be clear that this is not a general observation as illustrated in Figure 8.8. Observe as well that both divergence airspeeds at $\sigma_T^2 = 0.5$ for the 1DOF system corresponds to the two asymptotic values for large frequency ratio in Figure 8.8.

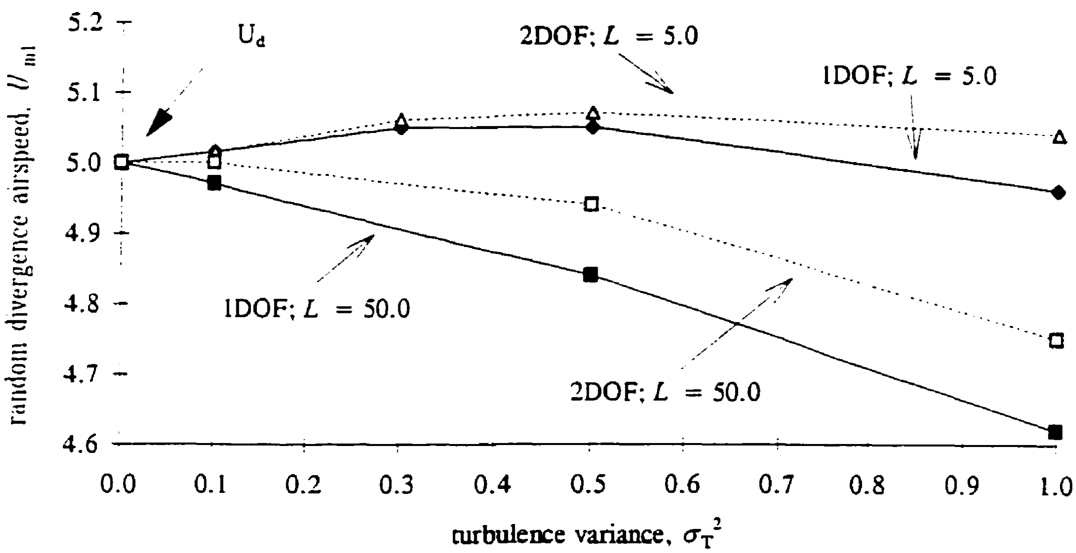

Figure 8.9 - Comparison of divergence airspeed of 1DOF (in pitch) and 2DOF airfoil, as a function of turbulence variance and for two scales of turbulence.

Note that we have also investigated the effect of the static unbalance, x_θ, by changing its value for different locations of the CG ahead of the EA. No significant shift in divergence airspeed has been observed. On the other hand, bringing the CG aft of the EA destabilises considerably the airfoil, but this is attributed to the airfoil experiencing flutter and no longer divergence.

As a final comment, we add that the observed dependance of the random divergence airspeed on frequency ratio and coupling with the heave DOF indicates that the mechanism accounting for the shift in divergence airspeed due to longitudinal turbulence is different from the mechanism defining the deterministic instability. As shown earlier, these parameters do not intervene in deterministic divergence since it is a purely static torsional stiffness problem. The fact that $\bar{\omega}$ plays a role is due to the heave coupling terms in the pitch equation of motion (equation 2.28). Furthermore, realising that this coupling acts via the inertia and damping terms, while there is no coupling with heave stiffness, we say that random divergence is a dynamic instability.

8.4 Nonlinear Response

Two aspects of the nonlinear response to combined turbulence have retained our attention. They are briefly discussed.

8.4.1 Probability structure

The probability structure of the response depends on which state(s) is(are) considered. As introduced in Section 8.2 and similarly with the fluttering airfoil, the pitch marginal PDF transitions from a uni- to a bi-modal shape at a smaller speed than does the heave. Contrary to flutter, however, the heave rate and pitch rate do not transition. They stay uni-modal with zero mean.

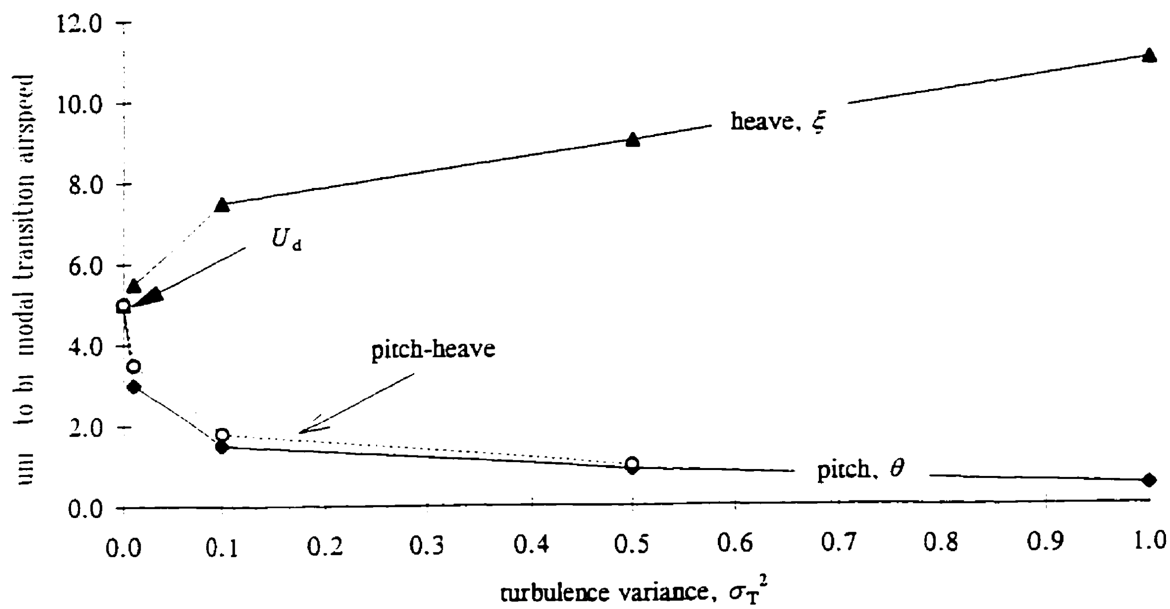

Figure 8.10 - Transition airspeeds of pitch and heave marginal PDFs, and of the bi-dimensional PDF of nonlinear airfoil in combined turbulence, as a function of turbulence variance; L = 50.0, k_3 = 400.0.

Shown in Figure 8.10 is the transition airspeed for both pitch and heave as a function of turbulence variance. It shows a strong dependance of the probability structure of the aeroelastic response on turbulence variance, especially at lower levels. Furthermore, the heave is always postponed and the pitch is always advanced relative to the deterministic pitchfork bifurcation.

The latter observation on the pitch is different from the fluttering airfoil since for flutter we observed postponement of the pitch transition at small and intermediate levels of turbulence, followed by advancement for high level turbulence. Also shown for comparison purposes is the pitch-heave bi-dimensional PDF transition airspeed which is reproduced from Figure 8.5. We deduce from this comparison that the pitch-heave probability density is essentially dictated by the pitch dynamics.

The mechanism of uni- to bi-modal transition of the diverging pitch and heave is different than from the fluttering problem; although the fundamental cause is the same in both cases, which is the vertical turbulence-nonlinear interaction. It can be appreciated from the study of the bi-dimensional PDF, as shown in Figure 8.11.

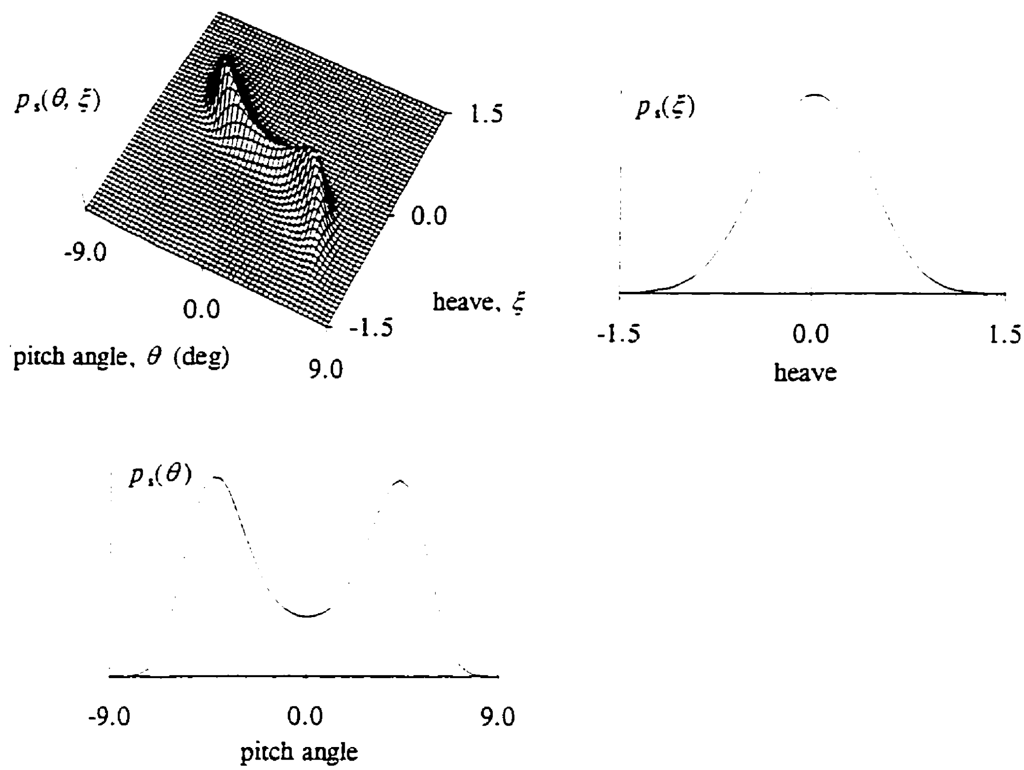

Figure 8.11 - Marginal and bi-dimensional PDF of nonlinear airfoil pitch-heave in combined turbulence; $U_m = 6.0$, $\sigma_T^2 = 0.5$, $L = 50.0$, $k_3 = 400.0$.

The example chosen exhibits a bi-modal density in pitch-heave. The S-shape of the bi-dimensional PDF is a direct consequence of nonlinear-turbulence interaction. We have also observed an S-shape at smaller airspeeds, where the bi-dimensional PDF is uni-modal. It is believed that the curvature towards a limit value in pitch can be attributed to the location of the nonlinearity on the torsional spring. Physically, the restraining mechanism of the nonlinear torsional spring is felt more strongly by the pitch motion than by the heave, especially for large amplitudes since the nonlinear stiffness loses its strength for small amplitude. This translates into a slowing down of the pitch motion at large amplitude which is more important than the slowing down of the heave motion, hence an accumulation of probability at relatively high pitch angle whereas the heave probability is distributed more homogeneously. The final outcome at this airspeed is a bi-modal pitch marginal PDF and a uni-modal heave PDF bi-modal, as shown also in Figure 8.11.

Also note that the random fixed points, as defined by the peaks of the bi-dimensional distribution are located at $\theta \approx 4.0$ deg, $\xi \approx -0.25$ and $\theta \approx -4.0$ deg, $\xi \approx 0.25$. In comparison the deterministic fixed points are located at $\theta = 1.90$ deg, $\xi = -0.06$ and $\theta = -1.90$ deg, $\xi = 0.06$. They are displaced significantly by turbulence.

Effect of a nonlinear spring in heave

We briefly discuss the impact of adding a structural non-linearity in heave via a hardening cubic spring. Note that the non-linearity on the torsional spring is maintained. The heave stiffness term in the aeroelastic equations of motion (equation (2.28)), is modified according to equation (8.6). k_{3h} is defined as the (non-dimensional) nonlinear cubic stiffness coefficient in heave.

$$\frac{\overline{\omega}^2}{U_m^2} \rightarrow k_{3h} \frac{\overline{\omega}^2}{U_m^2} \tag{8.6}$$

Figure 8.12 shows the transition airspeed of the marginal PDF of the heave response for three values of k_{3h}. In comparison with the linear spring (in heave), $k_{3h} = 0.0$, which is the case also shown in Figure 8.10, a hardening of the nonlinear spring in heave has for effect to advance the uni- to bi-modal transition of its corresponding motion. This result supports the argumentation that the location of the non-linearity, be it purely on the torsional spring or on the translational spring as well, dictates the advancement of the transition airspeed of their respective motion.

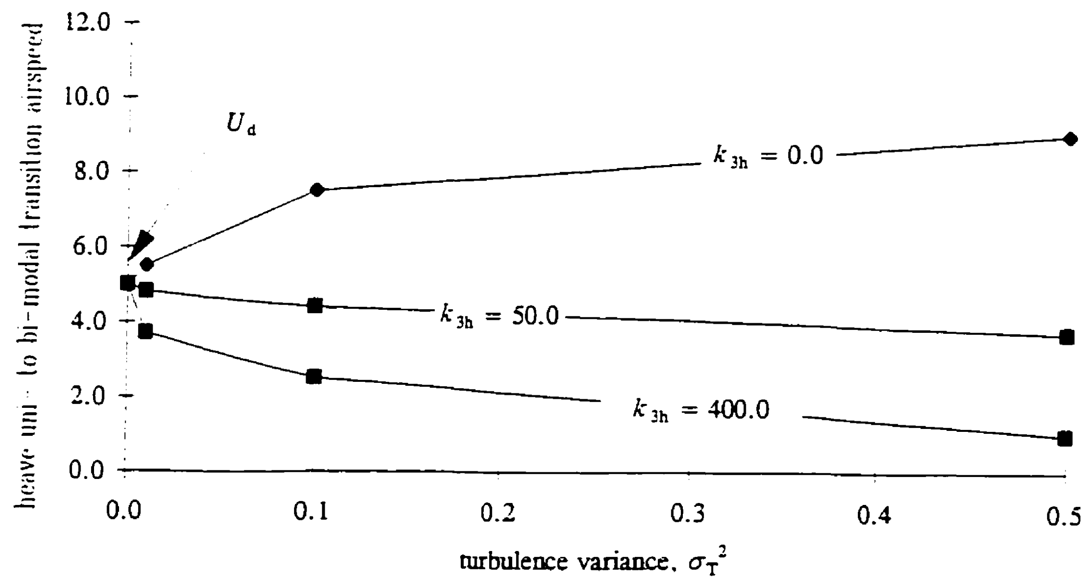

Figure 8.12 - Uni- to bi-modal transition airspeed of heave marginal PDF of nonlinear airfoil in combined turbulence for three values of the nonlinear cubic stiffness coefficient in heave, as a function of turbulence variance; L = 50.0, k_3 = 400.0.

8.4.2 Basin hopping

There exist many forms of basin hopping like the bi-modal PDF and the time history plot exhibiting low frequency coherent oscillations, but perhaps its most distinctive signature is the PSD. Shown in Figure 8.13 is the heave response PSD to combined turbulence at U_m = 9.0 for three turbulence levels. The deterministic divergence/pitchfork occurs at U = 5.0. Also shown, in Figure 8.14, are the corresponding sample time histories in heave, and pitch, for the same airspeed and turbulence conditions.

The PSD at each of the three turbulence variances is typical of a certain type of dynamic behaviour described as follows. For the smaller variance, σ_T^2 = 0.01, the two important features in the PSD are the high sharp peak at zero frequency followed by a low density flat spectrum at higher frequencies. This is indicative of a dominant intra-well motion. The turbulence level is relatively small, such that the dynamics is caught within one domain of attraction for a relatively long period of time, as exemplified by the sample time history, and steady state intra-well motion is experienced. Basin hopping occurs but very rarely and irregularly.

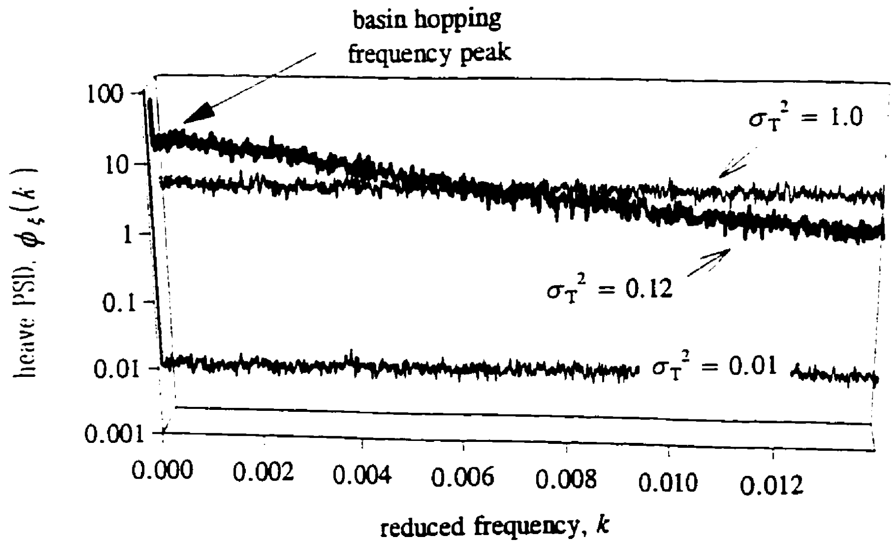

Figure 8.13 - PSD of heave response of nonlinear airfoil in combined turbulence, for three turbulence variances; L = 5.0, k_3 = 400.0, U_m = 9.0; N = 100,000,000, $\Delta\tau$ = 0.1.

Jumping ahead to the high turbulence level, σ_T^2 = 1.0, a much different type of dynamics is observed, since it is dominated by inter-well motion. The PSD displays a flat spectrum, similarly with the low level turbulence, but no peak at the zero frequency. The latter observation that there is no peak at k = 0.0 indicates that the motion does not have the time to settle within one domain of attraction as it is hopping between the two attractors. From the former observation that the spectrum is flat, we conclude that the hopping is highly irregular and white noise like.

Stepping back to the intermediate level turbulence, shown as σ_T^2 = 0.12 in Figure 8.13, we make three observations. First, there is a peak at zero frequency which indicates intra-well motion. Second, the spectral density of the non-zero frequencies is of the same order of magnitude as of the zero frequency peak. From these two observations, we retain the interpretation that both intra- and inter-well motions are experienced with approximately the same degree. This interpretation can also be appreciated by looking at the time history of sample heave and pitch responses, Figure 8.14. The phase plane plot is also shown in Figure 8.15 for this turbulence variance.

The third observation concerns the small, but nevertheless present, hump centred at $k \approx$ 0.0005. This hump indicates coherent oscillation, or *pseudo-regular oscillation* (see Chapter 1), due to basin hopping. We have observed that increasing or decreasing the turbulence variance moves this hump toward higher or lower frequencies, respectively. However, we have also observed that the range of turbulence variance for which it can be detected is small, $0.05 \leq \sigma_T^2 \leq 0.15$.

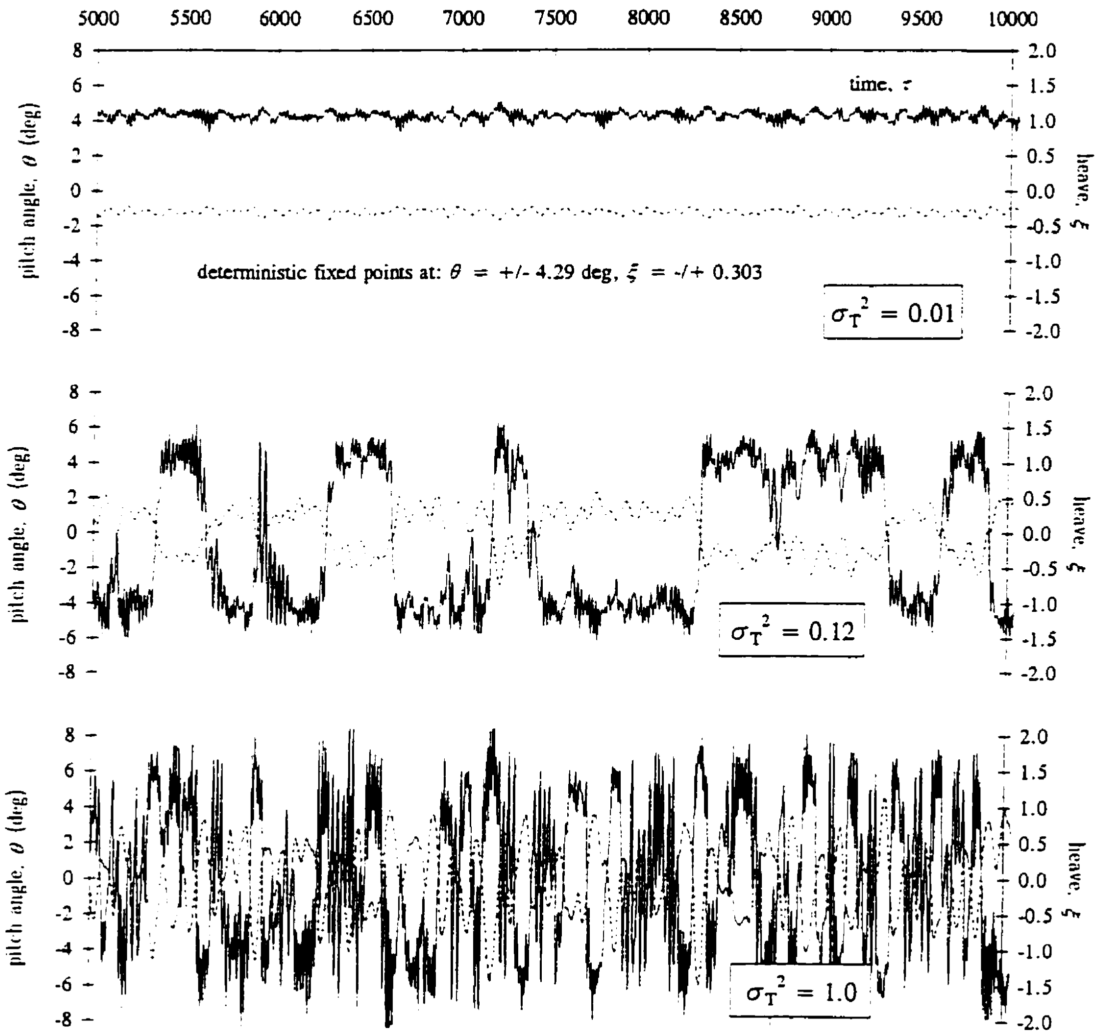

Figure 8.14 - Sample time histories of nonlinear airfoil heave (---) and pitch (—) responses in combined turbulence, for three turbulence variances; $L = 5.0$, $k_3 = 400.0$, $U_m = 9.0$.

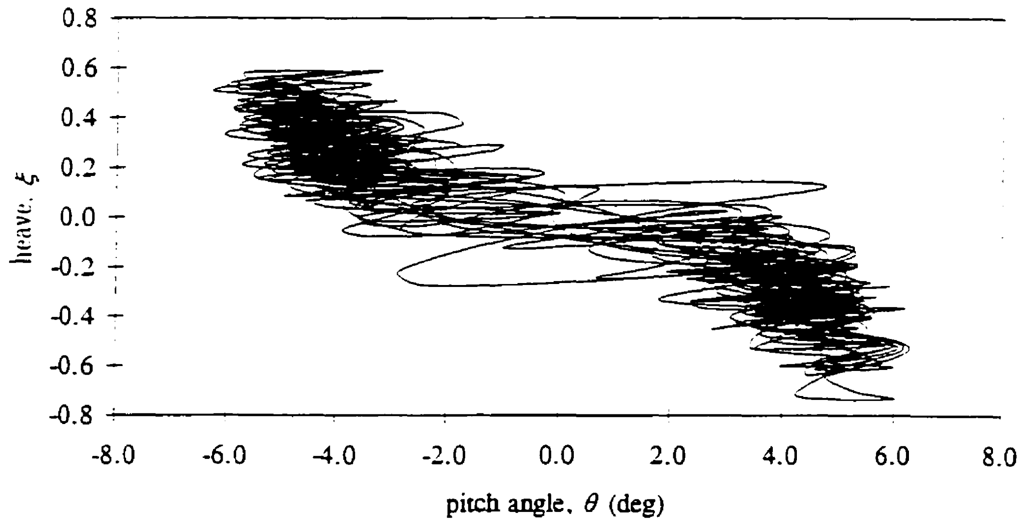

Figure 8.15 - Sample phase plane plot of nonlinear airfoil heave and pitch responses in combined turbulence; L = 5.0, σ_T^2 = 0.12, k_3 = 400.0, U_m = 9.0.

Keeping the same turbulence variance but changing the mean airspeed has a similar effect. For σ_T^2 = 0.12, we have detected pseudo-regular oscillations for only a small range of airspeeds, $8.5 \leq U_m \leq 9.5$. For smaller airspeeds, inter-well motion becomes more dominant; for higher airspeeds, the dynamics tend to be dominated by intra-well motion since the zero-frequency peak becomes stronger. We point out that this observation is not trivial in the sense that the magnitude of the aerodynamic forcing increases with airspeed, even though we have kept the turbulence variance constant. It indicates that the attraction towards either of the two random fixed points is stronger than the increasing random external aerodynamic forcing. This interpretation was also indirectly corroborated by observing the time to reach steady state in the response PDF. We noticed that steady state, as indicated by the PDF, was reached in less iterations at lower airspeeds than at higher airspeeds.

The difficulty in detecting pseudo-regular oscillations due to the lack of sharpness of the hump, as well as due to the small range of parameters (airspeed and turbulence variance) for which it is observed may be an indication that this phenomena is not the norm for this aeroelastic problem. Consequently, it is likely that basin hopping occurs on a very irregular basis. Finally, it is noted that basin hopping is a very small frequency phenomena and is a pure product of the nonlinear-turbulence interaction. Not shown, but in comparison, the PSD of the airfoil response displays other (sharper) peaks at much higher frequencies whose origin can be traced back to the underlying deterministic system.

8.5 Concluding Remarks

In summary, the following remarks are presented.

1. The nonlinear airfoil in pure longitudinal turbulence experiences a three-step bifurcation characterized by, first, a dynamical bifurcation followed by two P-bifurcations. The airspeed region between the D- and the first P-bifurcation displays uni-modal pitch and heave probability densities with a sharp peak centred at zero. The region between the two P-bifurcations is tri-modal. Finally, the second P-bifurcation separates the tri-modal from a bi-modal PDF region, thus is defined by the disappearance of the central sharp peak. The heave rate and pitch rate densities stay uni-modal through out this airspeed range.

2. When vertical turbulence is considered, with or without longitudinal turbulence, the D-bifurcation disappears and only one P-bifurcation remains. The pre-bifurcation motion is represented by a uni-modal pitch-heave bi-dimensional probability density. In the post-bifurcation regime, the bi-dimensional pitch-heave PDF is bi-modal. Furthermore, we argued that the P-bifurcation is advanced by turbulence, namely its vertical component.

3. This point applies strictly to the linear airfoil in combined turbulence and to the nonlinear airfoil in pure longitudinal turbulence. This is so since the D-bifurcation which indicates the loss of stability of the fixed point, hence divergence, does not exist for the nonlinear airfoil in combined turbulence. Divergence can be advanced or postponed by longitudinal turbulence. We have observed a complex dependence on turbulence variance and scale, as well on the frequency ratio. This latter dependence indicates that the coupling with the heave DOF plays a role in random divergence. In turn, we have interpreted this observation as an indication that random divergence is a dynamic instability. Finally, our results indicate that, in general, the shift in divergence airspeed is relatively small.

4. We have observed that the probability structure of the aeroelastic response is strongly dependent on turbulence variance, especially at low levels. Furthermore, the pitch PDF transitions from a uni- to a bi-modal shape at a smaller airspeed than the heave, while the pitch rate and heave rate remain uni-modal. We have explained the difference in transition airspeed between the pitch and heave via their bi-dimensional PDF projection which exhibits a S-like shape leading to a build-up of probability for high pitch angles. Physically, we have argued that the specific form of the S-shape, and related advancement of the pitch transition airspeed, can be attributed to the location of the non-linearity on the torsional spring. In support of this argumentation, we have shown that adding a non-linearity on the heave spring can advance the heave transition airspeed.

5. Coherent, or *pseudo-regular*, oscillations due to basin hopping were detected for a small range of turbulence variance and airspeed. These coherent oscillations take the form of a small hump in the very low frequency range of the aeroelastic response PSD. The lack of sharpness of the hump, coupled with the small range of parameters for which it is detected, indicate that in general basin hopping is likely to occur on a very irregular basis for the diverging nonlinear airfoil.

6. For large turbulence variance, we have found that basin hopping occurs frequently such that the dynamics is determined in a large part by inter-well motion. In contrast, for small turbulence variance intra-well motion becomes dominant.

Chapter 9

CONCLUSION

9.1 Synthesis

In this thesis we have applied the ideas of Random Dynamical Theory, and specifically the principles of the still maturing discipline of random bifurcation, pioneered by Arnold (for *dynamical* bifurcations) and Horsthemke and Lefever (for *phenomenological* bifurcations), to the problem of a flexible nonlinear airfoil in two-dimensional turbulent flow. The D-bifurcation is defined according to a change in sign of the largest Lyapunov exponent of the linearized system. The P-bifurcation corresponds a qualitative change in the probability density of the motion.

The archetypal typical section model, in its deterministic idealization, is relatively simple. It can however generate complex behaviour in the nonlinear regime, as demonstrated by various authors. Relaxing the deterministic idealization by introducing a "reality" element, in the form of random turbulence, increases the complexity of the model, and its analysis, significantly. In turn, its random dynamics become highly intricate, even when the underlying deterministic attractor is a simple fixed point or a limit cycle oscillation. New types of dynamic behaviour appear which require a different conceptual approach, as formalised by random bifurcation theory, and which also necessitate an accrued reliance on their probabilistic and statistical representation.

Turbulence enters the problem in two forms. One is vertical and acts as an external random forcing, or additive noise in dynamical terms. The second form is the longitudinal component which acts directly on the parameters, hence parametric random excitation or multiplicative noise. A fundamental attribute of our treatment of the problem is the deliberate choice to consider the turbulent excitation not as a perturbation noise of the otherwise deterministic system and dynamics, but as an essential element like any other (deterministic) parameters or external forcing. In this light, we have ultimately been searching for random dynamical objects in the sense of Millona's passive and active noise paradigms. It would have made no sense to proceed otherwise, since the underlying deterministic dynamics was known from the start.

In the pursuit of our two objectives we have made full use of the flexibility and highly controlled research environment of the numerical laboratory. We have done so by switching on or off, at will, the longitudinal and vertical turbulent excitations, as well as their more specific contribution on the system parameters, in order to gain a more profound understanding of the overall turbulent problem. We have also been able to easily control and modify the turbulence spectral content, via the scale of turbulence, and its intensity via its variance, thus assessing their effects. These controlled actions would have been extremely difficult, if not impossible, to realize in a physical laboratory.

Nonetheless, the multi-dimensionality of the aeroelastic system has introduced an element of uncontrollability due to the random nature of the dynamics which could not be fully overcome by the numerical experimentation. It has been argued that the most natural representation of the random dynamics is its probability density function, which ideally should be of the same dimension as the system from which it is generated. We are, however, fundamentally restricted to a two-dimensional PDF, with the third dimension representing the probability density. This has, in general, resulted in a cautious interpretation of the results, and specifically with regard to the identification of the bifurcation and associated pre- and post-bifurcation motion types.

We have concentrated our efforts on the investigation of the random fluttering airfoil experiencing a supercritical Hopf bifurcation in its nonlinear deterministic representation. As a second problem, we have also treated the divergence/supercritical pitchfork, but in less detail. These two problems have been studied with the principal aim of capturing their bifurcation, stability and response characteristics when excited by turbulent flow. Essentially, this has been our first objective. A secondary objective has been to examine the relative contribution of the longitudinal component of turbulence, since it is often neglected in more traditional aeroelastic analyses. At the end of Chapters 4 to 8, we have presented the results of our research in the form of detailed summarizing remarks. In what follows, emphasis is put on what we believe are the most significant results of this thesis. Broad conclusions are also drawn.

We have found that bifurcations in the airfoil's aeroelastic response are fundamentally modified by the presence of turbulent flow in a number of ways. This is true for both the Hopf and pitchfork bifurcations. In the deterministic case, the D- and P-bifurcation coincide at the instability point. The loss of stability of the fixed point indicated by the D-bifurcation, where the largest Lyapunov exponent becomes zero, corresponds exactly to a change in qualitative behaviour of the dynamics. For the excited nonlinear airfoil, due to vertical turbulence, the D-bifurcation disappears since the largest Lyapunov exponent does not experience any discontinuity. The P-bifurcation remains, but its location on the mean airspeed axis changes, seemingly toward smaller airspeeds. For reasons mentioned earlier with regard to the theoretical requirement to have a multi-dimensional PDF, we cannot, however, ascertain that the P-bifurcation is actually advanced.

Another aspect of the bifurcation concerns the pre- and post-bifurcation types of motion. We have observed different random motions and tried, in a first effort, to interpret them according to a deterministic point of view. Based on the probability density function representation, this has been possible for the fixed point type of motion. It is characterized by a uni-modal Gaussian-like shape in the marginal PDF and a uni-modal bell shape in the bi-dimensional PDF of the displacement displacement-rate. With regard to the LCO, the crater-like features of the bi-dimensional PDF supports the interpretation of a random LCO for low level turbulence. In contrast, we have observed that at intermediate and high level turbulence the basic LCO structure is lost, and a new type of motion appears which has no apparent deterministic analogue. Nevertheless, we have been able to account for some of its features in light of the deterministic motion. We have argued that the observed random motion at one particular airspeed and turbulence variance is related to the deterministic motion at a higher airspeed. The explanation is that increasing the turbulence variance or airspeed have the same effect in that the response amplitude is increased, in turn increasing nonlinear effects. This explanation has been corroborated by the observation and interpretation of the aeroelastic spectral content, which displayed an increase in the relative strength of the super-harmonics, in comparison with the fundamental frequency, with increasing turbulence variance. The same phenomena exists for the deterministic LCO as the airspeed is increased.

For the linear airfoil, the traditional nonlinear concept of bifurcation is not required although the D-bifurcation, defined by the largest Lyapunov exponent, does exist for both the excited and non-excited (linear) airfoil. We have associated the notion of D-bifurcation to flutter and divergence, since these two instability types correspond to a loss of stability of a fixed point, as indicated by the D-bifurcation, without regard to the post-instability, hence, nonlinear behaviour. We have argued that the flutter instability is always advanced by turbulence, due to its longitudinal component. A parametric resonance analysis, using a narrow-band excitation, has provided a numbers of answers in this regard. Specifically, it has shown that the longitudinal turbulence spectral density in the low and very low frequency range, coupled with principal and secondary combination difference type parametric resonances, account, for the most part, for the advancement in flutter speed. On the other hand, we have found that longitudinal turbulence may advance or postpone divergence. Furthermore, the magnitude of the shift in divergence airspeed is generally much less significant than for flutter.

In addition, since the D-bifurcation disappears for the (vertical turbulence) excited nonlinear airfoil, we have proposed the theoretical interpretation that flutter and divergence no longer exists in this case. This is in some ways reminiscent of deterministic divergence where a bias is considered as introduced in Chapter 1 (Figure 1.5). Divergence of the linear airfoil is not affected by a bias; although the response increases as the divergence airspeed is approached, divergence exists and its airspeed does not change. For the nonlinear airfoil with a bias, divergence disappears since the fixed point does not lose stability.

From perhaps a more practical point of view, we have observed that the probability structure of the nonlinear aeroelastic response, in both flutter/Hopf and divergence/pitchfork conditions, is strongly dependent on which state variable is considered. The uni- to bi-modal transitions do not occur at the same airspeed for pitch, heave and their time derivatives. Although the specific mechanism of the transition is different for the diverging and fluttering airfoil, their root cause is the same, that is the interplay between nonlinearity and turbulence, specifically vertical turbulence.

In this light, it is interesting to briefly compare this effect of vertical turbulence with the longitudinal component. Vertical turbulence appears to effectively "decouple" the state variable motions. In contrast, longitudinal turbulence tends to have a coupling effect, as was discussed for coalescence flutter and divergence. For the former, we have argued that the observed advancement of the random modal frequency coalescence could be interpreted as being due to a coupling effect of longitudinal turbulence. For the latter, the impact of the frequency ratio on the shift in random divergence shows that the heave motion plays a role for this instability type, which in the deterministic case is a 1DOF pitch problem for which heave motion has no effect.

With our second objective in mind, we have observed other effects of longitudinal turbulence and systematically analysed them in the context of the flutter/Hopf problem. They are a general destabilisation and a tendency to force the dynamics to be centred around the origin, the latter effect being especially evident for the nonlinear airfoil in pure longitudinal turbulence. Of these two competing effects, we found that destabilisation is, in general, the strongest. Furthermore, it affects the dynamics of the airfoil at all airspeeds, not necessarily just in the vicinity of the instability or bifurcation point.

The general decrease in stability of the airfoil due to longitudinal turbulence is embodied by a larger mean-square response to external excitation and specifically to vertical turbulence. Depending on scale of turbulence, turbulence variance and airspeed, the increase in response level can be significant for the linear airfoil. For the nonlinear airfoil, the contribution of the longitudinal component of turbulence diminishes as nonlinear effects increase. Overall, we have noted that longitudinal turbulence plays a minor role relative to vertical turbulence in the airfoil dynamics.

Also of interest are the noise-induced and noise-controlled peaks that are exhibited by the nonlinear response PSD. Some of these observations were not expected. For instance, contrary to intuition we observed a shift of the fundamental peak, representing the random LCO, towards smaller frequencies, as well as its narrowing, subsequent to a widening, with increasing variance. No physical explanation was proposed but we noted some similar observations in the physics literature. In contrast, we expected to observe a clear peak in the diverging nonlinear airfoil response spectrum, indicative of coherent or pseudo-regular oscillation due to basin hopping between the two stable fixed points. Rather, a small hump at very low frequencies was observed and for only a small range of airspeed and turbulence variance. This lead us to think that, in general, basin hopping for the diverging nonlinear airfoil is likely to take place on a very irregular basis.

9.2 Theoretical Perspectives

The bifurcation analysis in the specific context of the airfoil in turbulent flow has enabled us to shed some additional light on the problem of a general randomly excited nonlinear dynamical system. We have argued that the theoretical basis of the general problem has not yet reached a mature level. In support of this statement, we have offered the example of the debate concerning the D- versus P-bifurcations in terms of the more relevant and rigorous bifurcation theory. Furthermore, we have discussed areas where contradictory results, and subsequent interpretations, exist in the literature. They concern the motion type and shift in the bifurcation point for additive noise excitation. With regard to these points of discord and based on our investigation, we have proposed the following remarks.

First, related to the D- versus P-bifurcations we have determined that the D-bifurcation is destroyed by vertical turbulence in favour of a single P-bifurcation. In other words, the bifurcation scenario of the turbulent excited airfoil is essentially dictated by the vertical component of turbulence. We have therefore questioned the robustness of the bifurcation scenario under pure multiplicative noise and extended the concept of bifurcation robustness and structural stability applied to deterministic systems in this manner. Because both multiplicative and additive noise are present in any real system, the bifurcation scenario generally observed for pure multiplicative noise is qualitatively not robust.

We have also suggested that this applies regardless of the relative intensity of both noise components, since any small amount of additive noise will destroy the D-bifurcation. This is a question that warrants further attention, from both a theoretical and practical point of view. We have just alluded to the theoretical tenets of this question. In practice, it may become relevant when the parametric and external excitations have different sources, and when the intensity of the parametric excitation is much larger that the intensity of the latter. In this case, the interest lies in how much of the bifurcation characteristics in pure parametric excitation remain when a small amount of external noise is added.

On the second point of discord, we have in part reconciled apparent conflicting results obtained by some authors. We have argued that the observed differences in motion type could be accounted for due to additive noise intensity, as explained earlier with regard to the post-bifurcation LCO dynamics for low level turbulence in comparison with intermediate and high level turbulence. The question of the shift of the P-bifurcation due to vertical turbulence remains open, although we have speculated on an advancement.

Accordingly, we believe that the results of this research go beyond the specific context of the turbulent excited flexible airfoil. Our research is relevant in two ways for the general random nonlinear problem. It provides results from a systematic analysis of a nonlinear system excited by multiplicative and additive noise and for which the specific contributions of both noise components were investigated in isolation and in combination. It also provides results from a highly controlled research environment of a "real" system. In this sense, this research helps to bridge the gap between analytical treatments, which are limited by a number of simplifying assumptions such as low-dimensionality, white noise and/or Gaussian response, and real physical experimentation where random excitation and response are very difficult to control and monitor.

9.3 Recommendations for Future Research

Potential for future research exists in both depth and breadth. Depth-wise we have, throughout this thesis, already pointed out a number areas which require further attention. Although the flutter/Hopf problem has been investigated in detail, some questions are left unanswered. Specifically, the peculiar behaviour observed in the aeroelastic spectral response would benefit from a targeted analysis. Furthermore, an investigation of other types of nonlinearities would also be important.

Certainly our treatment of the divergence/pitchfork problem has been less systematic and more descriptive than for the flutter/Hopf case. In this sense, a number of questions remains open. In particular, we believe that a more profound and exhaustive investigation of basin hopping is warranted. Since the spectral signature of *pseudo-regular oscillations* appears to be lacking the sharpness that we were looking for, we believe that the response PDF representation is perhaps a more fertile ground to better understand this phenomena. The analysis of the response probability density function could be particularly useful for the problem with a bias since the two competing fixed points, and their respective basin of attraction, will have different properties.

More generally, the PDF is a useful tool to visualise and analyse the structure of competing attractors. Random noise can be exploited to probe the dynamics of the multi-stable system. As introduced in Chapter 1, the probability structure may be used as an indication of the relative strength of attractors. The relative height of each modal PDF peak and their respective width are relevant characterisation parameters. This is the basic idea behind the approach taken by some researchers. For example, Kaneko [1998] studied the structure and relative strength of attractors, as well as their basin volume, by considering their return rate (probability) after being perturbed with a randomly selected input. Note that probability density functions are also used to characterize deterministic chaotic attractors [Hsu and Kim, 1985].

In terms of breadth, numerous problems are potentially significant either from a theoretical point of view or for their practical implications. A logical extension to the two problems treated in this thesis is the nonlinear airfoil experiencing a subcritical Hopf bifurcation in its deterministic model. This problem is particularly relevant from the point of view of basin hopping where the two stable competing attractors are a fixed point and a limit cycle oscillation. Accordingly, a study of the PDF of the response may provide some important clues on the structure of the basin of attraction of these two attractors. Also of interest is the fact that basin hopping is possible at pre-flutter speeds, hence, strongly nonlinear dynamics is expected to be observed at airspeeds lower than the flutter speed. It may have important implications with regards to the understanding of relatively recent aeroelastic instabilities experienced by the CF18 aircraft [Dickinson, 1996].

Another problem that comes to mind is nonlinear panel flutter excited by very low level turbulence, which implies a very small vertical turbulence intensity, and parametrically excited with a high level structural vibration. This is a practical form of the theoretical problem raised in Section 9.2. Of interest may be the probability structure of the response and its potentially beneficial impact on panel structural fatigue, considering that for pure parametric excitation the LCO dynamics is expected to be forced to occur close to the origin.

The dual problem of chaos and randomness is certainly an extremely complex and challenging one. A great number of papers have been published in the physics literature for the general problem. It could be worthwhile to apply the ideas developed in physics to the specific case of the nonlinear airfoil.

In theory, the turbulent excited airfoil operating in dynamic stall condition is also potentially significant. This is so since the nonlinearity, which originates from the aerodynamics for a stalled airfoil, is directly (parametrically) excited by turbulence, thus enabling the appearance of *pure noise-induced transitions*. In practice, one important aspect may alter the significance of this research topic. We know of no validated aerodynamic model capable of reproducing arbitrary motion in dynamic stall conditions. To our knowledge, the proven applicability of existing models is limited to simple harmonic motion.

Finally, the results of this thesis may serve to establish a database of simulated aeroelastic data. We believe that the enclosed data, and analysis, can be useful to test and validate, similar to a test bench, aeroelastic flight test data analysis techniques. In those terms, this thesis directly addresses one of the recommendations from the last North Atlantic Treaty Organization (NATO) Advisory Group for Aerospace Research & Development (AGARD) specialist meeting on aeroelasticity flight testing [AGARD-CP-566, 1995].

REFERENCES

Abarbanel, H.D.I., Brown, R., and Kennel, M.B., "Variation of Lyapunov Exponents on a Strange Attractor", Journal of Nonlinear Science, Vol. 1, 1991, pp. 175-199.

Abdel-Motagaly, K., Duan, B., and Mei, C., "Nonlinear Panel Response at High Acoustic excitations and supersonic Speeds", AIAA-99-1380, 1999, pp. 1963-1972.

AGARD, "High Angle-of-Attack Aerodynamics", AGARD Lecture Series, AGARD-LS-121, 1982.

AGARD, "The Flight of Flexible Aircraft in Turbulence - State-of-the-Art in the Description and Modelling of Atmospheric Turbulence", AGARD Report, AGARD-R-734, 1987.

AGARD, "Aircraft Dynamic Loads Due to Flow Separation", AGARD Conference Proceedings, AGARD-CP-483, 1990.

AGARD, "Advanced Aeroservoelastic Testing and Data Analysis", AGARD Conference Proceedings, AGARD-CP-566, 1995.

Alighanbari, H., "Flutter Analysis and Chaotic Response of an Airfoil Accounting For Structural Nonlinearities", PhD Thesis, McGill University, Montreal, Canada, 1995.

Alighanbari, H., and Price, S.J., "The Post-Hopf-Bifurcation Response of an Airfoil in Incompressible Two-Dimensional Flow", Non-linear Dynamics, Vol. 10, 1996, pp. 381-400.

Anishchenko, V.S., and Neiman, A.B., "Stochastic Synchronization", *Stochastic Dynamics* (Edited by L. Schimansky-Geier and T. Pöschel), Springer-Verlag, Berlin, 1997, pp. 155-166.

Anonymous, "Revised Discrete Gust Load Design Requirements; Final Rule - FAR, 14 CFR Part 25", Federal Register, DOT, Vol. 61, No. 28, 1996, pp. 5218-5222.

Anonymous, "Fortran Subroutines for Statistical Analysis", IMSL, Inc. STAT/LIBRARY, 1987.

Argyris, J., Faust, G., and Haase, M., "An Exploration of Chaos; An Introduction for Natural Scientists and Engineers", Texts on Computational Mechanics, Vol. VII, North-Holland, Amsterdam, 1994.

Ariaratnam, S.T., "Bifurcation in Nonlinear Stochastic Systems", *New Approaches to Nonlinear Problems in Dynamics* (Edited by P.J. Holmes), S.I.A.M. Publications, 1980, pp. 470-474.

Ariaratnam, S., "Some Illustrative Examples of Stochastic Bifurcations", *Nonlinearity and Chaos in Engineering Dynamics* (Edited by Thompson, J. and Bishop, S.), John Wiley & Sons, Ltd., Chichester, 1994, pp. 267-274.

Ariaratnam S.T. and Tam D.S.F., "Random Vibration and Stability of a Linear Parametrically Excited Oscillator", ZAMM 59, 1979, pp. 79-84.

Arnold, L., "Stochastic Differential Equations: Theory and Applications", John Wiley & sons Inc., 1974.

Arnold, L., "Random Dynamical Systems", *Dynamical Systems*, Lectures given at the 2nd session of the CIME, Springer-Verlag, Berlin, 1995, pp. 1-43.

Arnold, L.,"Random Dynamical Systems", Springer-Verlag, Berlin, 1998.

Arnold, L. and Chueshov, I., "Order-Preserving Random Dynamical Systems: Equilibria, Attractors, Applications", Dynamics and Stability of Systems, Vol. 13, No. 3, 1998, pp. 265-280.

Arnold, L., Crauel, H., "Random Dynamical Systems", Proceedings of a Conference on Lyapunov Exponents, Lecture Notes in Mathematics, Springer-Verlag, Vol. 1486, Berlin, 1991, pp. 1-22.

Arnold, L., Doyle, M., and Sri Namachchivaya, N., "Small Noise Expansion of Moment Lyapunov Exponents for Two-Dimensional Systems", Dynamics and Stability of Systems, Vol. 12, No. 3, 1997, pp. 187-211.

Arnold, L. and Kedai, X., "Invariant Measures for Random Dynamical Systems, and a Necessary Condition for Stochastic Bifurcation from a Fixed Point", Random & Computational Dynamics, Vol. 2, No. 2, 1994, pp. 165-182.

Arnold, L., Kliemann, W., and Oeljeklaus, E., "Lyapunov Exponents of Linear Stochastic Systems",Proceedings of a Workshop on Lyapunov Exponents, Lecture Notes in Mathematics, Springer-Verlag, Vol. 1186, Berlin, 1986, pp. 85-125.

Barnes, T.J., "Overview of the Activities of the ad hoc Committee of International Gust Specialists", AGARD-R-798, 1994, pp. 1-1 to 1-8.

Baxendale, P., "Invariant Measures for Nonlinear Stochastic Differential Equations", Proceedings of a Conference on Lyapunov Exponents, Lecture Notes in Mathematics, Springer-Verlag, Vol. 1486, Berlin, 1991, pp. 123-140.

Benzi, R., Parisi, G., Sutera, A., and Vulpiani, A., "Stochastic Resonance in Climatic Change", Tellus, Vol. 34, 1982, pp. 10-16.

Bisplinghoff, R., and Ashley, H., "Principles of Aeroelasticity", John Wiley and Sons, Inc., New York, 1962.

Breitbach E., "Effects of Structural Non-Linearities on Aircraft Vibration and Flutter", AGARD Rep. 665, 1978.

Bucher, C.G., "Sample Stability of Multi-Degree-of-Freedom Systems", Proceedings of a Conference on Lyapunov Exponents, Lecture Notes in Mathematics, Springer-Verlag, Vol. 1486, Berlin, 1991, pp. 322-330.

Bucher, C.G., and Lin, Y.K., "Effect of Spanwise Correlation of Turbulence Field on the Motion Stability of Long-Span Bridges", Journal of Fluids and Structures, Vol. 2, 1988, pp. 437-451.

Bucher, C.G., and Lin, Y.K., " Stochastic Stability of Bridges Considering Coupled Modes", Journal of Engineering Mechanics, ASCE, Vol. 114, No. 12, 1988, pp. 2055-2071.

Cai, G., and Lin, Y.K., "Response Spectral Densities of Strongly Nonlinear Systems Under Random Excitation", Probabilistic Engineering Mechanics, Vol. 12, No. 1, 1997, pp. 41-47.

Cartmell, M., "Introduction to Linear, Parametric and Nonlinear Vibrations", Chapman and Hall, London, 1990.

Casdagli, M., "Chaos and Deterministic Versus Stochastic Nonlinear Modelling", Journal of the Royal Statistical Society, B, Vol. 54, No. 2, pp. 303-328, 1991.

Costello, M., Prasad, J.V.R., Schrage, D.P., and Gaonkar, G.H., "Some Issues on Modeling Atmospheric Turbulence Experienced by Helicopter Rotor Blades", Journal of the American Helicopter Society, Vol. 37, No. 2, 1992, pp. 71-75.

Dickinson, M., "CF-18/GBU-24 Flight Flutter Test Report", Bombardier Inc. Report, RAU-261-165, 1996.

Dinyavari, M.A.H, and Friedmann, P.P., "Application of Time-Domain Unsteady Aerodynamics to Rotary-Wing Aeroelasticity", AIAA Journal, Vol. 24, No. 9, 1986, pp. 1424-1432.

Ditzinger, T., Ning, C., and Hu, G., "Resonancelike Responses of Autonomous Nonlinear Systems to White Noise", Physical Review E, Vol. 50, No. 5, November 1994, pp. 3508-3516.

Done, G., "Past and Future Progress in Fixed and Rotary Wing Aeroelasticity", Aeronautical Journal, 1996, pp. 269-279.

Dowell, E.H., "Panel Flutter: A Review of the Aeroelastic Stability of Plates and Shells", AIAA Journal, Vol. 8, No. 3, 1970, pp. 385-399.

Dowell, E.H., "Aeroelasticity of Plates and Shells", Noordhoff International Pub., Leyden, The Netherlands, 1974.

Dowell, E.H., "A Simple Method for Converting Frequency Domain Aerodynamics to the Time Domain", NACA TM 81844, 1980.

Dowell, E.H., Curtiss, Jr., H., and Sisto, F., "A modern Course in Aeroelasticity", Sijthoff & Noordhoff, Alphen aan den Rijn, The Netherlands, 1978.

Dowell, E.H., and Ilgamov, M., "Studies in Nonlinear Aeroelasticity", Springer-Verlag, New York, 1988.

Dowell, E.H., and Voss, H.M., "Experimental and Theoretical Panel Flutter Studies in the Mach Number Range 1.0 to 5.0", AIAA Journal, Vol. 3, No. 12, 1965, pp. 2292-2304.

D'Souza, A., and Garg, V., "Advanced Dynamics; Modeling and Analysis", Prentice-Hall, Inc., Englewood Cliffs, 1984.

Dykman, M., Luchinsky, D., Mannella, R., McClintock, P., Soskin, S., Stein, N., and Stocks, N., "Stochastic Resonance", *Nonlinearity and Chaos in Engineering Dynamics* (Edited by Thompson, J. and Bishop, S.), John Wiley & Sons, Ltd., Chichester, 1994.

Dykman, M.I., and McClintock, P.V.E., "Power Spectra of Noise-Driven Nonlinear Systems and Stochastic Resonance", Physica D, Vol. 58, 1992, pp. 10-30.

Eastep, F.E., and McIntosh, Jr., S.C., "Analysis of Nonlinear Panel Flutter and Response Under Random Excitation or Nonlinear Aerodynamic Loading", AIAA Journal, Vol. 9, No. 3, 1971, pp. 411-418.

Ebeling, W., Herzel, H., Richert, W., and Schimansky-Geier, L., "Influence of Noise on Duffing-Van der Pol Oscillators", ZAMM, Vol. 66, No. 3, 1986, pp. 141-146.

Eckmann, J.-P., Kamphorst, S., Ruelle, D., and Ciliberto, S., "Liapunov Exponents from Time Series", Physical Review A, Vol. 34, No. 6, December 1986, pp. 4971-4979.

Eckmann, J.-P., and Ruelle, D., "Ergodic Theory of Chaos and Strange Attractors", Reviews of Modern Physics, Vol. 57, No. 3, Part 1, 1985, pp. 617-656.

Edwards, J.W., Ashley, H., and Breakwell, J.V., "Unsteady Aerodynamic Modeling for Arbitrary Motions", AIAA Journal, Vol. 17, No. 4, 1979, pp. 365-374.

Farmer, J.D., "Chaotic Attractors of an Infinite-Dimensional Dynamical System", Physica 4D, 1982, pp. 366-393.

Fishman, G.S. and Moore III, L.R., "An Exhaustive Analysis of Multiplicative Congruential Random Number Generators With Modulus 2^{31} - 1", SIAM Journal on Scientific and Statistical Computing, Vol. 7, No. 1, 1986, pp. 24-45.

Fox, R.F., Gatland, I.R., Roy, R., and Vemuri, G., "Fast, Accurate Algorithm for Numerical Simulation of Exponentially Correlated Colored Noise", Physical Review A, Vol. 38, No. 11, 1988, pp. 5938-5940.

Fox, R.F., "Numerical Simulations of Stochastic Differential Equations", Journal of Statistical Physics, Vol. 54, No. 5/6, 1989, pp. 1353-1366.

Friedmann, P., "Renaissance of Aeroelasticity and Its Future", Journal of Aircraft, Vol. 36, No. 1, 1999, pp. 105-121.

Friedmann, P.P., "Arbitrary Motion Unsteady Aerodynamics and Its Application to Rotary-Wing Aeroelasticity", Journal of Fluids and Structures, Vol. 1, 1987, pp. 71-93.

Friedmann, P.P., and Robinson, L.H., "Influence of Unsteady Aerodynamics on Rotor Blade Aeroelastic Stability and Response", AIAA Journal, Vol. 28, No. 10, 1990, pp. 1806-1812.

Fronzoni, L., "Analogue Simulations of Stochastic Processes by Means of Minimum Component Electronic Devices", *Noise in Nonlinear Dynamical Systems, Experiments and Simulations* (Edited by F. Moss and P.V.E. McClintock), Vol. 3, Cambridge University Press, Cambridge, 1989, pp. 222-242.

Fronzoni L., Mannella, P., McClintock, P., and Moss, F., "Postponement of Hopf Bifurcations by Multiplicative Colored Noise", Physical Review A, Vol. 36, No.2, July 1987, pp. 834-841.

Fung, Y.C., "An Introduction to the Theory of Aeroelasticity", John Wiley & Sons, Inc., New York, 1955.

Gaonkar, G.H., "Gust Response of Rotor and Propeller Systems", Journal of Aircraft, Vol. 18, No. 5, 1981, pp. 389-395.

Garrick, I.E., "On Some Reciprocal Relations in the Theory of Nonstationary Flows", NACA Rept. 629, 1938.

Gelb, A., and Vander Velde, W.E., "Multiple-Input Describing Functions and Nonlinear System Design", McGraw-Hill, Inc., New York, 1968.

Grassberger, P., and Procaccia, I., "Measuring the Strangeness of Strange Attractors", Physica 9D, 1983, pp. 189-208.

Guckenheimer, J., and Holmes, P., "Nonlinear Oscillations, Dynamical Systems, and Bifurcations of Vector Fields", Applied Mathematical Sciences, Springer-Verlag, New York, 1990.

Hänggi, P., "Colored Noise in Continuous Dynamical Systems: a Functional Calculus Approach", *Noise in Nonlinear Dynamical Systems* (Edited by F. Moss and P.V.E. McClintock), Vol. 1, 1989, pp. 307-328.

Heo, H., "Non-Linear Stochastic Flutter of Aeroelastic Structural Systems", PhD Thesis, Texas Tech University, 1985.

Hoblit, F., "Gust Loads on Aircraft: Concepts and Applications", AIAA Education Series, AIAA, Inc., Washington, D.C., 1988.

Holmes P.J., "Bifurcations to Divergence and Flutter in Flow-Induced Oscillations: a Finite Dimensional Analysis", Journal of Sound and Vibration, Vol. 53, No. 4, 1977, pp. 471-503.

Horsthemke W. and Lefever R., "Noise-Induced Transitions; Theory and Applications in Physics, Chemistry and Biology", Springer-Verlag, Berlin, 1984.

Houbolt, J.C., "A Recurrence Matrix Solution for the Dynamic Response of Elastic Aircraft", Journal of the Aeronautical Sciences, Vol. 17, No. 9, 1950, pp. 540-550.

Houbolt, J., Steiner, R., and Pratt, K., "Dynamic Response of Airplanes to Atmospheric Turbulence Including Flight Data on Input and Response", NASA Tech. Rep. R-199, 1964.

Ibrahim, R.A., "Parametric Random Vibration", Research Studies Press, Ltd., Letchworth, 1985.

Ibrahim, R.A., and Heo, H., "Stochastic Response of Nonlinear Structures with Parameter Random Fluctuations", AIAA Journal, Vol. 25, No. 2, 1987, pp. 331-338.

Ibrahim, R.A., Orono, P.O., and Madaboosi, S.R., "Stochastic Flutter of a Panel Subjected to Random In-Plane Forces Part I: Two Mode Interaction", AIAA Journal, Vol. 28, No. 4, 1990, pp. 694-702.

Ibrahim, R.A. and Orono, P.O., "Stochastic Non-Linear Flutter of a Panel Subjected to Random In-Plane Forces", International Journal of Non-Linear Mechanics, Vol. 26, No. 6, 1991, pp. 867-883.

Jones, D.J., and Lee, B.H.K., "Time Marching Numerical Solution of the Dynamic Response of Nonlinear Systems", National Research Council Canada, NAE-AN-25, 1985.

Jones, R.T., "Operational Treatment of the Nonuniform Lift Theory to Airplane Dynamics", NACA TN 667, 1938.

Kabashima, S. and Kawakubo, T., "Observation of a Noise-Induced Phase Transition in a Parametric Oscillator", Physics Letters, Vol. 70A, Nos 5/6, April 1979, pp. 375-376.

Kaneko, K., "On the Strength of Attractors in a High-dimensional System: Milnor Attractor Network, Robust Attraction, and Noise-Induced Selection", Physica D, Vol. 124, 1998, pp. 322-344.

Kantz, H., "A Robust Method to Estimate the Maximal Lyapunov Exponent of a Time Series", Physics Letters A, Vol. 185, 1994, pp. 77-87.

Katafygiotis, L., Papadimitriou, C., and Tsarkov, Y., "Mean-Square Stability of Linear Stochastic Dynamical Systems Under Parametric Wide-Band Excitations", Probabilistic Engineering Mechanics, Vol. 12, No. 3, 1997, pp. 137-147.

Khasminskii, R., "Stochastic Stability of Differential Equations", Sijthoff & Noordhoff, Alphen aan den Rijn, the Netherlands, 1980.

Kloeden, P.E., and Platen, E., "Numerical Solution of Stochastic Differential Equations", Springer-Verlag, Berlin, 1992.

Knobloch, E. and Weisenfeld, K.A., "Bifurcations in Fluctuating Systems: The Center Manifold Theory", Journal of Statistical Physics, Vol. 33, No. 3, 1983, pp. 611-637.

Knuth, D.E., "The Art of Computer Programming", Vol. 2, Addison Wesley Longman, Inc., 1998.

Küssner, H.G., "Zusammenfassender Bericht uber den instationaren Auftrieb von Flugeln", Luftfahrtforschung, Bd. 13, 1936, pp. 410-424.

Küssner, H.G., "Zusammenfassender Bericht uber den instationaren Auftrieb von Flugeln", Luftfahrtforschung, Bd. 13, 1936, pp. 410-424.

Lee, B.H.K., Brown, D., Tang, F.C., and Plosenski, M., "Flowfield in the Vicinity of an F/A-18 Vertical Fin at High Angles of Attack", Journal of Aircraft, Vol. 30, No. 1, 1993, pp. 69-74.

Lee, B.H.K, Brown, D., Zgela, M., and Poirel, D., "Wind Tunnel Investigation and Flight Tests of Tail Buffet on the CF-18 Aircraft", AGARD Conference on Aircraft Dynamic Loads Due to Flow Separation, AGARD-CP-483, 1990, pp. 1-1 to 1-26.

Lee, B.H.K., and Desrochers, J., "Flutter Analysis of a Two-Dimensional Airfoil Containing Structural Nonlinearities", National Research Council Canada, LR-618, 1987.

Lee, B.H.K. Gong, L., and Wong, Y.S., "Analysis and Computation of Nonlinear Dynamic Response of a Two-Degree-of-Freedom System and Its Application in Aeroelasticity", Journal of Fluids and Structures, Vol. 11, 1997, pp. 225-246.

Lee, B.H.K., and Leblanc, P., "Flutter Analysis of a Two-Dimensional Airfoil With Cubic Non-Linear Restoring Force", National Research Council Canada, NAE-AN-36, 1986.

Lee, B.H.K., Price, S.J., and Wong, Y.S., "Nonlinear Aeroelastic Analysis of Airfoils: Bifurcation and Chaos", Progress in Aerospace Sciences, Vol. 35, 1999, pp. 205-334.

Lee, B.H.K., and Tron, A., "Effects of Structural Nonlinearities on Flutter Characteristics of the CF-18 Aircraft", Journal of Aircraft, Vol. 26, No. 8, 1989, pp. 781-786.

Lefever, R. and Turner, J.W., "Sensitivity of a Hopf Bifurcation to Multiplicative Colored Noise", Physical Review Letters, Vol. 56, No. 16, April 1986, pp. 1631-1634.

Leishman, G.J., "Unsteady Lift of a Flapped Airfoil by Indicial Concepts", Journal of Aircraft, Vol. 31, No. 2, 1994, pp. 288-297.

Le Maitre, O., Huberson, S., and Souza De Cursi, E., "Unsteady Model of Sail and Flow Interaction", Journal of Fluids and Structures, Vol. 13, 1999, pp. 37-59.

Leng, G., Sri Namachchivaya, N, and Talwar, S., "Robustness of Nonlinear Systems Perturbed by External Random Excitation", Journal of Applied Mechanics, Vol. 59, 1992, pp. 1015-1022.

Li, Q.C., and Lin, Y.K., "New Stochastic Theory for Bridge Stability in Turbulent Flow. II", Journal of Engineering Mechanics, Vol. 121, No. 1, 1995, pp. 102-116.

Lin, C.C., "Statistical Theories of Turbulence", Princeton University Press, Princeton, 1961.

Lin, Y.K., Fujimori, Y., and Ariaratnam, S.T., "Rotor Blade Stability in Turbulent Flows - Part I", AIAA Journal, Vol. 17, No. 6, 1979, pp. 545-552.

Lin, Y.K., "Stochastic Stability of Wind-Excited Long-Span Bridges", Probabilistic Engineering Mechanics, Vol. 11, 1996, pp. 257-261.

Lin, Y.K., and Li, Q.C., "New Stochastic Theory for Bridge Stability in Turbulent Flow", Journal of Engineering Mechanics, Vol. 119, No. 1, 1993, pp. 113-127.

Lin Y.K. and Prussing J.E., "Concepts of Stochastic Stability in Rotor Dynamics", Journal of the American Helicopter Society, Vol. 27, No. 2, 1982, pp. 73-74.

Liu, J.-K., and Zhao, L.-C., "Bifurcation Analysis of Airfoils in Incompressible Flow", Journal of Sound and Vibration, Vol. 154, No. 1, 1992, pp. 117-124.

Livne, E., "Integrated Aeroservoelasticity Optimization: Status and Direction", Journal of Aircraft, Vol. 36, No. 1, 1999, pp. 122-145.

Longtin, A., "Noise-Induced Transitions at a Hopf Bifurcation in a First-Order Delay-Differential Equation", Physical Review A, Vol. 44, No. 8, 1991, pp. 4801-4813.

Longtin, A., Milton, J.G., Bos, J.E., and Mackey, M.C., "Noise and Critical Behavior of the Pupil Light Reflex at Oscillation Onset", Physical Review A, Vol. 41, No. 12, 1990, pp. 6992-7005.

Lugiato, L.A., Broggi, G., Merri, M., and Pernigo, M.A., "Control of Noise by Noise and Applications to Optical Systems", *Noise in Nonlinear Dynamical Systems* (Edited by F. Moss and P.V.E. McClintock), Vol. 2, Cambridge University Press, Cambridge, 1989, pp. 293-346.

Lusebrink, H., and Sonder, R., "Gust Design Procedures", AGARD-AG-317 (Edited by Houbolt, J.), 1991, pp. 66-116.

Mackey, M.C., Longtin, A., and Lasota, A., "Noise-Induced Global Asymptotic Stability", Journal of Statistical Physics, Vol. 60, Nos. 5/6, 1990, pp. 735-751.

Mannella, R., "Computer Experiments in Non-Linear Stochastic Physics", *Noise in Nonlinear Dynamical Systems, Experiments and Simulations* (Edited by F. Moss and P.V.E. McClintock), Vol. 3, Cambridge University Press, Cambridge, 1989, pp. 189-221.

McClintock, P., and Moss, F., "Analogue Techniques for the Study of Problems in Stochastic Nonlinear Dynamics", *Noise in Nonlinear Dynamical Systems, Experiments and Simulations* (Edited by F. Moss and P.V.E. McClintock), Vol. 3, Cambridge University Press, Cambridge, 1989, pp. 243-274.

McLachlan, N., "Theory and Application of Mathieu Functions", Dover Publications, Inc., New York, 1964.

Mei, C., Abdel-Motagaly, K., and Chen, R., "Review of Nonlinear Panel Flutter at Supersonic and Hypersonic Speeds", Paper Presented at the CEAS/AIAA/ICASE/NASA LaRC International Forum on Aeroelasticity and Structural Dynamics, Williamsburg, VA., June 22-25, 1999.

Meijer, J., and Cunningham, Jr., A., "Development of a Method to Predict Transonic Limit Cycle Oscillation Characteristics of Fighter Aircraft", AGARD-CP-507, 1992, pp. 23-1 - 23-21.

Millonas, M., "Fluctuations and Order; The New Synthesis", Springer-Verlag, New York, 1996.

Mitchell R.R. and Kozin F., "Sample Stability of Second Order Linear Differential Equations with Wide Band Noise Coefficients", SIAM J. Appl. Math., Vol. 27, No.4, December 1974, pp. 571-605.

Nayfeh, A., and Mook, D., "Nonlinear Oscillations", John Wiley & Sons, New York, 1979.

Newland, D.E., "An Introduction to Random Vibrations and Spectral Analysis", Longman Group Ltd., London, 1975.

Nicolis, C., "Stochastic Aspects of Climatic Transitions - Response to Periodic Forcing", Tellus, Vol. 34, 1982, pp. 1-9.

Nicolis, C., and Nicolis, G., "Normal Form Analysis of Stochastically Forced Dynamical Systems", Dynamics and Stability of Systems, Vol. 1, No. 3, 1986, pp. 249-253.

Peterson, L.D., and Crawley, E.F., "Improved Exponential Time Series Approximation of Unsteady Aerodynamic Operators", Journal of Aircraft, Vol. 25, No. 2, 1988, pp. 121-127.

Poirel, D., and Landry, N., "DND Flutter Clearance Methodology - The CF-18/480 USG EFT Category II Experience", CASI 40th Annual Conference, Toronto, May, 1993.

Poirel, D., and Price, S.J., "A Numerical Investigation of the Stability and Post-Flutter Response of a 2D Nonlinear Airfoil in Longitudinal Atmospheric Turbulence", AIAA 37th Structures, Structural Dynamics and Materials Conference, AIAA-96-1341-CP, 1996, pp. 204-214.

Poirel, D., and Price, S.J., "Post-Instability Behavior of a Structurally Nonlinear Airfoil in Longitudinal Turbulence", Journal of Aircraft, Vol. 34, No. 5, pp. 619-626.

Poirel, D., and Price, S.J., "Dynamic Behavior of a Structurally Nonlinear Airfoil in Atmospheric Turbulence", AIAA 40th Structures, Structural Dynamics and Materials Conference, AIAA-99-1473-CP, 1999.

Poirel, D., and Price, S.J., "Structurally Nonlinear Fluttering Airfoil in Turbulent Flow", AIAA Journal (*submitted for publication*).

Pratt, K., and Walker, W., "A Revised Gust-Load Formula and a Re-Evaluated of V-G Data Taken on Civil Transport Airplanes From 1933 to 1950", NACA Rep. 1206, 1954.

Press, W.H., Flannery, B.P., Teukolsky, S.A. and Vetterling, W.T., "Numerical Recipes in Fortran 77: The Art of Scientific Computing", Cambridge University Press, Cambridge, 1986.

Price, S.J. Alighanbari, H., and Lee, B.H.K., "The Aeroelastic Response of a Two-Dimensional Airfoil With Bilinear and Cubic Structural Nonlinearities", Journal of Fluids and Structures, Vol. 9, 1995, pp. 175-193.

Prussing J.E., "Stabilization of an Unstable Linear System by Parametric White Noise", Journal of Applied Mechanics, Vol. 48, brief notes, March 1981, pp. 198-199.

Prussing, J.E., and Lin, Y.K., "Rotor Blade Flap-Lag Stability in Turbulent Flows", Journal of the American Helicopter Society, Vol. 27, No. 2, 1982, pp. 51-57.

Prussing, J.E., and Lin, Y.K., "A Closed-Form Analysis of Rotor Blade Flap-Lag Stability in Hover and Low-Speed Flight in Turbulent Flow", Journal of the American Helicopter Society, Vol. 28, No. 3, 1983, pp. 42-46.

Pugachev, S., and Sinitsyn, I., "Stochastic Differential Systems; Analysis and Filtering", John Wiley & Sons, Ltd., Chichester, 1987.

Romberg, O., and Popp, K., "The Influence of Upstream Turbulence on the Stability Boundaries of a flexible Tube in a Bundle", Journal of Fluids and Structures, Vol. 12, 1998, pp. 153-169.

Roy, R.V., and Spanos, P.D., "Power Spectral Density of Nonlinear System Response: The Recursion Method, Transactions of the ASME, Vol. 60., 1993, pp. 358-365.

Sancho, J.M., San Miguel, M., Katz, S.L. and Gunton, J.D., "Analytical and Numerical Studies of Multiplicative Noise", Physical Review A, Vol. 26, No. 3, 1982, pp. 1589-1609.

Saucray, J., Artigues, C., Squeglia, G., and Guillot, J., "International Standardisation of Regulations for Gust Loading Calculations", Aeronautical Journal, 1991, pp. 370-378.

Schenk-Hoppé, K.R., "The Stochastic Duffing-van der Pol Equation", PhD thesis, Institut für Dynamische System, Universität Bremen, 1996.

Schenk-Hoppé, K.R., "Bifurcation Scenarios of the Noisy Duffing-van der Pol Oscillator", Nonlinear Dynamics, Vol. 11, 1996, pp. 255-274.

Schimansky-Geier, L., Tolstopjatenko, A.V., and Ebeling, W., "Noise Induced Transitions Due to External Additive Noise", Physics Letters, Vol. 108A, No. 7, 1985, pp. 329-332.

Schreiber, T., "Interdisciplinary Application of Nonlinear Time Series Methods", Physics Reports, Vol. 308, 1999, pp. 1-64.

Sears, W.R., "Operational Methods in the Theory of Airfoils in Non-Uniform Motion", Journal of the Franklin Institute, Vol. 230, 1940, pp. 95-111.

Sigeti, D., and Horsthemke, W., "Pseudo-Regular Oscillations Induced by External Noise", Journal of Statistical Physics, Vol. 54, Nos. 5/6, 1989, pp. 1217-1222.

Silchenko, A., Kapitaniak, T., and Anishchenko, V., "Noise-Enhanced Phase Locking in a Stochastic Bistable System Driven by a Chaotic Signal", Physical Review E, Vol. 59, No. 2, 1999, pp. 1593-1599.

Spicic, S.R., and Morino, L., "Dynamic Behavior of Fluttering Two-Dimensional Panels on an Airplane in Pull-Up Maneuver", AIAA Journal, Vol. 29, No. 8, 1991, pp. 1304-1312.

Sri Namachchivaya, N., "Hopf Bifurcation in the Presense of Both Parametric and External Stochastic Excitations", Journal of Applied Mechanics, Vol. 55, 1988, pp. 923-930.

Sri Namachchivaya, N., and Doyle, M., "Stochastic Dynamics", Nonlinearity and Chaos in Engineering Dynamics (Edited by Thompson, J. and Bishop, S.), John Wiley & Sons, Ltd., Chichester, 1994.

Sri Namachchivaya, N. and Liang, Y., "P-Bifurcations in the Stochastic Version of the Duffing-van der Pol Equation", ZAMM, Vol. 76, 1996, pp. 231-234.

Sri Namachchivaya, N., and Van Roessel, H.J., "Maximal Lyapunov Exponent and Rotation Numbers for Two Coupled Oscillators Driven by Real Noise", Journal of Statistical Physics, Vol. 71, Nos 3/4, 1993, pp. 549-567.

Stocks, N.G., Mannella, R., and McClintock, P.V.E., "Effect of External Fluctuations on the Fréedericksz Transition in an Analogue Simulator", Journal of Statistical Physics, Vol. 54, Nos. 5/6, 1989, pp. 1383-1396.

Tang, D.M., and Dowell, E.H., "Response of a Nonrotating Rotor Blade to Lateral Turbulence Part I: Theory", Journal of Aircraft, Vol. 32, No. 1, 1995, pp. 145-153.

Theodorsen, T., "General Theory of Aerodynamic Instability and the Mechanism of Flutter", NACA Rept. No. 496, 1935, pp. 413-433.

Trame, L., Williams, L., and Yurkovich, R., "Active Aeroelastic Oscillation Control on the F/A-18 Aircraft", AIAA-85-1858-CP, 1985, pp. 94-104.

Vaicaitis, R., Dowell, E.H., and Ventres, C.S., "Nonlinear Panel Response by a Monte Carlo Approach", AIAA Journal, Vol. 12, No. 5, 1974, pp. 685-691.

van der Wall, B.G., "The Influence of Variable Flow Velocity on Unsteady Airfoil Behavior", UM-AERO 91-46, M.S. Thesis, University of Maryland, College Park, 1991. Also available as DLR-FB 92-22.

van der Wall, B.G., and Leishman, J.G., "On the Influence of Time-Varying Flow Velocity on Unsteady Aerodynamics", Journal of the American Helicopter Society, Vol. 39, No. 4, 1994, pp. 25-36.

Von Kármán, T. and Sears, W.R., "Airfoil Theory for Non-Uniform Motion", Journal of the Aeronautical Sciences, Vol. 5, No. 10, 1938, pp. 379-390.

Wagner, H., "Uber die Entstehung des Dynamischen Auftriebs von Tragflugeln", Zeitschrift für Angewandte Mathematik and Mechanik, Bd. 5, Heft 1, 1925, pp. 17-35.

Wedig, W., "Lyapunov Exponents and Invariant Measures of Equilibria and Limit Cycles", Proceedings of a Conference on Lyapunov Exponents, Lecture Notes in Mathematics, Springer-Verlag, Vol. 1486, Berlin, 1991, pp. 309-321.

Weisenfeld, K., "Noisy precursors of Nonlinear Instabilities", Journal of Statistical Physics, Vol. 38, No. 5/6, 1985, pp. 1071-1097.

White, F.M., "Viscous Fluid Flow", McGraw-Hill Book, Inc., New York, 1974.

Wolf, A., Swift, J., Swinney, H., and Vastano, J., "Determining Lyapunov Exponents From a Time Series", Physica 16D, 1985, pp. 285-317.

Woolston, D.S., Runyan, H.L., and Andrews, R.E., "An Investigation of Effects of Certain Types of Structural Nonlinearities on Wing and Control Surface Flutter.", Journal of the Aeronautical Sciences, 1957, pp. 57-63.

Xie, W.-C., "Lyapunov Exponents and their Applications in Structural Dynamics", PhD Thesis, University of Waterloo, Waterloo, Ontario, Canada, 1990.

Yoon, Y., and Ibrahim, R., "Parametric Random Excitation of Nonlinear Coupled Oscillators", Nonlinear Dynamics, Vol. 8, 1995, pp. 385-413.

APPENDIX A -
TRANSFORMATION OF INTEGRO-DIFFERENTIAL EQUATIONS INTO DIFFERENTIAL EQUATIONS

We start with the circulatory portion of the lift, or moment, relations due to arbitrary motion of the airfoil and longitudinal turbulence shown as expression (A.1), and similarly due to vertical turbulence shown as expression (A.2). These two expressions are obtained directly from equation (2.23).

$$\left[w^{\bullet}_{3/4}(t)\,\varphi(0) - \int_0^t w^{\bullet}_{3/4}(s)\,\frac{d\,\varphi\,(t\text{-}s)}{ds}\,ds \right] \tag{A.1}$$

$$\left[w^{\bullet}_{\mathrm{T}}(t)\,\psi(0) - \int_0^t w^{\bullet}_{\mathrm{T}}(s)\,\frac{d\,\psi(t\text{-}s)}{ds}\,ds \right] \tag{A.2}$$

The only differences between the two are that expression (A.1) is expressed in terms of the downwash at the three-quarter chord point and Wagner's function, whereas as expression (A.2) is expressed in terms of the vertical turbulent velocity and Küssner's function. Otherwise, their form is the same, and we can consider the following expression to represent both:

$$\left[w^{\bullet}(t)\,\Theta(0) - \int_0^t w^{\bullet}(s)\,\frac{d\Theta\,(t\text{-}s)}{ds}\,ds \right] \tag{A.3}$$

$\Theta(t)$, which represents Wagner's or Küssner's function, is approximated by a two-state representation (see equation 2.4 and 2.12) as follows:

$$\Theta(t) = 1 - A\,e^{-at} - B\,e^{-bt} \tag{A.4}$$

Taking the derivative, and substituting it in expression (A.3) gives:

$$\frac{d\Theta(t-s)}{ds} = -Aa\,e^{-a(t-s)} - Bb\,e^{-b(t-s)} \tag{A.5}$$

$$\left[w^{\bullet}(t)\,\Theta(0) + \int_0^t w^{\bullet}(s)\,[Aa\,e^{-a(t-s)} + Bb\,e^{-b(t-s)}]\,ds \right] \tag{A.6}$$

We then take the Laplace transform of expression (A.6).

$$\mathcal{L}\left\{\left[w^{\bullet}(t)\,\Theta(0) + \int_0^t w^{\bullet}(s)\,[Aa\,e^{-a(t-s)} + Bb\,e^{-b(t-s)}]\,ds \right]\right\} = w^{\bullet}(\wp)\Theta(0) + Aa\frac{w^{\bullet}(\wp)}{\wp+a} + Bb\frac{w^{\bullet}(\wp)}{\wp+b}$$

$$= w^{\bullet}(\wp)\Theta(0) + \frac{\wp w^{\bullet}(\wp)(Aa+Bb) + w^{\bullet}(\wp)(A+B)ab}{(\wp+a)(\wp+b)} \tag{A.7}$$

Defining

$$z^{\bullet}(\wp) \equiv \frac{w^{\bullet}(\wp)}{(\wp+a)(\wp+b)} \tag{A.8}$$

and substituting $z^{\bullet}(\wp)$ into equation (A.7) gives:

$$\mathcal{L}\left\{\left[w^{\bullet}(t)\Theta(0) + \int_0^t w^{\bullet}(s)\,[Aa e^{-a(t-s)} + Bb e^{-b(t-s)}]\,ds \right]\right\} = w^{\bullet}(\wp)\Theta(0) + \wp z^{\bullet}(\wp)(Aa+Bb) + z^{\bullet}(\wp)(A+B)ab$$

Finally, we take the inverse Laplace transform (and putting $z^{\bullet}(t=0) = 0$ as is usually done since initial conditions have effectively no impact on the long term steady state behaviour), such that expression (A.6) becomes:

$$\left[w^*(t)\Theta(0) + \int_0^t w^*(s)[Aae^{-a(t-s)} + Bbe^{-b(t-s)}]ds \right] = \mathcal{L}^{-1}\left\{ w^*(s)\Theta(0) + s z^*(s)(Aa+Bb) + z^*(s)(A+B)ab \right\}$$

$$= w^*(t)\Theta(0) + \dot{z}^*(t)(Aa+Bb) + z^*(t)(A+B)ab \qquad \text{(A.9)}$$

where $z^*(t)$ and $\dot{z}^*(t)$ are the two new state variables which represent the two aerodynamic lag states in Wagner's or Küssner's function approximations. They are obtained from the inverse Laplace transform of equation (A.8) in this manner. Equation (A.8) is first re-arranged

$$z^*(s)(s+a)(s+b) = w^*(s)$$

$$z^*(s)(s^2 + s(a+b) + ab) = w^*(s)$$

$$\mathcal{L}^{-1}\left\{ z^*(s)(s^2 + s(a+b) + ab) = w^*(s) \right\}$$

and neglecting the initial conditions (i.e. $z^*(0) = 0$ and $\dot{z}^*(0) = 0$), we finally have the following differential equation that represents the aerodynamic lag states:

$$\ddot{z}^*(t) + \dot{z}^*(t)(a+b) + z^*(t)ab = w^*(t) \qquad \text{(A.10)}$$

With the proper variable substitution for a, b and $w^*(t)$, equation (A.10) becomes equation (2.26 a) for Wagner's lag states and equation (2.26 b) for Küssner's lag states. With similar variable substitution, equation (A.9) is substituted back into equations (2.23 a) and (2.23 b) to give equations (2.25 a) and (2.25 b).

APPENDIX B -
TRANSFORMATION OF TURBULENCE SPECTRUM INTO TIME DOMAIN

B.1 Dryden Vertical Turbulence

The Dryden vertical turbulent velocity PSD is given in equation (2.22 b)

$$\Phi_{VT}(\omega) = \sigma_T^{*2}\left(\frac{L^*}{\pi U^*_m}\right)\frac{1+3\,[L^*\,\omega\,/U^*_m]^2}{[1+[L^*\,\omega/U^*_m]^2]^2} \tag{2.22 b}$$

which can also be written as:

$$\Phi_{VT}(\omega) = |H(\omega)|^2\Phi_{WN} \tag{B.1}$$

where Φ_{WN} is the PSD of a Gaussian white noise of intensity, $\Phi_{WN} = 1.0$, and

$$|H(\omega)|^2 = \sigma_T^{*2}\left(\frac{L^*}{\pi U^*_m}\right)\frac{1+3\,[L^*\,\omega\,/U^*_m]^2}{[1+[L^*\,\omega/U^*_m]^2]^2} \tag{B.2}$$

$$|H(\omega)| = \sigma_T^{*}\left(\frac{L^*}{\pi U^*_m}\right)^{1/2}\frac{(1+3\,[L^*\,\omega\,/U^*_m]^2)^{1/2}}{[1+[L^*\,\omega/U^*_m]^2]} \tag{B.3}$$

We are looking for a transfer function, $H(\omega)$, which relates Gaussian white noise, G^*_{WN}, as an input and vertical turbulence, $w^*_T(\omega)$, as an output, thus satisfying equation (B.3). This is shown in equation (B.4).

$$w^{*}_{T}(\omega) = H(\omega)\, G^{*}_{WN} \tag{B.4}$$

Hoblit [1988] gives the following transfer function expressed in the Laplace domain:

$$H(s) = \sigma^{*}_{T}\left(\frac{L^{*}}{\pi U^{*}}\right)^{1/2} \frac{1+\sqrt{3}\,[L^{*} s\;/U^{*}]}{[1+L^{*} s/U^{*}]^{2}} \tag{B.5}$$

Note that by using $s = i\omega$, we have verified that the norm, or modulus, of $H(s)$, i.e. $|H(i\omega)|$, satisfies equation (B.3). Also note that U^{*} becomes U^{*}_{m} for the more general problem when longitudinal turbulence is also considered.

The time domain vertical turbulent velocity is obtained by substituting equation (B.5) into the Laplace domain representation of equation (B.4), and then taking its inverse Laplace transform as follows:

$$w^{*}_{T}(s) = \sigma^{*}_{T}\left(\frac{L^{*}}{\pi U^{*}}\right)^{1/2} \frac{1+\sqrt{3}\,[L^{*} s\;/U^{*}]}{[1+L^{*} s/U^{*}]^{2}} G^{*}_{WN}(s) \tag{B.6}$$

$$w^{*}_{T}(s)\,[1+L^{*} s/U^{*}_{m}]^{2} = \sigma^{*}_{T}\left(\frac{L^{*}}{\pi U^{*}_{m}}\right)^{1/2} (1+\sqrt{3}\,[L^{*} s\;/U^{*}_{m}])G^{*}_{WN}$$

$$w^{*}_{T}(s)\,(1+2L^{*} s/U^{*}_{m}+[L^{*} s/U^{*}_{m}]^{2}) = \sigma^{*}_{T}\left(\frac{L^{*}}{\pi U^{*}_{m}}\right)^{1/2} (1+\sqrt{3}\,[L^{*} s\;/U^{*}U^{*}_{m}])G^{*}_{WN}$$

$$w^{*}_{T}(s)+s w^{*}_{T}(s)2L^{*}/U^{*}_{m}+[s w^{*}_{T}(s)]^{2}[L^{*}/U^{*}_{m}]^{2} = \sigma^{*}_{T}\left(\frac{L^{*}}{\pi U^{*}_{m}}\right)^{1/2} (G^{*}_{WN}(s)+sG^{*}_{WN}(s)\sqrt{3}L^{*}\;/U^{*}_{m}) \tag{B.7}$$

We take the inverse Laplace transform equation (B.7), assuming all initial conditions to be zero.

$$\ddot{w}^*_{\mathrm{T}}(t)+\dot{w}^*_{\mathrm{T}}(t)2L^*/U^*_{\mathrm{m}}+w^*_{\mathrm{T}}(t)[L^*/U^*_{\mathrm{m}}]^2 = \sigma^*_{\mathrm{T}}\left(\frac{L^*}{\pi U^*_{\mathrm{m}}}\right)^{1/2}(G^*_{\mathrm{WN}}(t)+\dot{G}^*_{\mathrm{WN}}(t)\sqrt{3}L^*/U^*_{\mathrm{m}}) \quad \text{(B.8)}$$

Finally, re-arranging equation (B.8) gives:

$$\ddot{w}^*_{\mathrm{T}}(t)+\dot{w}^*_{\mathrm{T}}(t)2U^*_{\mathrm{m}}/L^*+w^*_{\mathrm{T}}(t)[U^*_{\mathrm{m}}/L^*]^2 = \sigma^*_{\mathrm{T}}\left(\frac{U^{*3}_{\mathrm{m}}}{\pi L^{*3}}\right)^{1/2}G^*_{\mathrm{WN}}(t)+\sigma^*_{\mathrm{T}}\left(\frac{3U^*_{\mathrm{m}}}{\pi L^*}\right)^{1/2}\dot{G}^*_{\mathrm{WN}}(t) \quad \text{(B.9)}$$

By definition, since white noise is nowhere continuous, it is not differentiable [Horsthemke and Lefever, 1984]. Accordingly, equation (B.9) is integrated once before it is numerically modelled. The final expression is equation (2.24 b) reproduced below.

$$\dot{w}^*_{\mathrm{T}}+w^*_{\mathrm{T}}\frac{2U^*_{\mathrm{m}}}{L^*}=-\frac{U^{*2}_{\mathrm{m}}}{L^{*2}}\int_0^t w^*_{\mathrm{T}}dt+\sigma^*_{\mathrm{T}}\left(\frac{U^{*3}_{\mathrm{m}}}{\pi L^{*3}}\right)^{1/2}\int_0^t G^*_{\mathrm{WN}}dt+\sigma^*_{\mathrm{T}}\left(\frac{3U^*_{\mathrm{m}}}{\pi L^*}\right)^{1/2}G^*_{\mathrm{WN}} \quad \text{(2.24 b)}$$

B.2 Dryden Longitudinal Turbulence

The same process is followed for the longitudinal component of the Dryden turbulence model, except that Hoblit [1988] does not give a transfer function. Based on the form of the transfer function for vertical turbulence, we have tried different expressions for longitudinal turbulence and found the following appropriate function:

$$H(s) = \sigma^*_{\mathrm{T}}\left(\frac{2L^*}{\pi U^*_{\mathrm{m}}}\right)^{1/2}\frac{1}{1+L^*s/U^*_{\mathrm{m}}} \quad \text{(B.10)}$$

The squared modulus of $H(s)$ must satisfies the longitudinal turbulence PSD (divided by Φ_{WN} = 1.0) given in equation (2.22 a). Accordingly, let $s = i\omega$ in equation (B.10):

$$H(i\,\omega) = \sigma^{*}_{T}\left(\frac{2L^{*}}{\pi U^{*}_{m}}\right)^{1/2}\frac{1}{1+L^{*}\,i\,\omega\,/\,U^{*}_{m}}$$

$$H(\omega) = \sigma^{*}_{T}\left(\frac{2L^{*}}{\pi U^{*}_{m}}\right)^{1/2}\frac{1}{1+L^{*}\,i\,\omega/\,U^{*}_{m}}\;\frac{1-L^{*}\,i\,\omega/\,U^{*}_{m}}{1-L^{*}\,i\,\omega/\,U^{*}_{m}}$$

$$|H(\omega)|^{2} = \sigma^{*2}_{T}\left(\frac{2L^{*}}{\pi U^{*}_{m}}\right)\left|\frac{1}{1+L^{*}\,i\,\omega/\,U^{*}_{m}}\;\frac{1-L^{*}\,i\,\omega/\,U^{*}_{m}}{1-L^{*}\,i\,\omega/\,U^{*}_{m}}\right|^{2}$$

After some algebra we get equation (B.11) which demonstrates that the transfer function, equation (B.10), satisfies the Dryden longitudinal turbulent velocity PSD in equation (2.22 a).

$$|H(\omega)|^{2} = \sigma^{*2}_{T}\left(\frac{2L^{*}}{\pi U^{*}_{m}}\right)\frac{1}{1+[\,L^{*}\;\omega/\;U^{*}_{m}\,]^{2}} = \frac{\Phi_{LT}}{\Phi_{WN}} \tag{B.11}$$

Note that Φ_{WN} = 1.0. The Laplace domain representation of longitudinal turbulence is given in equation (B.12).

$$u^{*}_{T}(s) = \sigma^{*}_{T}\left(\frac{2L^{*}}{\pi U^{*}_{m}}\right)^{1/2}\frac{1}{1+L^{*}\,s\,/\,U^{*}_{m}}\,G^{*}_{WN}(s) \tag{B.12}$$

From the inverse Laplace transform of equation (B.12), the time domain longitudinal turbulence is obtained, as shown in equation (2.24 a):

$$\dot{u}^{*}_{T} + u^{*}_{T}\frac{U^{*}_{m}}{L^{*}} = \sigma_{T}\left(\frac{2U^{*}_{m}}{\pi L^{*}}\right)^{1/2} G^{*}_{wn} \tag{2.24 a}$$

B.3 Narrow Band Parametric Excitation

In this case the transfer function, that relates Gaussian white noise to an excitation velocity whose PSD is given by equation (5.10), can be obtained from Yoon and Ibrahim [1995] and Newland [1975]. It is given in equation (B.13) in non-dimensional form, where here $s = ik$.

$$H(s) = \frac{\sigma_T (2\zeta r^3 / \pi)^{1/2}}{s^2 + 2\zeta r s + r^2} \tag{B.13}$$

Note that we have also verified that the modulus squared of the transfer function satisfies equation (5.10). After taking the inverse Laplace transform of $u(s) = H(s)\, G_{WN}(s)$, the time domain expression is as follows:

$$u'' + 2\zeta r\, u' + r^2 u = \sigma_T (2\zeta r^3 / \pi)^{1/2} G_{wn}(t) \tag{B.14}$$

APPENDIX C -
STATE SPACE MODEL
(VECTOR AND MATRIX) COEFFICIENTS

The coefficients of the vector and matrices in equation (3.1) are the following:

$$\{B(\tau)\} = \{0, 0, 0, 0, 0, 0, 0, w_T(\tau)/U_m\} \tag{C.1}$$

$$[A(\tau)] = \begin{bmatrix} 0 & 0 & 1 & 0 & 0 & 0 & 0 & 0 \\ 0 & 0 & 0 & 1 & 0 & 0 & 0 & 0 \\ \multicolumn{2}{c}{-[\mathrm{MSA}]^{-1}[\mathrm{KSA}]} & \multicolumn{2}{c}{-[\mathrm{MSA}]^{-1}[\mathrm{DSA}]} & \multicolumn{2}{c}{-[\mathrm{MSA}]^{-1}[\mathrm{KDW}]} & \multicolumn{2}{c}{-[\mathrm{MSA}]^{-1}[\mathrm{KDK}]} \\ 0 & 0 & 0 & 0 & 0 & 1 & 0 & 0 \\ \mathrm{unf} & 0 & (1/2-a_h) & 1 & -b_1 b_2 & -b_1-b_2 & 0 & 0 \\ 0 & 0 & 0 & 0 & 0 & 0 & 0 & 1 \\ 0 & 0 & 0 & 0 & 0 & 0 & -b_3 b_4 & -b_3-b_4 \end{bmatrix} \tag{C.2}$$

$$[A_3] = \begin{bmatrix} \multicolumn{2}{c}{-[\mathrm{MSA}]^{-1}\begin{bmatrix} k_3/U_m^2 & 0 \\ 0 & 0 \end{bmatrix}} & \begin{matrix} 0 & 0 & 0 & 0 & 0 & 0 \\ 0 & 0 & 0 & 0 & 0 & 0 \end{matrix} \\ 0 & 0 & 0 & 0 & 0 & 0 & 0 & 0 \\ 0 & 0 & 0 & 0 & 0 & 0 & 0 & 0 \\ 0 & 0 & 0 & 0 & 0 & 0 & 0 & 0 \\ 0 & 0 & 0 & 0 & 0 & 0 & 0 & 0 \\ 0 & 0 & 0 & 0 & 0 & 0 & 0 & 0 \\ 0 & 0 & 0 & 0 & 0 & 0 & 0 & 0 \end{bmatrix} \tag{C.3}$$

where

$$[\mathrm{MSA}] = \begin{bmatrix} 1 + \dfrac{a_h^2 + 1/8}{\mu r_\theta^2} & , & \dfrac{x_\theta}{r_\theta^2} - \dfrac{a_h}{\mu r_\theta^2} \\ x_\theta - \dfrac{a_h}{\mu} & , & 1 + \dfrac{1}{\mu} \end{bmatrix}$$

$$[\mathrm{KSA}\ ] = \begin{bmatrix} \dfrac{1}{U_m^2} + \dfrac{(1/2 - a_h)}{\mu r_\theta^2} - \dfrac{2(a_h + 1/2)\mathrm{unsf}\ \ \varphi(0)}{\mu r_\theta^2} & , & 0 \\ \dfrac{1}{\mu} + \dfrac{2\mathrm{unsf}\ \ \varphi(0)}{\mu} & , & \dfrac{\overline{\omega}^2}{U_m^2} \end{bmatrix}$$

$$[\mathrm{DSA}\ ] = \begin{bmatrix} \dfrac{2\zeta_\theta}{U_m} + \dfrac{\mathrm{unf}(1/2 - a_h)}{\mu r_\theta^2} - \dfrac{2(a_h + 1/2)(1/2 - a_h)\mathrm{unf}\,\varphi(0)}{\mu r_\theta^2} & , & -\dfrac{2(a_h + 1/2)\mathrm{unf}\,\varphi(0)}{\mu r_\theta^2} \\ \dfrac{\mathrm{unf}}{\mu} + \dfrac{2(1/2 - a_h)\mathrm{unf}\,\varphi(0)}{\mu} & , & \dfrac{2\zeta_h \overline{\omega}}{U_m} + \dfrac{2\mathrm{unf}\,\varphi(0)}{\mu} \end{bmatrix}$$

$$[\mathrm{KDW}] = \begin{bmatrix} -\dfrac{2(a_h + 1/2)b_1 b_2 \mathrm{unf}\,(A_1 + A_2)}{\mu r_\theta^2} & , & -\dfrac{2(a_h + 1/2)(A_1 b_1 + A_2 b_2)\mathrm{unf}}{\mu r_\theta^2} \\ \dfrac{2 b_1 b_2 \mathrm{unf}\,(A_1 + A_2)}{\mu} & , & \dfrac{2(A_1 b_1 + A_2 b_2)\mathrm{unf}}{\mu} \end{bmatrix}$$

$$[\mathrm{KDK}] = \begin{bmatrix} -\dfrac{2(a_h + 1/2)b_3 b_4 (A_3 + A_4)}{\mu r_\theta^2} & , & -\dfrac{2(a_h + 1/2)(A_3 b_3 + A_4 b_4)}{\mu r_\theta^2} \\ \dfrac{2 b_3 b_4 (A_3 + A_4)}{\mu} & , & \dfrac{2(A_3 b_3 + A_4 b_4)}{\mu} \end{bmatrix}$$

APPENDIX D -

RUNGE-KUTTA PROGRAM LISTING

```
c
c      BASIC PROGRAM; RUNGE-KUTTA (FOURTH-ORDER) ALGORITHM
c
c      THIS PROGRAM CALCULATES THE DYNAMIC BEHAVIOR OF AN
c      OSCILLATING AIRFOIL IN PITCH AND HEAVE AS A FUNCTION OF
c      AIRSPEED.
c
c      THE AERODYNAMIC IS UNSTEADY INCOMPRESSIBLE AND LINEAR (IE
c      TWO TERMS WAGNER FUNCTION). THE STRUCTURE HAS A
c      NONLINEAR TORSIONAL STIFFNESS DUFFING TYPE.
c
c      ALL PARAMETERS ARE NONDIMENSIONAL. HOWEVER, THE INPUT
c      AND OUTPUT OF THE PITCH ANGLE IS IN DEGREES.
c
c      THE INTEGRAL OF THE AERODYNAMIC CIRCULATORY TERMS HAS
c      BEEN MODIFIED TO NEW STATE VARIABLES. THE VAN DER WALL
c      MODELLING IS USED.
c
c      THE INTEGRAL OF THE KUSSNER GUST ENTRY FUNCTION HAS BEEN
c      MODIFIED TO NEW STATE VARIABLES. TWO TERMS ARE ALSO USED
c      FOR KUSSNER FUNCTION.
c
c      EIGHT STATES (IE STRUCTURAL AND AERODYNAMICS) ARE
c      CALCULATED SIMULTANEOUSLY USING AN EIGHT BY EIGHT MATRIX
c      A(τ), WHILE THE TURBULENCE STATE EQUATIONS ARE SOLVED ON
c      THEIR OWN AT EACH TIME STEP.
c
c      THE TWO TURBULENCE COMPONENTS RECEIVE RANDOM NUMBERS
c      FROM DIFFERENT RAN1NEW ROUTINES; HENCE ARE UNCORRELATED.
c      USES RAN1NEW.FOR, IE RAN1 FROM "Numerical Recipes", 2nd edition,page
c      271. THESE UNIFORMLY DISTRIBUTED RANDOM NUMBERS ARE THEN
c      TRANSFORMED INTO GAUSSIAN NUMBERS WITH THE BOX-MUELLER
c      ALGORITHM AND INTO WHITE NOISE. THE TWO WHITE NOISE
c      PROCESSES ARE FINALLY FED INTO NUMERICAL FILTERS THAT
c      REPRESENT THE VERTICAL AND LONGITUDINAL DRYDEN
c      TURBULENCE SPECTRA.
c
c      THE DATA CAN BE SAVED IN FILE "ana.in" FOR FURTHER ANALYIS.
c      THE FILE "info.in" CONTAINS THE VALUES OF THE PROGRAM
c      VARIABLES AND SYSTEM PARAMETERS WHICH DEFINE THE DATA.
c
```

```
c*************************************************************************
c
c   DEFINITION OF PROGRAM VARIABLES AND AEROELASTIC-TURBULENCE
c   SYSTEM PARAMETERS TYPES
c
      parameter (idim=8, idims=4, idimw=2, idimk=2, idimg=2)
      character*60 noise, component, ainfo
      real*8 x(idim), k1(idim), k2(idim), k3(idim), k4(idim),
     * mu, pi, ita, its, lw, ls, lg, ldg, lkwn, lwn, vwn,
     * msa(idims/2,idims/2), dsa(idims/2,idims/2), ksa(idims/2,idims/2),
     * mksa(idims/2,idims/2), mdsa(idims/2,idims/2), msadw(2), msakw(2),
     * a(idim,idim), an(idim,idim), kn(idims/2,idims/2), kalpha, ksigma,
     * mksan(idims/2,idims/2), kqw, dwn, sumvwn, sumvgint,
     * k1vg, k2vg, k3vg, k4vg, k1lg, k2lg, k3lg, k4lg,
     * kw(2), dw(2), k33, k31, k44, kk(2), dk(2), msadk(2), msakk(2)
c
c   INPUT AND DEFINITION OF PROGRAM VARIABLES
c
c     nmax = MAXIMUM NUMBER OF ITERATIONS
c     nrss = ITERATION AT STEADY STATE
c     um = AIRSPEED
c     a = ALPHA (PITCH)
c     s = SIGMA (HEAVE)
c     ap = d ALPHA/ dt
c     sp = d SIGMA/ dt
c     idum1, idum2, idum3, idum4 : SEEDS FOR RANDOM NUMBER GENERATOR
c
      pi=3.1415927
      dtr=pi/180.
      rtd=180./pi
      write (6,*)'What is maximum number of iterations, nmax=?'
      read  (6,*)nmax
      write (6,*)'What is the steady state response iteration, nrss?'
      read  (6,*)nrss
      write (6,*)'What is the airspeed, um?'
      read  (6,*)um
      write (6,*)'Of what state variable do you want info? a, s, ap
     * or sp?'
      read  (6,67)ainfo
      itna=1
      idum1=-2
      idum2=-3
      idum3=-4
      idum4=-5
      sumvwn=0.
      sumvgint=0.
```

```
      vwn=0.
      lwn=0.
      ldg=0.
      vdg=0.
c
c  INPUT OF AEROELASTIC-TURBULENCE SYSTEM PARAMETERS
c
c  A. STRUCTURAL PARAMETERS
c
c   xalpha = DISTANCE FROM EA TO CG DIVIDED BY SEMI-CHORD
c   ah = DISTANCE FROM EA TO MID-CHORD DIVIDED BY SEMI-CHORD
c   wbs = RADIAL FREQUENCY RATIO
c   ssigma = NONDIMENSIONAL DAMPING HEAVE COEFFICIENT
c   salpha = NONDIMENSIONAL DAMPING PITCH COEFFICIENT
c   balpha1 = NONDIMENSIONAL LINEAR STIFFNESS PITCH COEFFICIENT
c   balpha3 = NONDIMENSIONAL CUBIC STIFFNESS PITCH COEFFICIENT
c   ralpha = RADIUS OF GYRATION
c
      write (6,*)'What is the static unbalance, xalpha?'
      read  (6,*)xalpha
      write (6,*)'What is the distance between EA and C/2, ah?'
      read  (6,*)ah
      write (6,*)'What is the frequency ratio, wbs?'
      read  (6,*)wbs
      ralpha=.5
      ssigma=0.
      salpha=0.
      balpha1=1.
      write (6,*)'What is the non-linear stiffness parameter, balpha3?'
      read  (6,*)balpha3
c
c  B. AERODYNAMIC PARAMETERS
c
c   mu = AIRFOIL/MASS RATIO
c   lw, a1w, a2w, b1w, b2w : WAGNER FUNCTION COEFFICIENTS
c   a1k, a2k, b1k, b2k : KUSSNER FUNCTION COEFFICIENTS
c
      mu=100.
      lw=1.
      a1w=.165
      b1w=.0455
      a2w=.335
      b2w=.3
      a1k=.5792
      b1k=.1393
      a2k=.4208
```

```
      b2k=1.802
c
c   C. TURBULENCE PARAMETERS
c
c    no = NO TURBULENT EXCITATION
c    dg = DRYDEN GUST(TURBULENCE) EXCITATION
c    lg = LONGITUDINAL GUST
c    vg = VERTICAL GUST
c    bg = BOTH GUST COMPONENTS
c    ls = SCALE OF TURBULENCE
c    dgvar = DRYDEN GUST VARIANCE
c
      write (6,*)'What noise input do you want - no or dg?'
      read  (6,67)noise
   67 format(a2)
      if (noise.eq.'dg') then
        write (6,*)'What noise component do you want - lg, vg or bg?'
        read  (6,67)component
        write (6,*)'What is the scale of turbulence, ls?'
        read  (6,*)ls
        write (6,*)'What is the Dryden gust variance?'
        read  (6,*)dgvar
        spsd=1.
        lkwn=(dgvar*2./(pi*ls))**.5
        dwn=(dgvar/(pi*ls/3.))**.5
        kqw=(-1./ls**2)
        vkwn=(dgvar/(pi*ls**3))**.5
      end if
c
c   INPUT OF AEROELASTIC SYSTEM STATE INITIAL CONDITIONS, AT t=0, i=1
c
      write (6,*)'What is the initial alpha (in deg) ?'
      read  (6,*)alphado
      alphao=alphado*dtr
      x(1)=alphao
      write (6,*)'What is the initial alphap(in deg) ?'
      read  (6,*)alphapdo
      alphapo=alphapdo*dtr
      x(3)=alphapo
      write (6,*)'What is the initial sigma ?'
      read  (6,*)sigmao
      x(2)=sigmao
      write (6,*)'What is the initial sigmap ?'
      read  (6,*)sigmapo
      x(4)=sigmapo
      do 304 i=idims+1,idim
```

```
      x(i)=0.
 304 continue
c
c   CALCULATION AND INPUT OF TIME STEP
c
c    dtalpha = TIME STEP BASED ON NATURAL UNCOUPLED PITCH
c    AEROELASTIC MODE
c    dtsigma = TIME STEP BASED ON NATURAL UNCOUPLED HEAVE
c    AEROELASTIC MODE
c    dtdg = TIME STEP BASED ON DRYDEN GUST CORRELATION TIME
c    dt = CHOSEN TIME STEP
c
      kalpha=(((1./um**2)-2.*(ah+.5)*(lw-a1w-a2w)/(mu*ralpha**2))/
     *          (1.+(1./8.+ah**2)/(mu*ralpha**2)))**.5
      ksigma=(wbs/um)/(1.+1./mu)**.5
      talpha=2.*pi/kalpha
      tsigma=2.*pi/ksigma
      dtalpha=talpha/128.
      dtsigma=tsigma/128.
      dtdg=ls/50.
      write (6,*)'dtalpha =', dtalpha
      write (6,*)'dtsigma =', dtsigma
      write (6,*)'dtdg =', dtdg
      write (6,*)'What is dt?'
      read  (6,*)dt
c
c   DEFINITION OF OUTPUT VARIABLES
c
c    na = RATE AT WHICH DATA POINTS ARE SAMPLED FOR STORAGE. FOR
c    EXAMPLE
c    na = 1 MEANS THAT ALL DATA POINTS ARE STORED, OR na = 10 MEANS
c    THAT EVERY 10 DATA POINTS ARE STORED.
c    isana = ITERATION AT WHICH THE DATA STARTS TO BE STORED.
c    imana = ITERATION AT WHICH THE DATA STOPS TO BE STORED.
c
      open (9, file='info.in')
      write (6,*)'What is the sampling rate to save data, na?'
      read  (5,*)na
      write (6,*)'What is the first and last iter to be saved?'
      read  (5,*)isana, imana
      open (13, file='ana.in')
c
c   OUTPUT OF PROGRAM VARIABLES, SYSTEM PARAMETERS AND
c   STATE INITIAL CONDITIONS
c
      write (9,*)
```

```
      write (9,*)'The recorded state variable is ', ainfo
      write (9,29)nmax
   29 format('nmax=',i10)
      write (9,30)nrss
   30 format('nrss=',i7)
      write (9,37)ls
   37 format('ls=',f9.5)
      write (9,19)dgvar
   19 format('Dryden gust variance=', f6.3)
      write (9,38)ah
   38 format('ah=',f5.2)
      write (9,36)wbs
   36 format('wbs=',f7.4)
      write (9,56)ralpha
   56 format('ralpha=',f6.4)
      write (9,40)xalpha
   40 format('xalpha=',f6.4)
      write (9,41)salpha
   41 format('salpha=',f6.4)
      write (9,44)ssigma
   44 format('ssigma=',f6.4)
      write (9,43)balpha1
   43 format('balpha1=',f5.2)
      write (9,42)balpha3
   42 format('balpha3=',f9.2)
      write (9,46)mu
   46 format('mu=',f6.1)
      write (9,48)alphado
   48 format('alphado=',f7.3)
      write (9,49)alphapdo
   49 format('alphapdo=',f5.2)
      write (9,54)sigmao
   54 format('sigmao=',f7.3)
      write (9,55)sigmapo
   55 format('sigmapo=',f5.2)
      write (9,50)um
   50 format('um=',f6.2)
      write (9,*)'The time step is, dt =', dt
      write (9,*)'The noise component is ', component
      write (9,*)
      write (9,*)
      write (9,*)
c
c   AEROELASTIC SYSTEM MATRIX CALCULATION (TIME-INVARIANT PART)
c
      do 300 i=1,idim
```

```
      do 301 j=1,idim
      a(i,j)=0.
      an(i,j)=0.
301 continue
300 continue
      ita=-2.*(ah+.5)/(mu*ralpha**2)
      its=2./mu
      msa(1,1)=1.+((1./8.+ah**2)/(mu*ralpha**2))
      msa(1,2)=(xalpha/ralpha**2)-(ah/(mu*ralpha**2))
      msa(2,1)=xalpha-(ah/mu)
      msa(2,2)=1.+(1./mu)
      k33=b1w*b2w
      d33=b1w+b2w
      d31=-(.5-ah)
      d32=-1.
      k44=b1k*b2k
      d44=b1k+b2k
      kn(1,2)=0.
      kn(2,1)=0.
      kn(2,2)=0.
      ksa(1,2)=0.
      ih=idims/2
      deta=msa(1,1)*msa(2,2)-msa(1,2)*msa(2,1)
      tempmsa11=msa(1,1)
      msa(1,1)=msa(2,2)/deta
      msa(1,2)=-msa(1,2)/deta
      msa(2,1)=-msa(2,1)/deta
      msa(2,2)=tempmsa11/deta
      kn(1,1)=balpha3/um**2
      ksa(2,2)=(wbs/um)**2
      a(1,3)=1.
      a(2,4)=1.
      a(5,6)=1.
      a(6,3)=-d31
      a(6,4)=-d32
      a(6,5)=-k33
      a(6,6)=-d33
      a(7,8)=1.
      a(8,7)=-k44
      a(8,8)=-d44
c
c   ITERATION IN TIME OF EQUATIONS OF MOTION
c
      do 10 it=2, nmax
      t=dt*float(it-1)
c
```

```
c   CALCULATION OF WHITE NOISE AND DRYDEN TURBULENCE
c
     if (noise.eq.'no') then
        unf=1.
        unsf=1.
        vg=0.
     else if (noise.eq.'dg') then
        lg=ldg
        vg=vdg
        spsd=1.
        wnvar=spsd*pi/dt
        sumvgint=sumvgint+vdg
        vgint=sumvgint*dt
        sumvwn=sumvwn+vwn
        vwnint=sumvwn*dt
        b=vkwn*vwnint+dwn*vwn+kqw*vgint
        urn1=ran1(idum1)
        urn2=ran2(idum2)
        urn3=ran3(idum3)
        urn4=ran4(idum4)
        lwn=cos(2.*pi*urn1)*(-2.*log(urn2)*wnvar)**.5
        vwn=cos(2.*pi*urn3)*(-2.*log(urn4)*wnvar)**.5
        unf=1.+lg/um
        unsf=1.+(2.*lg/um)+(lg/um)**2
        if (component.eq.'vg') then
          unf=1.
          unsf=1.
        else if (component.eq.'lg') then
          vg=0.
        end if
     end if
c
c   AEROELASTIC SYSTEM MATRIX CALCULATION (TIME-VARYING PART)
c
     dsa(1,1)=(2.*salpha/um)+((.5-ah)*unf/(mu*ralpha**2))
    * -(2.*(.5+ah)*(.5-ah)*(lw-a1w-a2w)/(mu*ralpha**2))*unf
     dsa(1,2)=-2.*(.5+ah)*(lw-a1w-a2w)*unf/(mu*ralpha**2)
     dsa(2,1)=(1.*unf/mu)+(2.*(.5-ah)*(lw-a1w-a2w)*unf/mu)
     dsa(2,2)=(2.*ssigma*wbs/um)+(2.*(lw-a1w-a2w)*unf/mu)
     ksa(1,1)=-2.*(.5+ah)*(lw-a1w-a2w)*unsf/(mu*ralpha**2)
    *        +(balpha1/um**2)
     ksa(2,1)=2.*(lw-a1w-a2w)*unsf/mu
     dw(1)=ita*(a1w*b1w+a2w*b2w)*unf
     dw(2)=its*(a1w*b1w+a2w*b2w)*unf
     kw(1)=ita*b1w*b2w*.5*unf
     kw(2)=its*b1w*b2w*.5*unf
```

```
      k31=-unf
      dk(1)=ita*(a1k*b1k+a2k*b2k)
      dk(2)=its*(a1k*b1k+a2k*b2k)
      kk(1)=ita*b1k*b2k
      kk(2)=its*b1k*b2k
      msadk(1)=msa(1,1)*dk(1)+msa(1,2)*dk(2)
      msadk(2)=msa(2,1)*dk(1)+msa(2,2)*dk(2)
      msakk(1)=msa(1,1)*kk(1)+msa(1,2)*kk(2)
      msakk(2)=msa(2,1)*kk(1)+msa(2,2)*kk(2)
      mksa(1,1)=msa(1,1)*ksa(1,1)+msa(1,2)*ksa(2,1)
      mksa(1,2)=msa(1,1)*ksa(1,2)+msa(1,2)*ksa(2,2)
      mksa(2,1)=msa(2,1)*ksa(1,1)+msa(2,2)*ksa(2,1)
      mksa(2,2)=msa(2,1)*ksa(1,2)+msa(2,2)*ksa(2,2)
      mksan(1,1)=msa(1,1)*kn(1,1)+msa(1,2)*kn(2,1)
      mksan(1,2)=msa(1,1)*kn(1,2)+msa(1,2)*kn(2,2)
      mksan(2,1)=msa(2,1)*kn(1,1)+msa(2,2)*kn(2,1)
      mksan(2,2)=msa(2,1)*kn(1,2)+msa(2,2)*kn(2,2)
      mdsa(1,1)=msa(1,1)*dsa(1,1)+msa(1,2)*dsa(2,1)
      mdsa(1,2)=msa(1,1)*dsa(1,2)+msa(1,2)*dsa(2,2)
      mdsa(2,1)=msa(2,1)*dsa(1,1)+msa(2,2)*dsa(2,1)
      mdsa(2,2)=msa(2,1)*dsa(1,2)+msa(2,2)*dsa(2,2)
      msadw(1)=msa(1,1)*dw(1)+msa(1,2)*dw(2)
      msadw(2)=msa(2,1)*dw(1)+msa(2,2)*dw(2)
      msakw(1)=msa(1,1)*kw(1)+msa(1,2)*kw(2)
      msakw(2)=msa(2,1)*kw(1)+msa(2,2)*kw(2)
      do 302 i=1,idims/2
      do 303 j=1,idims/2
      a(i+idims/2,j)=-mksa(i,j)
      a(i+idims/2,j+idims/2)=-mdsa(i,j)
      an(i+idims/2,j)=-mksan(i,j)
303   continue
302   continue
      a(3,5)=-msakw(1)
      a(3,6)=-msadw(1)
      a(4,5)=-msakw(2)
      a(4,6)=-msadw(2)
      a(6,1)=-k31
      a(3,7)=-msakk(1)
      a(3,8)=-msadk(1)
      a(4,7)=-msakk(2)
      a(4,8)=-msadk(2)
c
c  RK SCHEME INTEGRATION
c
c         x1=alpha
c         x2=sigma
```

```
c           x3=alpha'
c           x4=sigma'
c           x5=Z1 (Wagner function)
c           x6=Z1'(Wagner function)
c           x7=Z2 (Kussner function)
c           x8=Z2'(Kussner function)
c           ldg=longitudinal Dryden gust
c           vdg=vertical Dryden gust
c
      do 320 i=1,idim
      k1(i)=0.
      do 330 j=1,idim
      k1(i)=a(i,j)*x(j)+an(i,j)*x(j)**3+k1(i)
330 continue
320 continue
      do 340 i=1,idim
      k2(i)=0.
      do 350 j=1,idim
      k2(i)=a(i,j)*(x(j)+k1(j)*dt/2.)
     *     +an(i,j)*(x(j)+k1(j)*dt/2.)**3+k2(i)
350 continue
340 continue
      do 360 i=1,idim
      k3(i)=0.
      do 370 j=1,idim
      k3(i)=a(i,j)*(x(j)+k2(j)*dt/2.)
     *     +an(i,j)*(x(j)+k2(j)*dt/2.)**3+k3(i)
370 continue
360 continue
      do 380 i=1,idim
      k4(i)=0.
      do 390 j=1,idim
      k4(i)=a(i,j)*(x(j)+k3(j)*dt)
     *     +an(i,j)*(x(j)+k3(j)*dt)**3+k4(i)
390 continue
380 continue
      do 400 i=1,idim
      x(i)=x(i)+(dt/6.)*(k1(i)+2.*k2(i)+2.*k3(i)+k4(i))
400 continue
      x(8)=x(8)+vg*dt/um
      if (noise.eq.'dg') then
         k1vg=(-2./ls)*vdg+b
         k2vg=(-2./ls)*(vdg+k1vg*dt/2.)+b
         k3vg=(-2./ls)*(vdg+k2vg*dt/2.)+b
         k4vg=(-2./ls)*(vdg+k3vg*dt)+b
         vdg=vdg+(dt/6.)*(k1vg+2.*k2vg+2.*k3vg+k4vg)
```

```
          k1lg=(-1./ls)*ldg+lwn*lkwn
          k2lg=(-1./ls)*(ldg+k1lg*dt/2.)+lwn*lkwn
          k3lg=(-1./ls)*(ldg+k2lg*dt/2.)+lwn*lkwn
          k4lg=(-1./ls)*(ldg+k3lg*dt)+lwn*lkwn
          ldg=ldg+(dt/6.)*(k1lg+2.*k2lg+2.*k3lg+k4lg)
       end if
c
c   OUTPUT OF AEROELASTIC SYSTEM STATE TIME HISTORIES
c
       if (ainfo.eq.'a') then
              sv=x(1)*rtd
       else if (ainfo.eq.'s') then
              sv=x(2)
       else if (ainfo.eq.'ap') then
              sv=x(3)*rtd
       else if (ainfo.eq.'sp') then
              sv=x(4)
       end if
       if (it.le.imana .and. it.ge.isana) then
          if (itna.eq.na) then
            write (13,*) t, sv
            itna=0
          end if
          itna=itna+1
       end if
c
c   RETURN FOR ITERATION
c
 10 continue
c
c   FILE CLOSURES AND PROGRAM TERMINATION
c
       close(9)
       close(13)
       stop
       end
c
c   RANDOM NUMBER GENERATORS
c
      FUNCTION RAN1(IDUM1)
      INTEGER IDUM1, IA, IM, IQ, IR, NTAB, NDIV
      REAL RAN1, AM, EPS, RNMX
      PARAMETER (IA=16807, IM=2147483647, AM=1./IM, IQ=127773, IR=2836,
     *NTAB=32, NDIV=1+(IM-1), EPS=1.2E-7, RNMX=1.-EPS)
      INTEGER J, K, IV(NTAB), IY
      SAVE IV, IY
```

```
      DATA IV/NTAB*0/, IY/0/
      IF (IDUM1.LT.0.OR.IY.EQ.0) THEN
         IDUM1=MAX(-IDUM1,1)
         DO 11 J=NTAB+8,1,-1
         K=IDUM1/IQ
         IDUM1=IA*(IDUM1-K*IQ)-IR*K
         IF (IDUM1.LT.0) IDUM1=IDUM1+IM
         IF (J.LE.NTAB) IV(J)=IDUM1
 11      CONTINUE
         IY=IV(1)
      ENDIF
      K=IDUM1/IQ
      IDUM1=IA*(IDUM1-K*IQ)-IR*K
      IF (IDUM1.LT.0) IDUM1=IDUM1+IM
      J=1+IY/NDIV
      IY=IV(J)
      IV(J)=IDUM1
      RAN1=MIN(AM*IY,RNMX)
      RETURN
      END
c
      FUNCTION RAN2(IDUM2)
      INTEGER IDUM2, IA, IM, IQ, IR, NTAB, NDIV
      REAL RAN2, AM, EPS, RNMX
      PARAMETER (IA=16807, IM=2147483647, AM=1./IM, IQ=127773, IR=2836,
     *NTAB=32, NDIV=1+(IM-1), EPS=1.2E-7, RNMX=1.-EPS)
      INTEGER J, K, IV(NTAB), IY
      SAVE IV, IY
      DATA IV/NTAB*0/, IY/0/
      IF (IDUM2.LT.0.OR.IY.EQ.0) THEN
         IDUM2=MAX(-IDUM2,1)
         DO 11 J=NTAB+8,1,-1
         K=IDUM2/IQ
         IDUM2=IA*(IDUM2-K*IQ)-IR*K
         IF (IDUM2.LT.0) IDUM2=IDUM2+IM
         IF (J.LE.NTAB) IV(J)=IDUM2
 11      CONTINUE
         IY=IV(1)
      ENDIF
      K=IDUM2/IQ
      IDUM2=IA*(IDUM2-K*IQ)-IR*K
      IF (IDUM2.LT.0) IDUM2=IDUM2+IM
      J=1+IY/NDIV
      IY=IV(J)
      IV(J)=IDUM2
      RAN2=MIN(AM*IY,RNMX)
```

```
      RETURN
      END
c
      FUNCTION RAN3(IDUM3)
      INTEGER IDUM3, IA, IM, IQ, IR, NTAB, NDIV
      REAL RAN3, AM, EPS, RNMX
      PARAMETER (IA=16807, IM=2147483647, AM=1./IM, IQ=127773, IR=2836,
     *NTAB=32, NDIV=1+(IM-1), EPS=1.2E-7, RNMX=1.-EPS)
      INTEGER J, K, IV(NTAB), IY
      SAVE IV, IY
      DATA IV/NTAB*0/, IY/0/
      IF (IDUM3.LT.0.OR.IY.EQ.0) THEN
         IDUM3=MAX(-IDUM3,1)
         DO 11 J=NTAB+8,1,-1
         K=IDUM3/IQ
         IDUM3=IA*(IDUM3-K*IQ)-IR*K
         IF (IDUM3.LT.0) IDUM3=IDUM3+IM
         IF (J.LE.NTAB) IV(J)=IDUM3
11       CONTINUE
         IY=IV(1)
      ENDIF
      K=IDUM3/IQ
      IDUM3=IA*(IDUM3-K*IQ)-IR*K
      IF (IDUM3.LT.0) IDUM3=IDUM3+IM
      J=1+IY/NDIV
      IY=IV(J)
      IV(J)=IDUM3
      RAN3=MIN(AM*IY,RNMX)
      RETURN
      END
c
      FUNCTION RAN4(IDUM4)
      INTEGER IDUM4, IA, IM, IQ, IR, NTAB, NDIV
      REAL RAN4, AM, EPS, RNMX
      PARAMETER (IA=16807, IM=2147483647, AM=1./IM, IQ=127773, IR=2836,
     *NTAB=32, NDIV=1+(IM-1), EPS=1.2E-7, RNMX=1.-EPS)
      INTEGER J, K, IV(NTAB), IY
      SAVE IV, IY
      DATA IV/NTAB*0/, IY/0/
      IF (IDUM4.LT.0.OR.IY.EQ.0) THEN
         IDUM4=MAX(-IDUM4,1)
         DO 11 J=NTAB+8,1,-1
         K=IDUM4/IQ
         IDUM4=IA*(IDUM4-K*IQ)-IR*K
         IF (IDUM4.LT.0) IDUM4=IDUM4+IM
         IF (J.LE.NTAB) IV(J)=IDUM4
```

```
11    CONTINUE
        IY=IV(1)
      ENDIF
      K=IDUM4/IQ
      IDUM4=IA*(IDUM4-K*IQ)-IR*K
      IF (IDUM4.LT.0) IDUM4=IDUM4+IM
      J=1+IY/NDIV
      IY=IV(J)
      IV(J)=IDUM4
      RAN4=MIN(AM*IY,RNMX)
      RETURN
      END
```

APPENDIX E -

HOUBOLT PROGRAM LISTING

```
c
c                    BASIC PROGRAM; HOUBOLT ALGORITHM
c
c
c   THE ALGORITHM IS AN EIGHT-ORDER HOUBOLT FINITE DIFFERENCE,
c   EXCEPT FOR THE TURBULENCE EQUATIONS OF MOTION WHICH ARE
c   SOLVED USING A FOURTH-ORDER RUNGE-KUTTA.
c
c**********************************************************************
c
c  DEFINITION OF PROGRAM VARIABLES AND AEROELASTIC-GUST SYSTEM
c  PARAMETERS TYPES
c
      parameter (idim=8, idims=4, idimw=2, idimk=2, idimg=2)
      character*60 noise, component, ainfo
      real*8 x(3), p(3,3), pz2, xz2,
     * mu, pi, ita, its, lw, ls, lg, ldg,
     * msa(idims/2,idims/2), dsa(idims/2,idims/2), ksa(idims/2,idims/2),
     * kn, vwn, lwn, kqw, dwn, sumvwn, sumvgint,
     * lkwn, k1vg, k2vg, k3vg, k4vg, k1lg, k2lg, k3lg, k4lg,
     * kw(2), dw(2), k33, k31, k44, kk(2), dk(2)
c
c  INPUT AND DEFINITION OF PROGRAM VARIABLES
c
      pi=3.1415927
      dtr=pi/180.
      rtd=180./pi
      write (6,*) 'What is maximum number of iterations, nmax=?'
      read  (6,*) nmax
      write (6,*)'What is the steady state response iteration, nrss?'
      read  (6,*)nrss
      write (6,*)'What is the airspeed, um?'
      read  (6,*) um
      write (6,*)'Of what state variable do you want info? a, s, ap
     * or sp?'
      read  (6,67)ainfo
      itna=1
      idum1=-2
      idum2=-3
      idum3=-4
      idum4=-5
      sumvwn=0.
```

```
      sumvgint=0.
      vwn=0.
      lwn=0.
      ldg=0.
      vdg=0.
      N=3
      NP=3
      M=1
      MP=1
c
c   INPUT OF AEROELASTIC-TURBULENCE SYSTEM PARAMETERS
c
c   A. STRUCTURAL PARAMETERS
c
      write (6,*)'What is the static unbalance, xalpha?'
      read  (6,*)xalpha
      write (6,*)'What is the distance between EA and C/2, ah?'
      read  (6,*)ah
      write (6,*)'What is the frequency ratio, wbs?'
      read  (6,*)wbs
      ralpha=.5
      ssigma=0.
      salpha=0.
      balpha1=1.
      write (6,*)'What is the non linear stiffness parameter, balpha3?'
      read (6,*)balpha3
c
c   B. AERODYNAMIC PARAMETERS
c
      mu=100.
      lw=1.
      a1w=.165
      b1w=.0455
      a2w=.335
      b2w=.3
      a1k=.5792
      b1k=.1393
      a2k=.4208
      b2k=1.802
c
c   C. TURBULENCE PARAMETERS
c
      write (6,*)'What noise input do you want - no or dg?'
      read  (6,67)noise
   67 format(a2)
      if (noise.eq.'dg') then
```

```
          write (6,*)'What noise component do you want - lg, vg or bg?'
          read  (6,67) component
          write (6,*)'What is the scale of turbulence, ls?'
          read  (6,*)ls
          write (6,*)'What is the Dryden gust variance?'
          read  (6,*)dgvar
          spsd=1.
          lkwn=(dgvar*2./(pi*ls))**.5
          dwn=(dgvar/(pi*ls/3.))**.5
          kqw=(-1./ls**2)
          vkwn=(dgvar/(pi*ls**3))**.5
        end if
c
c  INPUT OF AEROELASTIC SYSTEM STATE INITIAL CONDITIONS, AT t=0, i=1
c
        write (6,*)'What is the initial alpha (in deg) ?'
        read  (6,*)alphado
        alphao=alphado*dtr
        alphai=alphao
        write (6,*)'What is the initial alphap(in deg) ?'
        read  (6,*)alphapdo
        alphapo=alphapdo*dtr
        alphapi=alphapo
        write (6,*)'What is the initial sigma ?'
        read  (6,*)sigmao
        sigmai=sigmao
        write (6,*)'What is the initial sigmap ?'
        read  (6,*)sigmapo
        sigmapi=sigmapo
        aeroi=0.
        z2=0.
c
c  CALCULATION AND INPUT OF TIME STEP
c
        kalpha=(((1./um**2)-2.*(ah+.5)*(lw-a1w-a2w)/(mu*ralpha**2))/
     *       (1.+(1./8.+ah**2)/(mu*ralpha**2)))**.5
        ksigma=(wbs/um)/(1.+1./mu)**.5
        talpha=2.*pi/kalpha
        tsigma=2.*pi/ksigma
        dtalpha=talpha/128.
        dtsigma=tsigma/128.
        dtdg=ls/50.
        write (6,*)'dtalpha =', dtalpha
        write (6,*)'dtsigma =', dtsigma
        write (6,*)'dtdg =', dtdg
        write (6,*)'What is dt?'
```

```
      read  (6,*)dt
c
c   DEFINITION OF OUTPUT VARIABLES
c
      open (9, file='info.in')
      write(6,*)'What is the sampling rate to save data, na?'
      read (5,*)na
          write(6,*)'What is the first and last iter to be saved?'
          read (5,*)isana, imana
      open (13, file='ana.in')
c
c   OUTPUT OF PROGRAM VARIABLES, SYSTEM PARAMETERS AND
c   STATE INITIAL CONDITIONS
c
      write (9,*)
      write (9,*)'The recorded state variable is ', ainfo
      write (9,29)nmax
 29 format('nmax=',i10)
      write (9,30)nrss
 30 format('nrss=',i7)
      write (9,37)ls
 37 format('ls=',f9.5)
      write (9,19)dgvar
 19 format('Dryden gust variance=', f6.3)
      write (9,38)ah
 38 format('ah=',f5.2)
      write (9,36)wbs
 36 format('wbs=',f7.4)
      write (9,56)ralpha
 56 format('ralpha=',f6.4)
      write (9,40)xalpha
 40 format('xalpha=',f6.4)
      write (9,41)salpha
 41 format('salpha=',f6.4)
      write (9,44)ssigma
 44 format('ssigma=',f6.4)
      write (9,43)balpha1
 43 format('balpha1=',f5.2)
      write (9,42)balpha3
 42 format('balpha3=',f9.2)
      write (9,46)mu
 46 format('mu=',f6.1)
      write (9,48)alphado
 48 format('alphado=',f7.3)
      write (9,49)alphapdo
 49 format('alphapdo=',f5.2)
```

```
      write (9,54)sigmao
   54 format('sigmao=',f7.3)
      write (9,55)sigmapo
   55 format('sigmapo=',f5.2)
      write (9,50)um
   50 format('um=',f6.2)
      write (9,*)'The time step is, dt =', dt
      write (9,*)'The noise component is ', component
      write (9,*)
      write (9,*)
      write (9,*)
c
c   AEROELASTIC SYSTEM MATRIX CALCULATION (TIME-INVARIANT PART)
c
      ita=-2.*(ah+.5)/(mu*ralpha**2)
      its=2./mu
      msa(1,1)=1.+((1./8.+ah**2)/(mu*ralpha**2))
      msa(1,2)=(xalpha/ralpha**2)-(ah/(mu*ralpha**2))
      msa(2,1)=xalpha-(ah/mu)
      msa(2,2)=1.+(1./mu)
      k33=b1w*b2w
      d33=b1w+b2w
      d31=-(.5-ah)
      d32=-1.
      k44=b1k*b2k
      d44=b1k+b2k
      ksa(1,2)=0.
      kn=balpha3/um**2
      ksa(2,2)=(wbs/um)**2
      ih=idims/2
      c3=1.
      c2=0.
      c1=0.
      b3=0.
      b2=msa(1,1)
      b1=msa(1,2)
      a3=0.
      a2=msa(2,1)
      a1=msa(2,2)
      c9=-k33
      c6=-d33
      c7=0.
      c5=-d31
      c4=-d32
      b7=-ksa(1,2)
      a7=-ksa(2,2)
```

```
c
c  ITERATION IN TIME OF EQUATIONS OF MOTION
c
      do 10 it=2, nmax
      t=dt*float(it-1)
c
c  CALCULATION OF WHITE NOISE AND DRYDEN TURBULENCE
EXCITATION
c
      if (noise.eq.'no') then
        unf=1.
        unsf=1.
        vg=0.
      else if (noise.eq.'dg') then
        lg=ldg
        vg=vdg
        spsd=1.
        wnvar=spsd*pi/dt
        sumvgint=sumvgint+vdg
        vgint=sumvgint*dt
        sumvwn=sumvwn+vwn
        wvgint=sumvwn*dt
        b=vkwn*wvgint+dwn*vwn+kqw*vgint
        urn1=ran1(idum1)
        urn2=ran2(idum2)
        urn3=ran3(idum3)
        urn4=ran4(idum4)
        lwn=cos(2.*pi*urn1)*(-2.*log(urn2)*wnvar)**.5
        vwn=cos(2.*pi*urn3)*(-2.*log(urn4)*wnvar)**.5
        unf=1.+lg/um
        unsf=1.+(2.*lg/um)+(lg/um)**2
        if (component.eq.'vg') then
          unf=1.
          unsf=1.
        else if (component.eq.'lg') then
          vg=0.
        end if
      end if
c
c  AEROELASTIC SYSTEM MATRIX CALCULATION (TIME-VARYING PART)
c
      dsa(1,1)=(2.*salpha/um)+((.5-ah)*unf/(mu*ralpha**2))
     * -(2.*(.5+ah)*(.5-ah)*(lw-a1w-a2w)/(mu*ralpha**2))*unf
      dsa(1,2)=-2.*(.5+ah)*(lw-a1w-a2w)*unf/(mu*ralpha**2)
      dsa(2,1)=(1.*unf/mu)+(2.*(.5-ah)*(lw-a1w-a2w)*unf/mu)
      dsa(2,2)=(2.*ssigma*wbs/um)+(2.*(lw-a1w-a2w)*unf/mu)
```

```
      ksa(1,1)=-2.*(.5+ah)*(lw-a1w-a2w)*unsf/(mu*ralpha**2)
     *      +(balpha1/um**2)
      ksa(2,1)=2.*(lw-a1w-a2w)*unsf/mu
      dw(1)=ita*(a1w*b1w+a2w*b2w)*unf
      dw(2)=its*(a1w*b1w+a2w*b2w)*unf
      kw(1)=ita*b1w*b2w*.5*unf
      kw(2)=its*b1w*b2w*.5*unf
      k31=-unf
      dk(1)=ita*(a1k*b1k+a2k*b2k)
      dk(2)=its*(a1k*b1k+a2k*b2k)
      kk(1)=ita*b1k*b2k
      kk(2)=its*b1k*b2k
      b5=-dsa(1,1)
      b4=-dsa(1,2)
      b6=-dw(1)
      a5=-dsa(2,1)
      a4=-dsa(2,2)
      a6=-dw(2)
      b8=-ksa(1,1)
      b9=-kw(1)
      a8=-ksa(2,1)
      a9=-kw(2)
      c8=-k31
      a11=-kk(2)
      b11=-kk(1)
      a10=-dk(2)
      b10=-dk(1)
c
c  AEROELASTIC SYSTEM INTEGRATION, HFD
c
      p(1,1)=2.*a1/dt**2-11.*a4/(6.*dt)-a7
      p(1,2)=2.*a2/dt**2-11.*a5/(6.*dt)-a8
      p(1,3)=2.*a3/dt**2-11.*a6/(6.*dt)-a9
      p(2,1)=2.*b1/dt**2-11.*b4/(6.*dt)-b7
      p(2,2)=2.*b2/dt**2-11.*b5/(6.*dt)-b8
      p(2,3)=2.*b3/dt**2-11.*b6/(6.*dt)-b9
      p(3,1)=2.*c1/dt**2-11.*c4/(6.*dt)-c7
      p(3,2)=2.*c2/dt**2-11.*c5/(6.*dt)-c8
      p(3,3)=2.*c3/dt**2-11.*c6/(6.*dt)-c9
      alphab=2.*alphai-alphaim1
      x(1)=sigmai*(5.*a1/dt**2-18.*a4/(6.*dt))
     *    +alphai*(5.*a2/dt**2-18.*a5/(6.*dt))
     *    +aeroi*(5.*a3/dt**2-18.*a6/(6.*dt))
     *    +sigmaim1*(-4.*a1/dt**2+9.*a4/(6.*dt))
     *    +alphaim1*(-4.*a2/dt**2+9.*a5/(6.*dt))
     *    +aeroim1*(-4.*a3/dt**2+9.*a6/(6.*dt))
```

```
*     +sigmaim2*(a1/dt**2-2.*a4/(6.*dt))
*     +alphaim2*(a2/dt**2-2.*a5/(6.*dt))
*     +aeroim2*(a3/dt**2-2.*a6/(6.*dt))
*     +z2*a11+a10*(11.*z2-18.*z2m1+9.*z2m2-2.*z2m3)/(6*dt)
      x(2)=sigmai*(5.*b1/dt**2-18.*b4/(6.*dt))
*     +alphai*(5.*b2/dt**2-18.*b5/(6.*dt))
*     +aeroi*(5.*b3/dt**2-18.*b6/(6.*dt))
*     +sigmaim1*(-4.*b1/dt**2+9.*b4/(6.*dt))
*     +alphaim1*(-4.*b2/dt**2+9.*b5/(6.*dt))
*     +aeroim1*(-4.*b3/dt**2+9.*b6/(6.*dt))
*     +sigmaim2*(b1/dt**2-2.*b4/(6.*dt))
*     +alphaim2*(b2/dt**2-2.*b5/(6.*dt))
*     +aeroim2*(b3/dt**2-2.*b6/(6.*dt))
*     -kn*alphab**3
*     +z2*b11+b10*(11.*z2-18.*z2m1+9.*z2m2-2.*z2m3)/(6*dt)
      x(3)=sigmai*(5.*c1/dt**2-18.*c4/(6.*dt))
*     +alphai*(5.*c2/dt**2-18.*c5/(6.*dt))
*     +aeroi*(5.*c3/dt**2-18.*c6/(6.*dt))
*     +sigmaim1*(-4.*c1/dt**2+9.*c4/(6.*dt))
*     +alphaim1*(-4.*c2/dt**2+9.*c5/(6.*dt))
*     +aeroim1*(-4.*c3/dt**2+9.*c6/(6.*dt))
*     +sigmaim2*(c1/dt**2-2.*c4/(6.*dt))
*     +alphaim2*(c2/dt**2-2.*c5/(6.*dt))
*     +aeroim2*(c3/dt**2-2.*c6/(6.*dt))
      call GAUSSJ(P,N,NP,X,M,MP)
      sigmaim3=sigmaim2
      alphaim3=alphaim2
      aeroim3=aeroim2
      sigmaim2=sigmaim1
      alphaim2=alphaim1
      aeroim2=aeroim1
      sigmaim1=sigmai
      alphaim1=alphai
      aeroim1=aeroi
      sigmai=x(1)
      alphai=x(2)
      aeroi=x(3)
      alphapi=(11.*alphai-18.*alphaim1+9.*alphaim2-2.*alphaim3)/(6.*dt)
      sigmapi=(11.*sigmai-18.*sigmaim1+9.*sigmaim2-2.*sigmaim3)/(6.*dt)
      pz2=2./dt**2+11.*d44/(6.*dt)+k44
      xz2=z2*(5./dt**2+18.*d44/(6.*dt))
*     +z2m1*(-4./dt**2-9.*d44/(6.*dt))
*     +z2m2*(1./dt**2+2.*d44/(6.*dt))
*     +vg/um
      z2m3=z2m2
      z2m2=z2m1
```

```
      z2m1=z2
      z2=xz2/pz2
c
c   TURBULENCE EQUATIONS INTEGRATION, RK
c
      if (noise.eq.'dg') then
        k1vg=(-2./ls)*vdg+b
        k2vg=(-2./ls)*(vdg+k1vg*dt/2.)+b
        k3vg=(-2./ls)*(vdg+k2vg*dt/2.)+b
        k4vg=(-2./ls)*(vdg+k3vg*dt)+b
        vdg=vdg+(dt/6.)*(k1vg+2.*k2vg+2.*k3vg+k4vg)
        k1lg=(-1./ls)*ldg+lwn*lkwn
        k2lg=(-1./ls)*(ldg+k1lg*dt/2.)+lwn*lkwn
        k3lg=(-1./ls)*(ldg+k2lg*dt/2.)+lwn*lkwn
        k4lg=(-1./ls)*(ldg+k3lg*dt)+lwn*lkwn
        ldg=ldg+(dt/6.)*(k1lg+2.*k2lg+2.*k3lg+k4lg)
      end if
c
c   OUTPUT OF AEROELASTIC SYSTEM STATE TIME HISTORIES
c
      if (ainfo.eq.'a') then
          sv=alphai*rtd
      else if (ainfo.eq.'s') then
          sv=sigmai
      else if (ainfo.eq.'ap') then
          sv=alphapi*rtd
      else if (ainfo.eq.'sp') then
          sv=sigmapi
      end if
      if (it.le.imana .and. it.ge.isana) then
        if (itna.eq.na) then
          write (13,*) t, sv
          itna=0
        end if
        itna=itna+1
      end if
c
c   RETURN FOR ITERATION
c
   10 continue
c
c   FILE CLOSURES AND PROGRAM TERMINATION
c
      close(9)
      close(13)
      stop
```

```
      end
c
c   RANDOM NUMBER GENERATORS
c
      FUNCTION RAN1(IDUM1)
      INTEGER IDUM1, IA, IM, IQ, IR, NTAB, NDIV
      REAL RAN1, AM, EPS, RNMX
      PARAMETER (IA=16807, IM=2147483647, AM=1./IM, IQ=127773, IR=2836,
     *NTAB=32, NDIV=1+(IM-1), EPS=1.2E-7, RNMX=1.-EPS)
      INTEGER J, K, IV(NTAB), IY
      SAVE IV, IY
      DATA IV/NTAB*0/, IY/0/
      IF (IDUM1.LT.0.OR.IY.EQ.0) THEN
         IDUM1=MAX(-IDUM1,1)
         DO 11 J=NTAB+8,1,-1
         K=IDUM1/IQ
         IDUM1=IA*(IDUM1-K*IQ)-IR*K
         IF (IDUM1.LT.0) IDUM1=IDUM1+IM
         IF (J.LE.NTAB) IV(J)=IDUM1
11       CONTINUE
         IY=IV(1)
      ENDIF
      K=IDUM1/IQ
      IDUM1=IA*(IDUM1-K*IQ)-IR*K
      IF (IDUM1.LT.0) IDUM1=IDUM1+IM
      J=1+IY/NDIV
      IY=IV(J)
      IV(J)=IDUM1
      RAN1=MIN(AM*IY,RNMX)
      RETURN
      END
c
      FUNCTION RAN2(IDUM2)
      INTEGER IDUM2, IA, IM, IQ, IR, NTAB, NDIV
      REAL RAN2, AM, EPS, RNMX
      PARAMETER (IA=16807, IM=2147483647, AM=1./IM, IQ=127773, IR=2836,
     *NTAB=32, NDIV=1+(IM-1), EPS=1.2E-7, RNMX=1.-EPS)
      INTEGER J, K, IV(NTAB), IY
      SAVE IV, IY
      DATA IV/NTAB*0/, IY/0/
      IF (IDUM2.LT.0.OR.IY.EQ.0) THEN
         IDUM2=MAX(-IDUM2,1)
         DO 11 J=NTAB+8,1,-1
         K=IDUM2/IQ
         IDUM2=IA*(IDUM2-K*IQ)-IR*K
         IF (IDUM2.LT.0) IDUM2=IDUM2+IM
```

```
         IF (J.LE.NTAB) IV(J)=IDUM2
 11      CONTINUE
         IY=IV(1)
      ENDIF
      K=IDUM2/IQ
      IDUM2=IA*(IDUM2-K*IQ)-IR*K
      IF (IDUM2.LT.0) IDUM2=IDUM2+IM
      J=1+IY/NDIV
      IY=IV(J)
      IV(J)=IDUM2
      RAN2=MIN(AM*IY,RNMX)
      RETURN
      END
c
      FUNCTION RAN3(IDUM3)
      INTEGER IDUM3, IA, IM, IQ, IR, NTAB, NDIV
      REAL RAN3, AM, EPS, RNMX
      PARAMETER (IA=16807, IM=2147483647, AM=1./IM, IQ=127773, IR=2836,
     *NTAB=32, NDIV=1+(IM-1), EPS=1.2E-7, RNMX=1.-EPS)
      INTEGER J, K, IV(NTAB), IY
      SAVE IV, IY
      DATA IV/NTAB*0/, IY/0/
      IF (IDUM3.LT.0.OR.IY.EQ.0) THEN
         IDUM3=MAX(-IDUM3,1)
         DO 11 J=NTAB+8,1,-1
         K=IDUM3/IQ
         IDUM3=IA*(IDUM3-K*IQ)-IR*K
         IF (IDUM3.LT.0) IDUM3=IDUM3+IM
         IF (J.LE.NTAB) IV(J)=IDUM3
 11      CONTINUE
         IY=IV(1)
      ENDIF
      K=IDUM3/IQ
      IDUM3=IA*(IDUM3-K*IQ)-IR*K
      IF (IDUM3.LT.0) IDUM3=IDUM3+IM
      J=1+IY/NDIV
      IY=IV(J)
      IV(J)=IDUM3
      RAN3=MIN(AM*IY,RNMX)
      RETURN
      END
c
      FUNCTION RAN4(IDUM4)
      INTEGER IDUM4, IA, IM, IQ, IR, NTAB, NDIV
      REAL RAN4, AM, EPS, RNMX
      PARAMETER (IA=16807, IM=2147483647, AM=1./IM, IQ=127773, IR=2836,
```

```
     *NTAB=32, NDIV=1+(IM-1), EPS=1.2E-7, RNMX=1.-EPS)
      INTEGER J, K, IV(NTAB), IY
      SAVE IV, IY
      DATA IV/NTAB*0/, IY/0/
      IF (IDUM4.LT.0.OR.IY.EQ.0) THEN
         IDUM4=MAX(-IDUM4,1)
         DO 11 J=NTAB+8,1,-1
         K=IDUM4/IQ
         IDUM4=IA*(IDUM4-K*IQ)-IR*K
         IF (IDUM4.LT.0) IDUM4=IDUM4+IM
         IF (J.LE.NTAB) IV(J)=IDUM4
11       CONTINUE
         IY=IV(1)
      ENDIF
      K=IDUM4/IQ
      IDUM4=IA*(IDUM4-K*IQ)-IR*K
      IF (IDUM4.LT.0) IDUM4=IDUM4+IM
      J=1+IY/NDIV
      IY=IV(J)
      IV(J)=IDUM4
      RAN4=MIN(AM*IY,RNMX)
      RETURN
      END
c
      SUBROUTINE GAUSSJ(A,N,NP,B,M,MP)
      PARAMETER (NMAX=50)
      REAL*8 A(NP,NP),B(NP,MP)
      DIMENSION IPIV(NMAX),INDXR(NMAX),INDXC(NMAX)
      DO 11 J=1,N
      IPIV(J)=0
11    CONTINUE
      DO 22 I=1,N
       BIG=0.
       DO 13 J=1,N
        IF(IPIV(J).NE.1)THEN
         DO 12 K=1,N
          IF (IPIV(K).EQ.0) THEN
           IF (ABS(A(J,K)).GE.BIG)THEN
            BIG=ABS(A(J,K))
            IROW=J
            ICOL=K
           ENDIF
          ELSE IF (IPIV(K).GT.1) THEN
           PAUSE 'Singular matrix'
          ENDIF
12        CONTINUE
```

```
      ENDIF
13    CONTINUE
      IPIV(ICOL)=IPIV(ICOL)+1
      IF (IROW.NE.ICOL) THEN
       DO 14 L=1,N
        DUM=A(IROW,L)
        A(IROW,L)=A(ICOL,L)
        A(ICOL,L)=DUM
14      CONTINUE
       DO 15 L=1,M
        DUM=B(IROW,L)
        B(IROW,L)=B(ICOL,L)
        B(ICOL,L)=DUM
15      CONTINUE
      ENDIF
      INDXR(I)=IROW
      INDXC(I)=ICOL
      IF (A(ICOL,ICOL).EQ.0.) PAUSE 'Singular matrix.'
      PIVINV=1./A(ICOL,ICOL)
      A(ICOL,ICOL)=1.
      DO 16 L=1,N
       A(ICOL,L)=A(ICOL,L)*PIVINV
16     CONTINUE
      DO 17 L=1,M
       B(ICOL,L)=B(ICOL,L)*PIVINV
17     CONTINUE
      DO 21 LL=1,N
       IF(LL.NE.ICOL)THEN
        DUM=A(LL,ICOL)
        A(LL,ICOL)=0.
        DO 18 L=1,N
         A(LL,L)=A(LL,L)-A(ICOL,L)*DUM
18       CONTINUE
        DO 19 L=1,M
         B(LL,L)=B(LL,L)-B(ICOL,L)*DUM
19       CONTINUE
       ENDIF
21     CONTINUE
22    CONTINUE
     DO 24 L=N,1,-1
      IF(INDXR(L).NE.INDXC(L))THEN
       DO 23 K=1,N
        DUM=A(K,INDXR(L))
        A(K,INDXR(L))=A(K,INDXC(L))
        A(K,INDXC(L))=DUM
23      CONTINUE
```

```
      ENDIF
24    CONTINUE
      RETURN
      END
```

APPENDIX F -
TRANSFER FUNCTION RELATING VERTICAL TURBULENCE TO PITCH AND HEAVE MOTION

We start with equations (2.23), without the nonlinearity nor longitudinal turbulence, which are then transformed in the Laplace domain and non-dimensionalised. This is given in equation (F.1).

$$[G(s)]\begin{Bmatrix}\theta\\ \xi\end{Bmatrix}=\begin{Bmatrix}\dfrac{2(a_h+1/2)}{\mu r_\theta^2}\left(\dfrac{A_3b_3}{s+b_3}+\dfrac{A_4b_4}{s+b_4}\right)\\ \dfrac{-2}{\mu}\left(\dfrac{A_3b_3}{s+b_3}+\dfrac{A_4b_4}{s+b_4}\right)\end{Bmatrix}\frac{w_T(s)}{U} \tag{F.1}$$

where

$$\begin{aligned}G_{11}(s)&=\left(1+\frac{a_h^2+1/8}{\mu r_\theta^2}\right)s^2\\&+\left(\frac{2\zeta_\theta}{U}+\frac{(1/2-a_h)}{\mu r_\theta^2}-\frac{2(a_h+1/2)(1/2-a_h)\,\varphi(0)}{\mu r_\theta^2}-\frac{2(a_h+1/2)(1/2-a_h)}{\mu r_\theta^2}\left(\frac{A_1b_1}{s+b_1}+\frac{A_2b_2}{s+b_2}\right)\right)s\\&+\left(\frac{1}{U^2}-\frac{2(a_h+1/2)\,\varphi(0)}{\mu r_\theta^2}-\frac{2(a_h+1/2)}{\mu r_\theta^2}\left(\frac{A_1b_1}{s+b_1}+\frac{A_2b_2}{s+b_2}\right)\right)\end{aligned} \tag{F.2a}$$

$$G_{12}(s)=\left(\frac{x_\theta}{r_\theta^2}-\frac{a_h}{\mu r_\theta^2}\right)s^2+\left(-\frac{2(a_h+1/2)\,\varphi(0)}{\mu r_\theta^2}-\frac{2(a_h+1/2)}{\mu r_\theta^2}\left(\frac{A_1b_1}{s+b_1}+\frac{A_2b_2}{s+b_2}\right)\right)s \tag{F.2b}$$

$$\begin{aligned}G_{21}(s)&=\left(x_\theta-\frac{a_h}{\mu}\right)s^2\\&+\left(\frac{1}{\mu}+\frac{2(1/2-a_h)\,\varphi(0)}{\mu}+\frac{2(1/2-a_h)}{\mu}\left(\frac{A_1b_1}{s+b_1}+\frac{A_2b_2}{s+b_2}\right)\right)s\\&+\left(\frac{2\,\varphi(0)}{\mu}+\frac{2}{\mu}\left(\frac{A_1b_1}{s+b_1}+\frac{A_2b_2}{s+b_2}\right)\right)\end{aligned} \tag{F.2c}$$

$$G_{22}(s)=\left(1+\frac{1}{\mu}\right)s^2+\left(\frac{2\zeta_h\bar{\omega}}{U}+\frac{2\varphi(0)}{\mu}+\frac{2}{\mu}\left(\frac{A_1b_1}{s+b_1}+\frac{A_2b_2}{s+b_2}\right)\right)s+\frac{\bar{\omega}^2}{U^2} \tag{F.2d}$$

Thus,

$$\begin{Bmatrix}\theta\\ \xi\end{Bmatrix}=[G(s)]^{-1}\begin{Bmatrix}\dfrac{2(a_h+1/2)}{\mu r_\theta^2}\left(\dfrac{A_3b_3}{s+b_3}+\dfrac{A_4b_4}{s+b_4}\right)\\ \dfrac{-2}{\mu}\left(\dfrac{A_3b_3}{s+b_3}+\dfrac{A_4b_4}{s+b_4}\right)\end{Bmatrix}\frac{w_T(s)}{U} \tag{F.3}$$

$$\begin{Bmatrix}\theta\\ \xi\end{Bmatrix}=\frac{\begin{bmatrix}G_{22} & -G_{12}\\ -G_{21} & G_{11}\end{bmatrix}}{\det[G(s)]}\begin{Bmatrix}\dfrac{2(a_h+1/2)}{\mu r_\theta^2}\left(\dfrac{A_3b_3}{s+b_3}+\dfrac{A_4b_4}{s+b_4}\right)\\ \dfrac{-2}{\mu}\left(\dfrac{A_3b_3}{s+b_3}+\dfrac{A_4b_4}{s+b_4}\right)\end{Bmatrix}\frac{w_T(s)}{U} \tag{F.4}$$

$$\begin{Bmatrix}\theta\\ \xi\end{Bmatrix}=\frac{\begin{bmatrix}G_{22} & -G_{12}\\ -G_{21} & G_{11}\end{bmatrix}}{U\det[G(s)]}\begin{Bmatrix}\dfrac{2(a_h+1/2)}{\mu r_\theta^2}\left(\dfrac{A_3b_3}{s+b_3}+\dfrac{A_4b_4}{s+b_4}\right)\\ \dfrac{-2}{\mu}\left(\dfrac{A_3b_3}{s+b_3}+\dfrac{A_4b_4}{s+b_4}\right)\end{Bmatrix}w_T(s) \tag{F.5}$$

Expressed in condensed form with the transfer functions, F_θ and F_ξ equation (F.5) gives:

$$\begin{Bmatrix}\theta\\ \xi\end{Bmatrix}=\begin{Bmatrix}F_\theta\\ F_\xi\end{Bmatrix}w_T(s) \tag{F.6}$$